TECHNICAL REPORT STANDARD PAGE

1. Title and Subtitle
Developing Load Distribution Formula for Louisiana Cast-in-place Reinforced Concrete Box Culverts

2. Author(s)
Ayman M. Okeil, Ph.D., P.E. (FL)
Navid Jafari, Ph.D.

3. Performing Organization Name and Address
Department of Civil and Environmental Engineering
3255 P.F. Taylor Hall
Louisiana State University
Baton Rouge, LA 70803

4. Sponsoring Agency Name and Address
Louisiana Department of Transportation and Development
P.O. Box 94245
Baton Rouge, LA 70804-9245

5. Report No.
HWA/LA. 692

6. Report Date
February 2024

7. Performing Organization Code
LTRC Project Number: 20-1ST
SIO Number: DOTLT1000342

8. Type of Report and Period Covered
Final Report
03/2020 – 12/2023

9. No. of Pages
204

10. Supplementary Notes
Conducted in Cooperation with the U.S. Department of Transportation, Federal Highway Administration

11. Distribution Statement

12. Key Words
live load distribution; reinforced concrete; culverts; buried structures; reliability live load distribution; reliability

13. Abstract
This report summarizes the results from an investigation of the behavior of cast-in-place (CIP) reinforced concrete (RC) box culverts. Load rating of CIP-RC box culverts has been a challenge for Departments of Transportation (DOTs) across the nation, including in Louisiana. Excessive conservatism built into the American Association of State Highway and Transportation Officials (AASHTO) Bridge Design Specifications (BDS) has led to situations where load posting, structural strengthening, or full replacement of culverts may be needed unless refined analysis methods are used to obtain more accurate results. Use of refined methods is a time-consuming burden to bridge engineers. Field inspections have not led to obvious conclusions that this class of culverts is under distress because of overloading, which was confirmed by an earlier project (Project 16-3ST)

sponsored by the Louisiana Transportation Research Center (LTRC) [1]. This project was initiated to explore the potential for developing a live load distribution (LLDF) formula that produces more consistent results, removes unnecessary conservatism, and conforms to safety levels targeted by AASHTO-LRFD BDS.

To address this challenge, a parametric study was conducted considering the key parameters known to influence the structural behavior of CIP-RC box culverts. The parametric study included 273 CIP-RC box culverts, which were analyzed using refined analysis methods to obtain more accurate results representing actual culvert behavior. Simplified analyses used by engineers were also conducted using several empirical LLDF formulas. A detailed study of the effects of various parameters on the straining actions was performed. Based on this study, the key parameters that affect live load distribution were identified, and a live load distribution formula was developed. The main advantage of the proposed formula is that it considers the secondary distribution of straining actions in the top slab, which is greatly affected by the wheel load position. Comparisons between AASHTO-LRFD BDS LLDF and the proposed LLDF formula were conducted to study how both formulae conform to AASHTO-LRFD BDS safety level requirements, as measured by the reliability index.

The predictions of straining actions using the proposed LLFD formula were found to produce more consistent predictions than the AASHTO-LRFD BDS LLDF formula. The unnecessary conservatism in predicting positive moments was removed, while the inconsistency in predicting shear forces and negative moments was greatly reduced. Therefore, it is recommended that CIP-RC box culverts be designed and load rated using the developed formula.

Project Review Committee

Each research project will have an advisory committee appointed by the LTRC Director. The Project Review Committee is responsible for assisting the LTRC Administrator or Manager in the development of acceptable research problem statements, requests for proposals, review of research proposals, oversight of approved research projects, and implementation of findings.

LTRC appreciates the dedication of the following Project Review Committee Members in guiding this research study to fruition.

LTRC Administrator/Manager

Walid Alaywan, Ph.D., P.E.
Senior Structures Research Manager

Members

Dana Feng, P.E., DOTD Bridge Design Section
Haylye Brown, DOTD Bridge Maintenance Section
Qiming Chen, LTRC
Corey Mayeux, LTRC
Paul Fossier, FHWA – Louisiana Division
(Former DOTD Bridge Design Section)

Directorate Implementation Sponsor

Chad Winchester, P.E.
DOTD Chief Engineer

Developing Load Distribution Formula for Louisiana Cast-in-place Reinforced Concrete Box Culverts

By
Ayman M. Okeil, Ph.D., P.E. (FL)
Navid Jafari, Ph.D.

Department of Civil and Environmental Engineering
3255-D Patrick F. Taylor Hall
Louisiana State University
Baton Rouge, LA 70803

LTRC Project No. 20-1ST
SIO No. DOTLT1000342

conducted for
Louisiana Department of Transportation and Development
Louisiana Transportation Research Center

February 2024

Abstract

This report summarizes the results from an investigation of the behavior of cast-in-place (CIP) reinforced concrete (RC) box culverts. Load rating of CIP-RC box culverts has been a challenge for Departments of Transportation (DOTs) across the nation, including in Louisiana. Excessive conservatism built into the American Association of State Highway and Transportation Officials (AASHTO) Bridge Design Specifications (BDS) has led to situations where load posting, structural strengthening, or full replacement of culverts may be needed unless refined analysis methods are used to obtain more accurate results. Use of refined methods is a time-consuming burden to bridge engineers. Field inspections have not led to obvious conclusions that this class of culverts is under distress because of overloading, which was confirmed by an earlier project (Project 16-3ST) sponsored by the Louisiana Transportation Research Center (LTRC) [1]. This project was initiated to explore the potential for developing a live load distribution (LLDF) formula that produces more consistent results, removes unnecessary conservatism, and conforms to safety levels targeted by AASHTO-LRFD BDS.

To address this challenge, a parametric study was conducted considering the key parameters known to influence the structural behavior of CIP-RC box culverts. The parametric study included 273 CIP-RC box culverts, which were analyzed using refined analysis methods to obtain more accurate results representing actual culvert behavior. Simplified analyses used by engineers were also conducted using several empirical LLDF formulas. A detailed study of the effects of various parameters on the straining actions was performed. Based on this study, the key parameters that affect live load distribution were identified, and a live load distribution formula was developed. The main advantage of the proposed formula is that it considers the secondary distribution of straining actions in the top slab, which is greatly affected by the wheel load position. Comparisons between AASHTO-LRFD BDS LLDF and the proposed LLDF formula were conducted to study how both formulae conform to AASHTO-LRFD BDS safety level requirements, as measured by the reliability index.

The predictions of straining actions using the proposed LLFD formula were found to produce more consistent predictions than the AASHTO-LRFD BDS LLDF formula. The unnecessary conservatism in predicting positive moments was removed, while the inconsistency in predicting shear forces and negative moments was greatly reduced. Therefore, it is recommended that CIP-RC box culverts be designed and load rated using the developed formula.

Acknowledgments

The authors gratefully acknowledge the financial support provided by the Louisiana Transportation Research Center (LTRC) (LTRC Project No. 20-1ST) and the Louisiana Department of Transportation and Development (DOTD)

The authors also acknowledge Ahmed Elshoura, graduate student in the Department of Civil and Environmental Engineering, for assistance in developing initial numerical models for analysis of culverts.

The authors would also like to thank Jenny Fu (DOTD), former Bridge Design Administrator, and Dana Fang (DOTD), Assistant Bridge Design Administrator, for initiating the idea behind this project, providing pertinent information throughout its execution, and for supporting the effort.

Finally, special thanks are due to Dr. Walid Alaywan (LTRC), Senior Structures Research Engineer, for his support of the research team and guidance throughout the project's execution.

Implementation Statement

This study demonstrates that the designing or load rating of cast-in-place (CIP) reinforced concrete (RC) box culverts using the American Association of State Highway and Transportation Officials (AASHTO) Bridge Design Specifications (BDS) live load distribution (LLDF) formula leads to inconsistencies in safety levels for some culverts and introduces unnecessary conservatism for others. The Louisiana Department of Transportation and Development (DOTD) stands to directly benefit from this project by reducing these inconsistencies and bringing culvert design into conformity with target safety levels acceptable by AASHTO-LRFD BDS as follows:

1. The proposed LLDF formula eliminates unnecessary conservatism in positive moment predictions, thus eliminating or reducing the number of culverts that will require load posting without the need to conduct refined analyses.
2. The proposed formula also eliminates unconservative shear force and negative moment predictions resulting from AASHTO-LRFD BDS LLDF formulae, which will enhance the safety of CIP-RC box culvert inventory.
3. As a last resort, culverts that are still not passing load rating requirements can be analyzed using refined analysis methods before resorting to load posting, structural strengthening, or other interventions.

Dissemination of the findings from this project can help with broader implementation of the proposed new LLDF formula. For implementation into the AASHTO LRFD Bridge Design Specifications, AASHTO Committee on Bridges and Structures (COBS) and its newly formed subcommittee on Soil Structures can help.

Table of Contents

List of Tables

List of Figures

Introduction

This report provides detailed investigation of wheel load distribution through earth fill for the design and load rating of cast-in-place (CIP) reinforced concrete (RC) box culverts. CIP-RC box culverts pose a challenge to bridge engineers in Louisiana and nationwide, as their load rating often results in low rating factors, which requires intervention by load posting, strengthening, or even replacement. Field inspections reveal that these culverts perform well with no signs of distress, which raises a question about current load rating procedures.

In this section, a brief review of how wheel loads are distributed for the design and load rating of CIP-RC box culverts is presented.

Live Load Distribution for CIP-RC Box Culverts

According to the NBI (National Bridge Inventory), culverts make up almost 140,000 out of the total national bridge inventory of over 616,000 [2], which translates into approximately 23% of the inventory. In Louisiana, the bridge inventory includes approximately 2,600 culverts. CIP-RC box culverts constitute a sizeable portion of the overall culvert inventory. Culverts have to be load rated like other bridges to ensure their structural integrity. However, following current load rating procedures for these culverts often yields unacceptable load rating factors even though their performance is acceptable with no signs of distress, such as cracking or excessive deformations. Unacceptable rating factors can lead to load posting, which restricts the use of the transportation network. Alternatively, upgrading these culverts may avoid load posting; however, the associated work may be cost prohibitive. Buried cast-in-place reinforced concrete culverts are known as a robust structural system that can withstand highway traffic because they behave as a highly statically indeterminate system. There are two main differences between the design of culverts and other types of bridges. First, single axle loads, and sometimes single wheel loads, are the controlling live load conditions for the design of culverts, as opposed to the gross vehicle weight (GVW) that controls the design of typical bridge spans. Second, the depth of the soil fill above any culvert is determined based on the hydraulics and roadway geometric conditions at the bridge site, which is known to vary greatly, and accordingly has a great impact on the live load effects on the buried culvert. In 2010, National Cooperative Highway Research Program (NCHRP) Project 15-29 produced Report 647, “Recommended Design Specifications for Live Load Distribution to Buried Structures” [3]. Simplified design equations (SDEs) for the structural response of buried structures based on three-dimensional (3D) analysis of 830

buried culverts were developed. The report also provides guidelines for conducting 2D and 3D modeling analyses for culverts that are not covered by the SDEs. In this work, the effect of pavement on live load distribution was ignored, which can have a significant effect on reducing actual pressures that reach the box. While this may be a conservative assumption for design purposes, it penalizes existing culverts with pavement over their top soil fill.

Live load effects from highway trucks are often assumed to spread as a surface load over an area whose dimensions can be determined based on a linear function of depth. Acceptable designs have been produced based on this approximation method for estimating the distribution of vehicular live loads through earth fill AASHTO Standard Specifications or Load Factor Design (LFD) [4]. Figure 1 shows a schematic of how live load pressures spread from the surface where the pressure is spread from the tire contact area (typically 10 in. x 20 in.) to a larger area at a given depth H. Three cases are shown representing (a) the case of a single wheel load, (b) the case of two single wheel loads from adjacent trucks in a passing mode, and (c) the case of two axles of the case described in (b). Currently, AASHTO (American Association of State Highway and Transportation Officials) LRFD (Load and Resistance Factor Design) Bridge Design Specifications [5] equations for estimating the distribution of vehicular live loads through earth fill led to increases in live load pressures on buried structures in comparison with AASHTO Standard Specifications [4]. Consequently, NCHRP sponsored an ongoing research project (Project 15-54) with the objective of proposing modifications to the culvert load rating specifications in AASHTO Manual for Bridge Evaluation [6] and revising AASHTO-LRFD accordingly. This is further exacerbated by the higher dynamic allowance in AASHTO-LRFD.

Figure 1. Area of live load distribution – (a) Single wheel (b) Two single wheels in passing mode (c) Two axles of two single wheels in passing mode (ACPA, 2011)

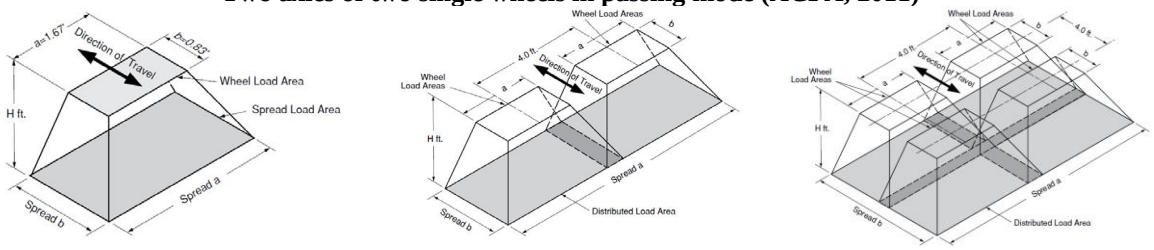

Reinforcement detailing also has its implications on reinforced concrete box culvert rating. Multi-cell structural systems are highly statically indeterminate and are therefore capable of resisting larger pressures than similar ones with lesser degrees of indeterminacy. However, the degree of indeterminacy of multi-cell box culverts may be reduced if the reinforcement

detailing at the corners is not capable of transferring the internal forces produced in such systems. Many of the CIP box culverts in Louisiana were built with old details that may fall under this category. Figure 2 shows one of these details, which reveals that (a) exterior wall reinforcement is not adequately embedded in the top or bottom slabs of the box and (b) a single layer of reinforcement in these walls, and at the ends of the top and bottom slabs, make them incapable of resisting negative moments that would generate in a fully rigid corner joint. Engineers have typically considered these connections to behave like hinges rather than rigid connections. The exact behavior of these corner joints can be confirmed from load test results.

Figure 2. Old LA-DOTD standard detail for a three-cell CIP box culvert

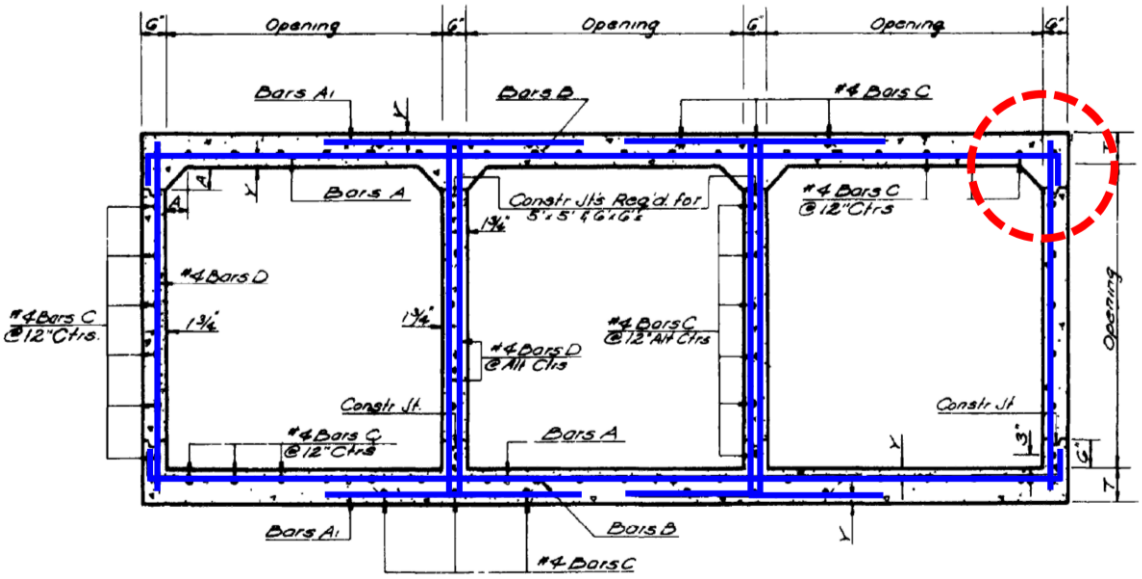

Current live load distribution estimation formulas in AASHTO-LRFD [5] specified governing equations for estimating axle load distribution for different earth fill height. Equation [1] can be used to estimate wheel load distribution dimensions, as shown in Figure 1-a, for culverts with low earth fill height (less than 2 ft., or 0.6 m.). On the other hand, Equation [2] represents wheel load distribution dimensions for culverts with fill height larger than 2 ft., or 0.6 m.

For $H_f \leq 2\ ft.$ (0.6 m.)

$$E_p(\text{in.}) = 96 + 1.44 * S\ (\text{ft.}) \quad [1]$$

$$E_s(\text{in.}) = L_T(\text{in.}) + LLDF * H_f\ (\text{in.})$$

For $H_f > 2\ ft.$ (0.6 m.)

$$E_p(\text{in.}) = 10 + LLDF * H_f\ (\text{in.}) \quad [2]$$

$$E_s(\text{in.}) = 20 + LLDF * H_f\ (\text{in.})$$

Where, H_f = earth fill height, E_p = distribution width in the direction perpendicular to span, E_s= distribution width parallel to span, S= Span length, L_T = length of tire contacting area parallel to span, and $LLDF$ = live load distribution factor. For culverts with low fill height, the distribution width perpendicular to span length E_p is based on a research study done in 2005. In that research, one of the main objectives of the study was to evaluate live load distribution width that can be applied to 2D FE modeling to obtain the same peak bending moments as 3D FE modeling [7]. Culverts with different conditions were studied; one-cell and two-cells, cast-in-place reinforced concrete, and precast concrete, with different span lengths, different element thicknesses, and different supporting conditions. Each culvert case was either 0 ft. or 2 ft. (0.6 m.) fill height.

Current AASHTO live load distribution equations are conservative, specifically for low fill height culverts, and give conservative internal forces for critical cross sections. This conservatism affects the rating process since it distributes live load to a narrower area, which in turn increases pressure intensity and internal forces and conducts low rating factors.

Load distribution width for axle load constitutes two components:

1. Distribution through the asphalt pavement and the soil layers, which can be called “primary distribution”
2. Distribution due to the slab flexural rigidity, called “secondary distribution”, which accounts for slab continuity in longitudinal direction, i.e. plate behavior.

In this study, the main target was to develop live load distribution formulas of axle load applicable for 2D FE models, in order to obtain the same internal forces (positive and negative moments) that result from 3D FE analysis. The formulas were developed so that the secondary distribution due to slab continuity is taken into account. Consequently, the formulas depended on conducting 3D FE analysis and comparing results with 2D FE analysis. The goal was to investigate how wide the live load needs to be distributed over 2D FE model to result in approximately the same values as 3D FE models. Furthermore, a parametric study to investigate the parameters that are in correlation with the distribution area was performed.

Earlier Research on Culverts in Louisiana

The Louisiana Transportation Research Center has funded several studies on buried culverts in the past. However, the work was mainly focused on metal culverts [8-11]. The light weight and flexibility of metal pipes make them an appealing alternative to other types of culverts. However, their susceptibility to corrosion is a disadvantage. In 1977, researchers started studying the durability of buried metal pipe culverts to address their corrosion in the harsh environments where they are commonly employed. This initiated the motivation for inspecting six different types of existing culvert metal pipes and four other new types to evaluate the rate and causes of corrosion and durability. The authors observed that asbestos-bonded, asphalt-coated galvanized steel culverts performed better than other types of culverts considered in the study after six years of in-service monitoring.

Several reports were published in the 1990s on coated metal pipe culverts [12-14]. The main focus of these studies was to investigate the feasibility of cathodic protection, both externally and internally, to prevent corrosion in corrugated steel pipes, hence reducing the costs of maintaining or replacing these types of culverts. In this research, cathodic protection was applied to retrofitted metal pipe externally and internally and monitored for two years. The same protection process was applied on a new metal pipe culvert and monitored for one year. The monitoring results indicated that cathodic protection was effective for existing pipes externally, but not internally. However, cathodic protection was effective for both internal and external corrosion protection for new culverts. The information from monitoring was used to develop a computer expert system software to assist designers in assessing the economics of employing cathodic protection systems in metal culverts in Louisiana.

Research Needs

As seen in the brief review of published efforts on live load rating of CIP-RC box culverts, live load distribution for design and load rating purposes has been the focus of many studies. Despite the differences in available live load distribution models, there is a consensus on the fact that current AASHTO-LRFD BDS provisions pose a challenge to bridge engineers, as these provisions produce conservative assessments that sometimes lead to load rating factors that require intervention by load positing, structural strengthening, or full replacement. This imposes an additional strain on the limited available resources.

The immediate research need for culvert load rating is to provide a modified procedure for both load rating CIP-RC box culverts in the DOTD's inventory that were built using old standard details as well as designing new culverts. The modified procedure will address the challenges resulting from current AASHTO-LRFD BDS provisions by removing unnecessary conservatism. The long-term need in Louisiana and nationwide is to fully understand the different factors that affect live load distribution, including fill height, pavement type, soil type, and a culvert's structural and geometric characteristics. Based on this understanding, new live load distribution formulas can be proposed.

This study builds on the findings from an earlier study (LTRC Project 16-3ST) in which field testing of eight culverts was conducted to assess the load rating of the selected culverts as a first step towards addressing long-term needs [1]. The project confirmed the structural integrity of the field-tested culverts despite the low ratings obtained using current load rating procedures.

This report presents the findings from a project whose purpose was to develop more rational live load distribution formula for the load rating and design of CIP-RC box culverts. A numerical modeling approach was adopted for the task. Three- and two-dimensional (3D and 2D) finite element (FE) models were used to model culverts with various configurations and design parameters to understand the behavior of CIP-RC box culverts. The FE results were then used to assess the quality of straining action predictions using AASHTO-LRFD BDS and to develop a new live load distribution formula. Finally, reliability assessment was conducted for culverts analyzed using the AASHTO-LRFD BDS and proposed live load distribution formulas.

Literature Review

The literature is rich with work on the behavior and design of buried structures. Some of these studies date to as early as several decades ago (e.g. [15; 16]). From early on, there was evidence that culverts were overdesigned. For example, Frederick and Tarhini [17] conducted field testing of prototypes, which revealed that observed strain levels were low.

The National Cooperative Highway Research Program sponsored several projects addressing culvert design. NCHRP Project 12-45, "Recommended Specifications for Large-Span Culverts", involved monitoring the performance of full-scale metal and concrete culverts during backfilling and under vehicle loads [18]. The experimental results were complemented with finite element analyses whose results were used to create simplified design equations. NCHRP Project 15-29, "Recommended Design Specifications for Live Load Distribution to Buried Structures", also produced simplified design equations for structural response based on 3D analysis of 830 buried culverts [3]. Finally, NCHRP Project 15-54, "Proposed Modifications to AASHTO Culvert Load Rating Specifications", has been recently completed [19].

For culverts with low fill height, the equation for distribution width perpendicular to span length E_p is based on a research study completed in 2005. In this study, one of the main objectives was to evaluate live load distribution width that can be applied to 2D FE modeling to obtain the same peak bending moments as 3D FE modeling [7]. Culverts with different conditions were studied: one-cell and two-cells, cast-in-place reinforced concrete, and precast concrete, with different span lengths, different element thicknesses, different supporting conditions, and each culvert with 0 ft. or 2 ft. (0.6 m.) fill height. In that study, 3D finite element analysis was used to model the culverts described earlier. To obtain the load distribution width corresponding to maximum shear, maximum positive moment, and maximum negative moment, the wheel load was placed at a distance d (the effective top slab thickness), mid-span, and several intermediate locations, respectively. Distribution width corresponding to peak shear force was the smallest followed by positive bending moment and negative bending moment, which can be considered as a controlling distribution [7]. Based on this result, a conservative axle live load distribution equation was developed to be used for the design and rating of culverts with earth fill height less than 2 ft. (0.6 m.).

Abolmaali and Garg [20] tested six culverts up to failure to evaluate the shear capacity for box culverts. They were loaded by AASHTO HS-20 wheel loads at shear-critical locations. Tests showed that fine flexural cracks were initiated inside the top slab at an applied load

equal to approximately the factored load. Then, by increasing the applied load, more positive and negative flexural crakes were propagated until it reached 156% of the factored load, at which shear cracks started to be detected [20]. Culverts were observed for total failure at loads equal to twice the factored load, and flexure and bond slippage was the failure mode [20]. Consequently, it can be concluded that shear behavior is not the controlling mode of failure. Moreover, a 3D simulation study including finite element analysis for the previously described study has been performed to detect the crack propagation and failure pattern. The results were the same; increasing the load up to twice the factored load led to widening the flexural cracks, and shear cracks started to surface [21]. Those findings contradict what has been concluded in AASHTO-LRFD distribution equation.

Abdel-Karim et al. [15] discussed the distribution of wheel loading within the aforementioned stages (pavement layers, embankment soil, and top slab) by conducting live load tests on culverts with fill heights ranging from 2 ft. (0.6 m) to 12 ft. (3.65m), and load pressures were measured using pressure cells. The study concluded that load pressure is generally distributed over a square area, but increasing fill height uniforms pressure intensity over a larger area with lower peak, except for 2 ft. (0.6 m) fill height. Furthermore, flexural rigidity of rigid pavement was shown to have considerable contribution in distribution loads within a wider area, with lower intensity specifically over low fill height culverts, owing to its higher flexural rigidity compared with soil rigidity. Moreover, the study proposed a method for calculating an additional width that represents the existence of rigid pavement by converting the pavement thickness into an equivalent fill height. The same behavior was also noticed for the top slab that helps for the additional dispersing of load, owing to the flexural rigidity of the top slab of the culvert.

Orton et al. [22] tested reinforced concrete culverts with fill depths ranging from 2.5 ft. (0.76 m.) to 13.5 ft. (4.1 m.) to determine live load effect on culvert behavior. By comparing measured and calculated strains and displacements, it was concluded that the AASHTO-LRFD specifications are overly conservative.

The accuracy of axle distribution equation stated in AASHTO-LRFD specifications was investigated by assessing the live load rating of three RC box culverts with different properties: span lengths, box dimensions, and earth fill heights. For each culvert, two different FE models were constructed. The first model is a 2D FE model using a structural-frame element for culvert component, and for wall and slab section; the second one is a 2D soil structural interaction. The models were calibrated by performing live load test and comparing test results with FE analyses. In the frame models, live loads were distributed based on AASHTO specifications, whereas they were dissipated according to the soil mesh in

the soil-structure interaction model. The research showed that both models are conservative, but more precise results were obtained from the 2D soil-structure interaction model. Moreover, increasing soil fill height resulted in improving the accuracy of both models [23]. Another study done by Wood et al. discussed the precision of live load distribution on RC box culverts. Comparison between three simplified FE models (structural-frame model, top-slab calibrated soil-structure model, and fully depth-calibrated soil-structure model) was conducted. In the first model, the soil was considered as a dead load only; it attenuated the wheel (concentrated) live load as recommended in the specifications [6], and it was found that it underrates culverts [24]. For the second model, axle line load is applied at the ground surface, and it is distributed to the walls, top slab, and the bottom slab of the culvert. More accurate load rating factors resulted using that model since it distributes stresses at the bottom slab and best captures the structural response. The fully depth-calibrated soil-structure model was found to obtain the most accurate and precise load factor since live loads are distributed differently according to the studied critical sections.

Acharya et al. [25] investigated the effect of the presence of rigid pavement and culvert span length on the live load distribution. It showed that the presence of rigid pavement enhanced the rating factor of culverts, owing to the additional live load distribution resulting from concrete pavement rigidity. An inverse correlation between load pressure intensity and span length was also found. In other words, increasing span length helped to distribute the live load within a wider area with less intensity, especially for culverts with low fill height.

Other parameters were studied in another study by Acharya et al. [26], in which RC box culverts with low fill height were tested with static and moving live load. The study aimed to understand the influence of vehicular axle load, its speed, and pavement type on top slab deflection of buried culverts. The tests were run under a static load at three different locations: concrete pavement, concrete shoulder with a thinner concrete pavement, and unsurfaced area, in addition to live load dynamic test. Tests showed that the deflection of top slab over the unsurfaced area due to the static load were 2-3 times higher than deflection under the concrete-paved road and shoulder as a result of the high stiffness of the concrete pavement. It was also observed that the dynamic load caused deflection with a higher magnitude than static loads due to impact effect.

Frederick and Tarhini [17] conducted a study to evaluate the design of precast reinforced concrete box culverts complying with ASTM Specifications C789 and C850 using AASHTO live load distribution provisions. The experimental program employed 1/6-size scale models and 1/24-size photo-elastic model of three culvert prototypes with different dimensions. By comparing the strains and deflections resulting from the model test and field test results of

the culvert prototypes, authors noticed that AASHTO live load distribution equation is conservative, and that the live load is dissipated over a wider area. It was concluded that culverts designed according to ASTM C850 were over-designed.

In general, current AASHTO-LRFD BDS live load distribution equation for low fill height culverts gives conservative internal forces at critical cross sections. This conservatism affects the rating process since it distributes live load to a narrower area, which in turn increases pressure intensity and internal forces and conducts low rating factors. In this study, the main target is to develop distribution equation E_p of axle load that can be used for 2D FE models to be able to obtain the same mid-span moment as 3D FE analysis. The proposed equation is based on conducting 3D FE analysis and comparing results with 2D FE analysis. A parametric study to quantify the correlation between 2D and 3D results for the distribution width E_p is also performed.

Secondary Distribution of Non-Uniform Loads on Slabs

Slabs are typically designed to resist uniformly distributed loads, which is easily handled by considering unit-width strips that are representative of the entire slab area. The complexity of the behavior of slabs increases substantially when subjected to non-uniform loads such as mast loads, partitions, and wheel loads. This topic has been investigated thoroughly by researchers since the 1930s [27]. Studies by Westergaard and others show that the portion of the slab that resists non-uniform loads extended beyond the projection of the load footprint on the slab. To some extent this concept has been implicitly adopted in AASHTO-LRFD BDS design provisions for bridge deck slabs and slab bridges. In AASHTO-LRFD BDS, the traditional design method identifies the strip width as a function of the span length. Other codes provide more explicit distribution width based on the position of the non-uniform load. For example, the Australian code has the following equation for determining the effective width (b_{ef}) of a slab that resists an applied non-uniform load:

$$b_{ef} = \text{load width} + 2.4\,a\left[1 - \frac{a}{L_n}\right] \quad [3]$$

Where, a is the distance from the non-uniform load to the closest support and L_n is the span length of the slab. This and similar expressions show that for load positions critical for shear (i.e., close to the support), the distribution width is smaller for flexure critical load positions (i.e., close to midspan). This is illustrated in Figure 3. This topic will be revisited when the new LLDF is developed later in the report.

Figure 3. Effect of load position of width or slab resisting non-uniform loads

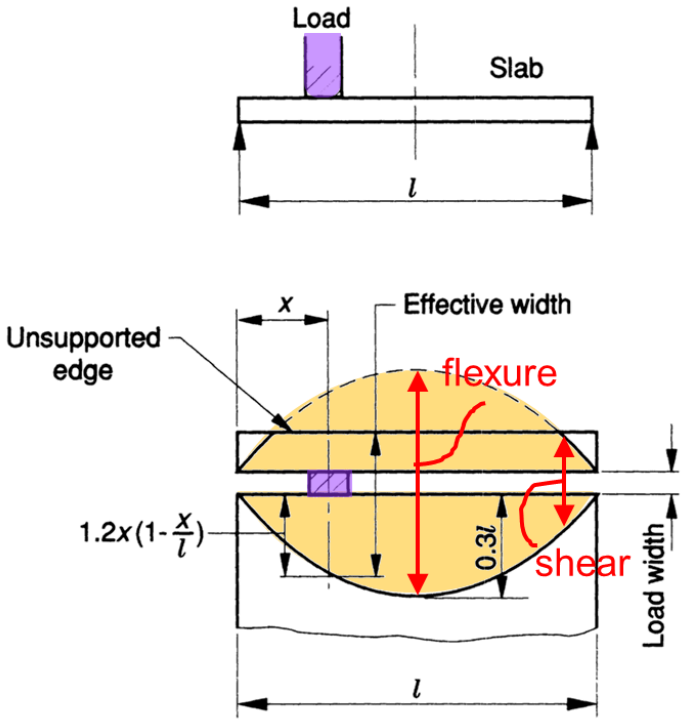

Objective

The primary objective of this project was to investigate live load distribution over buried cast-in-place (CIP) reinforced concrete (RC) box culverts in order to recommend the most appropriate live load distribution formulas (LLDF) for use in design and load rating.

The goals of the project were to:

1. Conduct a parametric investigation of buried RC-CIP box culverts covering key parameters known to affect distribution of wheel loads through the soil, both onto the culvert's top slab and structurally through the culvert.
2. Analyze results from the parametric study to help evaluate the best LLDF for the design and load rating of RC-CIP box culverts.
3. Study the reliability of RC-CIP box culverts using different LLDF to ensure conformity with AASHTO-LRFD BDS.
4. Provide DOTD with recommendations to assist in adoption in the *Bridge Design and Evaluation Manual (BDEM).*

Scope

This study focused on cast-in-place (CIP) reinforced concrete (RC) box culverts buried under low earth fill height. In Louisiana, load rating this class of culverts is challenging because the live load distribution formulas (LLDF) adopted in AASHTO-LRFD BDS appear to be conservative. The load rating challenge is further exacerbated by the fact that standard details for CIP-RC box culverts provide no resistance to negative moments at the outside top corners of the culverts despite their good performance in the field. This good performance is evidenced by routine field inspections and live load tests conducted through LTRC Project 16-3ST [1].

Thus, the scope of investigation is limited to CIP-RC box culverts with low earth fill heights ($\leq$ 2 ft.) considering AASHTO-LRFD BDS design axle loads, namely design truck and design tandem loads. 1-, 2-, and 3-barrel culverts with different sizes were considered in the investigation.

Methodology

To study both the live load distribution of design wheel loads through the soil onto the culvert and with the cast-in-place (CIP) reinforced concrete (RC) box culverts, detailed numerical models were used. The finite element (FE) method was chosen for this task, as it provides flexibility regarding the level of detail that can be considered in the model (e.g. modeling subgrade as springs, compression-only springs, or a continuum with contact elements).

Modeling of Buried Box Culverts

The numerical models used in this study were developed to provide a more exact assessment of live load distribution of wheel loads through the earth fill on top of the culvert and within the culvert itself. This distribution can only be captured using two-dimensional (2D) models after introducing empirical approximations that make the process inherently conservative. Conversely, three-dimensional (3D) models capture the distribution of wheel loads more accurately based on the mechanics of how the slab interacts with surrounding structural elements, rather than based on empirical assumptions. Since the use of 3D models is expensive and requires advanced knowledge of the finite element method, engineers typically use 2D models in the analysis of CIP-RC for design and load rating purposes. Therefore, all culverts investigated in this study were modeled using both models (2D and 3D), which are described next.

Three-dimensional (3D) Modeling of CIP-RC Culverts

Three-dimensional (3D) structural models represent the modeled structure in space without introducing simplifications that result from the elimination of the third dimension. For example, wheel loads attenuate through the soil and only affect a region of the culvert's top slab in the vicinity of the wheel load locations. The effect of the wheel load far from where it is applied becomes negligible as the distance from the wheel load increases. This effect is accounted for based on the structural response of the culverts as opposed to empirical simplifications of the transverse length of the culvert affected by the wheel load. Figure 4-a shows a 3D model of a 3-barrel culvert case with an axle load acting on the middle of the first barrel span. The culvert's top slab would deflect under the shown axle load, as can be seen in Figure 4-b. It is clear that the region affected by the axle load is limited near the application of the axle load. This region is clearer in Figure 4-c where the contour plot of the

vertical displacement highlights the region affected by the applied axle load. As stated earlier, the extent of this region transversely (i.e., perpendicular to traffic) is empirically estimated in 2D models.

Figure 4. Three-dimensional (3D) model of a 3-barrel culvert with one axle load

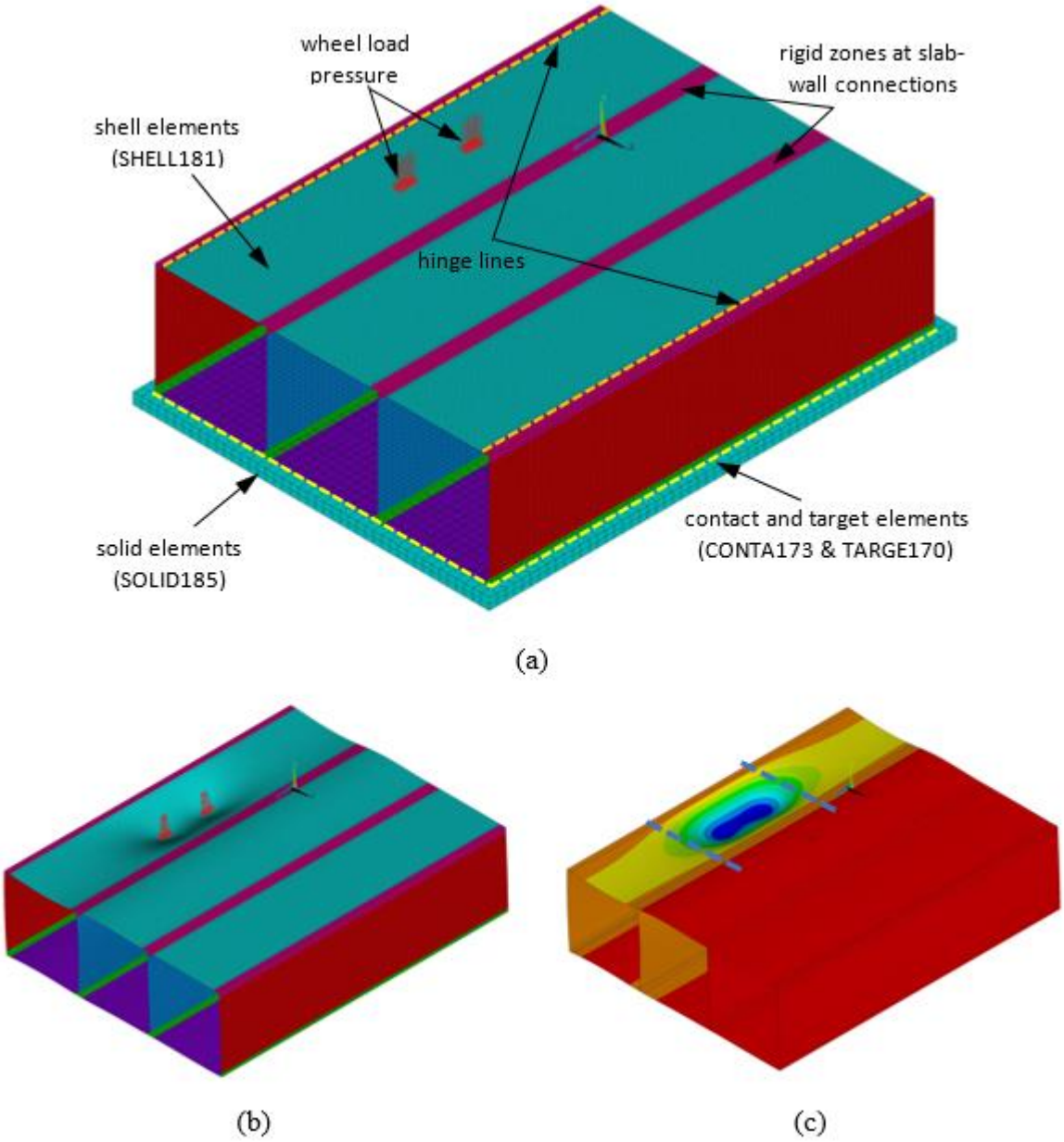

Details of 3D models

To capture the three-dimensional behavior of culverts, the PI investigated the use of solid and shell elements in an earlier study and compared their advantages and disadvantages [1]. In this study, the research team adopted the finding from the earlier study and chose to mode the culverts using shell elements found to be more efficient than the solid elements. Shell elements allow direct access to nodal solutions (moments, shear forces, etc.), while solid elements produce stresses that have to be integrated to obtain the shear forces and bending moments. Furthermore, solid elements are known to be stiff, and more elements are typically needed through the thickness to obtain acceptable results. Finally, the modeling of the zero-moment resistance at the exterior slab-wall connections would have been challenging if solid elements were used. The RT modeled the culverts using the general purpose finite element software package ANSYS [28]. ANSYS shell element SHELL181 with six degrees of freedom (DOFs, translations in the x, y, and z directions, and rotations about the x, y, and z-axes) at each of its four nodes was adopted for the 2D models. SHELL181 is suitable for analyzing thin to moderately thick shell structures. Figure 5 shows the geometric attributes of SHELL181.

Figure 5. Shell element SHELL181 used to model culvert walls and slabs [28]

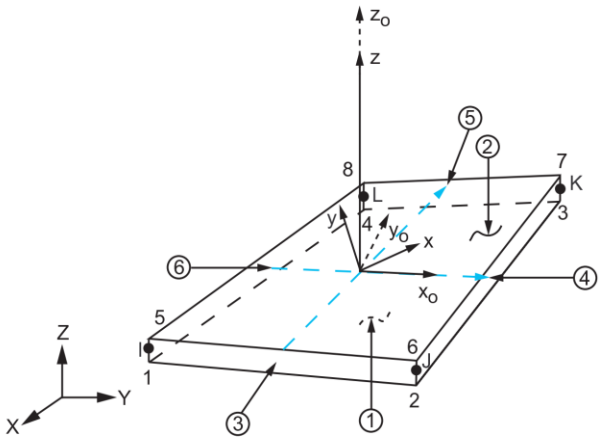

Another element type used in this study is the ANSYS solid element SOLID185. SOLID185 was used to model the soil subgrade under the culverts to represent the actual condition of the culvert's support. Simplifications of the support condition (e.g., assuming full restraint under the walls, partial parts of the bottom slabs, or individual springs) were deemed unnecessary. Instead, a full continuum solid element was used to simulate the subgrade support. SOLID185 is a 3D structural solid element with three DOFs (translations in the x, y, and z directions) at each of its eight nodes. Figure 6 shows the geometric attributes of SOLID185.

Figure 6. Solid element SOLID185 used to model soil subgrade [28]

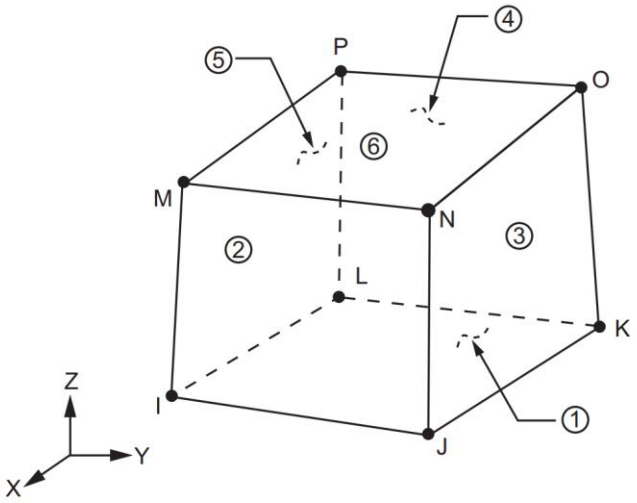

It should be noted that the culvert's bottom slab shell elements and the top of the soil subgrade solid elements were not rigidly connected. Contact elements were used to serve as interface between both elements. CONTA173 contact element was used to model this effect. Figure 7 shows the geometric attributes of CONTA173. It should be noted that a target surface needs to be defined for CONTA173 elements. This was done using TARGE170, which represents the target surface in space. Based on the properties of the elements involved in this interface modeling, the culvert's slab was allowed to move upward with no resistance. However, downward movement was resisted by the subgrade soil. Figure 8 shows the deformed shape of the 3-barrel culvert discussed earlier. It can be seen that the first barrel is directly affected by the axle load on the soil more than the third barrel. Note that due to the large scaling of the deformations, the bottom slab appears to sink into the soil.

Figure 7. Contact element CONTA173 used to bottom slab – subgrade interaction [28]

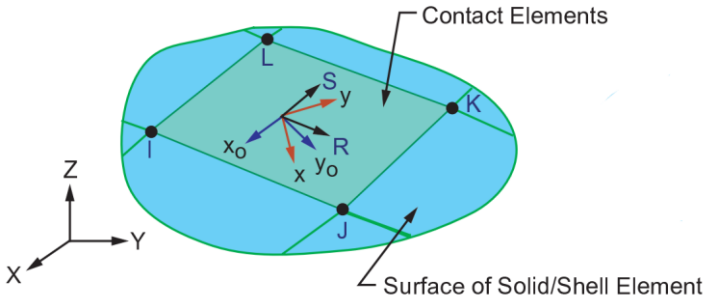

Figure 8. Deformation of a 3-barrel culvert showing interaction between bottom slab and soil subgrade

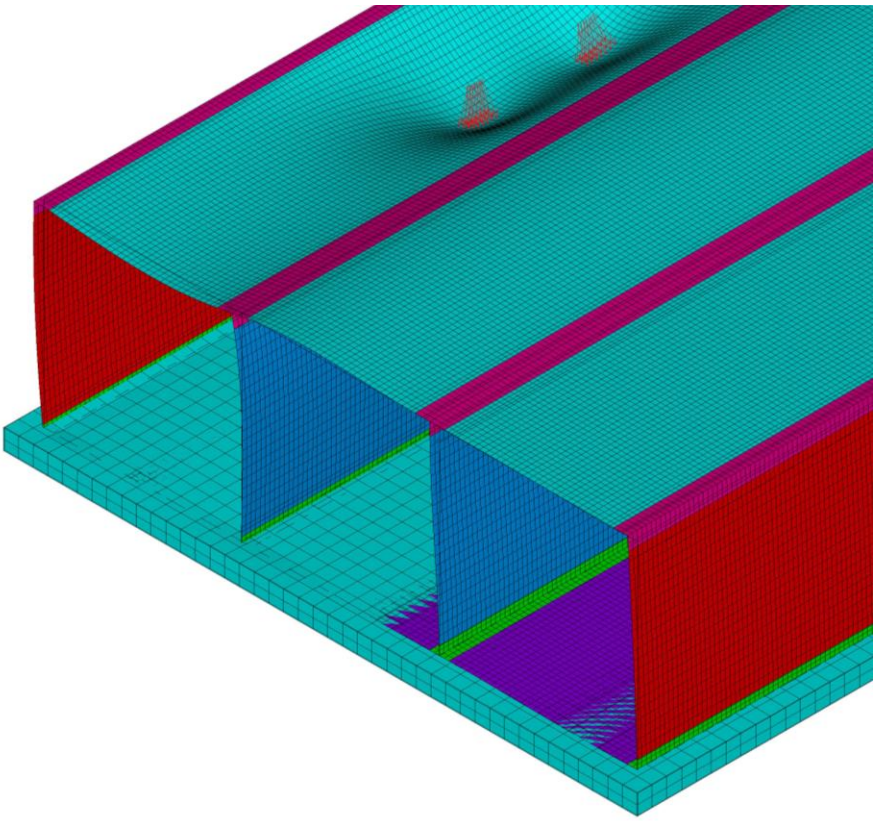

Shell elements are typically positioned at the midsection of the structural plate they represent (e.g., wall or slab), which means that an overlap exists at these joints. In this study, the wall-slab joint was modeled following the same method described in detail in LTRC Report 593 [1]. To model the offsets of the top and bottom slabs and the walls connected to them, rigid elements were used for the distance from the centers of the wall or slab to a point at the face of the member (i.e., half the slab or wall thickness). In the case of haunches, these haunches added to the rigidity of the connections and further increased the overlap between the slabs and the walls. Therefore, it was also assumed that the rigid element section extended beyond the aforementioned half slab or half wall thickness by one-half of the haunch length due to the presence of additional concrete thickness. These rigid areas are shown in Figure 4-a for the top corner location. The same is also true for bottom connections, albeit without a haunch. Because of the lack of negative moment resistance at the top outer corners, a hinge was assumed along the length of the culvert transversely, as can be seen in Figure 9. All other joints are capable of resisting bending moments; therefore, full continuity was assumed at these joints.

Figure 9. Typical wall- slab connection details in FE models

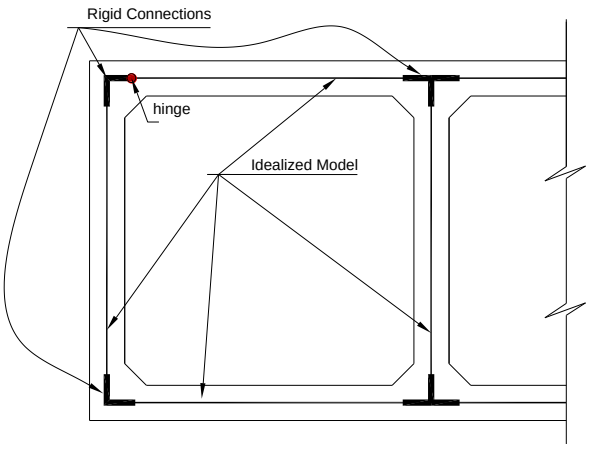

Loading of 3D Model

The following loads were applied on the 3D models:

- Self-weight of culvert concrete slabs and walls
- Earth fill weight over the top slab
- Wearing surface above the earth fill
- Wheel loads

Densities of 150 pcf and 120 pcf were used in calculating the self-weight for concrete and earth fill weight, respectively. A 29 psf was assumed for the wearing surface. The self-weight was applied in the first load step of the analysis as a gravity load using ACCEL command in ANSYS. Earth fill weight and wearing surface were applied as surface pressures over the entire top slab area. Wheel loads were also applied as a surface pressure on the top slab; however, they were only applied over a determined area based on the attenuation of wheel pressure through the earth fill. Figure 10 shows three cases of wheel pressure on the top slab of a 1-barrel culvert. The three cases represent earth fill heights equal to 0 ft., 1 ft., and 2 ft. As seen in the figure, the area of the top slab subjected to the attenuated wheel load pressure increases with the fill depth. For FH=0 ft, the area is equal to the contact area of the wheel, which is taken equal to 10 in. x 20 in. according to AASHTO-LRFD BDS [5]. It was assumed that wheel load was distributed through fill heights greater than 0 ft. at a slope of 2:1.

The 2:1 slope assumption is based on established information in the literature. As pressure passes from the tire, it spreads slightly in the pavement structure [29]. Once through the pavement, the pressure further spreads and attenuates through the cover soil [30]. Upon

reaching the culvert surface, the load transfers through the top slab. Moreover, AASHTO-LRFD BDS define the stress distribution based on fill depths less or greater than 2 ft. (0.6 m.), while this study is concerned with fill depths less than 2 ft. (0.6 m.). The 1992 AASHTO specifications promulgate a distribution width (B) as a function of the effective span length. This was updated in 2007 for the mobilization of positive and negative moments. However, the AASHTO guidelines greatly underestimate actual soil pressures [29; 31-33]. Accordingly, the 2:1 method was used in these analyses. This is an empirical approach based on the assumption that the area over which the load acts increases in a systematic way with depth. For rectangles of 20 in. and 10 in., the pressure at the surface decreases by approximately 72% at a depth of 1 ft. To verify the 2:1 method, the same computations were made using the Boussinesq Theory for a rectangularly loaded area. Boussinesq developed equations of the state of stress within a homogeneous, isotropic, linearly elastic half-space for a point load [34]. Newmark [35] derived the equation for the vertical stress under the corner of a uniformly loaded rectangular area. The average stress dissipation at 1 ft. of fill depth is approximately 71% of the applied surface pressure. Similar computations were made for a depth of 2 ft. Both methods result in similar approximate stress distributions. As a result, the 2:1 method was implemented in the numerical simulations conducted in this study.

Figure 10. Wheel load pressure on top slab for different fill heights.

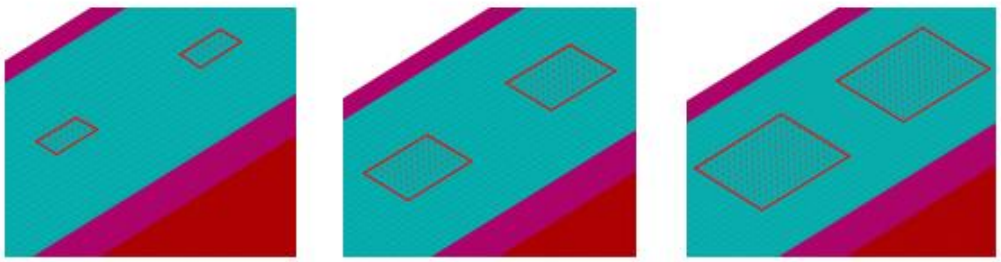

It should be noted that the meshing of the top slab was adjusted to make sure that the element dimensions fit the wheel pressure area exactly to avoid any unnecessary approximations due to pressure value adjustment, pressure area adjustment or both. This was achieved by defining areas before meshing that match exact dimensions of the wheel pressure area.

After determining the area affected by the wheel load pressure, this area was swept in the traffic direction to determine the maximum load effects for shear forces, positive and negative moments. This sweeping was necessary, as the critical wheel position cases for

shear are typically not the same as that for moments. Furthermore, the positions for the positive and negative moments also vary. Therefore, the wheel pressure was moved one element dimension at a time until the wheel pressure area exited the culvert at the other end. The number of wheel load positions in the traffic direction varied based on the culvert dimensions and fill height, which determines the size of the pressure area, as discussed earlier.

As required by AASHTO-LRFD BDS, both HL-93 design truck and design tandem were considered. Even though the tandem axle weight (25 kip) is less than that of the truck's axle weight (32 kip), its spacing is much smaller (4 ft. vs. 14 ft.), and therefore had to be considered in all analyzed cases. Figure 12 shows the case of a small culvert (6 ft.) with a design truck axle being swept across it. It is clear from the figure that a second axle with a 14 ft. spacing would not fit on a single barrel, nor on both barrels, for a negative moment case (i.e., one axle on each barrel). Figure 12 shows the case of a wide culvert (11 ft.) that would only fit one design truck axle. However, neither two nor three tandem axles can easily fit on one of the barrels.

Figure 11. Wheel load pressure on top slab (case of truck axle)

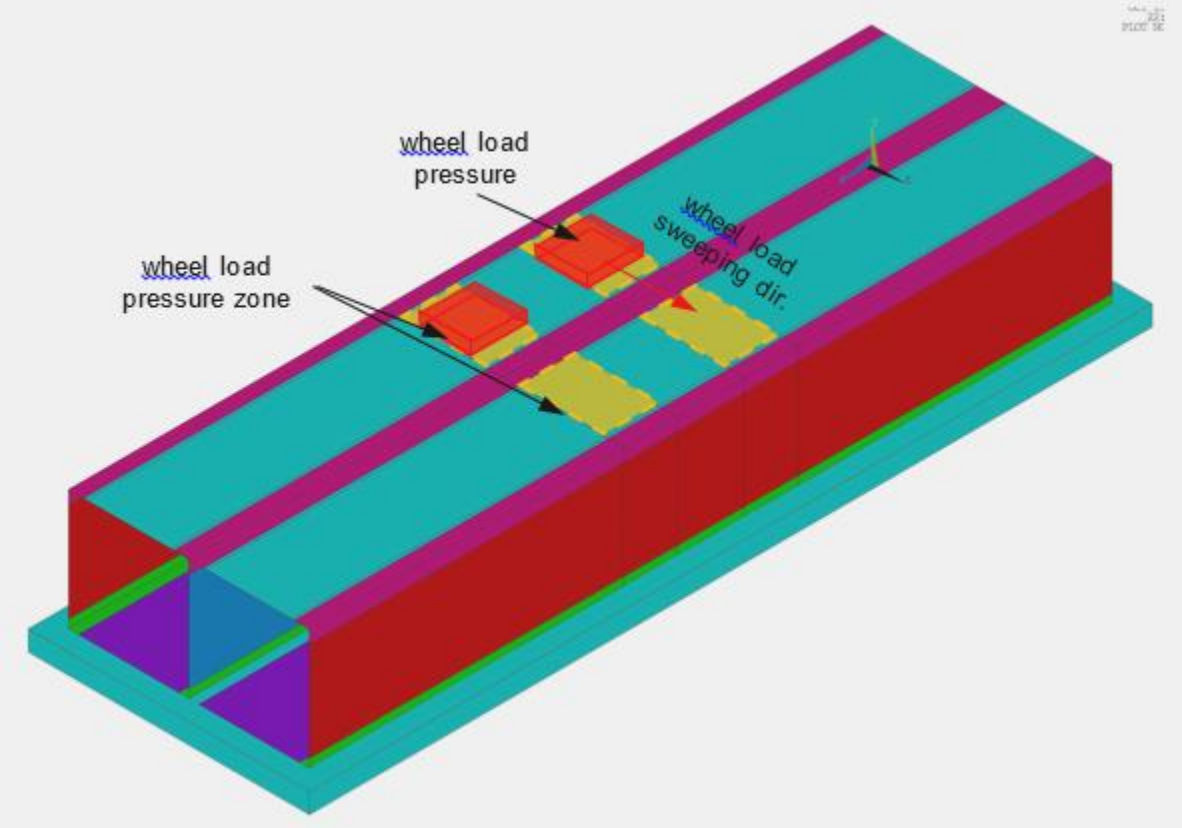

Figure 12. Wheel load pressure on top slab (case of wide culvert and tandem axle)

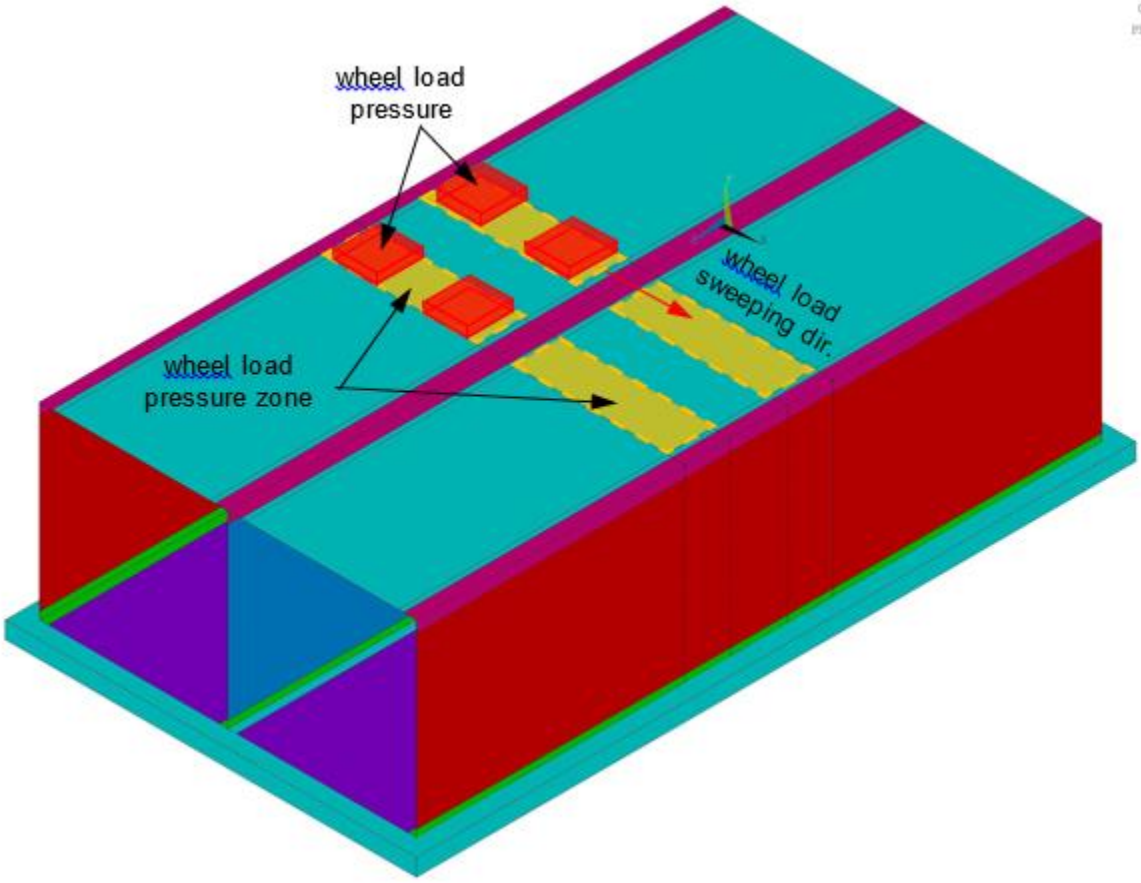

Details of 2D models

As stated earlier, engineers typically analyze culverts using 2D models for design and load rating. 2D models are easier to build and provide quick, direct answers to the user, unlike 3D models, which require advanced knowledge of the finite element method and a significant amount of post processing. By definition, 2D models do not represent the third dimension and are therefore considered an approximation of the exact behavior. The main source of approximation is the extent of the culvert transversely (perpendicular to traffic) that contributes to the resistance of the axle loads (see Figure 4-c). Hence, the goal of this study is to develop expressions for the equivalent width formula that provides acceptable accuracy over a wide range of culvert configurations and straining actions.

The 2D model in this study was built using BEAM188 element from the ANSYS element library. BEAM188 is based on Timoshenko's beam theory, which is suitable for slender to moderately thick beams. With three translation DOFs in the x, y, and z directions at each of

its two nodes, BEAM188 is capable of representing flexure, shear, and axial behavior. Figure 13 shows the geometric attributes of BEAM188. The element allows for the defining standard as well as general cross-sectional properties, including the orientation of the cross section in relation to the longitudinal axis of the element.

Figure 13. Beam element BEAM188 used to model culverts in 2D [28]

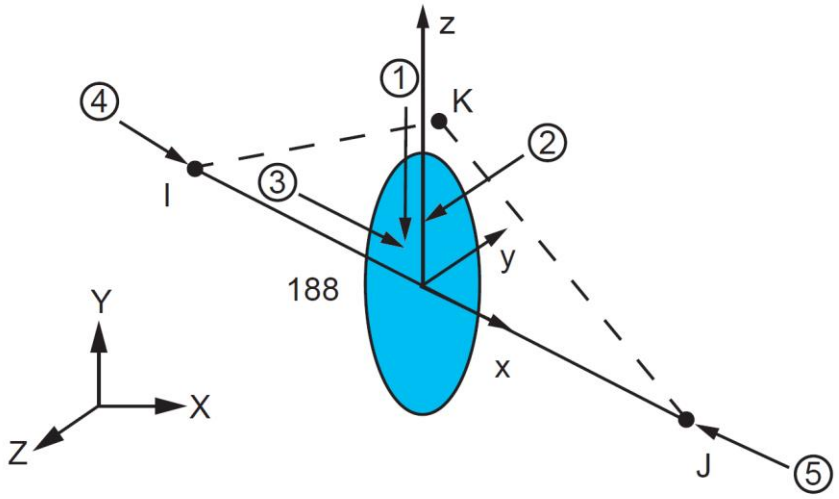

Error! Reference source not found. shows one of the 2D models for the case of a 3-barrel c ulvert (S =12 ft.). In **Error! Reference source not found.**-a, the boundary conditions of the model are shown, including the hinge condition at the outside corners of the top slab, to reflect the lack of negative moment reinforcement. It should be noted that out-of-plane boundary conditions have been added to the model to ensure stability, but these are not shown in the figure. **Error! Reference source not found.**-b shows the deformed shape of the m odel for the case of two axles of a design truck passing over the culvert– one axle on the first barrel and the other on the second barrel.

Figure 14. Two-dimensional (2D) model of a 3-barrel culvert with one axle load

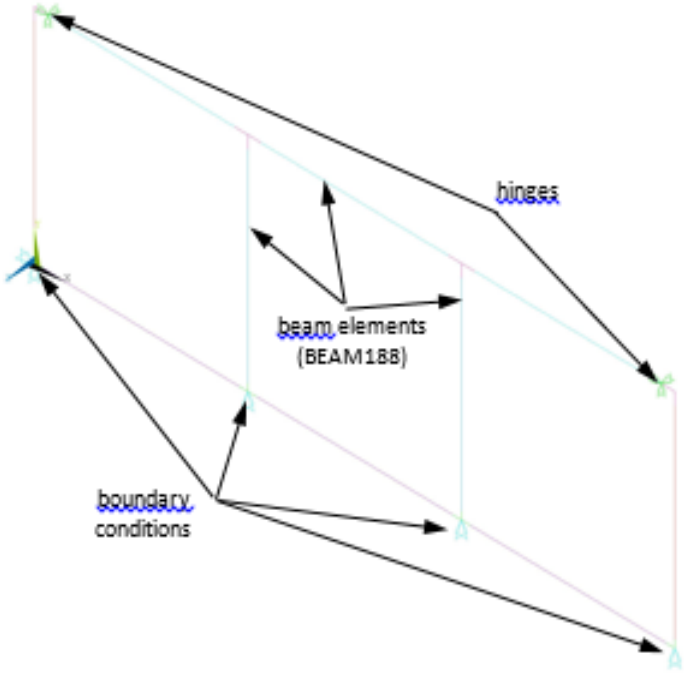

(a) boundary conditions

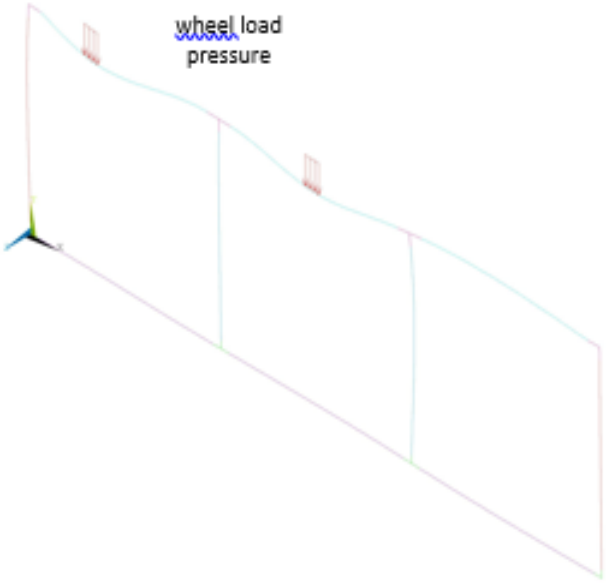

(b) deformed shape for a design truck case (two axles)

Extraction of Results

Extracting the results is a major step in the analysis process. Identifying critical sections in 3D models is not always straightforward, as maximum effect has to be explored in two directions, longitudinally and transversely. Special scripts were written for this purpose, where straining actions (shear force and bending moment) were explored in a strip width nominally equal to 1 ft. until the maximum live load shear force and the maximum live load bending moment were found. Once this nominal strip was identified, the straining actions due to other load cases (self-weight, earth fill, and wearing surface) were also recorded for the same strip for the purpose of conducting the reliability study discussed later. It should be noted that for the shear forces and negative moments, the search for the critical strip was only done transversally since the maximum values of these straining actions happen at the face of the interior supports.

Figure 15 shows the straining actions considered in this study. As stated earlier, the exact location of the critical strips for these straining actions vary based on the truck type, position, and number of axles. The extracted results are:

V_L = shear force left of 1st interior wall

V_R = shear force right of 1st interior wall

M_{pE} = positive moment around 1st exterior midspan

M_{nL} = negative moment left of 1st interior wall

M_{nR} = negative moment right of 1st interior wall

M_{pI} = positive moment around 1st interior midspan

Figure 15. Straining actions extracted in this study

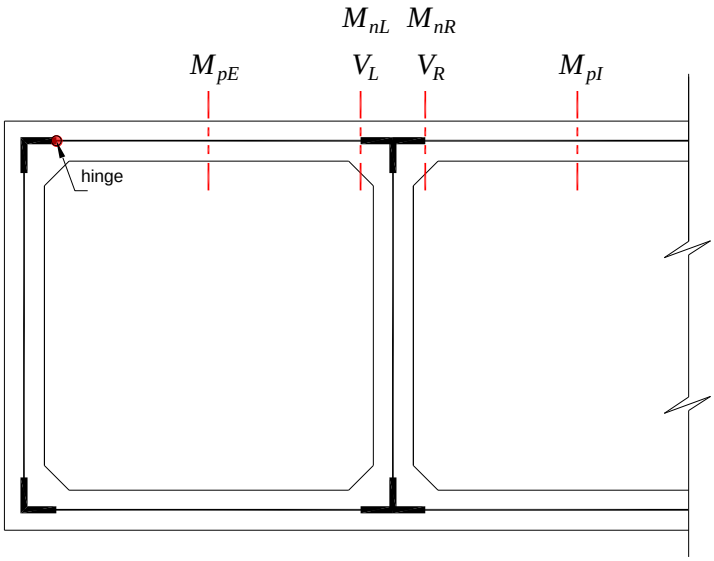

Mesh sensitivity study

As an approximate analysis method, the accuracy of FEM results is a function of several factors, including the mesh size. In addition to the possibility of missing critical stress locations if a coarse mesh size is used, the FEM approximation of the displacement field may also diverge further from the exact one. Therefore, choosing an appropriate mesh size is one of the important factors that need to be investigated before settling on a model. Typically, a mesh sensitivity study is conducted in which the element size is varied, and extracted results are compared. An acceptable mesh size is one where a mesh with smaller element sizes does not provide additional accuracy to the results (i.e., results have converged to the exact answer).

In this study, a single barrel case was investigated using five target element sizes: 2 in., 3 in., 4 in., 5 in., and 6 in. The models can be seen in Figure 16.

Figure 16. FE meshes used in sensitivity study (1-barrel case, *S*=10 ft., *FH*=0 ft. – (a) 6 in., (b) 5 in., (c) 4 in., (d) 3 I, (e) 2 in.)

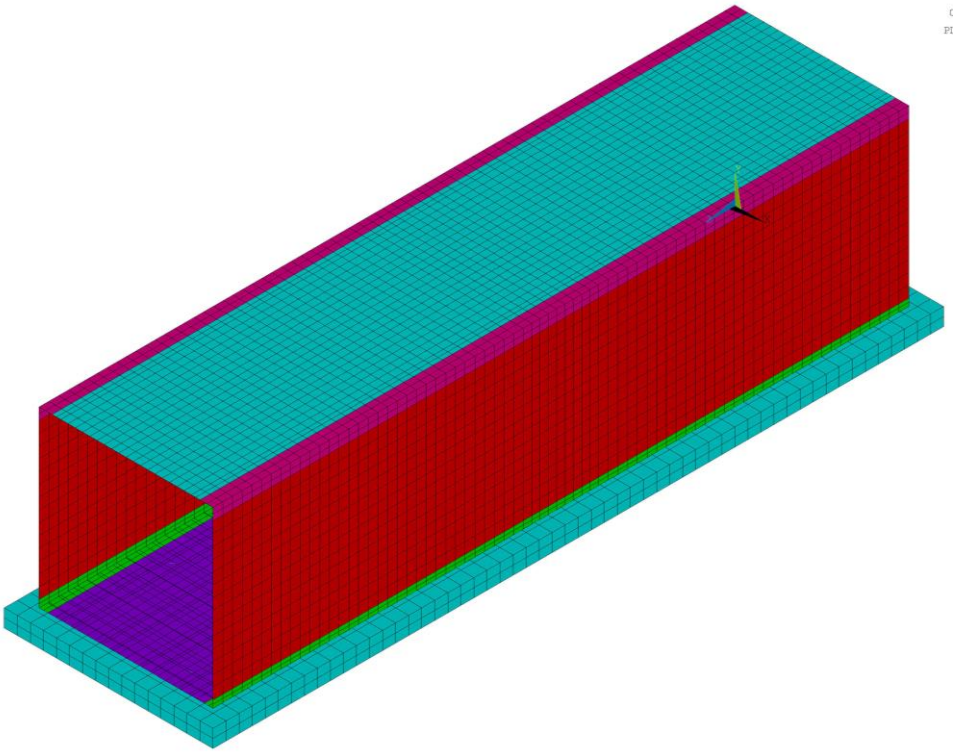

(a)

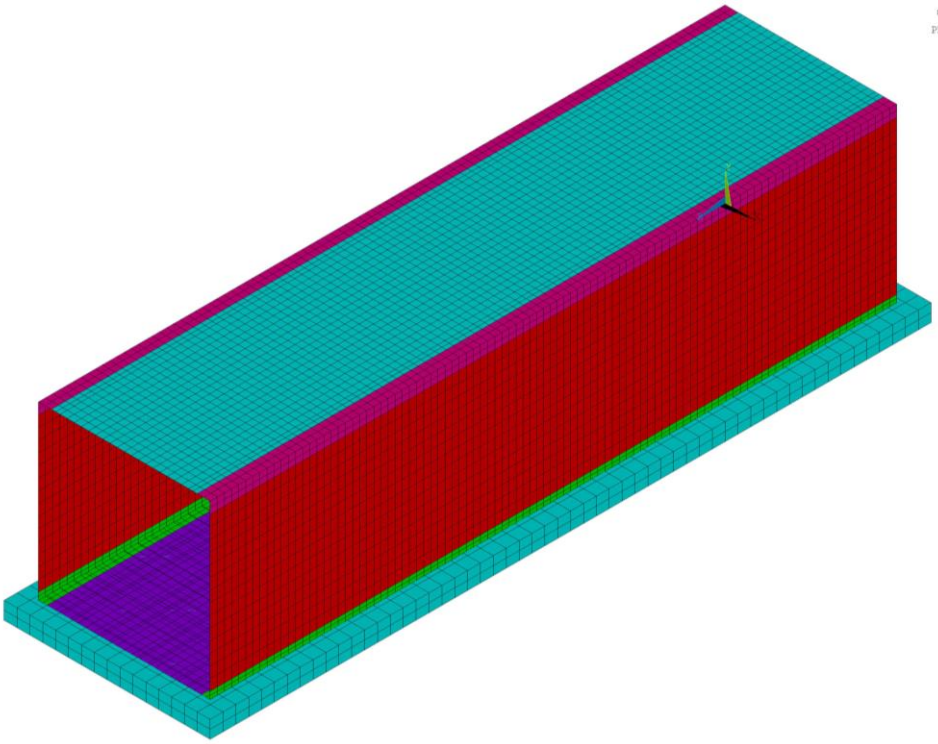

(b)

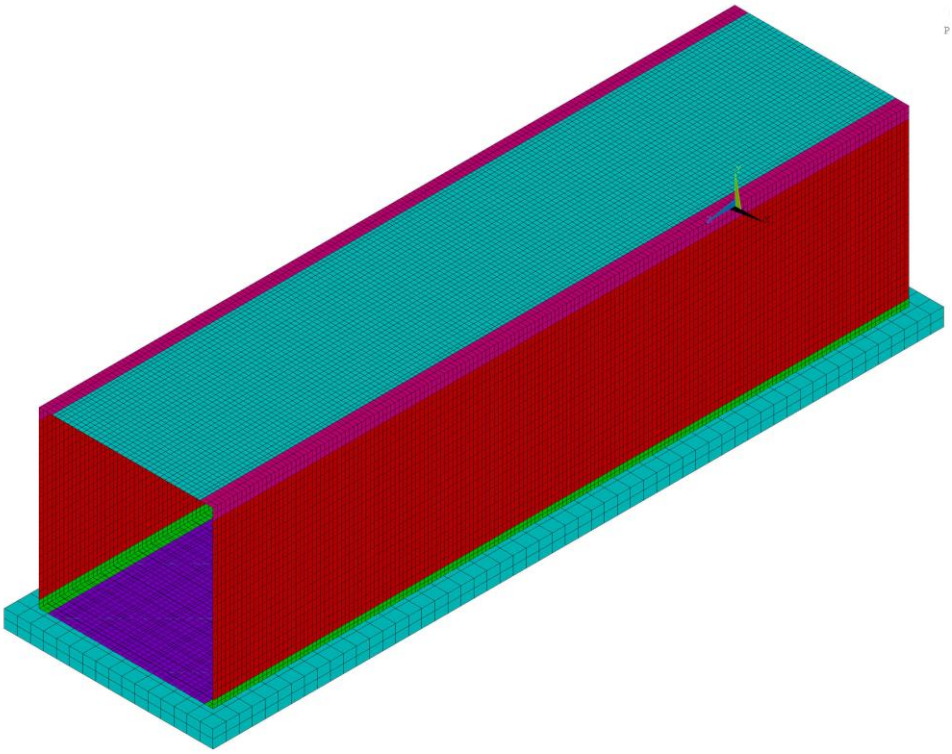

(c)

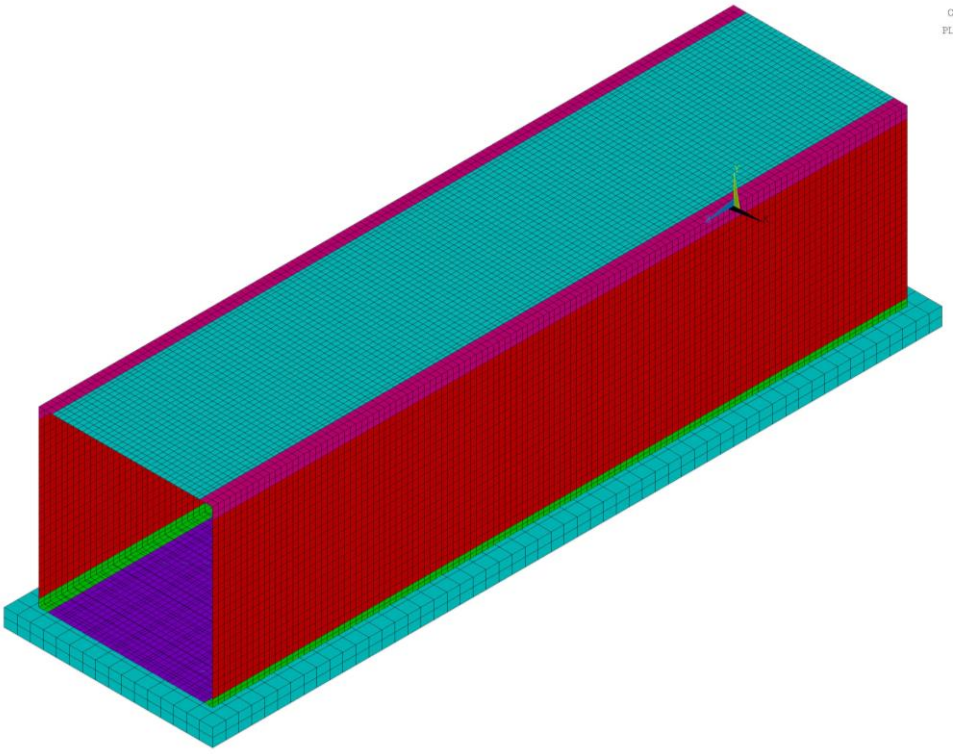

(d)

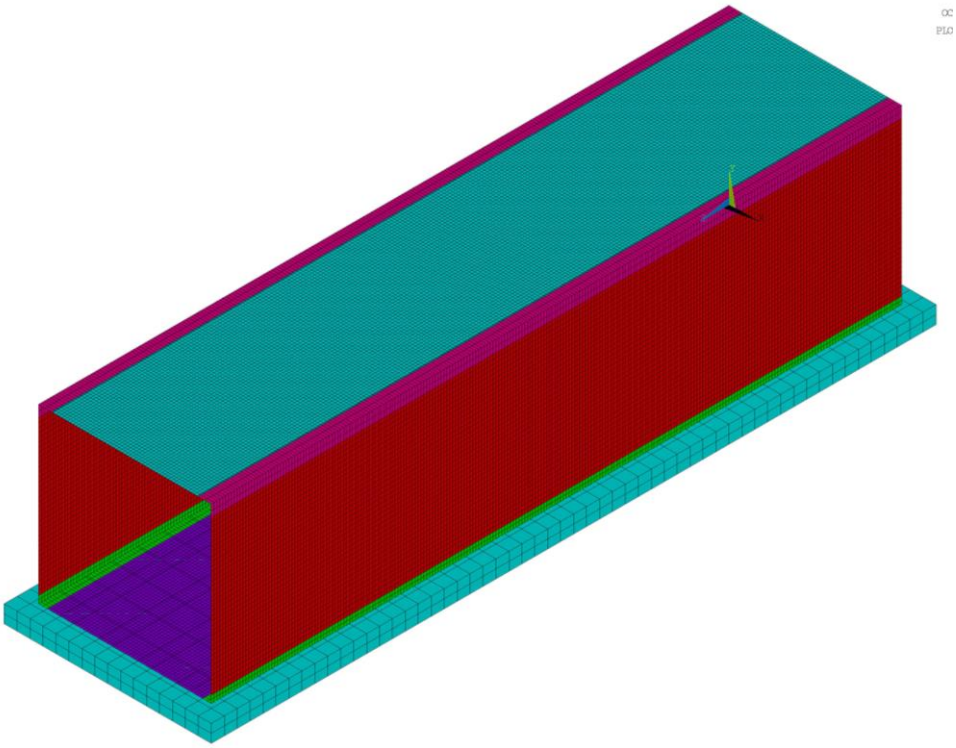

(e)

The maximum live load positive moment in the top slab was extracted from all these models and compared with the moment values from the smallest element size model, i.e., 2 in. It can be seen that a 6 in. model would introduce a mesh size accuracy error of about 3.5%. This mesh size accuracy error drops as the element size is reduced. The table also shows that a nominal element size of 3 in. is extremely close to that of a 2 in. element size model with a difference of about 0.3%. This means that the solution has almost converged. Therefore, it was deemed acceptable to use the 3 in. element size for all models in this study, especially since the number of elements, nodes, and degrees of freedom increases exponentially rather than linearly as the element size is reduced. Finally, this element size allows for averaging the results from four elements or five nodes when extracting the straining action results per foot, which is a good number of data points to obtain representative results.

Table 1. Sensitivity study results

Mesh Size	6 in.	5 in.	4 in.	**3 in.**	2 in.
M_{pE}^{LL} (lb.in./in.)	5463.5	5437.2	5323.5	**5295.3**	5277.8
$M_{pE}^{LL}/M_{pE-2\text{in.}}^{LL}$	1.035	1.030	1.009	**1.003**	1.000

Parametric Study

Four parameters were considered in developing a suite of culverts that covers a wide range of configurations representing the current inventory. These parameters are:

- Concrete Compressive Strength, f_c' – It is known that the concrete elastic modulus (E_c) is directly related to its compressive strength. Therefore, it is clear that f_c' is directly related to the stiffness of the culvert's structural elements, which will be investigated to study its effect of the results.
- Number of Barrels, NB – The straining actions (shear forces and bending moments) developing in box culverts vary based on the number of barrels, especially for the DOTD standard detail with the hinged behavior at the outside corners. For example, the top slab behaves almost like a simply supported beam in a 1-barrel configuration. For 2- and 3-barrel configurations, the top slab is a continuous one on at least one side, which affects how the straining actions are distributed.
- Top Slab Thickness, t_s – The other parameter that affects a structural member's stiffness is its dimension. Even though DOTD standard culvert details call for specific slab and wall thicknesses, (t_s) was varied as one of the parameters in this study. Wall thicknesses (t_w) were taken equal to the standard detail values. Varying t_w and t_s at the same time would not cause the intended effect of varying the relative stiffness of the culvert's members.
- Fill Height, FH – The depth of the fill height (FH) determines the extent of the area affected by the wheel load pressure. Therefore, FH is considered in this study.
- Culvert Barrel Span Length, S – The literature shows that the width of the top slab affected by wheel loads is affected by the ratio of the distance from the wheel load to the closest support (a) and to the barrel span length (S). As discussed earlier, the axle position will be swept over the culvert, i.e., a is varied. Therefore, considering S as one of the parameters is necessary. Furthermore, the barrel span length also determines how many axles are on one or two barrels.

Based on this information, a range was identified for each of the aforementioned parameters. Table 2 lists the range of parameters considered in this study, which includes three f_c' values, three t_s values, three FH values, and seven S values. This translates to 3 × 3 × 3 × 7 = 189 cases for each number of barrel configuration. Initially, the 1-barrel culvert case was analyzed to study the effect of each of the parameters. Later, the number of cases for the 2- and 3-barrel culvert configurations are further discussed. The culverts included in the parametric study were designated based on the parameter values for each case. For example, B2W8H8ST8WT8H2C4 is a case with 2 barrels (2B), an 8 ft. barrel width (W), an 8 ft.

barrel height (H), an 8 in. slab thickness (ST), an 8 in. wall thickness (WT), a 1 ft. fill height (H), and a 4000 psi concrete compressive strength (FC). Table D1, Table D2, and Table D3 list all the cases considered in this study.

Table 2. Range of parameters considered in this study

Parameter	Range
Concrete Compressive Strength f_c' (psi)	3,000; 4,000; 5,000
Number of Barrels, NB	1; 2; 3
Top Slab Thickness, t_s (in.)	$t_s^{\text{standard}} - 1$; t_s^{standard}; $t_s^{\text{standard}} + 1$
Fill Height, FH (ft.)	0; 1; 2
Culvert Barrel Span Length, S (ft.)	6; 7; 8; 9; 10; 11; 12

Reliability Assessment

Analysis models can only be implemented in design code provisions after conducting a thorough reliability investigation to ensure that they conform to acceptable AASHTO-LRFD safety levels. This reliability study is essential to overcome implementation barriers by conducting a comprehensive study that builds on the current provisions and is informed by historical provisions. This ensures that any proposed provisions provide adequate safety levels. Safety levels are typically presented in the form of a reliability index (β) that can be easily translated into a probability of failure (P_f) or probability of exceeding a certain design criterion according to the following equation:

$$P_f = \Phi(-\beta) \quad [4]$$

In this study, the focus will be on the *Strength I* limit state that typically controls the design and load rating of CIP-RC box culverts. Established procedures were based on principles of structural reliability similar to those used in the calibration of AASHTO's bridge design specifications [36], specifications for horizontally curved steel girder bridges [37] , and the LRFR bridge evaluation manual [38; 39]. These procedures were successfully used by the PI for the calibration of shear strengthening using FRP provisions through NCHRP Project 12-75 [40]. Figure 17 shows the overall process of the reliability analysis.

Figure 17. Overall process of the reliability analysis

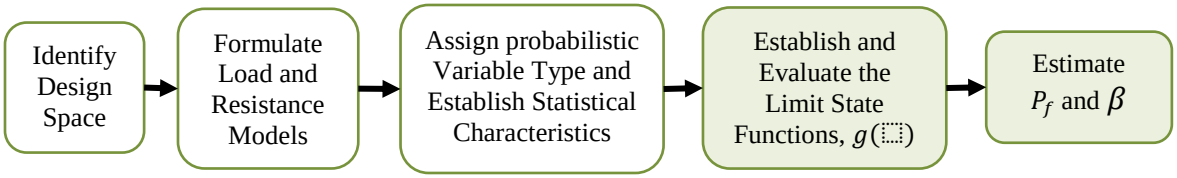

The basic form of the limit state function (g) for reliability analysis is:

$$g = R - Q \geq 0 \quad [5]$$

At the member level, R is the uncertain structural resistance and Q is the random load effects. The uncertain structural resistance (R) can be expressed as a function of the nominal resistance as obtained from the proposed design equations or analysis models (R_n) and the uncertainties stemming from material properties (M), fabrication (F), and a professional factor of design or analysis model (P). In addition to the randomness in load effects, as well as the uncertainties due to the use of approximate live load distribution equations, the derivation of resistance factors considered these three sources of uncertainty in the resistance models described below.

The limit state function for strength design at the member level, $g_{member}()$ reflect the aforementioned random variables on both the resistance and load sides of the design equation, including Q_{DC}, Q_{DW}, Q_{LL+IM}, and ξ_{LLDF} that represent the load demands due to component dead loads, wearing surface, live plus impact, and the accuracy of AASHTO live load distribution factor formulas, respectively.

Each bridge within the selected design space was evaluated for each design limit state. The probability of failure expressed by the reliability index (β) was determined (see Figure 18-a for the relationship between β and the probability of failure (P_f)). The First Order Reliability Method (FORM) was used in this study to find the design point, which is defined as the closest point on the failure surface ($g = 0$) to the origin of the standard forms domain of the random variables (see Figure 18-b). The reliability index (β) is then calculated in FORM in the standard form ($Z_i = (X_i - \mu_X)/\sigma_X$) domain where, μ_X and σ_X are the mean and standard deviation for each random variable (X_i) in its original domain. β values estimated using this procedure will be compared to pre-determined target reliability level (β_T), which is typically equal to 3.5 for calibrating strength limit states. For comparison purposes, β values resulting from existing provisions in AASHTO-LRFD BDS [5] were also considered. If the evaluated β did not meet β_T for a given limit state, the live load distribution formula was adjusted. The

culvert cases used in the parametric study discussed earlier will be used as the design space for the reliability study.

Figure 18. Reliability index, β, for limit state function $g(\ \ )$

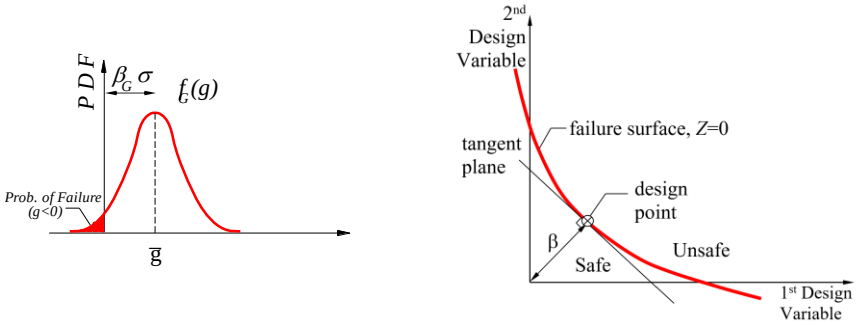

(a) PDF of limit state function, $g(\ \ )$ (b) Determining β using FORM

Resistance Models

The resistance models used in this study were flexure and shear resistance, which are well established in the literature. For example, the shear resistance of the top slab was only due to the concrete contribution (V_c), which, according to AASHTO-LRFD BDS, is given by the following equation:

$$V_c = 0.0316\beta_v\sqrt{f_c'}b_v d_v \qquad [6]$$

Where, b_v and d_v are the web width and effective depth of the cross section; f_c' is the concrete compressive strength; and β_v is a factor taken equal to 2.0 for non-prestressed members, with a depth less than 16.0 in. according to AASHTO-LRFD BDS 5.7.3.4.1. No stirrups are typically provided in slabs; therefore, no shear reinforcement contribution was considered. The following sections present the variabilities used in the current study. For each parameter treated as a random variable, a bias, coefficient of variation, and distribution type are given. For any random variable (X), the bias (λ_X) is defined as the ratio between of the mean value (μ_X) of the parameter it represents to its nominal value (X_n). The coefficient of variation ($COV(X)$) is the ratio between the standard deviation (σ_X) and the mean value (μ_X).

$$\lambda_X = \frac{\mu_X}{X_n} \quad [7]$$

$$COV(X) = \frac{\sigma_X}{\mu_X} \quad [8]$$

As seen from Equation [6], resistance models typically involve several parameters for which statistical parameters are needed. Concrete material statistical parameters have been derived in earlier studies using large datasets. Therefore, in this project, existing information was utilized. As an example, Nowak and Szersen [41] proposed an equation for the bias factor of concrete compressive strength ($\lambda_{f_c'}$) as a function of the nominal concrete compressive strength (f_c') and a COV equal to 10%. A literature review was performed to determine the statistical parameters and distribution types of all the material random variables. The fabrication factor (F) accounts for uncertainties in measured dimensions and other fabrication related parameters. A review of the literature indicates the information provided in Table 3 regarding certain fabrication related random variables.

Table 3. Material and fabrication random variables parameters [41-43]

Variable	Bias, λ	COV, %	Distribution Type
Concrete strength, f_c'	varies	10.0	Normal or lognormal
Dimensions (h, d, b)	1.00 – 1.03	0.5 – 7.0	Normal
Area of reinforcement	1.00	0.0 – 4.0	Normal

The professional factor accounts for the uncertainty in the prediction model. Determining this factor typically involves the compilation of a database of test results conducted on specimens failing with the desired mode of failure. Using the predicted ($Q_{pred.}$) and experimentally obtained resistance ($Q_{exp.}$), the bias ($\lambda_p = \mu(Q_{exp.}/Q_{pred.})$) and the coefficient of variation ($COV_p = \sigma(Q_{exp.}/Q_{pred.})/\mu(Q_{exp.}/Q_{pred.})$) for the professional factor will be determined. The modes of failure considered in this study were fundamental (flexure and shear), and can therefore be found in the literature. The aforementioned factors translate to the following biases and coefficients of variation for reinforced concrete members [36].

Table 4. Material and fabrication random variables parameters [36]

Variable	Material & Fabrication, MF		Professional Factor, P		Resistance Model, R	
	Bias, λ	COV (%)	Bias, λ	COV (%)	Bias, λ	COV (%)
Flexure, M	1.120	0.120	1.020	0.060	1.140	0.130
Shear, V	1.165	0.135	1.200	0.100	1.400	0.170

Load Models

The load, or demand, side (Q) of any limit state function is also represented as a random variable. Load models are typically determined based on field studies to determine the statistical characteristics of applied loads. Dead loads due to structural components (DC), wearing surface (DW), and highway truck loads (LL) can be easily found in the literature [44], which are listed in Table 5. In this study, the applicable load models from the literature was used. These include the dead loads, DC and DW. It should be noted that the live load model listed in Table 5 is for bridge girder design; in other words, it represents the statistics of the gross vehicle weight of highway trucks, which encompasses all axles of the trucks traveling over bridges. This information is determined by analyzing Weigh-In-Motion (WIM) data from several stations. Culvert design is controlled by one or two axles of a single truck. Therefore, another live load model is needed for the reliability analysis of culvert design.

Table 5. Bias and COV for load effects [45-48]

Variables	Statistical properties			Reference
	Bias λ	Coefficient of Variation CV	PDF	
Deck Dead Load	1.05	0.10	Normal	[45; 46]
Soil Self Weight	1.00	0.03	Normal	[47; 48]
Wearing Surface	1.00	0.25	Normal	[45; 46]
Live Load	Varies	Varies	Extreme Type I	[49]; current study

LTRC Project 07-2P characterized and developed truck load spectra and growth factors for current and future pavement design practices in Louisiana [49]. The truck load spectra was used to determine the statistical load model for individual truck axles representative of Louisiana highway truck traffic. LTRC Report 445 [49] provides histograms of the truck axles with different configurations and truck traffic classifications (TTC). For the purpose of the current study, the focus was on TTC 1 truck classification, which is for a major single-trailer route that is typically associated with principal arteries (e.g., interstate, defense, freeways, and expressways). Within this truck classification, two axle configurations were considered: a single axle and a tandem axle. Figure 19 and Figure 20 show the axle load spectra for the two axle configurations considered in this study.

Figure 19. Single axle load spectrum for combined vehicle classes for TTC 1 [49]

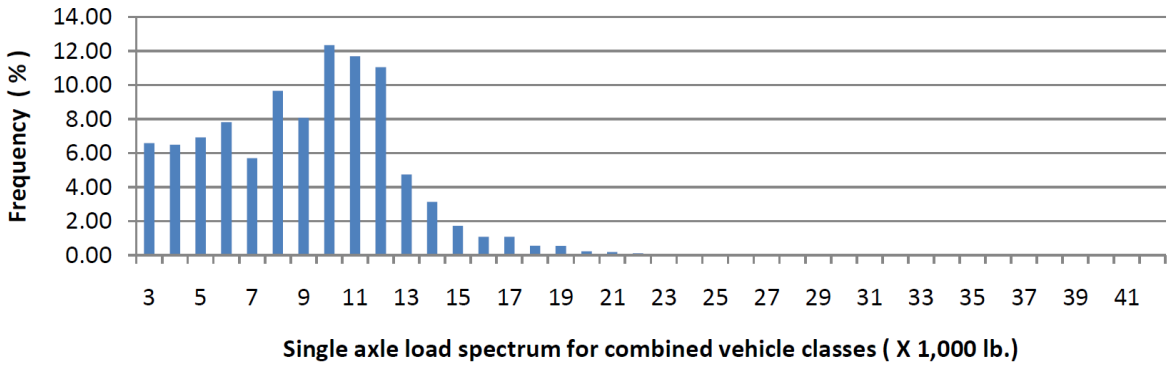

Figure 20. Tandem axle load spectrum for combined vehicle classes for TTC 1 [49]

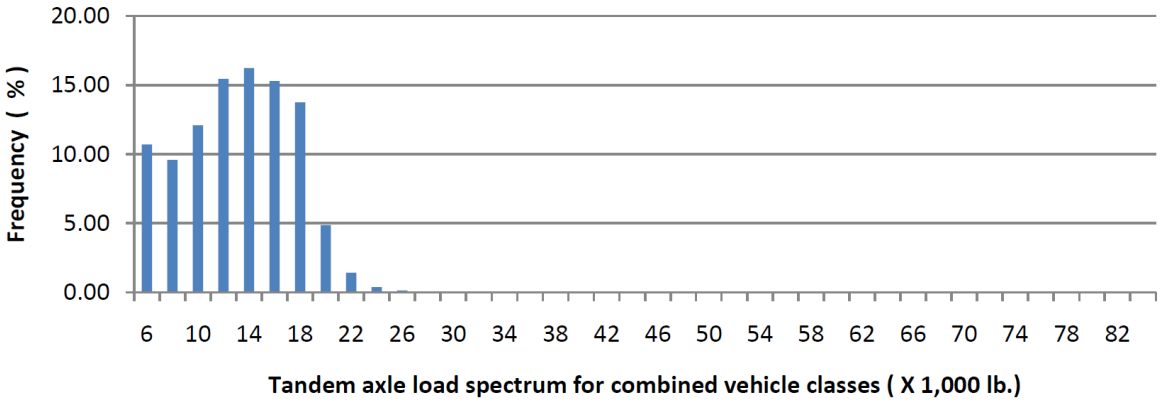

These spectra were analyzed statistically to determine the most suitable distribution type to establish an appropriate load model for culverts. Figure 21-a shows the histogram for the case of TTC 1 single axle load spectrum, which is fitted using a bimodal distribution selected as a mixture of two normal (Gaussian) distributions. It should be noted that distribution had to be scaled to maintain a 100% probability if all axle loads were considered, due to the truncations to eliminate lower axle loads in the WIM data. Figure 21-b shows a comparison between the selected bimodal distribution and a fitted normal distribution. It can be seen that the normal distribution is not a reasonable fit for the histogram data. This observation was confirmed via a Chi-square statistical test that showed that the bimodal distribution is acceptable for a 5% significance level [50]. Figure 22-a and 22-b show the same results for the TTC 1 tandem axle load spectrum.

Figure 21. Selected bimodal distribution for single axle load spectrum for combined vehicle classes for TTC 1

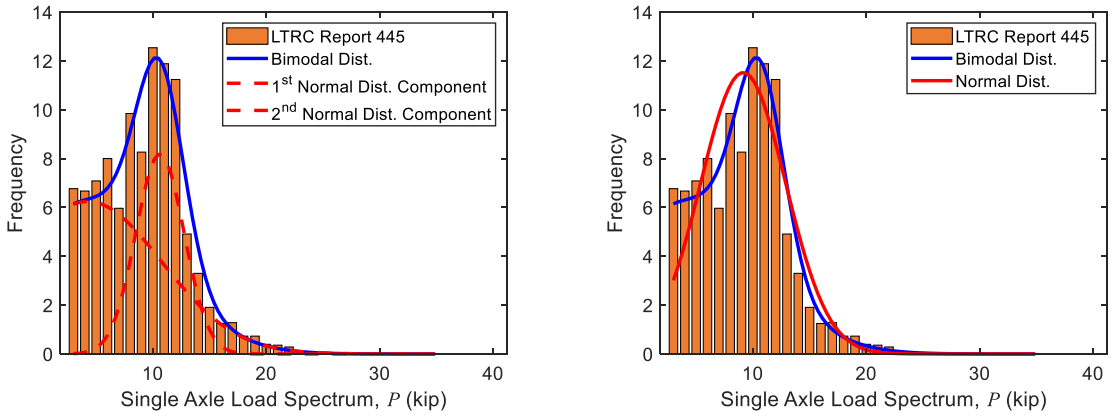

(a) (b)

Figure 22. Selected bimodal distribution for tandem axle load spectrum for combined vehicle classes for TTC 1

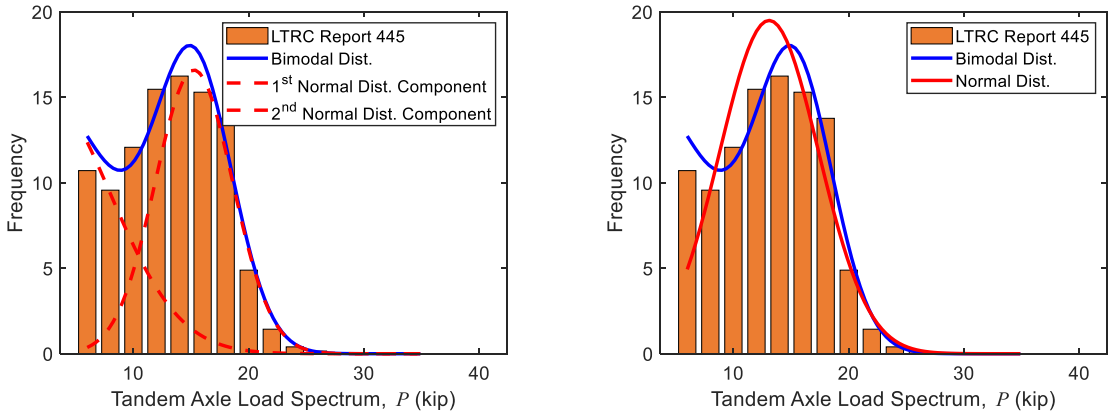

(a) (b)

It should be noted that the WIM data was collected over a limited time period of three years, between 2004 and 2006. AASHTO-LRFD BDS targets a 75-year design life. Therefore, the established statistical characteristics for the WIM monitoring period were extrapolated over a 75-year design period according to the Extreme Value Theory (EVT), which is used to quantify tail behavior of an independent continuous random variable. For this study, extreme values are the largest observations sampled with size n from a population. According to EVT, the probability distribution of the largest extreme value (M_n) extracted from the sample has a limiting distribution that converges the Generalized Extreme Value ($G(x)$) distribution:

$$\lim_{n\to\infty} Pr\left(\frac{M_n - a_n}{b_n} < x\right) \to G(x) \quad [9]$$

Where, a_n and b_n are normalizing constants [51; 52]. The Generalized Extreme Value distribution is a distribution family that has three forms: Type I (Gumbel), Type II (Frechet), and Type III (Weibull). Three parameters characterize the Generalized Extreme Value distribution, namely a location parameter (u), a scale parameter (α), and a shape parameter (ξ), as given in Equation [10]. As explained later, the cumulative distribution function (CDF) for Type I distribution (i.e., Gumbel distribution, with $\xi = 0$) is of interest in this study.

$$G_X(x) = exp\left(-\left[1 + \xi\left(\frac{x-\mu}{\alpha}\right)\right]^{-\frac{1}{\xi}}\right) \quad [10]$$

The cumulative distribution function of the extrapolated extreme value of axle loads for 75-year return period is expressed by:

$$F_X^{75\ yrs}(x) = \left[F_X^{3\ yrs}(x)\right]^N \quad [11]$$

$$= \exp(-\exp(-\frac{x-u_n}{\alpha_n}))$$

Where, α_n is the scale parameter and u_n is the location parameter of 75-year extrapolated extreme axle loads. For a Gumbel distribution, the scale parameter over a 75-year return period remains the same. However, the location parameter can be estimated as:

$$u_n = u + \alpha \text{ Ln } N \quad [12]$$

Where, N is the number of expected extreme events in a 75-year return period. The mean maximum value of the extrapolated data (μ_L) and standard deviation of mean maximum value (σ_L) can be determined using the following equations [51].

$$\mu_L = u_n + \gamma\ \alpha_n \quad [13]$$

$$\sigma_L = \frac{\pi}{\sqrt{6}}\alpha_n \quad [14]$$

Reliability Evaluation

Based on the aforementioned resistance and load statistical models, a reliability study was conducted for the shear and flexure strength limit states. Using the statistical characteristics for the sources of uncertainties described earlier (professional factor, P; material variabilities, M; fabrication tolerances, F) on the resistance side, as well as the uncertainties associated with dead and live loads published in the literature, and in addition to the uncertainties inherent in the live load distribution equation, it is possible to establish a limit state function for calculating the reliability index (β). The limit state function for strength design (*Strength I* limit state– $g_{Str.\ I}$) is given in Equation [15] and reflects the aforementioned random variables on both the resistance and load sides of the design equation.

$$g_{Str.\ I} = R_R - (Q_{DC} + Q_{EF} + Q_{DW} + \xi_{LLDF}Q_{LL+IM}) \quad [15]$$

Where, R_R is the random variable representing the resistance, and Q_{DC}, Q_{EF}, Q_{DW}, and Q_{LL+IM} are the random variables representing the load demands due to component dead loads, earth fill, wearing surface dead loads, and live load plus impact, respectively. The random variable (ξ_{LLDF}) was also included to account for the uncertainties introduced due to

the use of empirical live load distribution formulas that are typically used in design. Its bias ($\lambda_{\xi_{LLDF}}$) is taken from the results of the parametric study discussed earlier. The reliability index was evaluated using Theory of Reliability to obtain a reliability index (β) for each culvert design in the design space. Table 3 and Table 5 list the bias and coefficient of variation for load effects used in the study.

Discussion of Results

In this section, results obtained from the finite element analyses of a parametric study are presented. The parameters considered in the study are first discussed. Results from 3D and 2D models for each culvert and comparisons of both sets of results are investigated. Finally, a live load distribution formula is developed based on all the results obtained from the parametric study.

Investigation of Parameter Effects on 2D Model Accuracy

All results from the analyses performed in this study can be found in Appendix B (Table E1 through Table E12). The effect of each of the considered parameters are first analyzed in this section. To investigate the effect of each of the parameters described in the previous section, the 1-barrel case is considered. (Table E1, Table E4, Table E7, and Table E10). The live load distribution formula is adopted in AASHTO-LRFD BDS [5] in which the wheel load is distributed in two directions. In the direction parallel to the span, the axle load is distributed over a width on the top slab (E_{span}) equal to:

$$E_{span} = L_T + LLDF(H) \quad [16]$$

Where, L_T is the length of the tire contact area (10 in.), $LLDF$ is the live load distribution factor taken as 1.15, and H is the fill depth. In the direction perpendicular to the span, the width of the wheel pressure area (E) is:

$$E = 96 + 1.44\,S \quad [17]$$

Where, S is the barrel's clear span length in feet; however, the result is in inches.

The results will be presented in the form of a ratio between the 2D and 3D straining actions. This ratio is often referred to as *bias* (λ):

$$\lambda = \frac{R_n^{2D}}{R_n^{3D}} \quad [18]$$

Where, R_n^{2D} and R_n^{3D} are the straining actions extracted from the 2D and 3D models, respectively. The effect of each parameter was investigated separately by plotting the average

bias value (λ_{avg}) and coefficient of variation (COV) as an indication of the scatter of the ability of Equation [17] to predict the culvert response accurately. First, these results are presented in the form of histograms that show the distribution of λ. The variation of λ_{avg} with respect to key parameters are then be plotted to identify any trends to help assess existing live load distribution formulas and develop a new formula. Similar plots are also presented for the coefficient of variation (COV) for each straining action.

Effect of Barrel Span Length, S

Figure 23 shows the histograms of the bias (λ) for all straining actions extracted from the models analyzed in this study. The histograms are classified based on the barrel span length (S), for which seven values were considered in the parametric study. Each of the histograms show a vertical dashed line, which is the average of all bias values for each group of cases. It is clear that all bias values have an increasing trend from lower to higher S values, albeit more pronounced for positive moment biases than shear and negative moment biases. This is expected, as the wheel area distribution width is known to be larger for positive moments where the critical load case is typically when the wheel is close to midspan, as opposed to the other cases where the critical load case is controlled by wheel load positions close to the supporting walls, especially for shear cases. The proximity of the wheel load to the wall does not allow the top slab to distribute wheel pressure effectively. In other words, even though Equation [17] is a function of the span length (S), it seems it does not reflect the full ability of the top slab to distribute wheel load pressure.

The trends of the biases and the COV are shown in detail in Figure 24 through Figure 27. Figure 25-a and Figure 27-a show a clear increasing trend ($\lambda \gg 1.0$) that is conservative by at about 40% as a minimum. The conservatism in the exterior barrel positive moment reaches almost 80% ($\lambda \approx 1.80$), while only 55% ($\lambda \approx 1.55$) was observed for the interior barrel positive moment. This is due to the continuity of the interior barrel on both ends, which stiffens the top slab more than in the case of the exterior barrel, and hence reduces its ability to distribute wheel loads farther. For critical shear forces bias (λ_V), Figure 24-a also shows an increasing trend; however, the bias values are unconservative ($\lambda < 1.0$). This implies that even with the conservatism injected in positive moment biases, the shear forces are not as would be expected. As a result, developing one distribution formula that fits both shear forces and positive bending moments will be challenging. The same can be observed in Figure 26-a for the negative moment bias (λ_{M_n}), which increased for larger spans as a result of the ability to fit a second axle that is positioned closer to midspan, thus providing the slab with more room to distribute the wheel load pressure.

The COV shown in the figures reflect a range of 15%-25% for shear force bias ($COV(V)$), 8%–11% for exterior barrel positive moment bias ($COV(M_{pE})$), 4%–9% for negative moment bias ($COV(M_n)$), and 13%-18% for interior barrel positive moment bias ($COV(M_{pI})$).

Figure 23. Histogram of straining action bias for different barrel span lengths

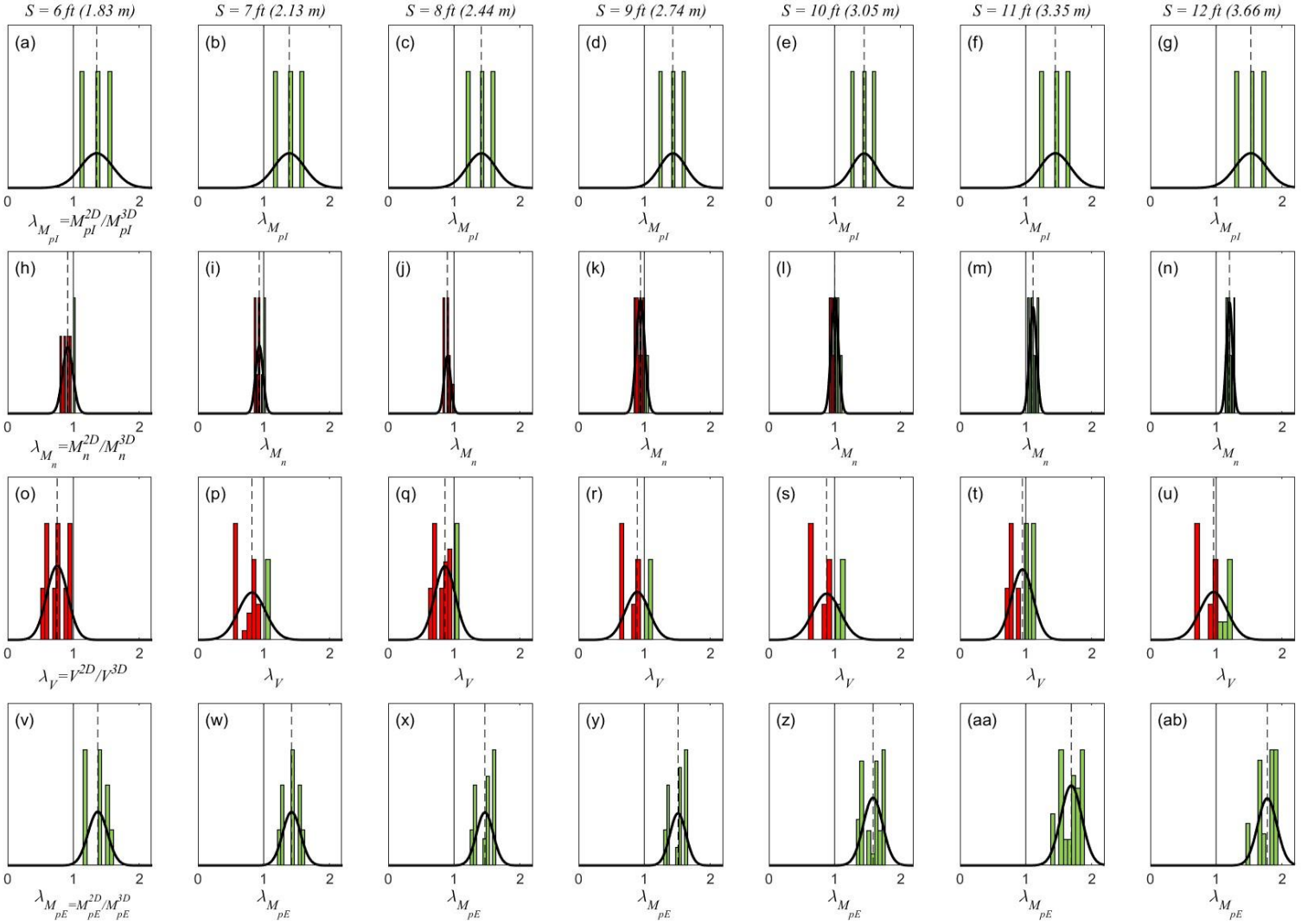

Figure 24. Trend of shear bias $\lambda_{V,avg}$ and COV vs. barrel span length, S

(a)

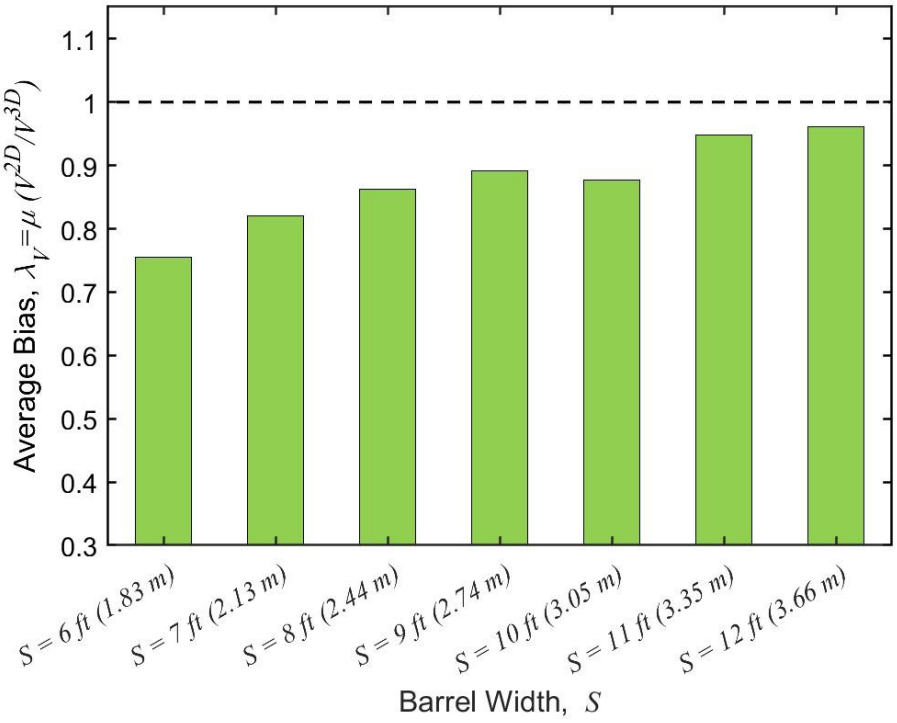

(b)

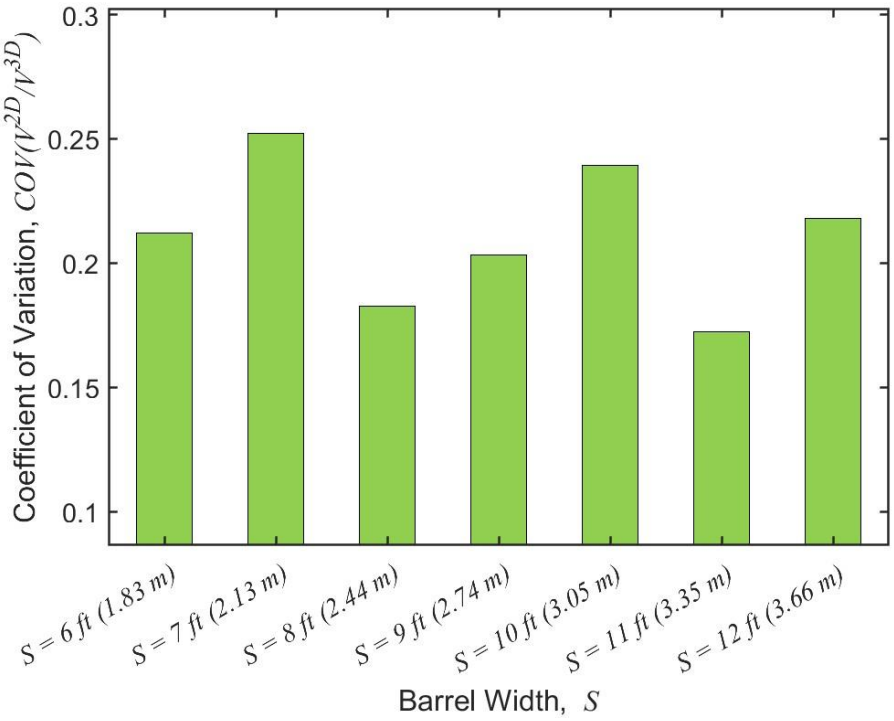

Figure 25. Trend of exterior positive moment bias $\lambda_{MpE,avg}$ and COV vs. barrel span length, S

(a)

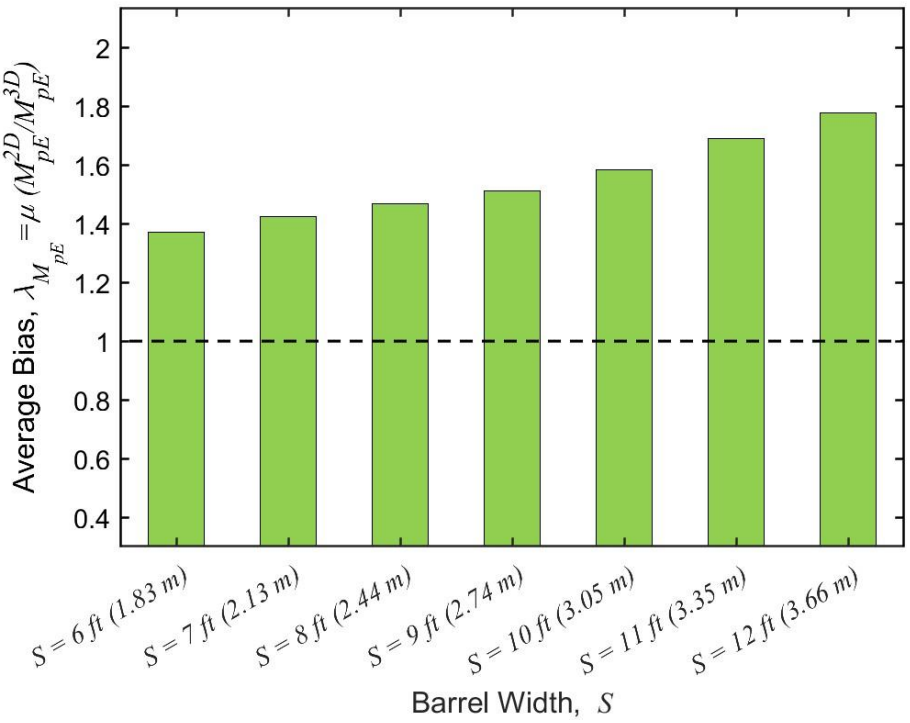

(b)

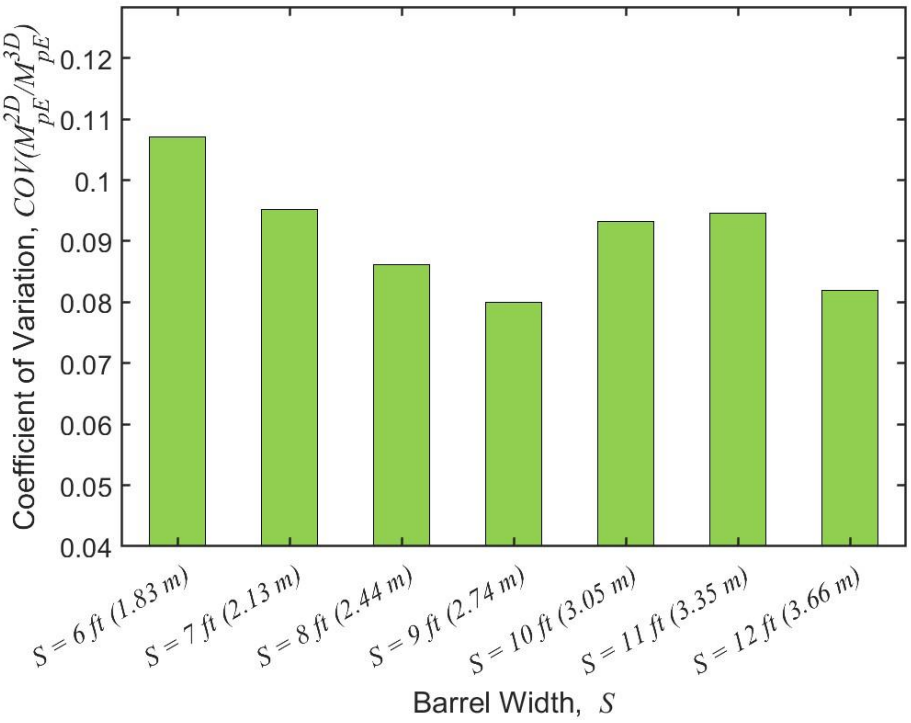

Figure 26. Trend of negative moment bias $\lambda_{Mn,avg}$ and COV vs. barrel span length, S

(a)

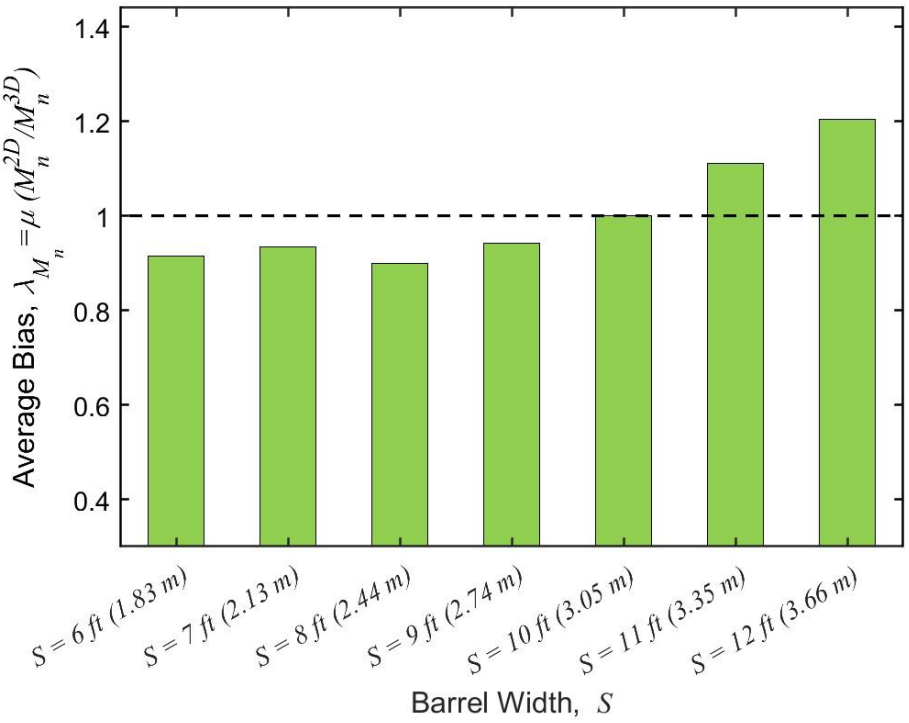

(b)

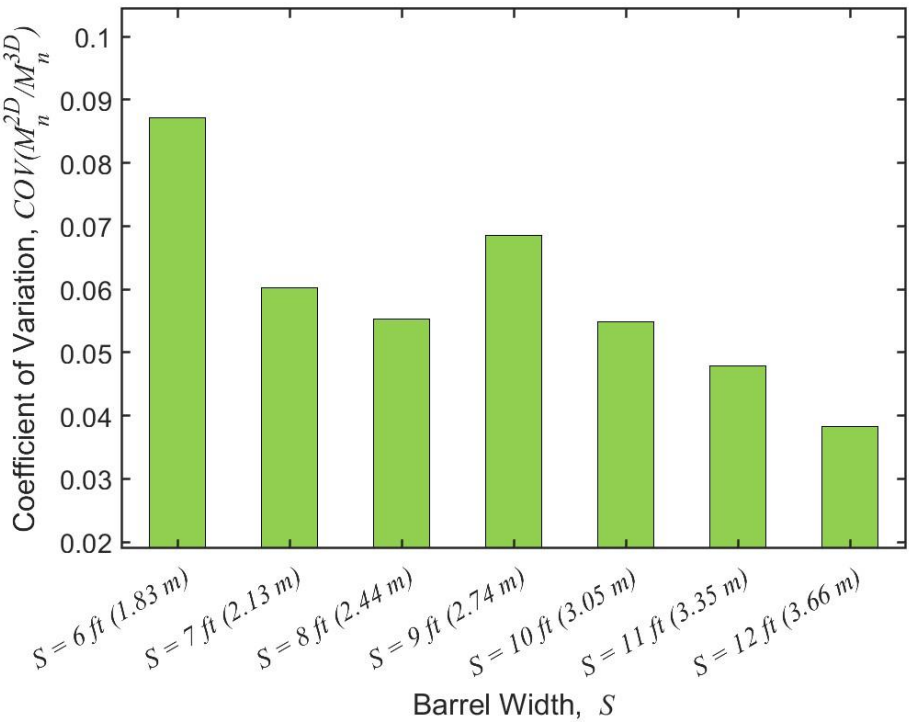

Figure 27. Trend of interior positive moment bias $\lambda_{MpI,avg}$ and COV vs. barrel span length, S

(a)

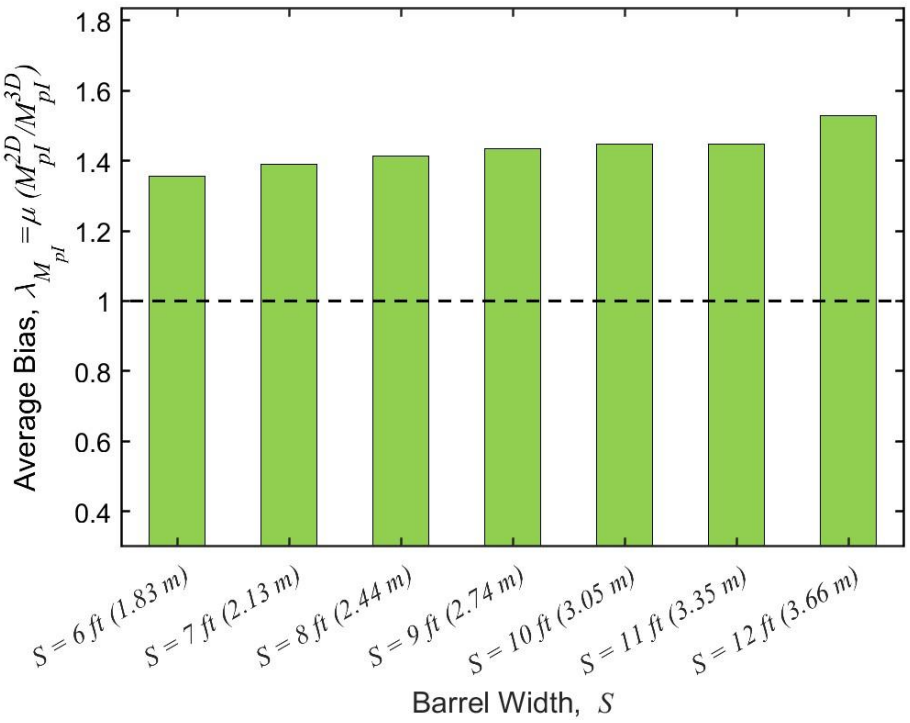

(b)

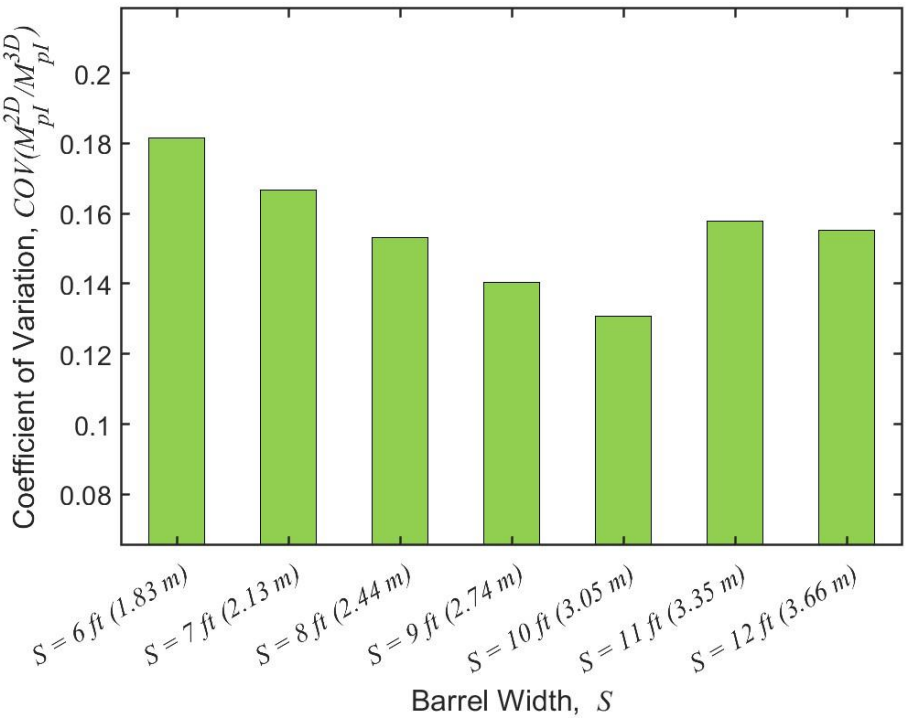

Effect of Fill Height, FH

Figure 28 shows the histograms of the bias (λ) for all straining actions extracted from the models analyzed in this study. One can observe that shear forces (λ_V) appear to be affected by the fill height more than Equations [16] and [17] imply. The average bias ($\lambda_{V,avg}$) is substantially negative for FH =0 ft., slightly negative for FH =1 ft., and positive for FH =2 ft. The trends of the shear bias and its COV are also shown in detail in Figure 29.

For positive bending moment bias ($\lambda_{M_{pE}}$) in the exterior barrel of culverts, Figure 23 shows that the bias is positive for all cases indicating conservatism in the range of 40% to 75% as can be seen in Figure 30-a. This is likely why many culverts struggle to pass load rating requirements. It should be noted that the scatter of the results increases with the increase in conservatism (see Figure 30-b). The negative moment bias values (λ_{M_n}) shown in Figure 31 are surprisingly on the mark, with bias values consistently around 1.0. Finally, Figure 32 shows the positive bending moment bias ($\lambda_{M_{pI}}$) in the interior barrel of culverts to have a conservative trend, like the positive bending moment in the exterior barrel. All cases show an increasing bias value indicating a conservatism inherent in Equations [16] and [17]. The reason for this conservatism is likely due to the fact that AASHTO-LRFD BDS formulas ignore the secondary distribution that the top slab introduces to the system, which is known to be a function of the barrel span length. Therefore, it appears that Equation [17] does not adequately reflect this secondary distribution.

Figure 28. Histogram of straining action bias for different fill height values

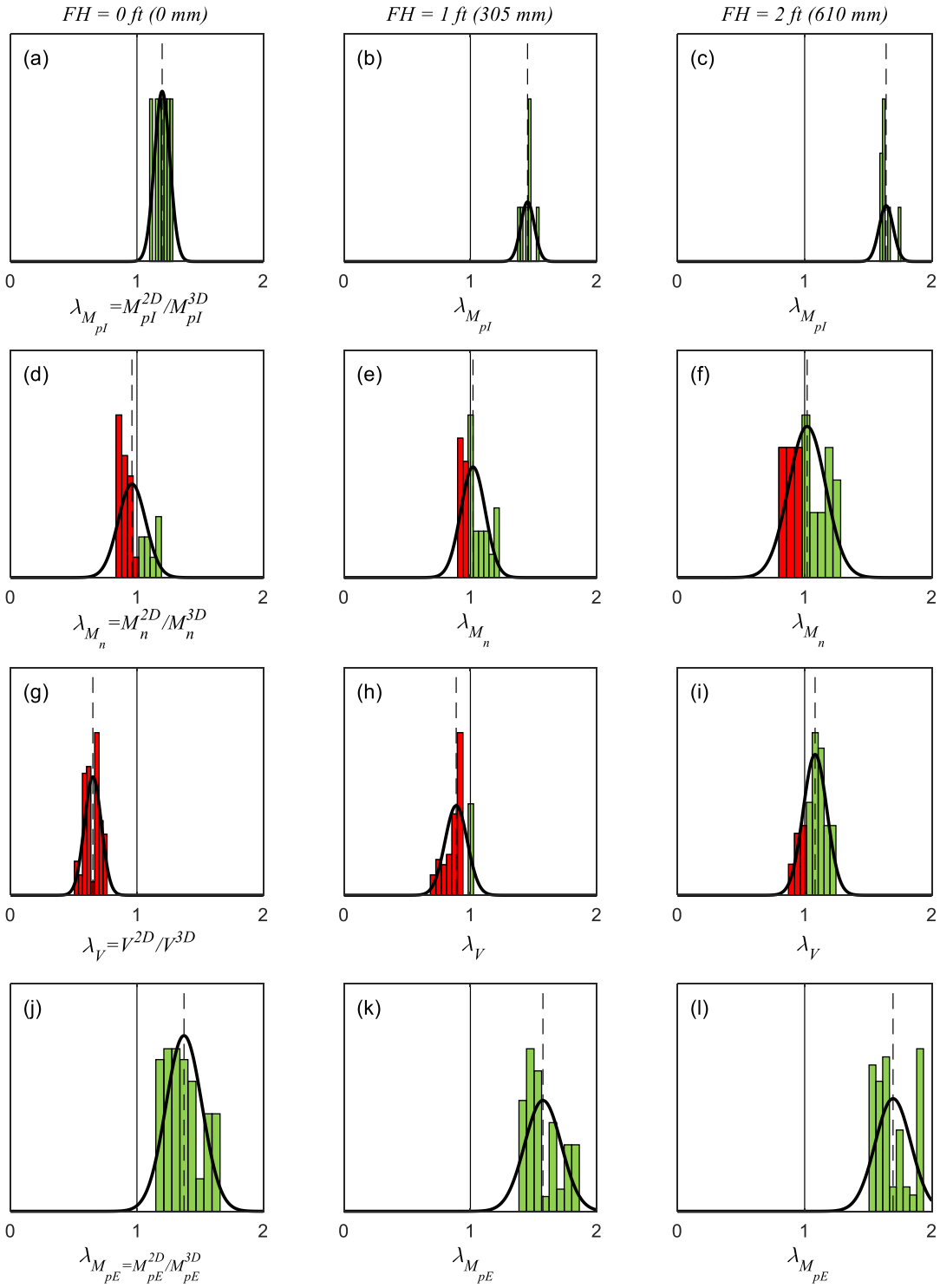

Figure 29. Trend of shear bias $\lambda_{V,avg}$ and COV vs. fill height

(a)

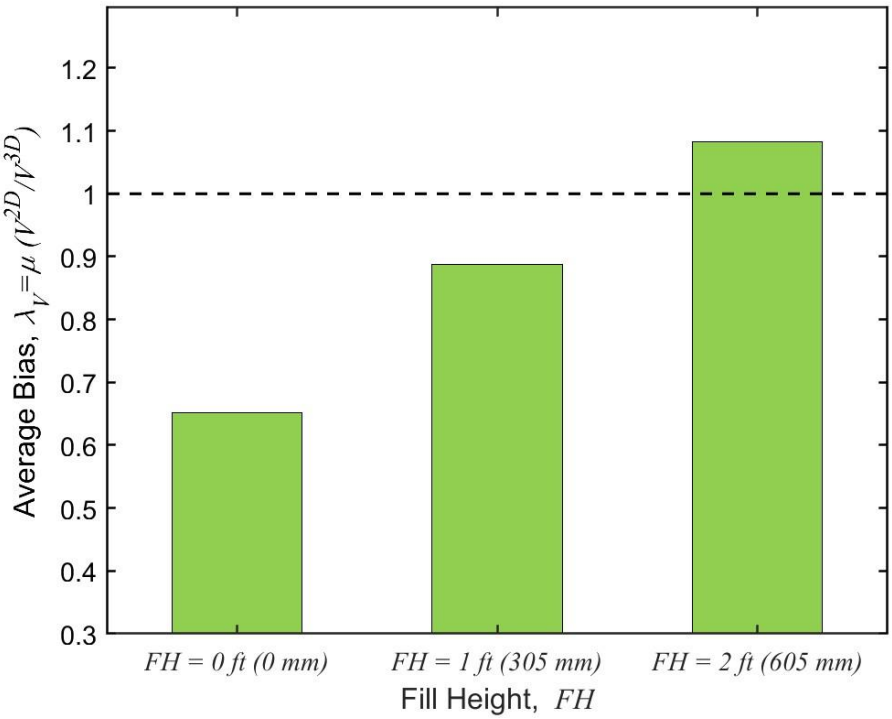

(b)

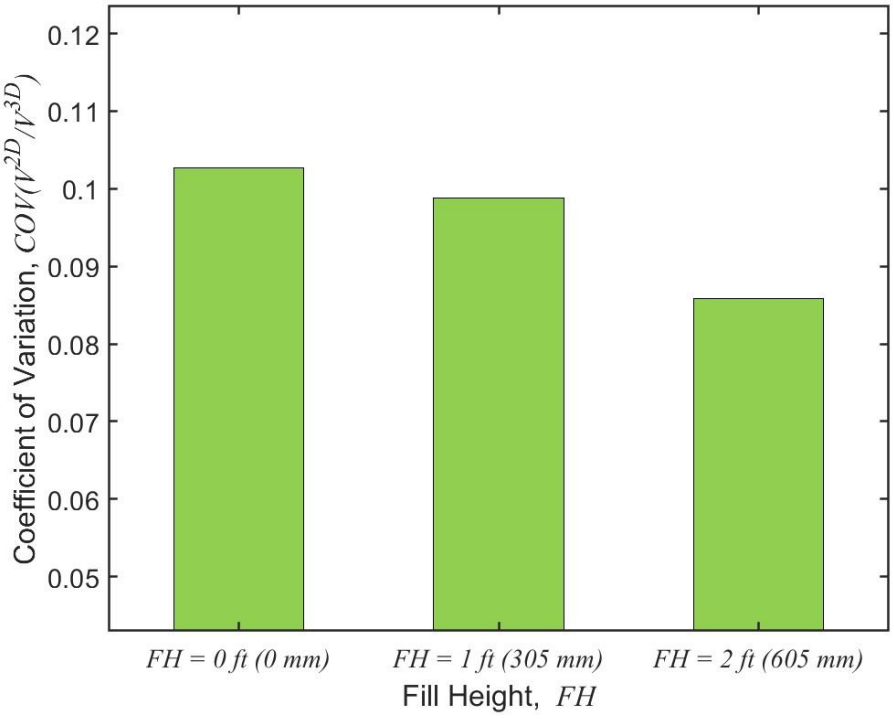

Figure 30. Trend of exterior positive moment bias $\lambda_{MpE,avg}$ and COV vs. fill height

(a)

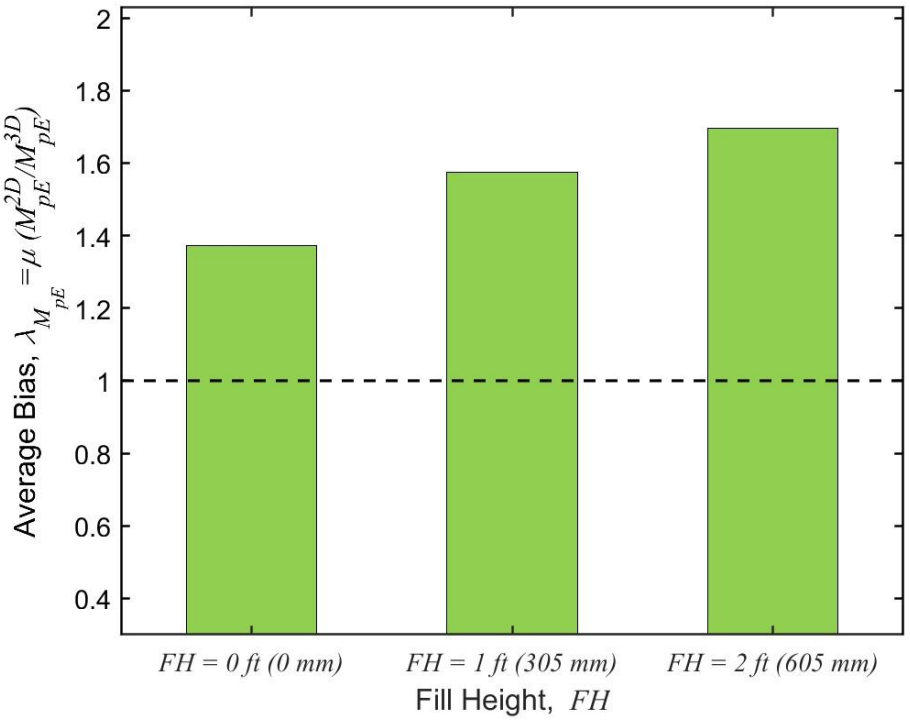

(b)

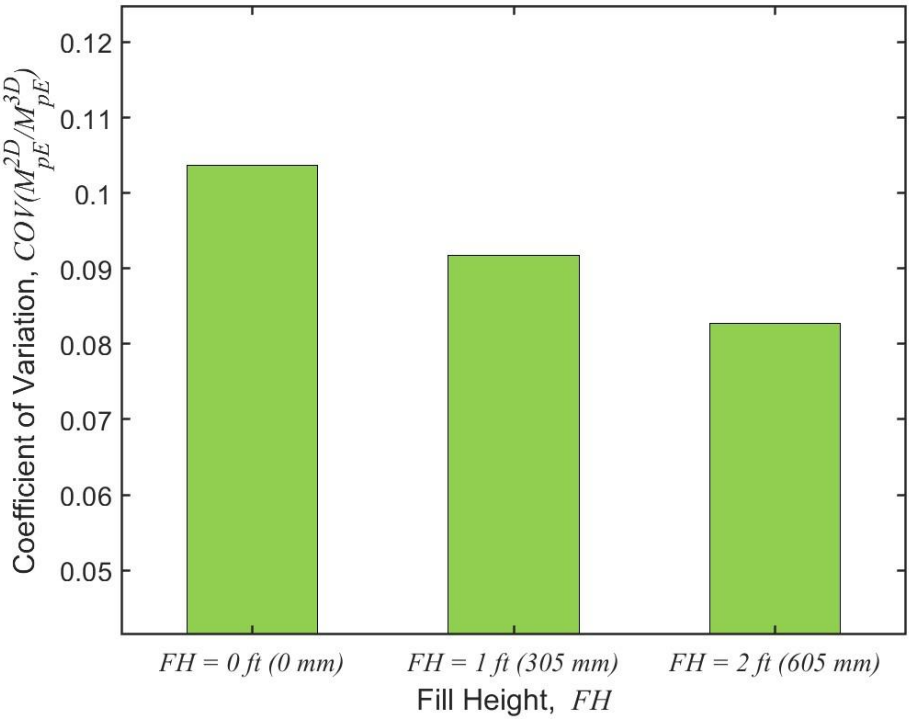

Figure 31. Trend of negative moment bias $\lambda_{Mn,avg}$ and COV vs. fill height

(a)

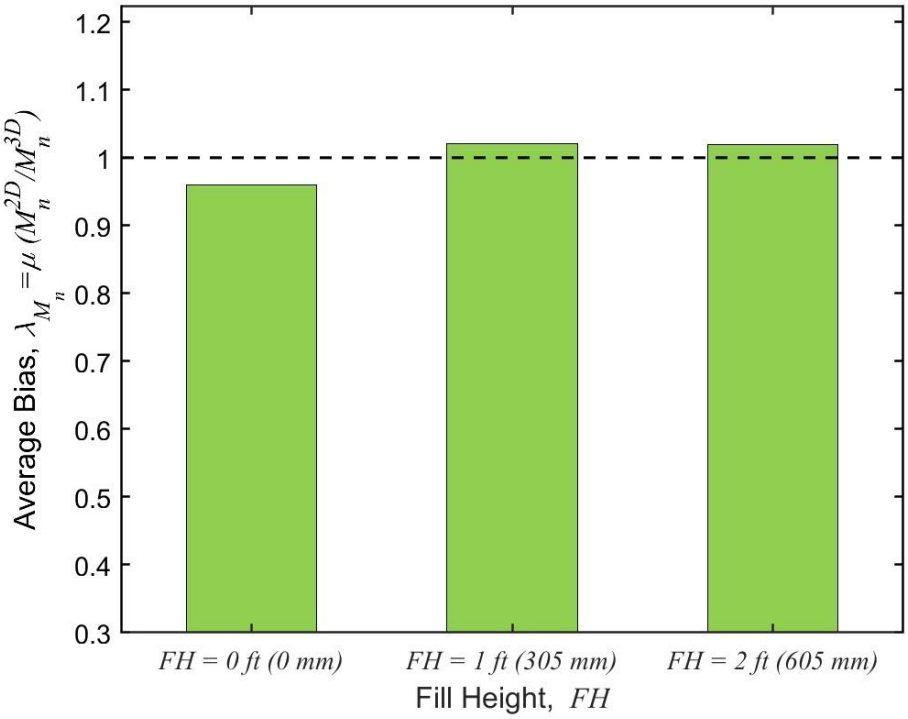

(b)

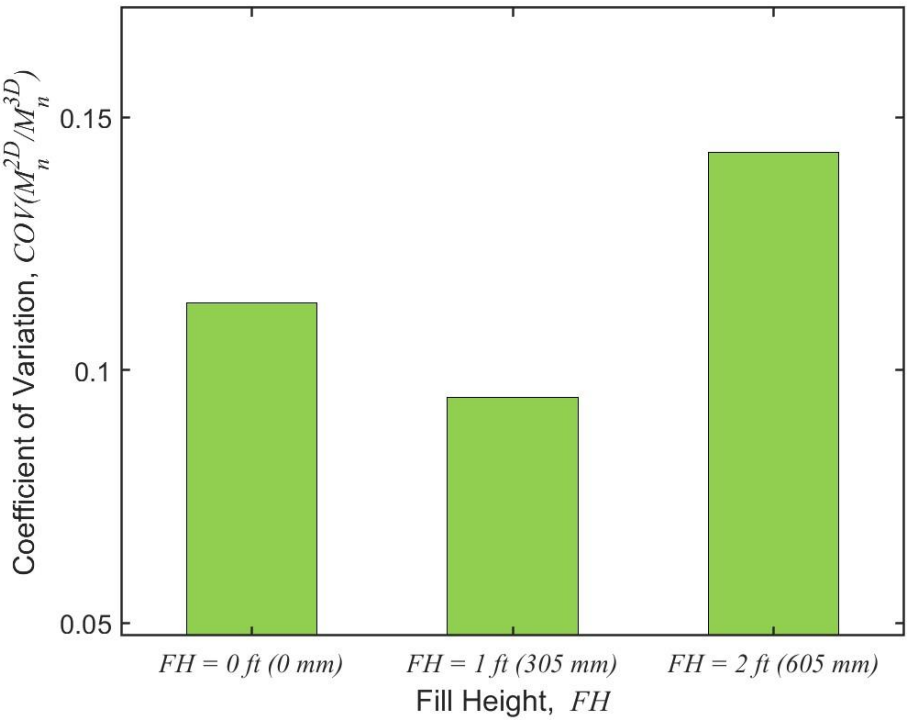

Figure 32. Trend of interior positive moment bias $\lambda_{Mpl,avg}$ and COV vs. fill height

(a)

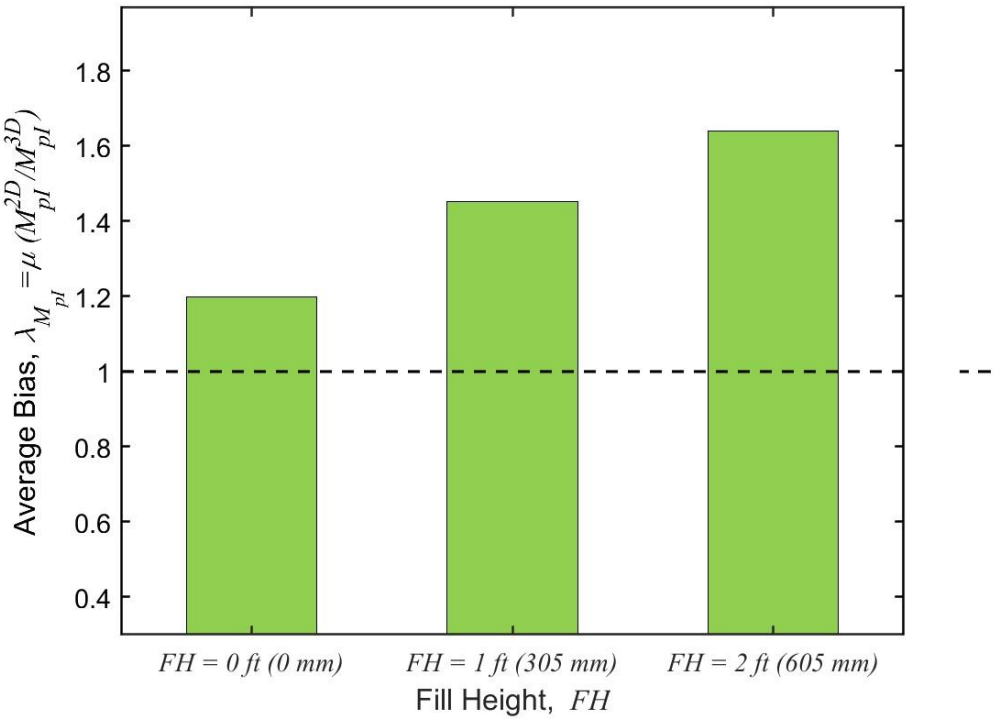

(b)

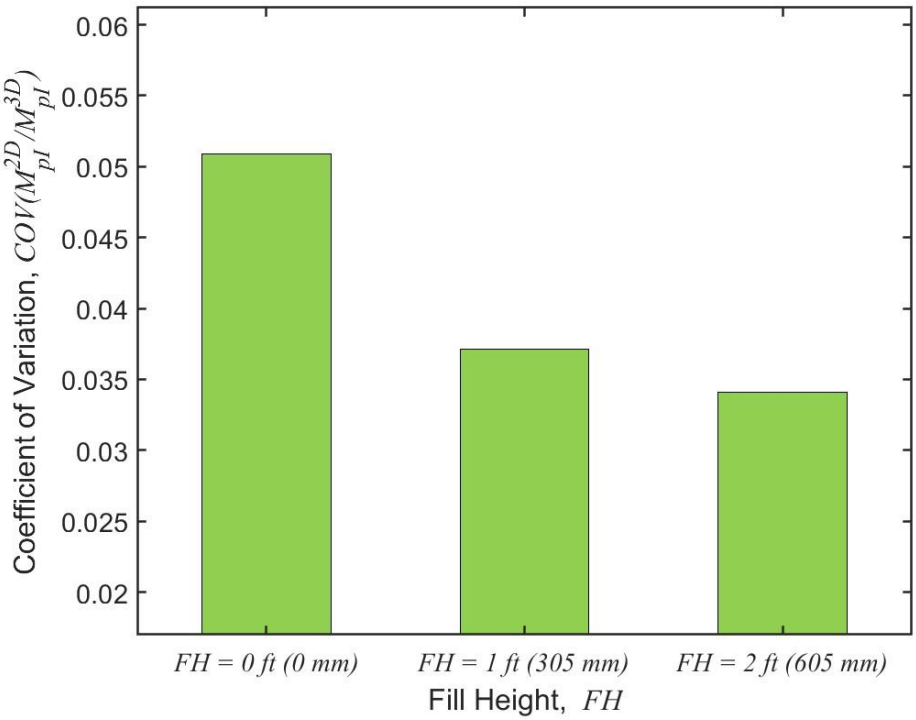

Effect of Culvert Concrete Compressive Strength, f'_c

Figure 33 shows the histograms of the bias (λ) for the shear force (V) and positive moment (M_{pE}) in 1-barrel cases. The histograms are shown for the concrete compressive strength (f'_c) values considered in the parametric study: 3000, 4000, and 5000 psi. It is clear that the concrete compressive strength (f'_c) does not affect the bias values nor does it affect the coefficient of variation, ($COV(\lambda_V)$). For statically indeterminate structures such as box culverts, the modulus of elasticity of concrete (E_c) typically affects the analysis results, and it is well known that E_c is a proportional to concrete compressive strength (f'_c). Hence, f'_c was included in the investigated parameters. However, the reason why results were not affected is attributed to the fact that increasing/decreasing f'_c for elements of the culvert (slabs and walls) keeps the relative stiffness of these elements the same. This is confirmed for the positive moment (M_{pE}). Figure 34 and Figure 35 show plots of the bias (λ) and coefficient of variation trends ($COV(\lambda_V)$), which do not change for both internal forces extracted from the 1-barrel cases, namely V and M_{pE}.

Based on these results, it was concluded that f'_c is not a parameter that affects the development of internal forces in box culverts. Therefore, it was not included in the subsequent analysis for 2-barrel and 3-barrel cases.

Figure 33. Histogram of straining action bias for different concrete compressive strengths, $f_c^{'}$

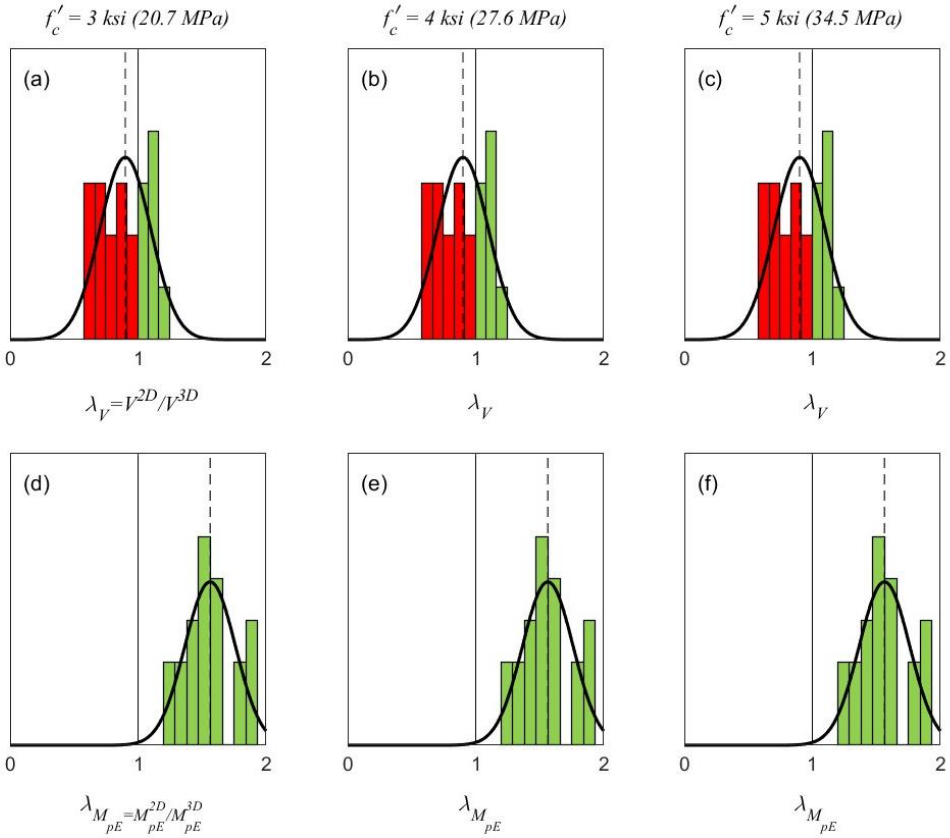

Figure 34. Trend of shear bias $\lambda_{V,avg}$ and COV vs. concrete compressive strengths, $f_c^{'}$

(a)

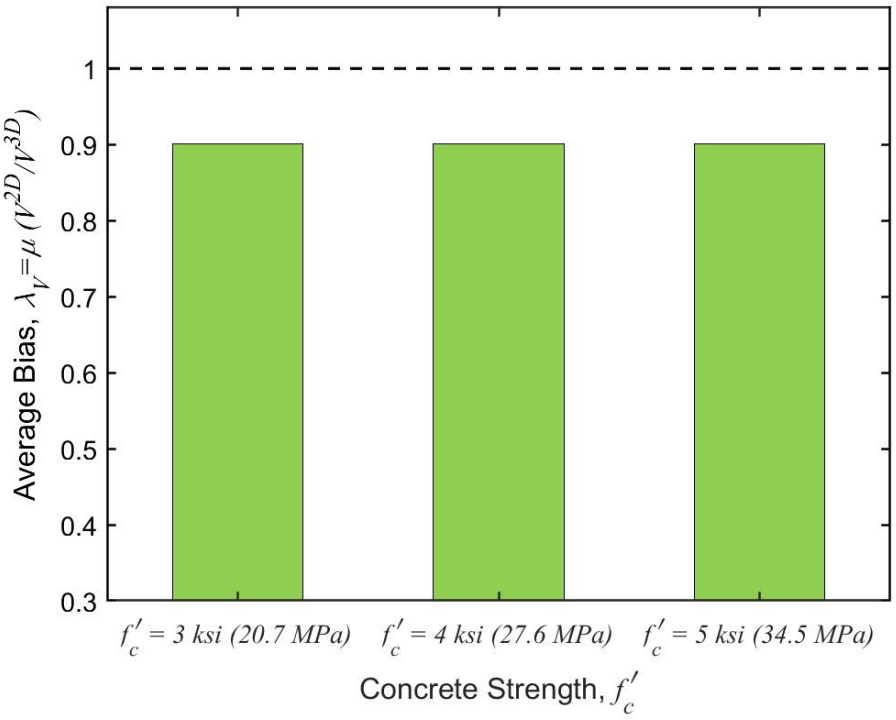

(b)

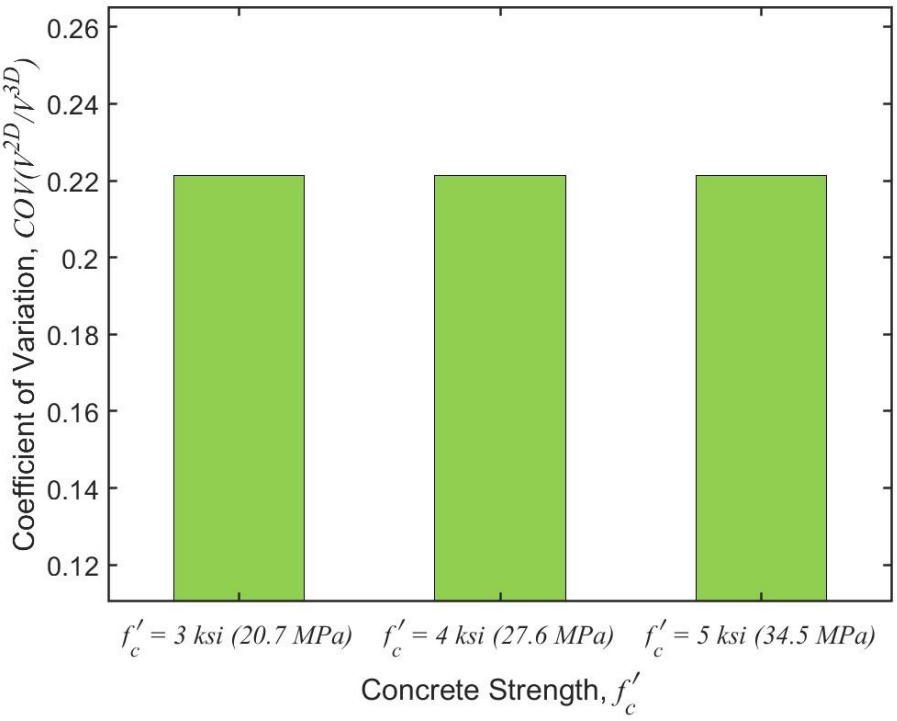

Figure 35. Trend of exterior positive moment bias $\lambda_{MpE,avg}$ and COV vs. concrete compressive strengths, $f_c^{'}$

(a)

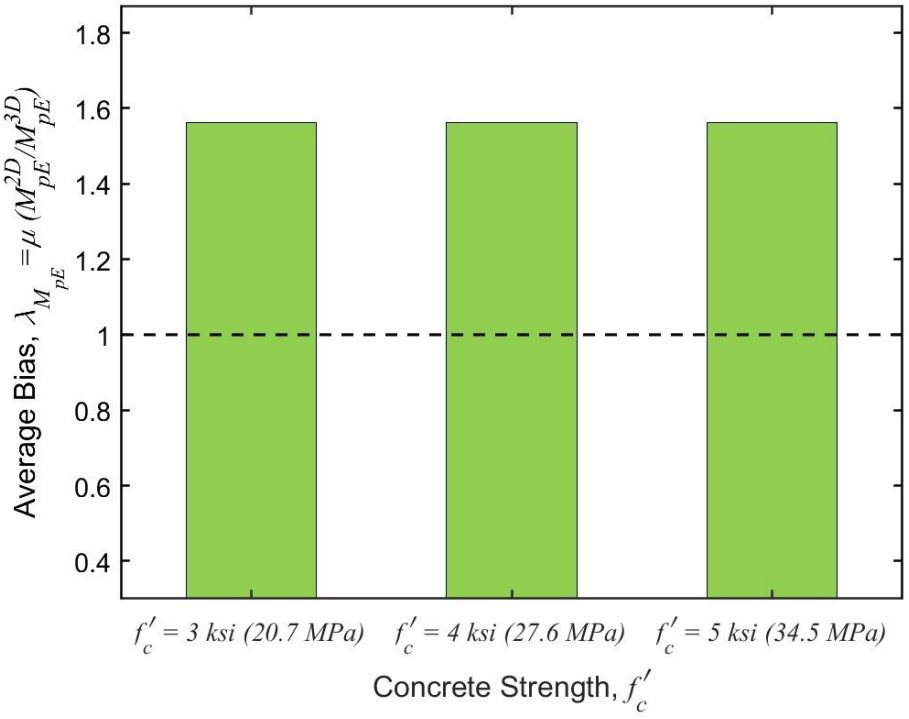

(b)

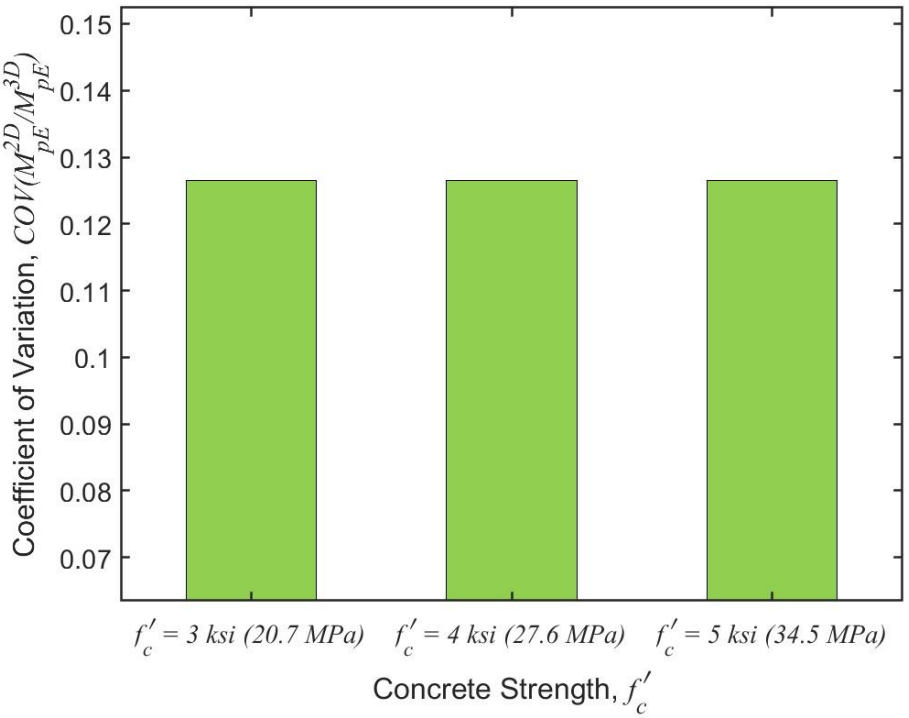

Effect of Number of Barrels, N_B

The available data allows for investigating the effect of number of barrels on the accuracy of results. Figure 36 shows the histograms of the bias (λ) for all straining actions extracted for this study. Obviously, some straining actions are not available for models with all numbers of barrels. For example, the negative moment (M_n) bias is only available for barrels with continuous top slabs, namely 2- and 3-barrels. Similarly, the bias for positive moment in interior barrels (M_{pI}) is only available in 3-barrel cases. The figure shows that there is no strong correlation between the number of barrels and the bias of straining actions. This can be explained by the previously discussed secondary distribution behavior that mainly relies on the wheel load position relative to the span length. The number of barrels will be included in this study simply because it allows for investigating more straining actions often encountered in the design and load rating of culverts (i.e., negative moment [M_n] and positive moment in interior barrels [M_{pI}]). For completeness, Figure 37 through Figure 40 show plots of the bias (λ) and coefficient of variation trends ($COV(\lambda)$) for all straining actions.

Figure 36. Histogram of straining action bias for different number of barrels

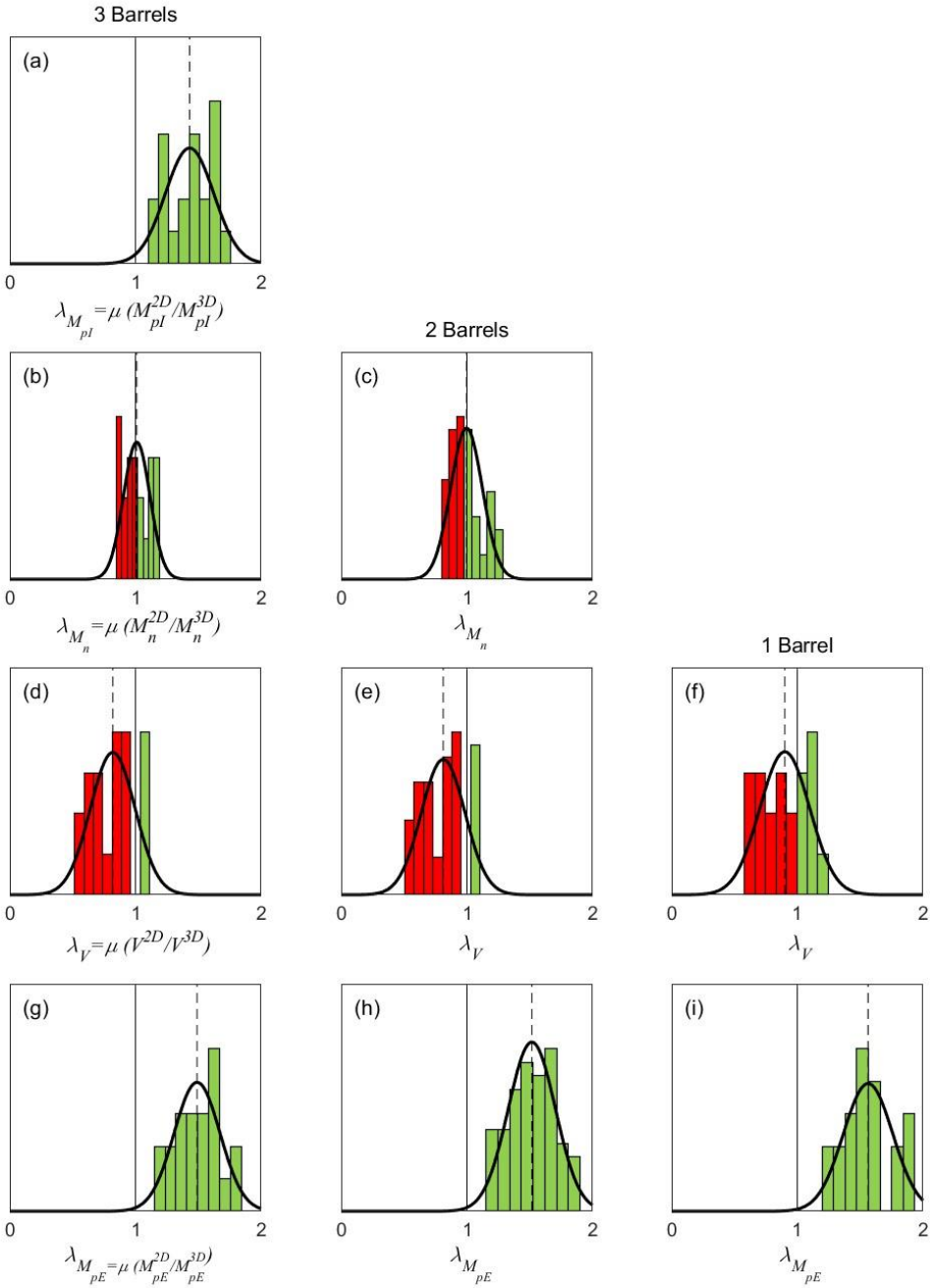

Figure 37. Trend of shear bias $\lambda_{V,avg}$ and COV for different number of barrels

(a)

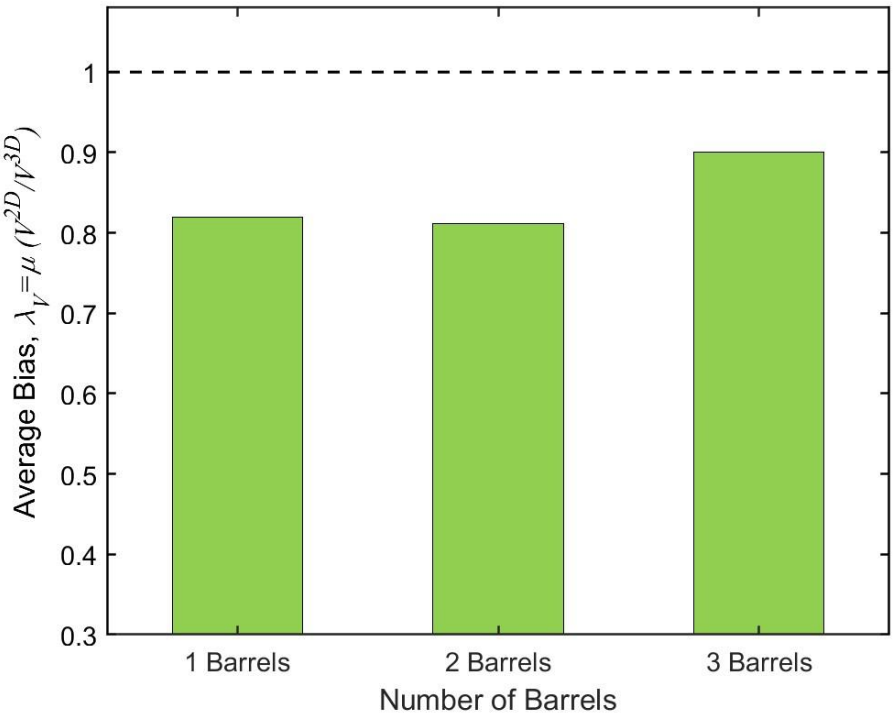

(b)

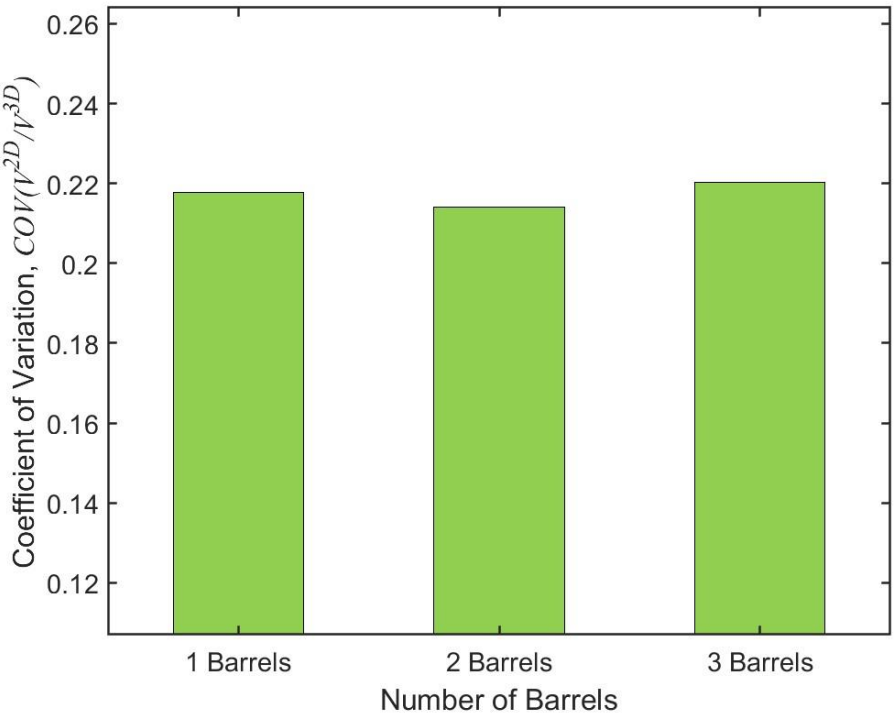

Figure 38. Trend of exterior positive moment bias $\lambda_{MpE,avg}$ and COV for different number of barrels

(a)

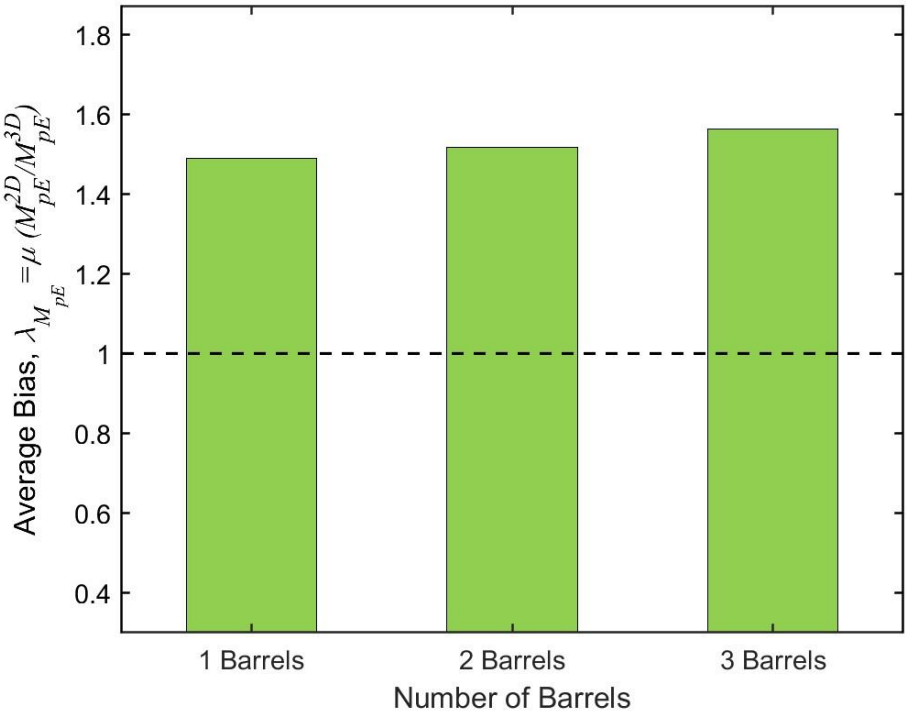

(b)

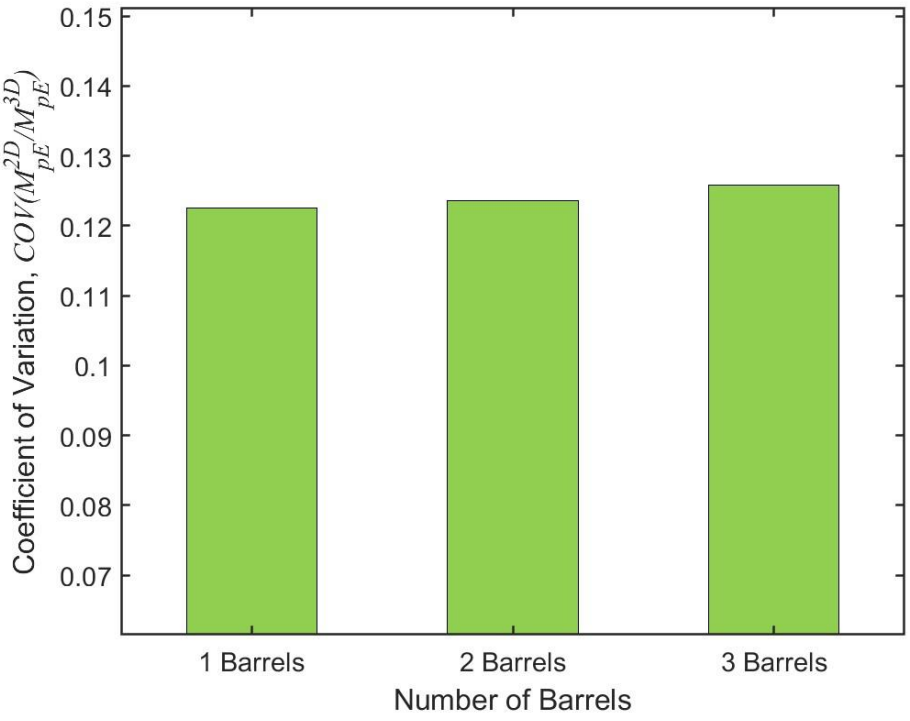

Figure 39. Trend of negative moment bias $\lambda_{Mn,avg}$ and COV for different number of barrels

(a)

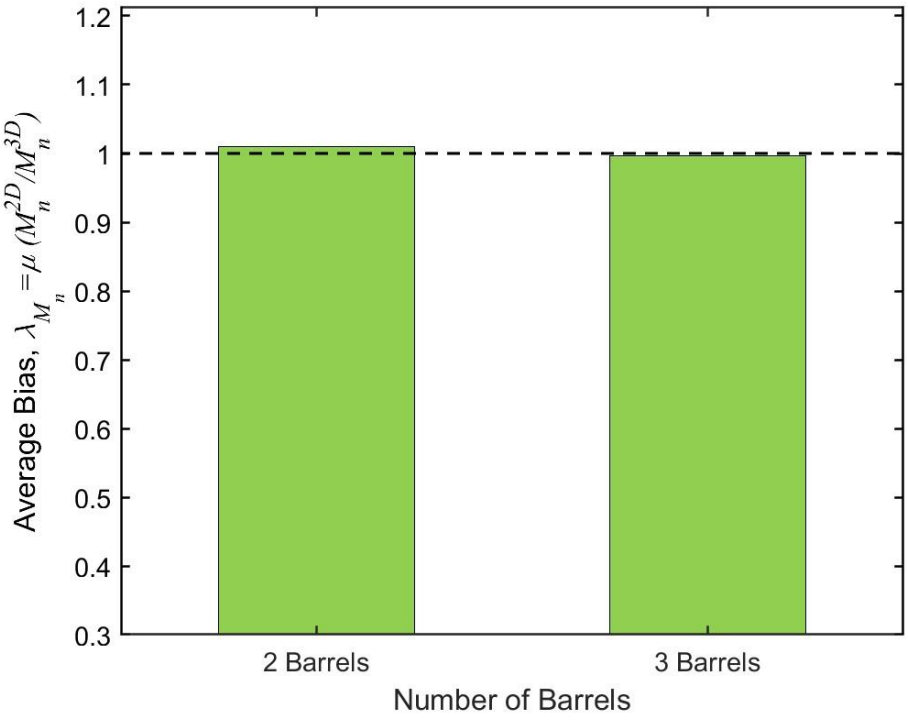

(b)

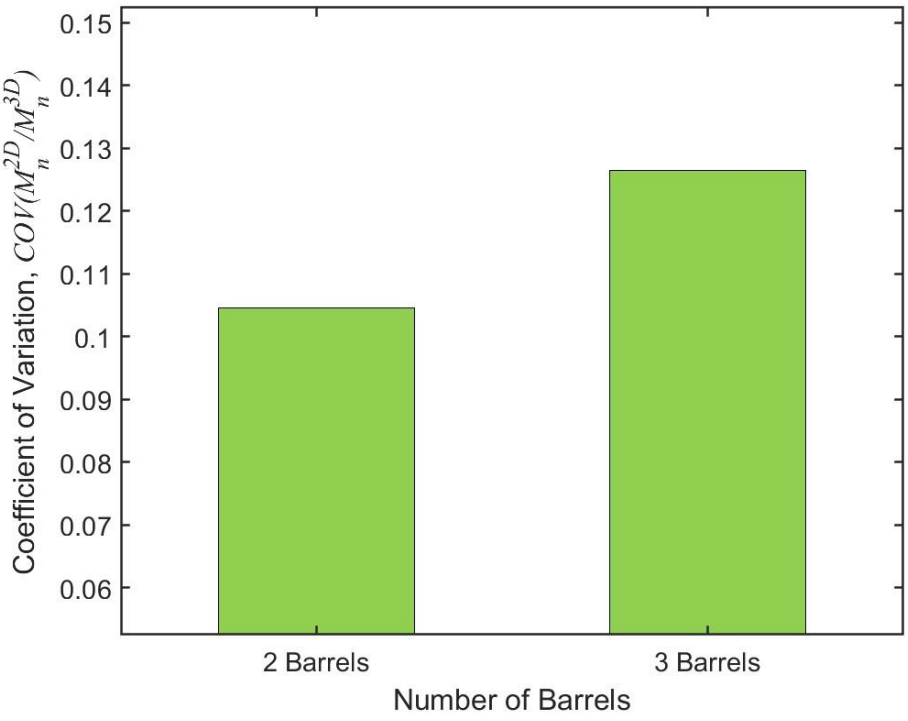

Figure 40. Trend of interior positive moment bias $\lambda_{MpI,avg}$ for different number of barrels

(a)

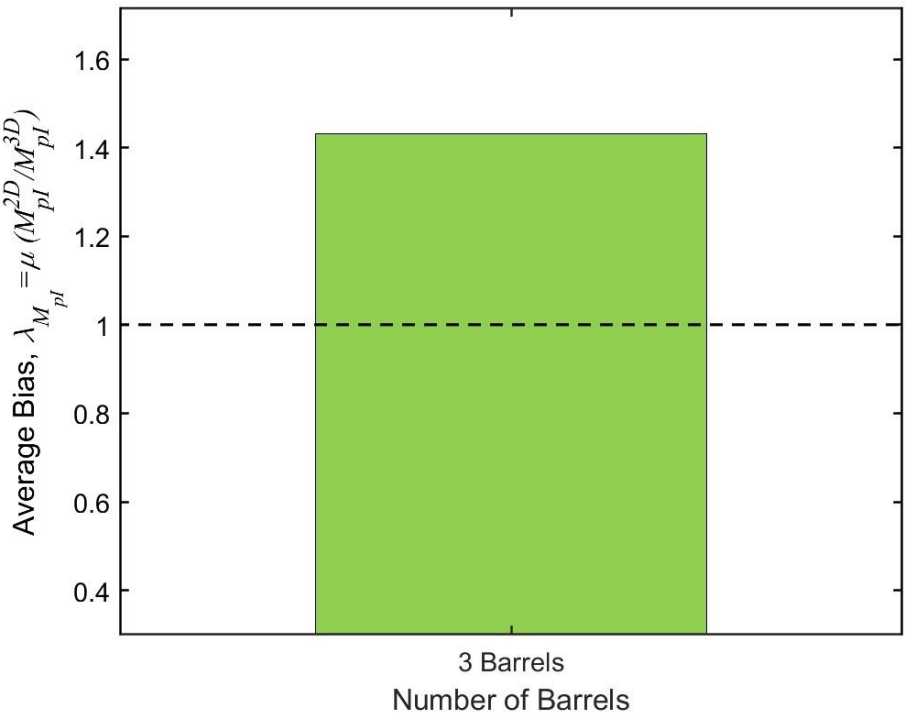

(b)

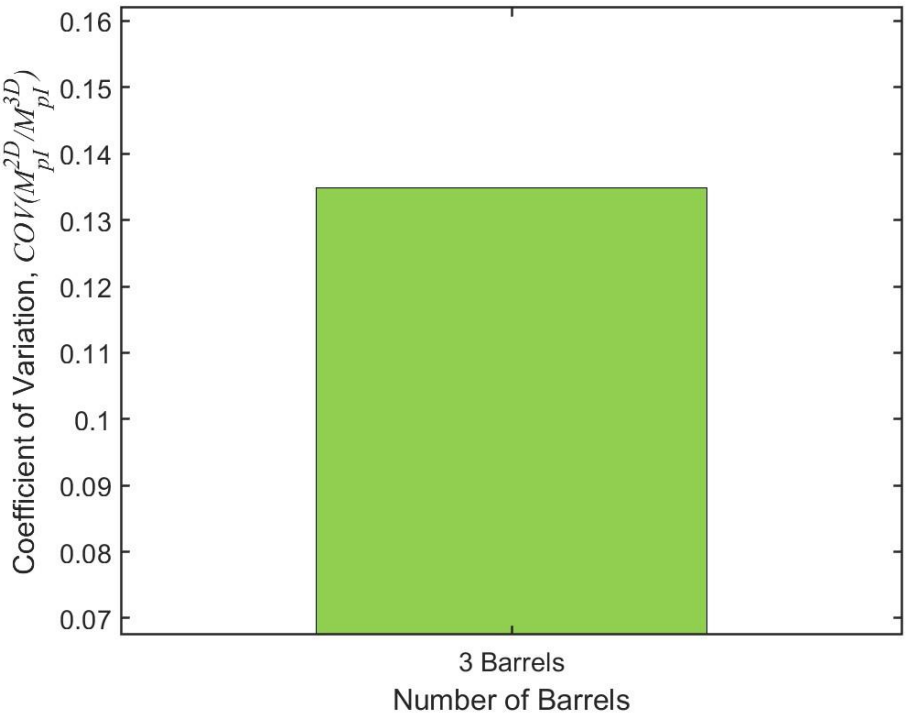

Effect of Span to top slab thickness ratio, S/t_s

The final parameter discussed is the slab thickness. The S/t_s ratio was selected instead of an absolute thickness because the most important parameter is the top slab stiffness, which affects the ability of the slab to distribute wheel loads. The histograms are shown for different span to top slab thickness ratios (S/t_s), which were grouped into three ranges: $S/t_s \leq 10$, $10 < S/t_s \leq 12$, and $S/t_s > 12$. Figure 41 shows the histograms of the bias (λ) for the shear force (V) and positive moment (M_{pE}) in 1-barrel cases. The figure shows that there is a correlation between the S/t_s ratio and the bias values for both shear and positive bending moment, albeit not as pronounced as for fill height (FH) or span length (S). The difference in the average bias (λ) for the different ranges is approximately 10%, which is lower than the values obtained for the other parameters, which reached up to 40%. Consequently, it was concluded that the ratio S/t_s is not a major parameter to be included in the proposed formula since its inclusion would add complexity to the formula, with little improvement in the prediction accuracy. Figure 42 and Figure 43 show plots of the bias (λ) and coefficient of variation trends ($COV(\lambda)$), which do not change for both internal forces extracted from the 1-barrel cases, namely V and M_{pE}. Therefore, the slab thickness parameter was not considered in the 3-barrel cases of the parametric study.

Figure 41. Histogram of straining action bias for different span to slab thickness ratios, S/t_s

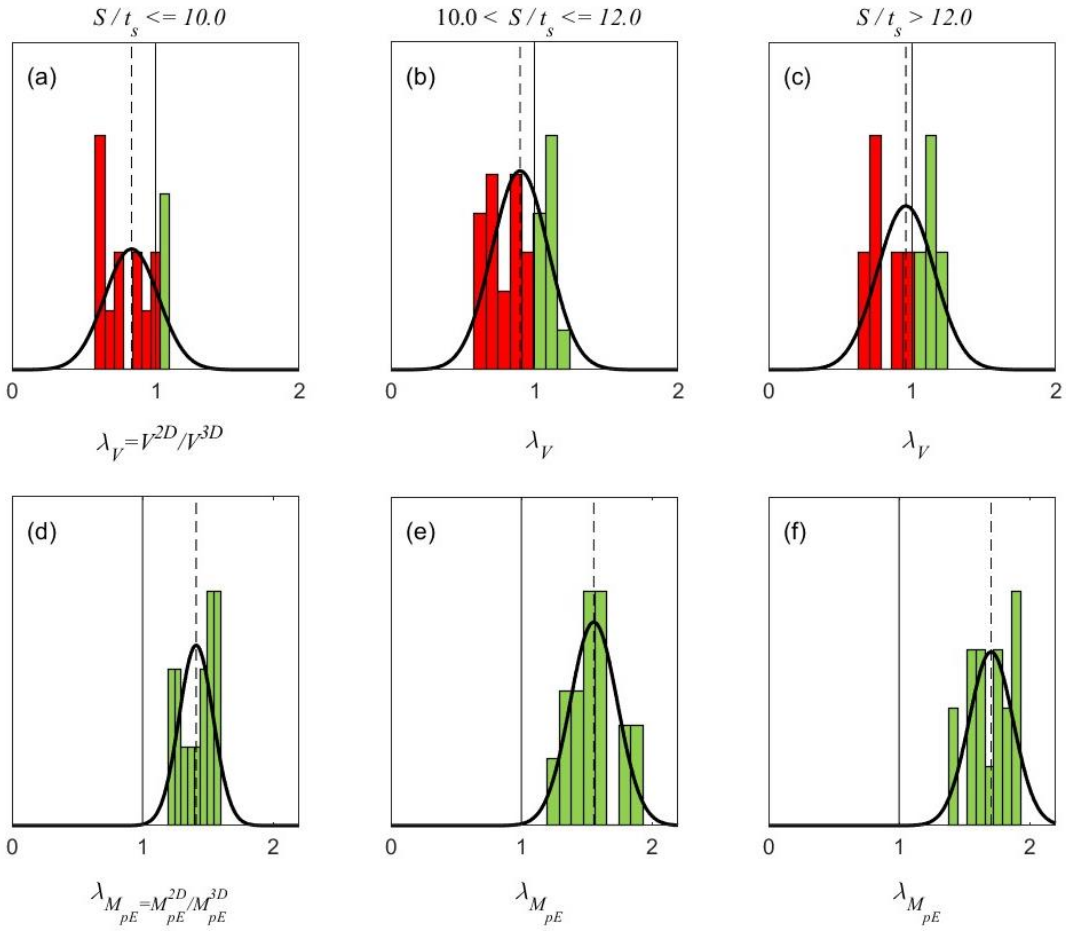

Figure 42. Trend of shear bias $\lambda_{V,avg}$ and COV for different secondary distributions coefficients, η

(a)

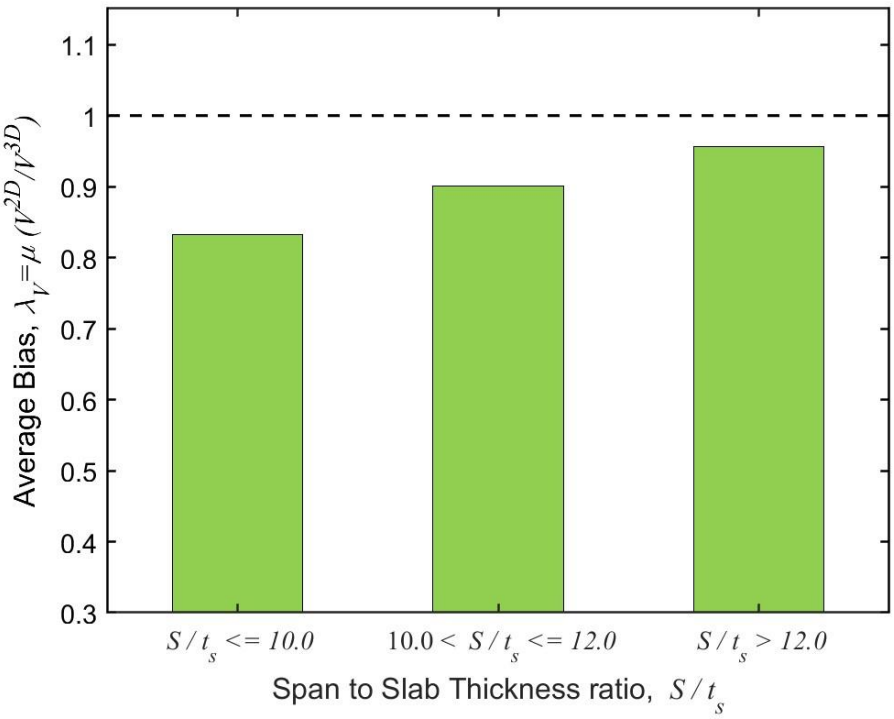

(b)

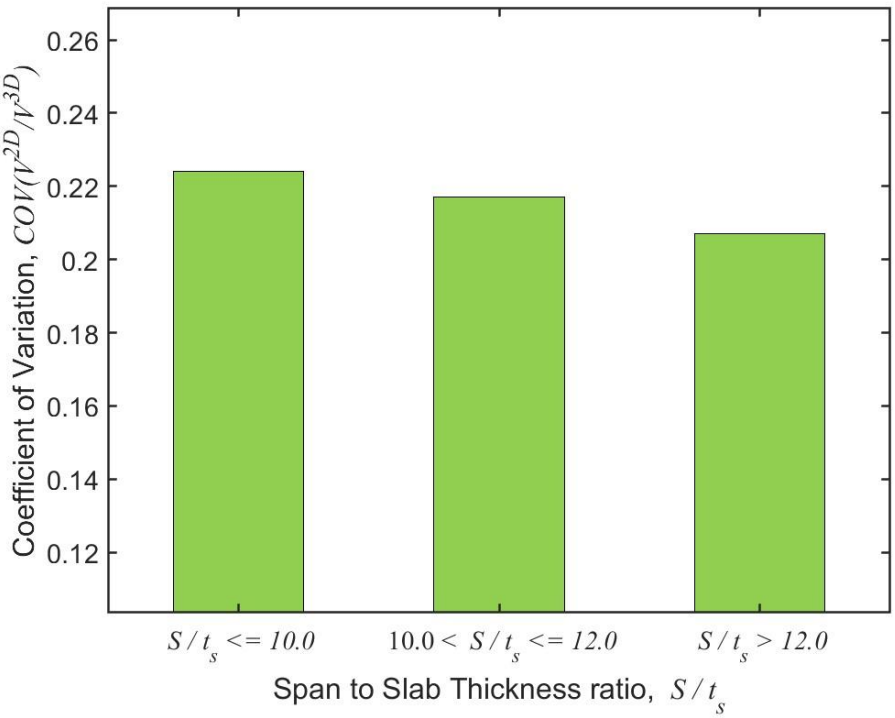

Figure 43. Trend of exterior positive moment bias $\lambda_{MpE,avg}$ and COV for different secondary distributions coefficients, η

(a)

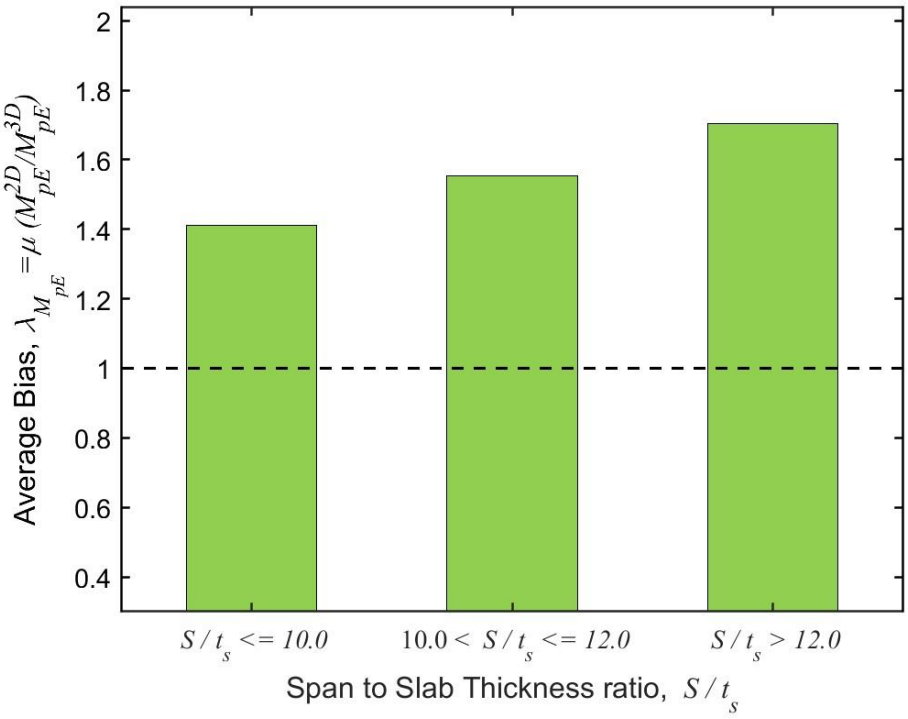

(b)

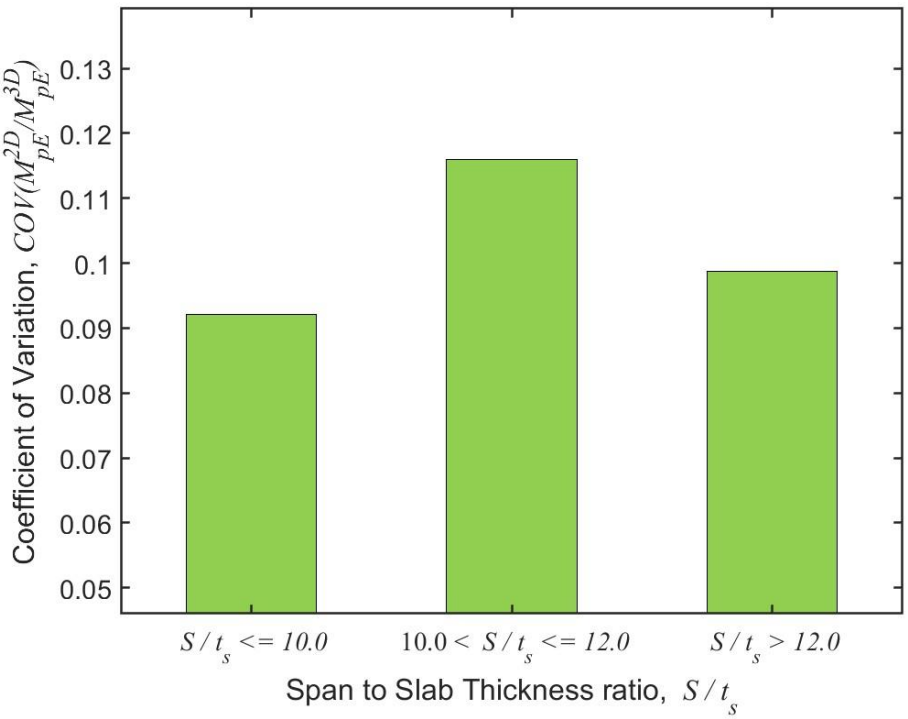

Development of New Live Load Distribution Formula

Parameters included in New Live Load Distribution Formula

Based on the parametric study results, it was determined that the main parameters that directly affects the straining action results are:

- Fill Height, FH
- Barrel Span Length, S

In addition to these parameters, the axle gauge (distance between wheels in one axle) clearly influences the top slab area width engaged in the resistance of wheel loads, as can be seen in Figure 4-c. The developed equation is based on the AASHTO-LRFD BDS equations for wheel load distribution (Equations [16] and [17]). Only Equation [17] was considered in the development of the modified live load distribution formula. The reason the focus was on Equation [17] is that current wheel load distribution formulas do not reflect the secondary distribution of wheel loads in the transverse direction, as discussed in the previous section.

To address this aspect of wheel load distribution, the following formula was investigated.

$$E = 92 + 1.15\,H + \eta\,S \qquad [19]$$

Where, H is the fill height (in.), S is the barrel span length (in.), and η is coefficient that will be calibrated to achieve the best results. η-values ranging from 0.1 to 0.5 will be considered.

The three terms of the formula shown in Equation [19] reflect the outer distance between wheels, the additional width that the earth fill helps distribute the wheel load, and the ability of the top slab to distribute the wheel load beyond the extents of the earth pressure, respectively. The first term is the standard distance of a design axle ($0.5 \times 20'' + 6' \times 12''/' + 0.5 \times 20'' = 92''$), while the second term is unchanged from AASHTO-LRFD BDS for the distribution in the direction parallel to the span length (AASHTO Eq. 4.6.2.10.2-2). Finally, the third term is a function of the span length as it is established in the literature that the ability of slabs to distribute non-uniform loads is a function of the distance from these loads to the closest support. For example, a load at mid-span would be distributed over a width equal to $0.5\,S$. For the many load cases considered in this study, the maximum effect for each critical case differs from one straining action type to another. For example, maximum positive moments are generated from wheel positions close to midspan. Conversely, maximum shear forces are caused by wheel loads close to the support. This

complexity was investigated by varying the η parameter to identify a suitable value that covers as many straining actions as possible.

Calibration of Secondary Distribution Effect in New Live Load Distribution Formula

Figure 44 shows the histograms of the bias (λ) for all straining actions extracted from the models analyzed in this study using the proposed formula (Equation [19]) with five η values (0.1 – 0.5). It can be seen that the average bias (dashed lines in individual figures) varies with the change in the distribution width (E) in the perpendicular direction to the span. As stated earlier, this is expected because a wider E dimension reflects the ability of the slab to distribute wheel pressure beyond the projection of the axle wheel through the soil onto the top slab, i.e., secondary distribution. By studying these average bias values, it is obvious that for positive moments (M_{pE} and M_{pI}) the average bias value is greater than 1.0 for most considered η values, and that it is closest to 1.0 for a value of $\eta = 0.4$. As stated earlier, the critical positive moments occur due to wheel position around midspan. For shear forces and negative moments (V and M_n) the average bias values are all less than 1.0, reflecting that little secondary distribution takes place for the wheel positions causing these critical values, which is closer to the culvert walls supporting the top slab. This means that deriving one formula for all straining action types will correlate well with some straining actions, while being conservative/unconservative to others.

The trends of the biases and the COV are shown in detail in Figure 45 through Figure 48 for V, M_{pE}, M_n, and M_{pI}, respectively. Figure 45-a through Figure 48-a show a clear decreasing trend of the average bias for all extracted straining actions; however, a clear divide is noted for the positive moments (M_{pE} and M_{pI}) and from the shear and negative moment (V and M_n) with the former being mostly conservative ($\lambda >$1.80) while the latter being unconservative ($\lambda <$1.80). The consistency of the prediction accuracy can be assessed by studying the scatter in the bias (λ), i.e., COV (R_n^{2D}/R_n^{3D}). It is clear that the divide carries over to the scatter as well, with COV values in the single digit percentage for positive moments (M_{pE} and M_{pI}) predictions, whereas values close to 15% are observed for the shear and negative moment (V and M_n) predictions.

Based on these results, it was determined that while a value for $\eta = 0.4$ is more suitable for predicting positive moments (M_{pE} and M_{pI}), it injects a high level of unconservatism for the shear and negative moment (V and M_n) predictions. Therefore, a value of $\eta = 0.3$ is investigated in the following sections to assess its performance over a wide range of cases and in comparison with existing formulas, especially AASHTO-LRFD BDS.

Figure 44. Histogram of straining action bias for different proposed formulas, $\eta = 0.1 - 0.5$

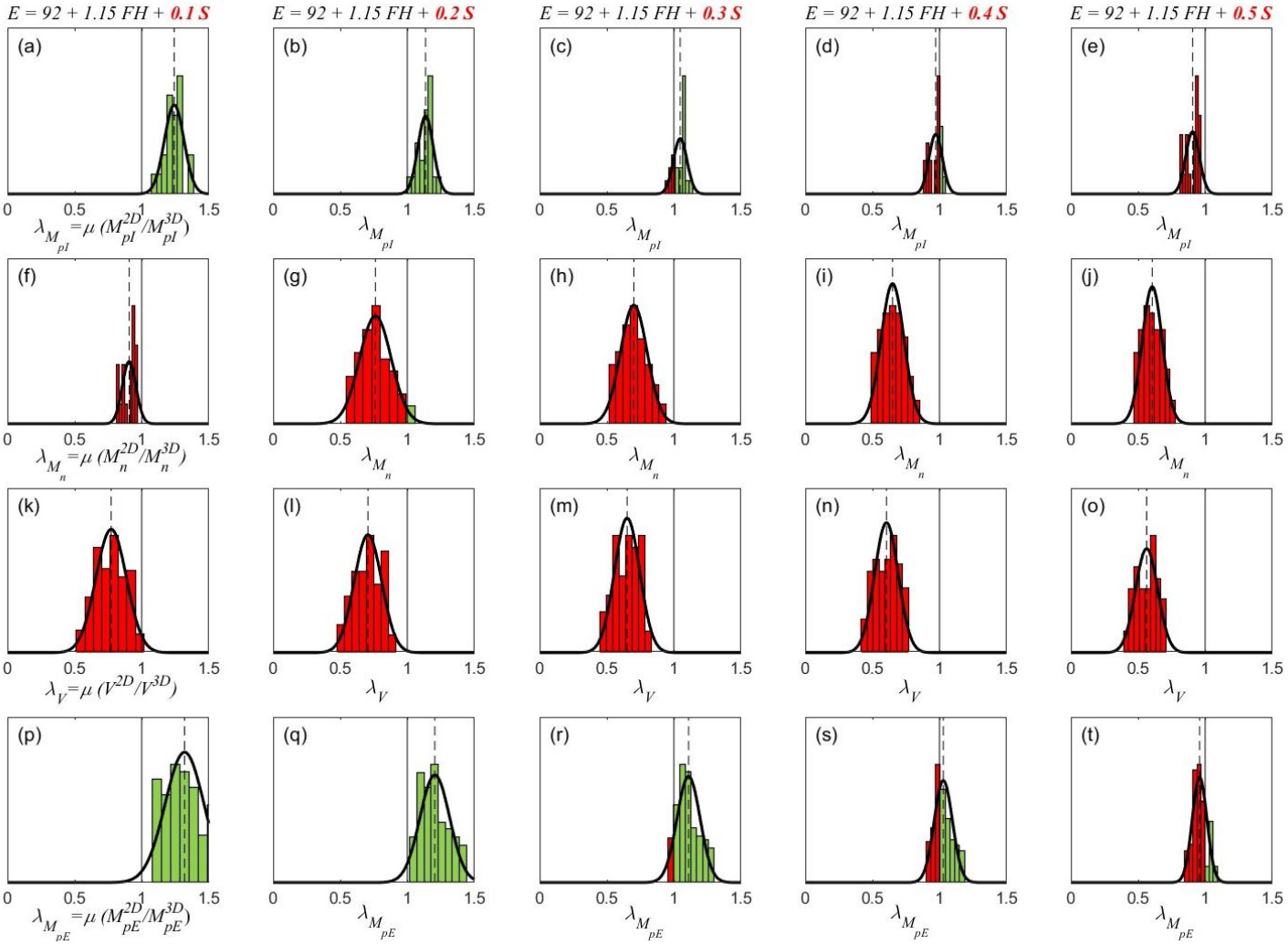

Figure 45. Trend of shear bias $\lambda_{V,avg}$ and COV for different secondary distributions coefficients, η

(a)

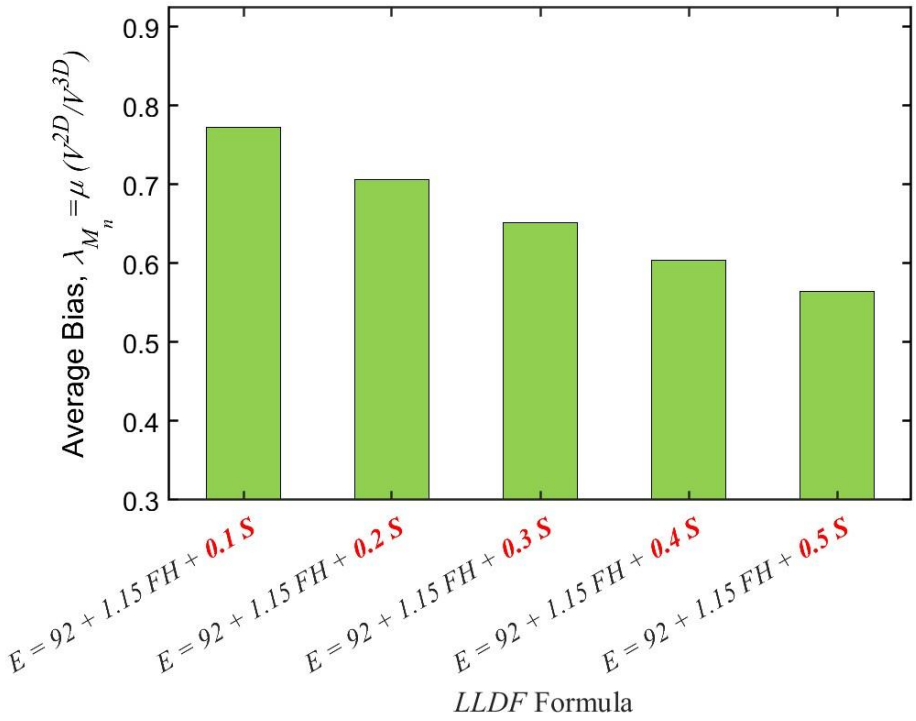

(b)

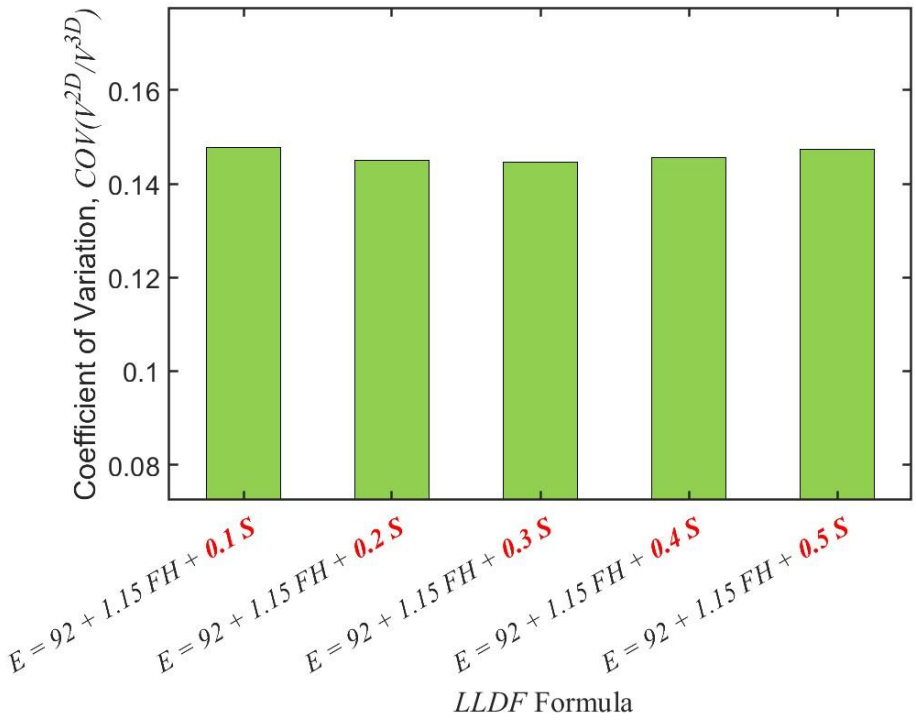

Figure 46. Trend of exterior positive moment bias $\lambda_{MpE,avg}$ and COV for different secondary distributions coefficients, η

(a)

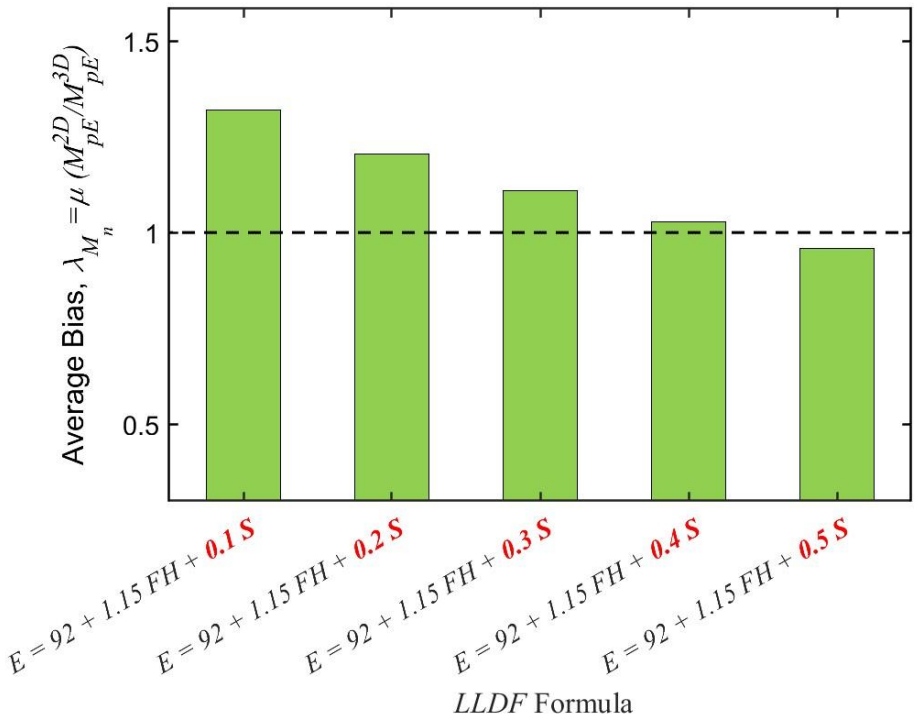

(b)

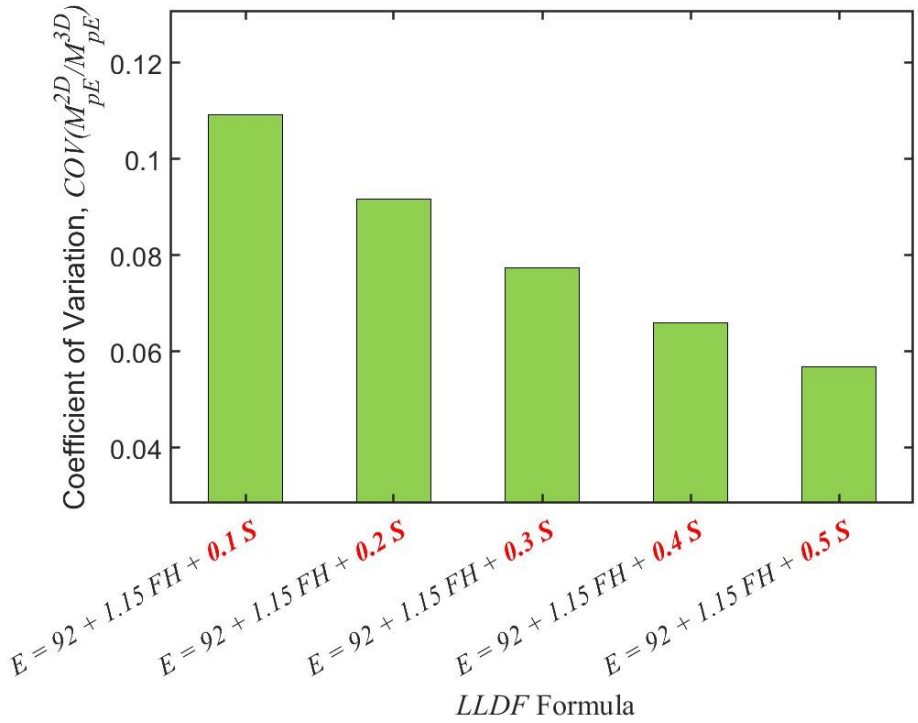

Figure 47. Trend of negative moment bias $\lambda_{Mn,avg}$ and COV for different secondary distributions coefficients, η

(a)

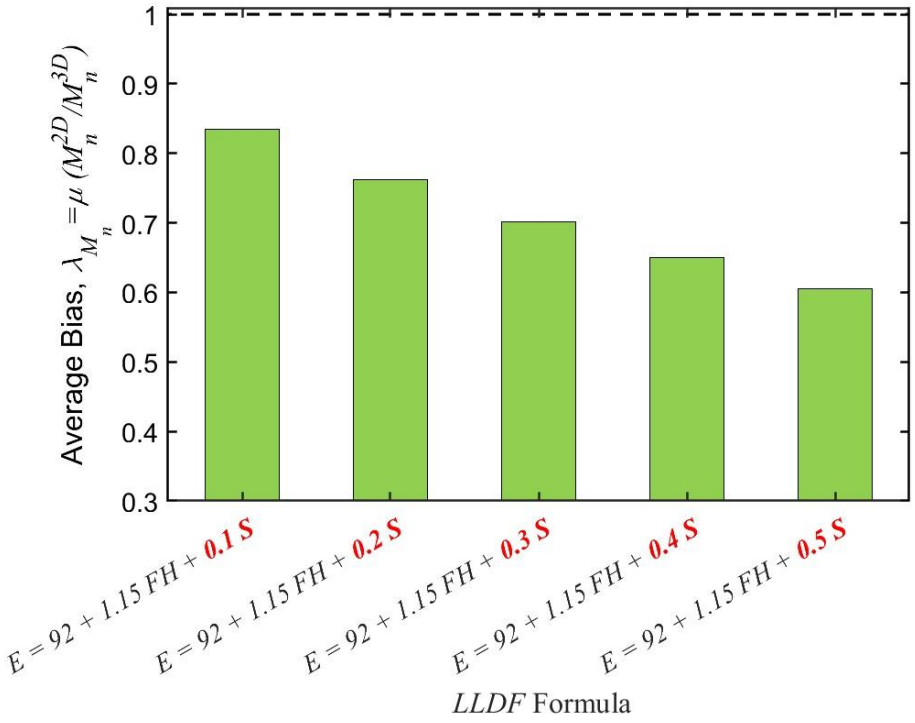

(b)

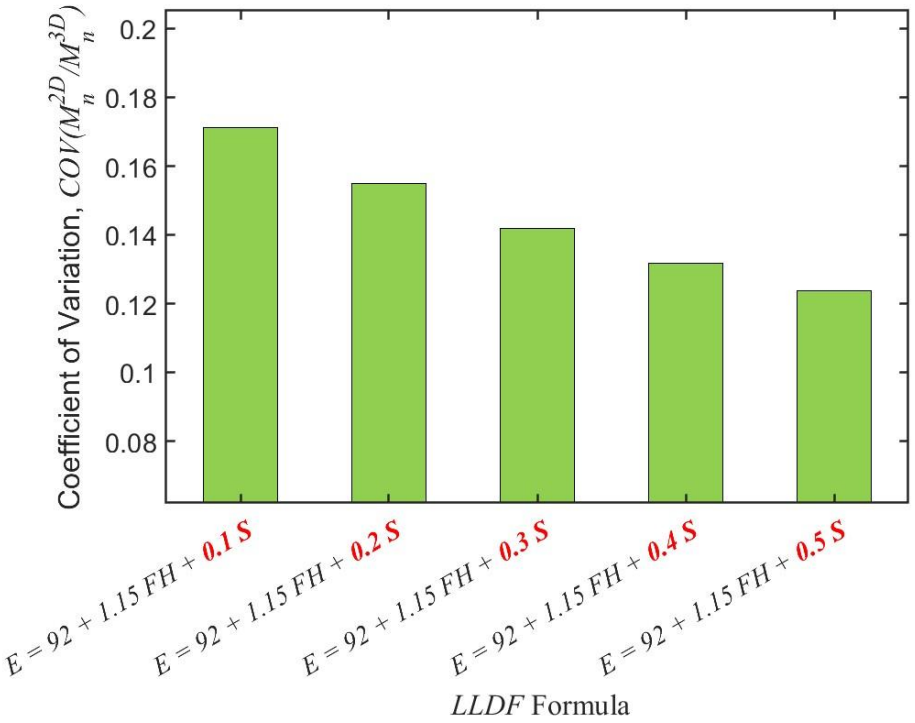

Figure 48. Trend of interior positive moment bias $\lambda_{MpI,avg}$ for different secondary distributions coefficients, η

(a)

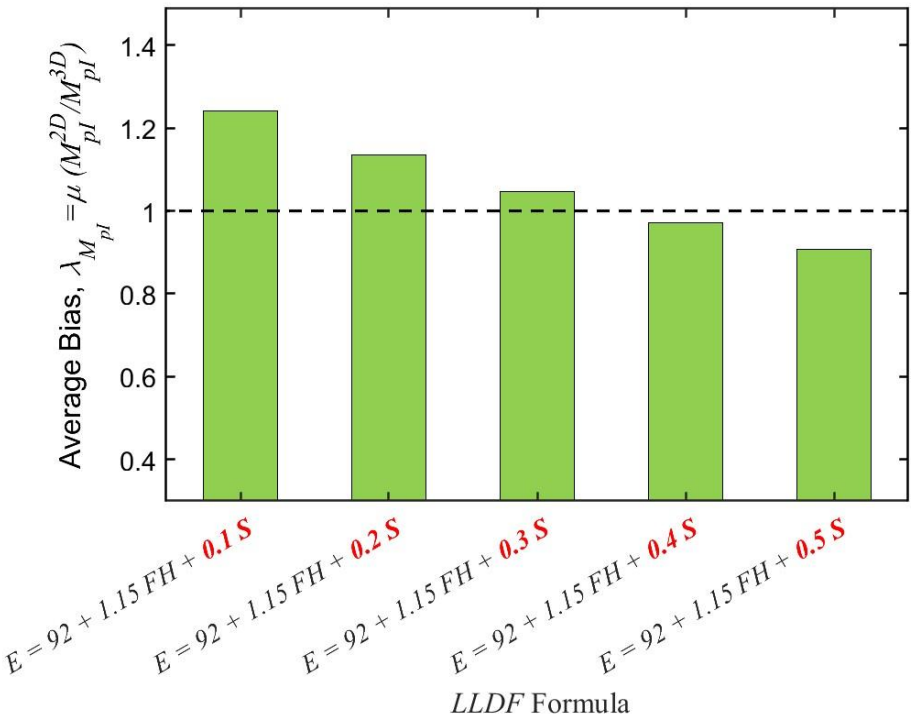

(b)

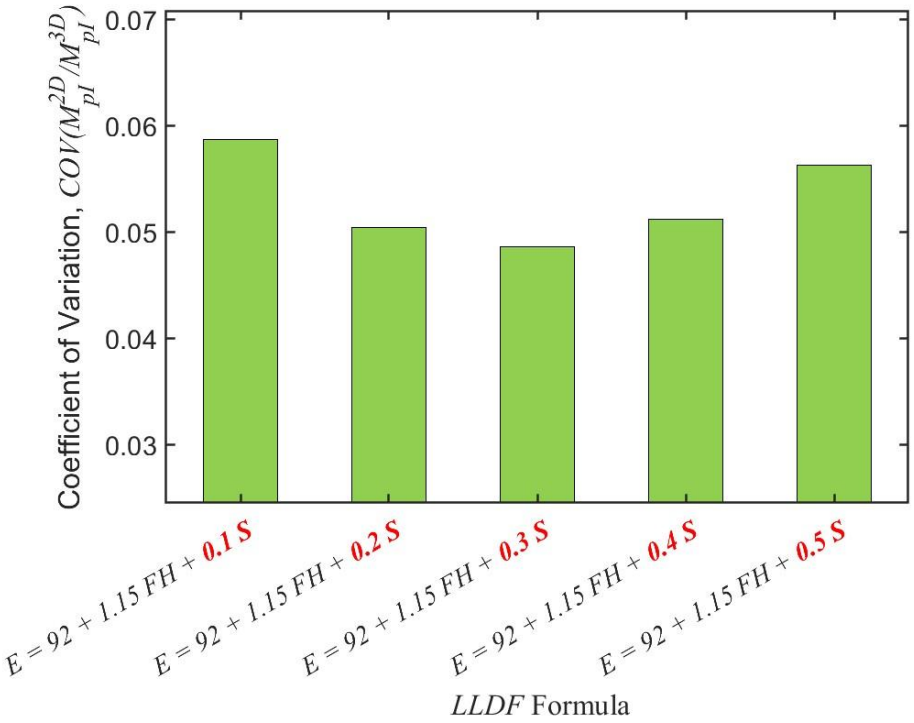

Comparisons between Predictions using Proposed Formula and AASHTO-LRFD BDS

In this section, comparisons are conducted between the predictions of the proposed formula and AASHTO-LRFD BDS formulas for wheel pressure distribution. In addition to the formulas adopted in AASHTO-LRFD BDS, another set of comparisons is presented using the recommendations of LTRC Project 16-3ST, in which rigid links were recommended in 2D models to reflect the rigid nature of the slab-wall connections [1]. Figure 49 shows the histograms of the bias (λ) for all straining actions extracted from the models analyzed in this study considering the three different live load distribution formulas (LLDF): AASHTO-LRFD BDS, modified AASHTO-LRFD BDS, and proposed formula (Equation [19]) with η value equal to 0.3. It can be seen that the average bias (dashed lines in individual figures) is closer to unity for the proposed formula for the positive moments (M_{pE} and M_{pI}). Furthermore, despite the lower bias values for the shear forces and negative moments V and M_n, it can be seen that the scatter is less when the proposed formula is used. These observations can be seen clearly in the comparisons of the bias (λ) and coefficient of variation (COV) in Figure 50 through Figure 53 for the biases of V, M_n, M_{pE} and M_{pI}, respectively. It is clear that the proposed formula results in coefficient of variations that are less than those obtained using AASHTO-LRFD BDS formula for all cases except for the bias for M_n, which is still close. As expected, the bias for shear forces and negative moments (V and M_n) are lower than 1.0, which is unconservative despite the lower scatter. This is due to the proposed formula emphasizing the positive moments (M_{pE} and M_{pI}). To remedy this deficiency, a multiplier coefficient can be used for the formula (ξ_{SA}) that reflects the type of straining action. In other words, ξ_{SA} would be equal to 1.0 for positive moments (M_{pE} and M_{pI}) and 0.6 for shear forces and negative moments (V and M_n).

Figure 49. Histogram of straining action bias obtained using different LLDF formulas

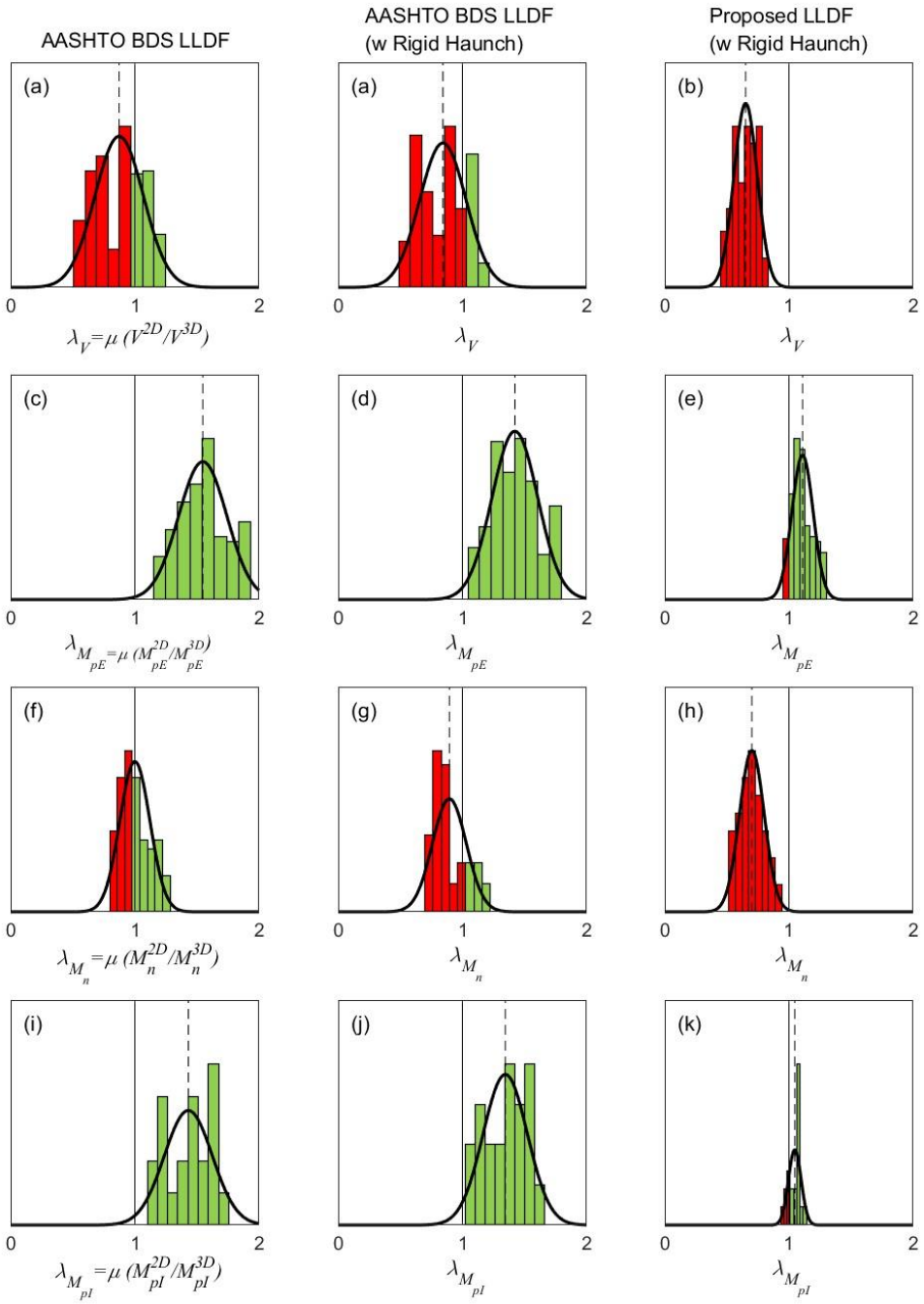

Figure 50. Trend of shear bias $\lambda_{V,avg}$ and COV for different LLDF formulas

(a)

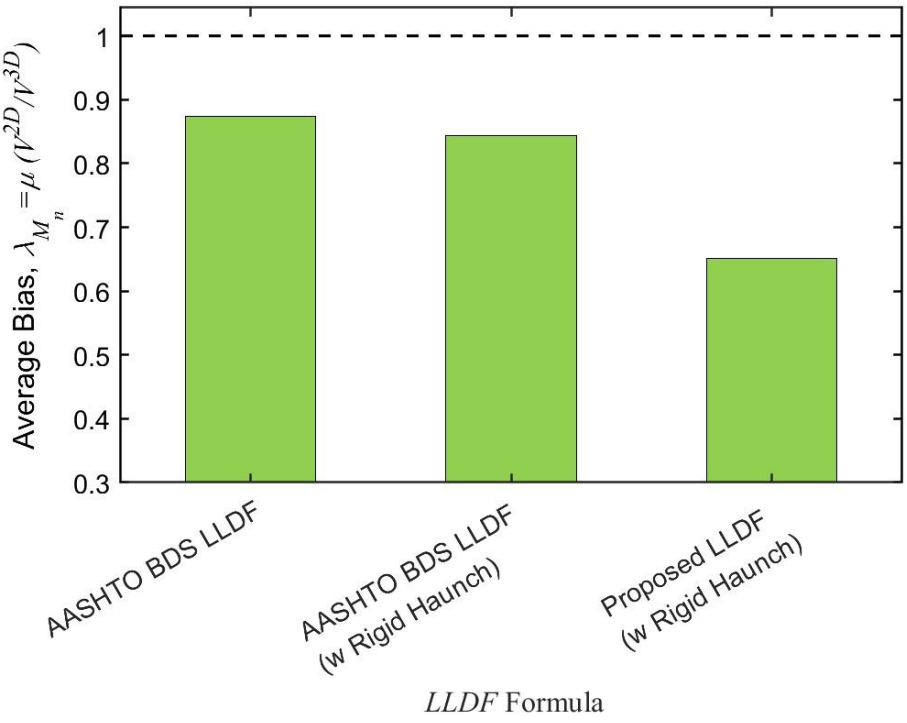

(b)

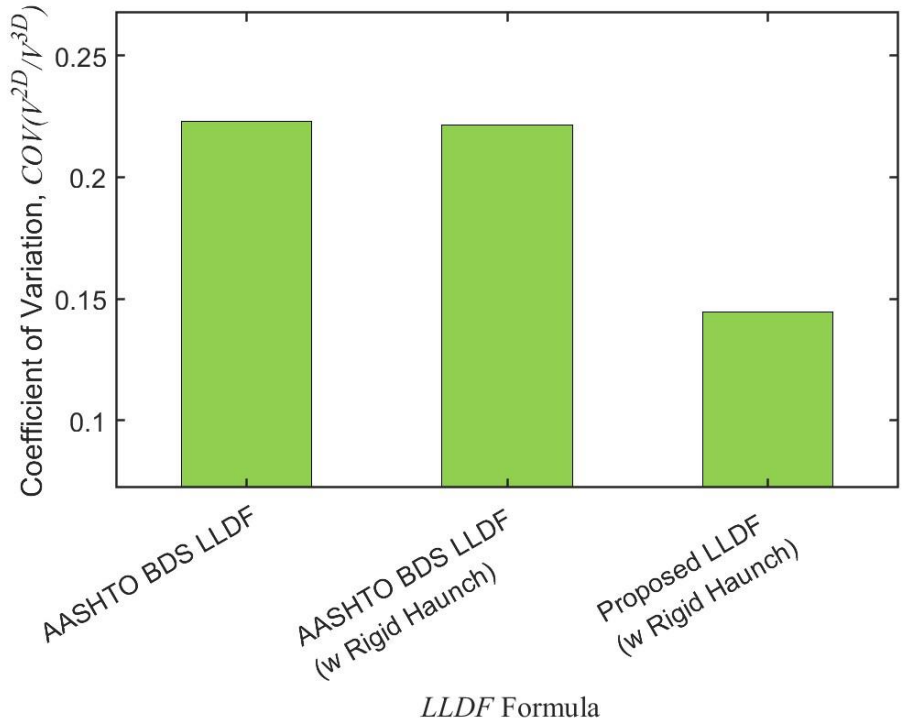

Figure 51. Trend of exterior positive moment bias $\lambda_{MpE,avg}$ and COV different LLDF formulas

(a)

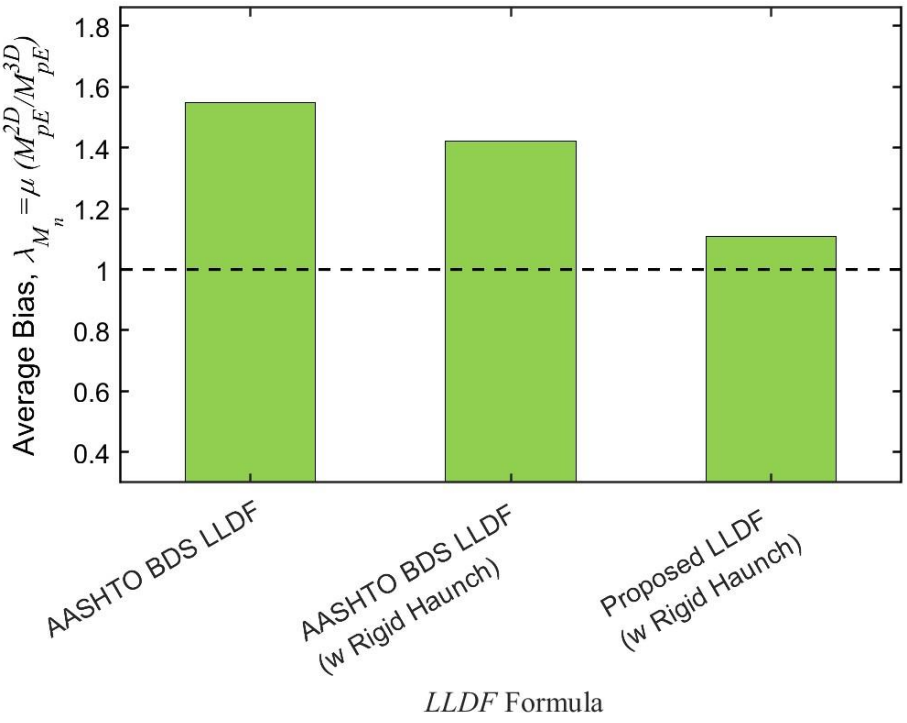

(b)

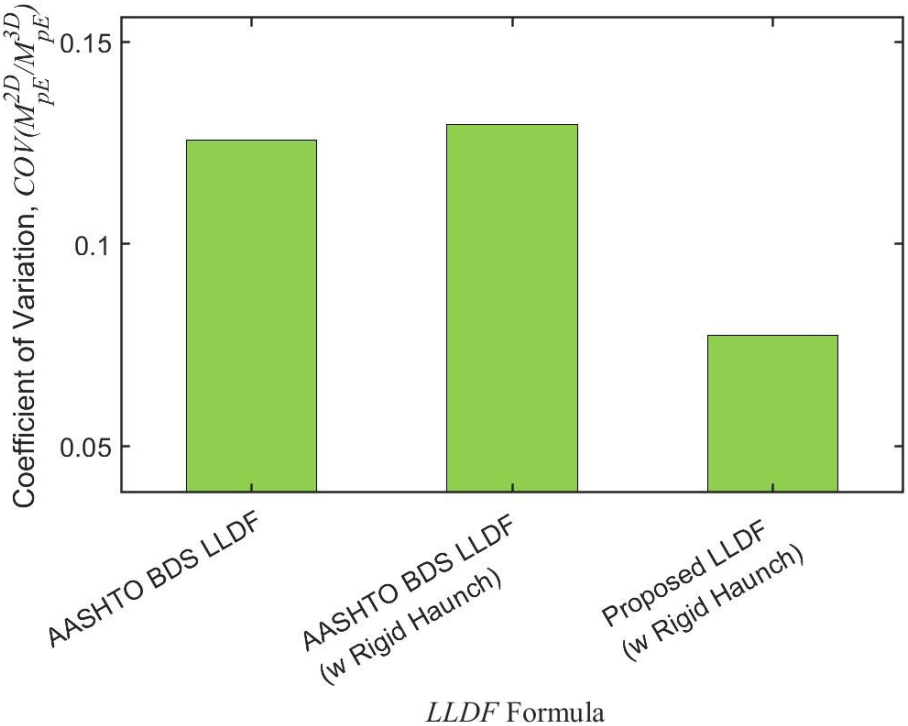

Figure 52. Trend of negative moment bias $\lambda_{Mn,avg}$ and COV different LLDF formulas

(a)

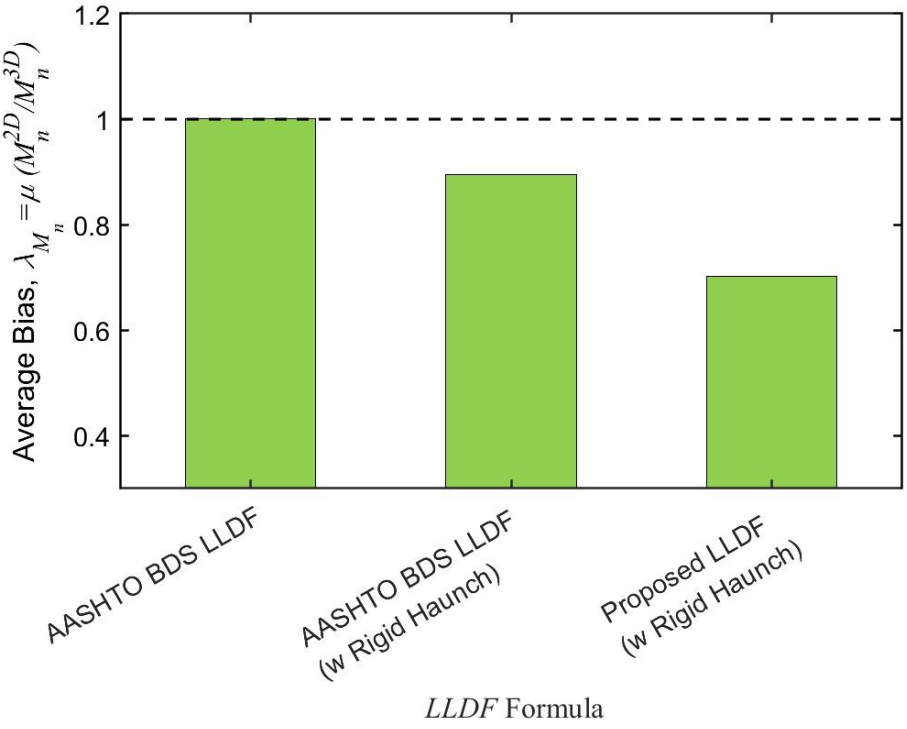

(b)

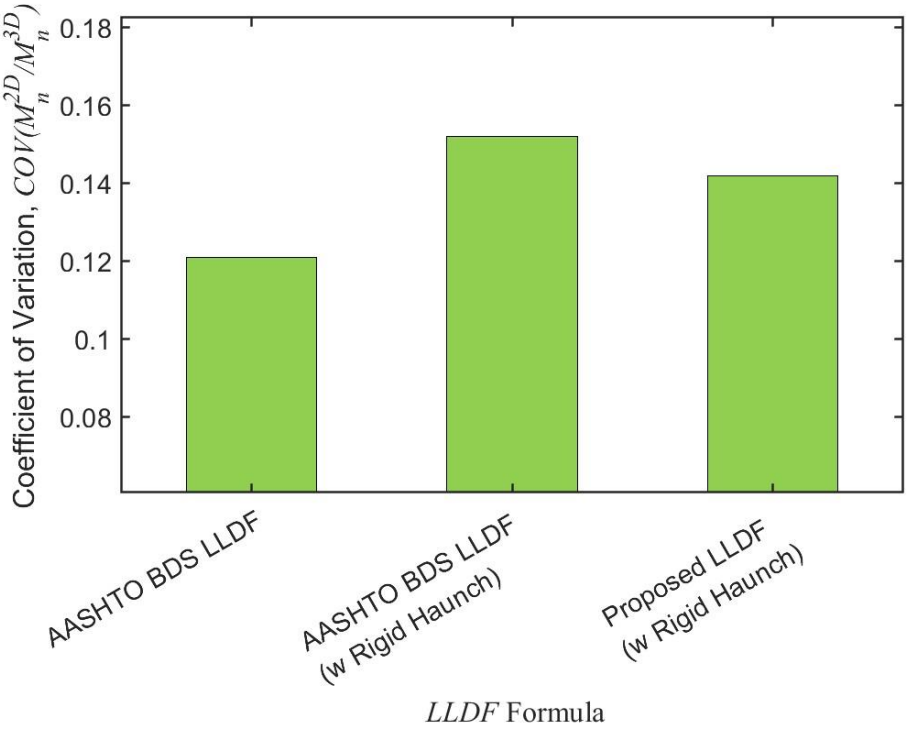

Figure 53. Trend of interior positive moment bias $\lambda_{Mpl,avg}$ different LLDF formulas

(a)

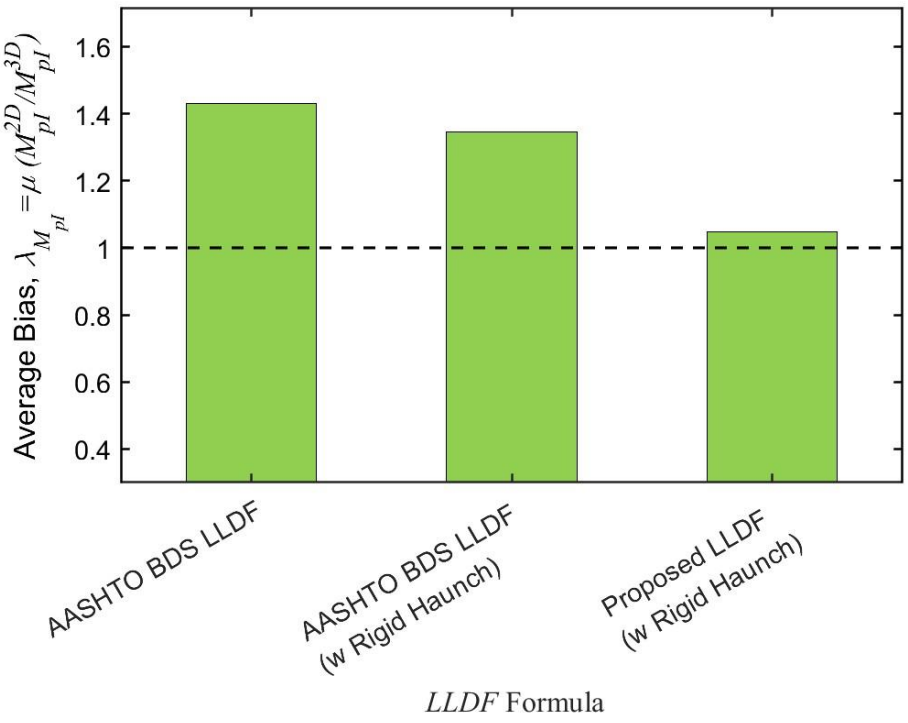

(b)

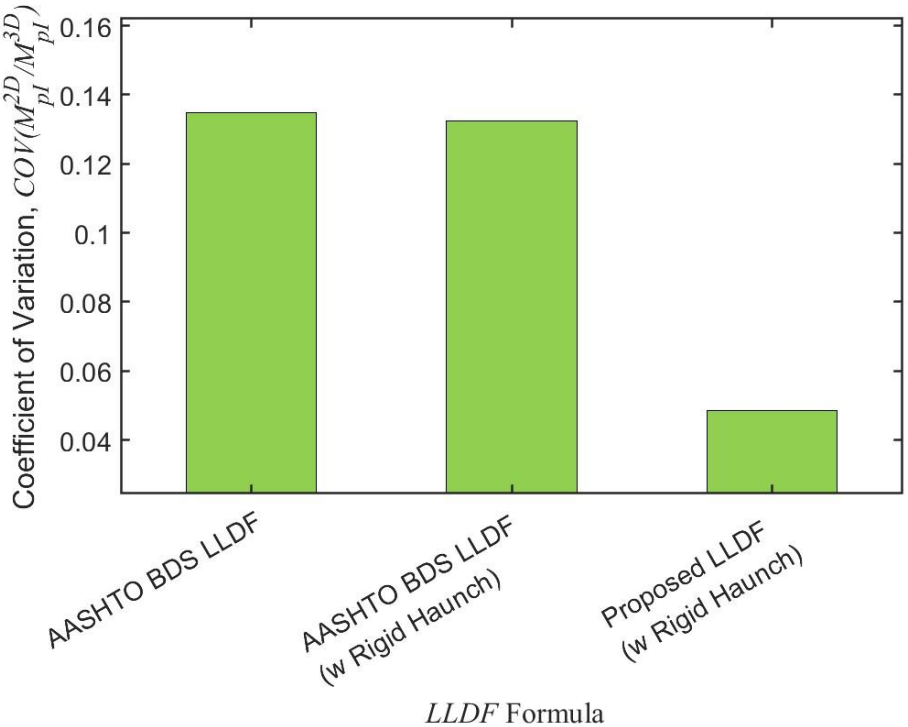

The previous figures are based on all results from the parametric study including 1-, 2-, and 3-barrels. To study the accuracy of the predictions for each group of cases, Figure 54, Figure 55, and Figure 56 are plotted for the 1-, 2-, and 3-barrel cases, respectively. It can be seen that the aforementioned observations hold true for all three groups. The proposed formula produces predictions with less scatter for all cases than AASHTO-LRFD BDS predictions. The average bias (λ) is clearly closer to 1.0 for positive moments (M_{pE} and M_{pI}) but not as close to 1.0 for the shear forces and negative moments (V and M_n).

Figure 54. Histogram of straining action bias obtained using different LLDF formulas (1-barrel cases)

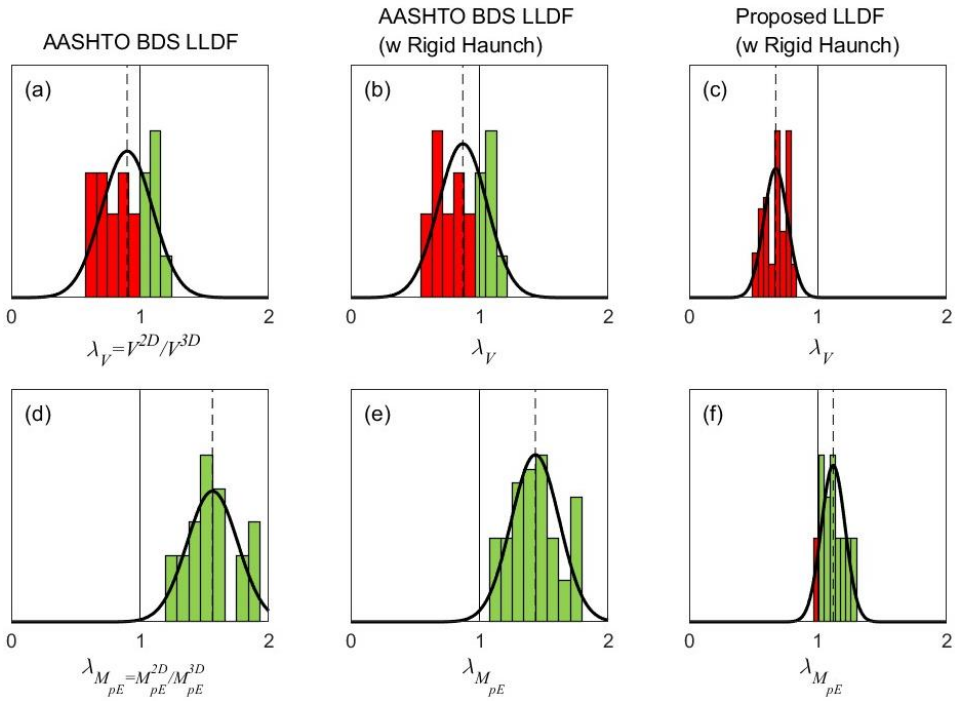

Figure 55. Histogram of straining action bias obtained using different LLDF formulas (2-barrel cases)

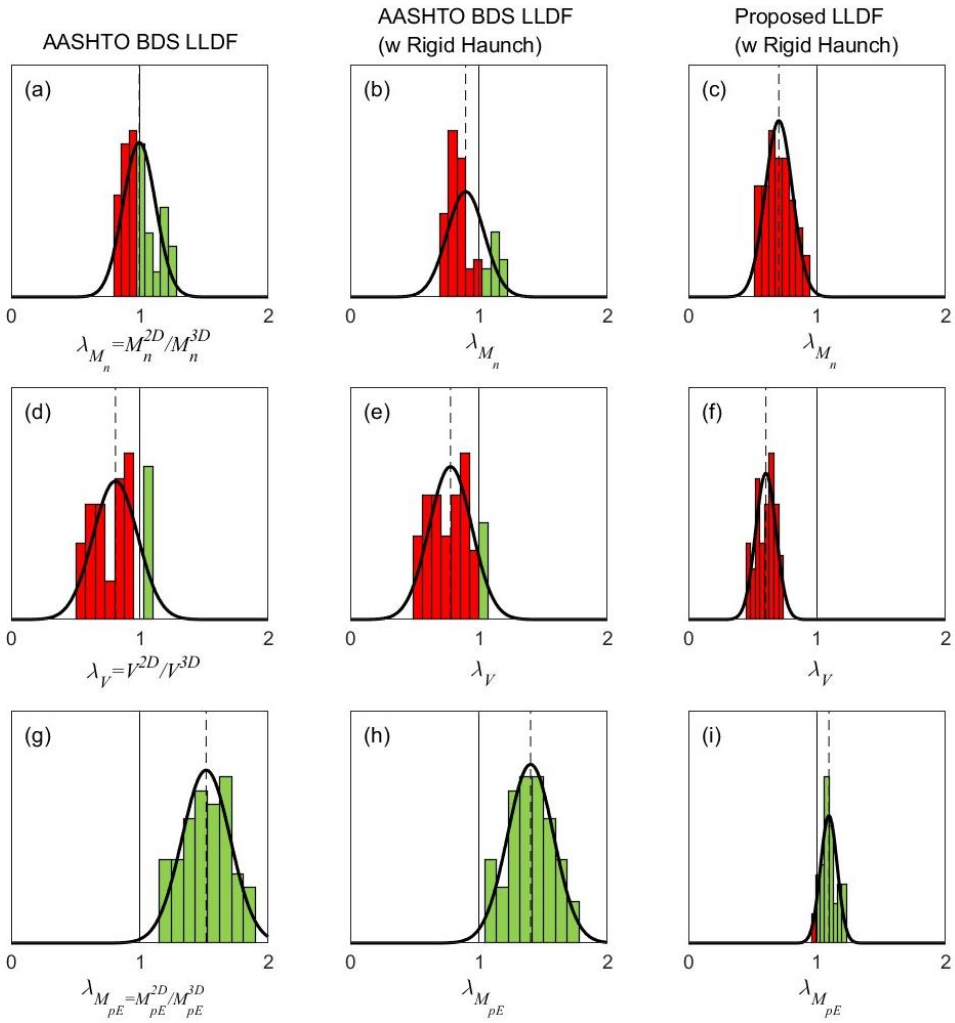

Figure 56. Histogram of straining action bias obtained using different LLDF formulas (3-barrel cases)

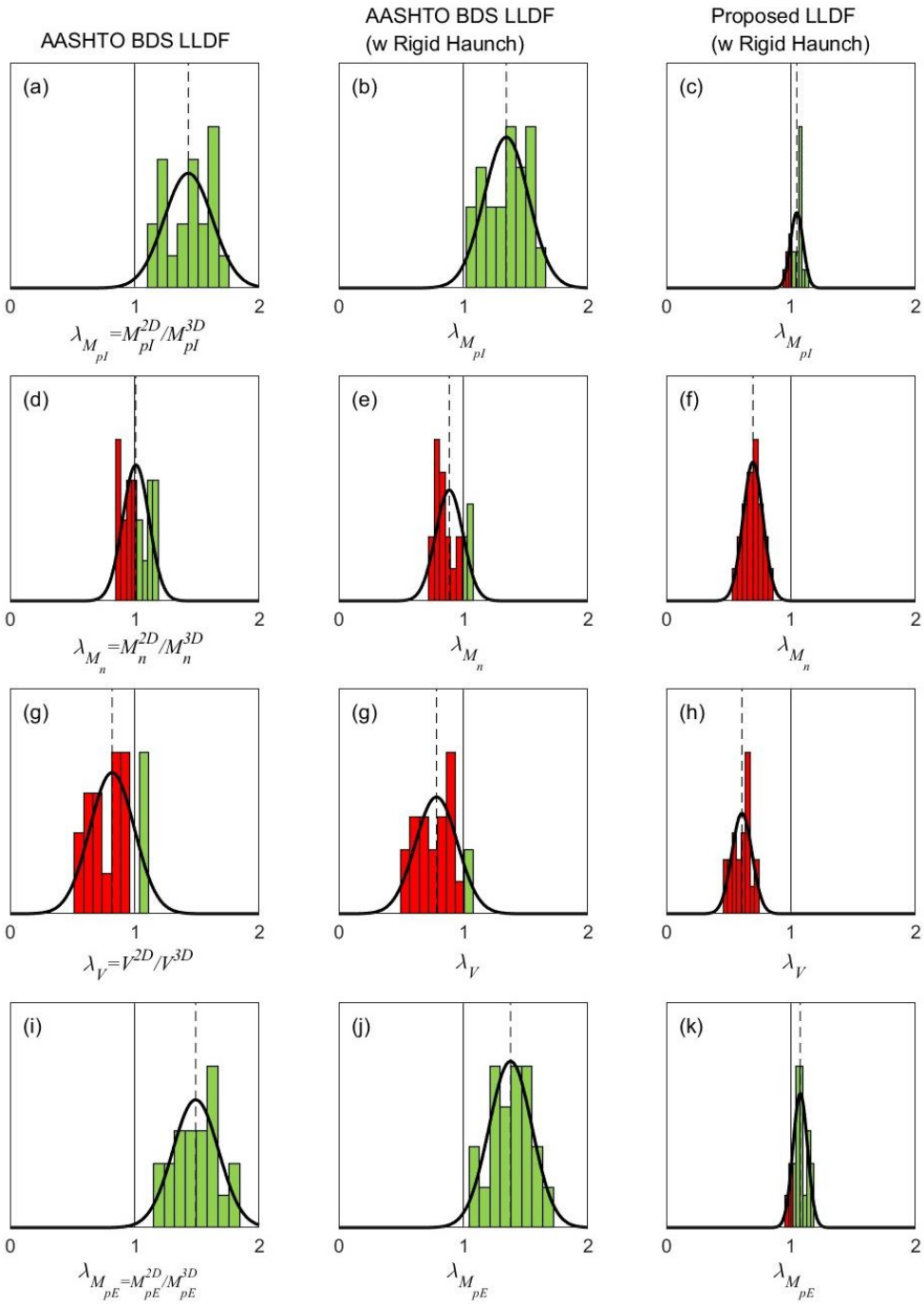

Proposed Formula

Based on the above discussions, it is proposed that the following formula be used to distribute wheel loads in the direction perpendicular to traffic:

$$E = \xi_{SA}(92 + 1.15\,H + 0.3\,S) \quad [20]$$

Where, ξ_{SA} is a straining action coefficient equal to 1.0 for positive moment sections (M_{pE} and M_{pI}) and equal to 0.6 for shear and negative moment sections (V and M_n). This formula is evaluated in the next section using a structural reliability criterion to ensure that it conforms to AASHTO-LRFD BDS safety levels. It is also be compared with AASHTO-LRFD BDS LLDF formula (Equation [17]).

For the sake of comparison between the proposed formula (Equation [20]) and AASHTO's LLDF formula (Equation [17]), a culvert with a span length equal to 10 ft. with fill depths equal to 0 ft., 1 ft., and 2 ft. are considered. Both methods use the same formula in the direction perpendicular to traffic (Equation [16]), and therefore are not evaluated. For the case of a fill depth equal to 0 ft., Equation [17] results in the following distribution width perpendicular to traffic:

$$E = 96 + 1.44\,S$$

$$= 96(\text{in.}) + 1.44 \times 10(\text{ft}) = 110.4\ \text{in.}$$

The proposed formula, on the other hand, produces the following distribution width for positive moments:

$$E = \xi_{SA}(92 + 1.15\,H + 0.3\,S)$$

$$= 1.0 \times [92(\text{in.}) + 1.15 \times 0(\text{in.}) + 0.3 \times 10(\text{ft}) \times 12(\text{in./ft.})]$$

$$= 128\ \text{in.}$$

and the following width for shear force and negative moments:

$$E = 0.6 \times [92 + 1.15 \times 0(\text{in.}) + 0.3 \times 10(\text{ft}) \times 12(\text{in./ft}.)]$$

$$= 76.8\ \text{in.}$$

The corresponding values for fill depths equal to 1 ft. and 2 ft. can be found in Table 6.

Table 6. Comparison of distribution width predictions

Fill Depth	AASHTO-LRFD BDS Equation [17] (in.)	Proposed Formula Equation [20] (in.)		Difference (%)
	M_{pE}, M_{pI}, V and M_n	M_{pE} and M_{pI}	V and M_n	
0	110.4	128.0	76.8	+15.9% and −30.4%
1	110.4	141.8	85.1	+28.4% and −22.9%
2	110.4	155.6	93.4	+40.9% and −15.4%

Reliability Assessment of Live Load Distribution Formulas

Reliability Evaluation

Reliability index (β) values were evaluated for all 273 culverts considered in this study. It was evaluated for both AASHTO-LRFD BDS LLDF formula (Equation [17]) and for the proposed LLDF formula (Equation [17]) from the current study. Figure 57 shows a plot of these results for AASHTO-LRFD BDS LLDF formula (Equation [17]). The four plots are for the following straining actions: shear force (V) positive moment in exterior span (M_{pE}) negative moment (M_n) and positive moment in interior span (M_{pI}) (refer to Figure 15 for the corresponding locations). It should be noted that for shear forces and negative moments, the minimum (i.e., critical) value of the two β-values to the left (V_{nl} or M_{nl}) and to the right (V_{nr} or M_{nr}) of the interior support was selected. Figure 58 shows the same plots for the cases evaluated using the proposed LLDF formula (Equation [20]).

It can be seen from the results in Figure 57 that AASHTO-LRFD BDS LLDF formula is both inconsistent and in some cases unconservative. Specifically, the AASHTO-LRFD BDS LLDF formula produces highly conservative β-values for positive moment sections (M_{pE} and M_{pI}, $\beta \gg 3.5$), whereas it produces β-values that are scattered around 3.5 for sections close to the support (V and M_n). This scatter includes many cases where $\beta \gg 3.5$ for V and M_n critical sections. In addition to not conforming to AASHTO-LRFD's target reliability index (β_{target}) it introduces an inconsistency in culverts designed or load rated using this LLDF formula.

Conversely, Figure 58 shows a more consistent distribution of β-values for all straining actions considered in this study. For all positive and negative moments considered in this study (M_{pE}, M_n and M_{pI}), β-values are consistently at or slightly above AASHTO-LRFD's target reliability index (β_{target}) of 3.5. Furthermore, β-values for the shear force (V) were consistently above β_{target}. The higher scatter in β-values for shear forces is attributed to the inherently higher variability of our ability to predict shear resistance, as reflected by a COV of 10% compared to only 6% for flexure. Furthermore, shear forces occur due to either one axle or two axles, with one of them close to the supporting wall. Therefore, the secondary distribution offered by the top slab should reflect two distribution widths, one for each axle, which is not easily implemented in an empirical formulation. The other straining actions are typically controlled by one axle position (two for negative moment, with one on each span) that are farther away from the supporting wall. Therefore, the secondary distribution width is more consistent in these cases and contributes to the superior performance of the proposed LLDF formula.

In summary, using the proposed LLDF formula results in more consistent predictions of straining actions for design and load rating of culverts. The benefits of using the proposed formula include removing unnecessary conservatism for positive moment straining actions (M_{pE} and M_{pI}) while at the same time greatly reducing the inconsistency of results for negative moments (V and M_n) and reducing the inconsistency of results for shear forces albeit to a lesser extent. In all cases, the proposed LLDF formula conforms to AASHTO-LRFD's target reliability index (β_{target}) of 3.5.

Figure 57. Reliability index, β, values at different sections (AASHTO-LRFD BDS)

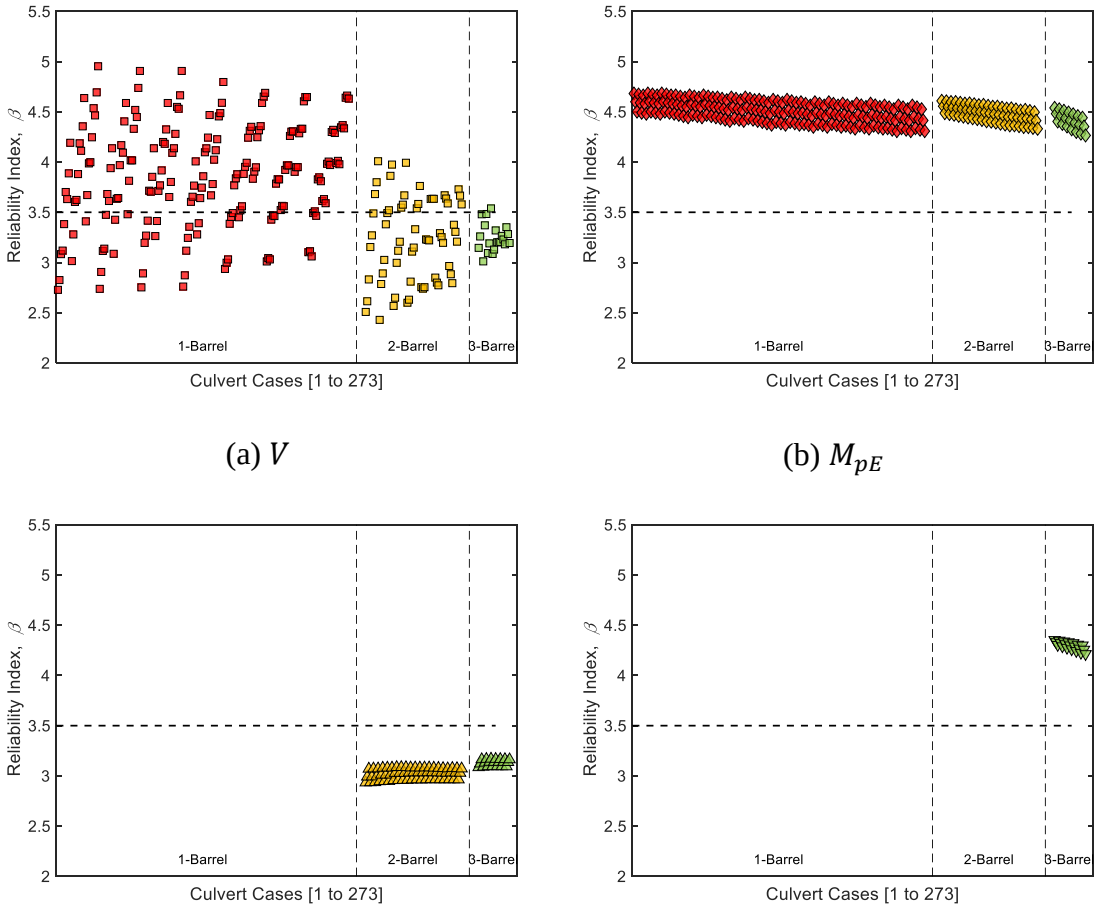

(a) V

(b) M_{pE}

(c) M_n

(d) M_{pI}

Figure 58. Reliability index, β, values at different sections (Proposed LLDF formula)

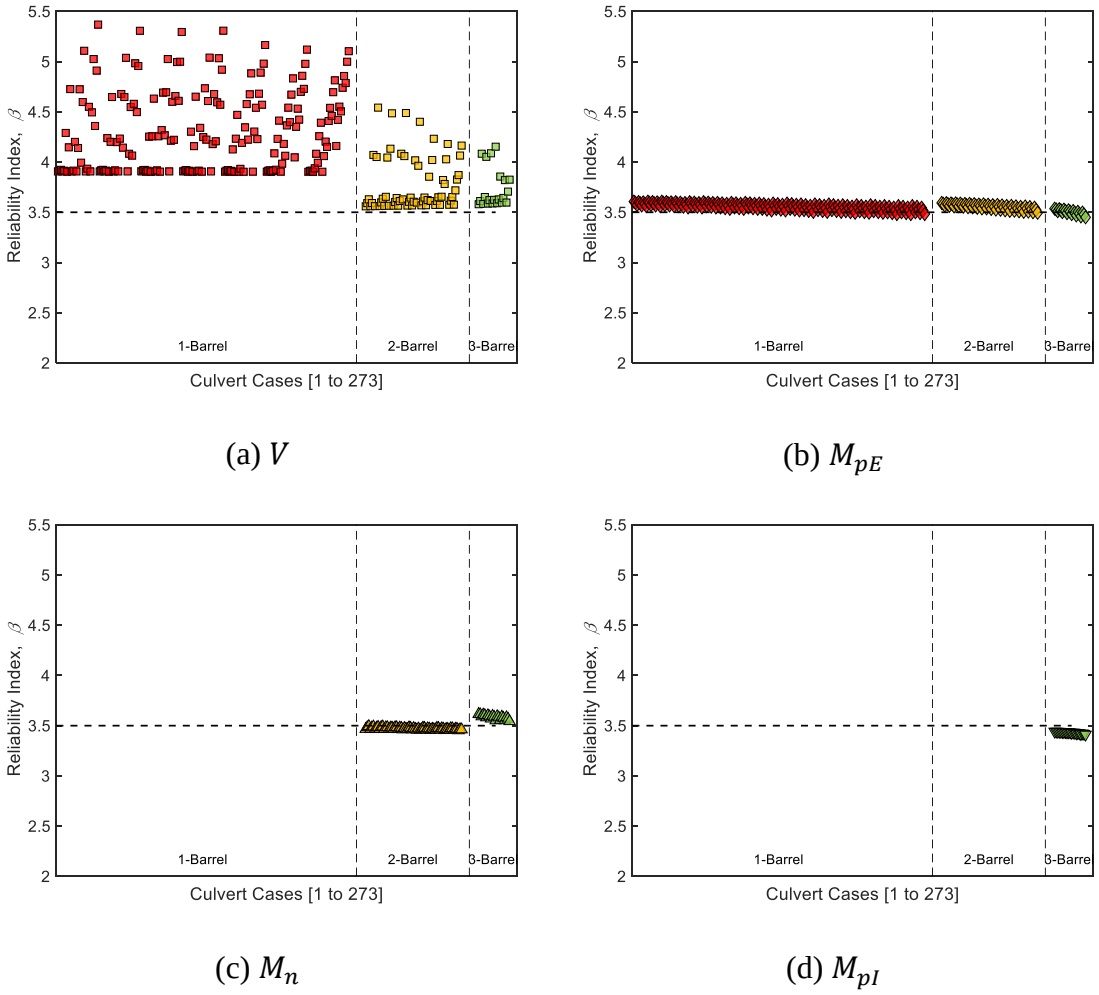

(a) V (b) M_{pE}

(c) M_n (d) M_{pI}

Application of Proposed LLDF Formula on Sample Culverts

In this section, the proposed LLDF formula is used in the load rating of two culverts that were selected to represent a small span (6 ft.) culvert and a long span (10 ft.) culvert. For both cases, straining actions are obtained using 2-D models loaded with wheel load pressures obtained using the proposed LLDF formula.

Figure 59. FE meshes for selected culverts: (a) 3-barrel 10 ft. × 7 ft., (b) 2-barrel 6 ft. × 4 ft.

(a)

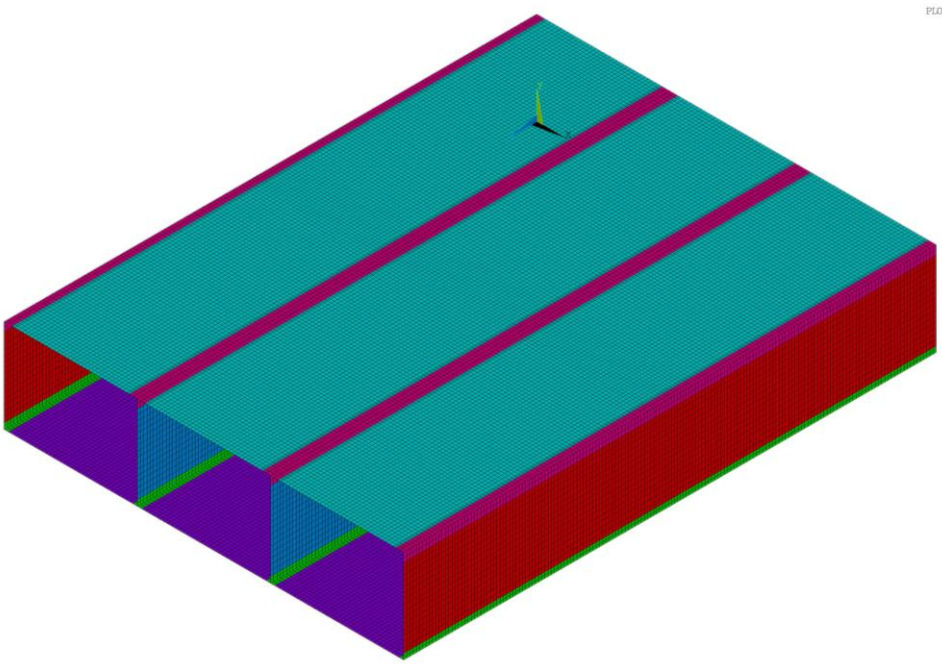

(b)

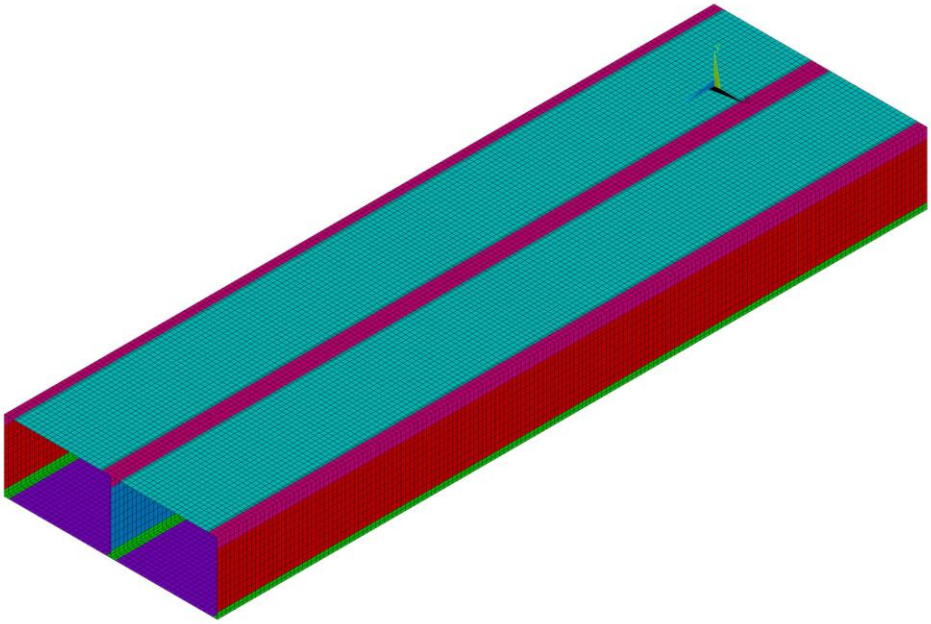

Culvert Case #1 ($S = 10$ ft.)

This 3-barrel culvert was selected to have non-square barrel openings to test the applicability of the proposed LLDF for configurations different than those used in its development. The rectangular barrel opening is 10 ft. × 7 ft., and the dimensions of the slabs (10 in.) and walls (8 in.) were selected from DOTD standards (CCSM10R90_1). It was analyzed for three fill heights (0 ft., 1 ft., and 2 ft.) using the 2D model described

twice in this report. The first set of results came from a model in which wheel load pressures were applied based on AASHTO LLDF, while the second set of results was for the 2D model with wheel load pressures based on the proposed LLDF. Table 7 lists the distribution widths used in the 2D model analysis, which are identical to the values demonstrated earlier (see Table 6) because both culverts had a barrel width equal to 10 ft. even though there is a difference in barrel height.

Table 7. Distribution widths for Culvert Case #1

Fill Depth	AASHTO-LRFD BDS Equation [17] (in.)	Proposed Formula Equation [20] (in.)	
	M_{pE}, M_{pI}, V and M_n	M_{pE} and M_{pI}	V and M_n
0	110.4	128.0	76.8
1		141.8	85.1
2		155.6	93.4

Table 8 lists the straining action predictions obtained using both 2D models, in addition to those obtained using the more accurate 3D model. The 3D model predictions were obtained to serve as a reference for comparing both 2D model results. Table 9 shows the differences between the 2D model and the 3D model predictions. It can be seen that AASHTO LLDF produces overly conservative positive moment predictions that reach 64% over those obtained using the 3D model. Furthermore, shear forces and negative moments are unconservative, consistently underpredicted by up to –40% for shear forces and –20% for negative moments. Conversely, the proposed LLDF produced conservative results consistently, with overpredictions equal to 13% on average, with a maximum conservative prediction of 30.7% and a maximum unconservative prediction of –14.6%.

Figure 60 illustrates the improvements that the proposed LLDF introduces to CIP-RC box culvert analysis using 2D models.

Table 8. Predictions of live load straining actions using 3D shell model, AASHTO LLDF, and proposed LLDF for Culvert Case #1

FH (ft)	3D Model Results						2D Model Results (AASHTO LLDF)						2D Model Results (Proposed LLDF)					
	M_{pE}	V_L	V_R	M_{nL}	M_{nR}	M_{pI}	M_{pE}	V_L	V_R	M_{nL}	M_{nR}	M_{pI}	M_{pE}	V_L	V_R	M_{nL}	M_{nR}	M_{pI}
0	-4536	-549.5	-531.7	4894	-4025	-3760	-5912	-348.4	-317.9	3886	-3304	-4770	-4919	-502.9	-454.1	6276	-5121	-3878
1	-3667	-384.0	-338.5	4592	-3643	-2935	-5450	-323.1	-290.1	3772	-3233	-4390	-4085	-421.7	-373.9	5509	-4524	-3210
2	-3123	-285.3	-226.4	4170	-3211	-2419	-5036	-285.9	-252.2	3577	-3107	-3967	-3401	-340.6	-295.9	4755	-3964	-2632

Units: lb./in. for shear; lb.-in./in. for bending moment

Table 9. Comparison of straining action predictions for Culvert Case #1 w.r.t. 3D model predictions

FH (ft)	Difference (AASHTO LRFD – Equation [17])						Difference (Proposed LLDF – Equation [20])					
	M_{pE}	V_L	V_R	M_{nL}	M_{nR}	M_{pI}	M_{pE}	V_L	V_R	M_{nL}	M_{nR}	M_{pI}
0	30.3%	**-36.6%**	**-40.2%**	**-20.6%**	**-17.9%**	26.9%	8.5%	**-8.5%**	**-14.6%**	28.2%	27.2%	3.1%
1	48.6%	**-15.9%**	**-14.3%**	**-17.9%**	**-11.3%**	49.6%	11.4%	9.8%	10.4%	20.0%	24.2%	9.4%
2	61.2%	0.2%	11.4%	**-14.2%**	**-3.2%**	64.0%	8.9%	19.4%	30.7%	14.0%	23.4%	8.8%

Figure 60. Plot of errors in straining action predictions for (a) AASHTO LLDF, and (b) Proposed LLDF for Culvert Case #1.

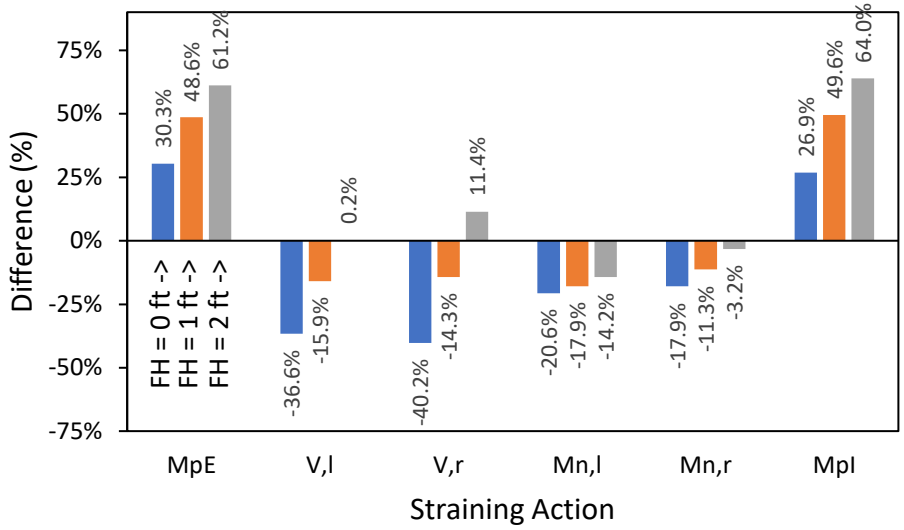

(a) AASHTO LLDF

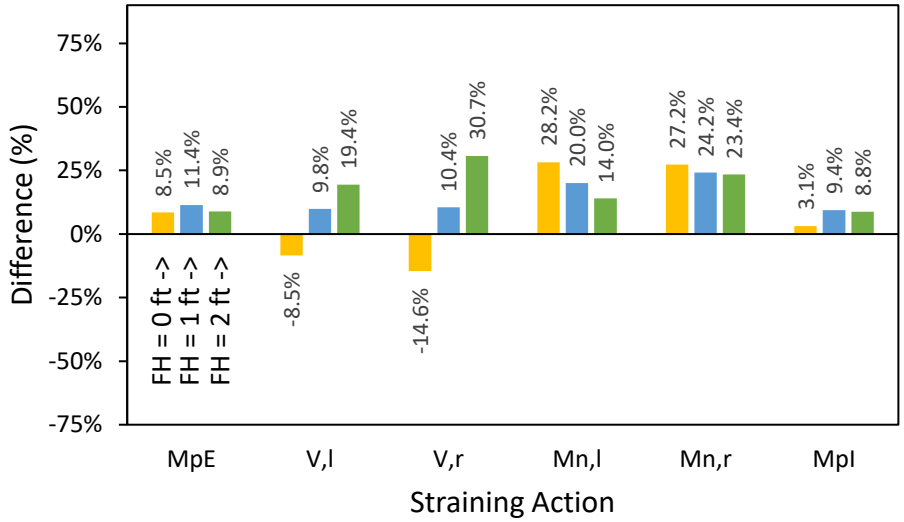

(b) Proposed LLDF

Culvert Case #2 ($S = 6$ ft.)

This 2-barrel culvert was also selected to have non-square barrel openings (6 ft. × 4 ft.), and the dimensions of the slabs (8 in.) and walls (6 in.) were selected from DOTD standards (CCSM6R90_1). It was analyzed for three fill heights (0 ft., 1 ft., and 2 ft.) using the 2D model, with wheel load pressures applied based both on AASHTO-LLDF

and the proposed LLDF. Table 7 lists the distribution widths used in the 2D model analysis.

Table 10. Distribution widths for Culvert Case #2

Fill Depth	AASHTO-LRFD BDS Equation [17] (in.)	Proposed Formula Equation [20] (in.)	
	M_{pE}, M_{pI}, V and M_n	M_{pE} and M_{pI}	V and M_n
0	104.6	113.6	68.2
1		127.4	76.4
2		141.2	84.7

Table 11 lists the three sets of straining action predictions obtained using both 2D models and the 3D model. Table 12 shows the differences between the 2D model and the 3D model predictions. It can be seen that AASHTO-LLDF produces overly conservative positive moment predictions that reach 37.9% over those obtained using the 3D model. Furthermore, shear forces and negative moments are unconservative, consistently underpredicted by up to –50.0% for shear forces and –27.7% for negative moments. Conversely, the proposed LLDF produced conservative results consistently, with overpredictions averaging 1.1%, with a maximum conservative prediction of 29.2% and a maximum unconservative prediction of –23.8% for shear and –4.7% for positive moments.

Figure 61 illustrates the improvements that the proposed LLDF introduces to CIP-RC box culvert analysis using 2D models.

Table 11. Predictions of live load straining actions using 3D shell model, AASHTO LLDF, and proposed LLDF for Culvert Case #2

FH (ft.)	3D Model Results					2D Model Results (AASHTO LLDF)					2D Model Results (Proposed LLDF)				
	M_{pE}	V_L	V_R	M_{nL}	M_{nR}	M_{pE}	V_L	V_R	M_{nL}	M_{nR}	M_{pE}	V_L	V_R	M_{nL}	M_{nR}
0	-3236	-548.3	-548.3	2987	-2987	-3372	-273.9	-273.9	2532	-2532	-3084	-417.7	-417.7	3860	-3860
1	-2344	-372.1	-372.1	2586	-2586	-2894	-248.7	-248.7	2359	-2285	-2361	-338.0	-338.0	3207	-3106
2	-1767	-256.0	-256.0	2156	-2156	-2437	-213.9	-213.9	1560	-1560	-1793	-262.4	-262.4	1913	-1913

Units: lb./in. for shear; lb.-in./in. for bending moment

Table 12. Comparison of straining action predictions for Culvert Case #2 w.r.t. 3D model predictions

FH (ft.)	Difference (AASHTO LRFD – Equation [17])					Difference (Proposed LLDF – Equation [20])				
	M_{pE}	V_L	V_R	M_{nL}	M_{nR}	M_{pE}	V_L	V_R	M_{nL}	M_{nR}
0	4.2%	**-50.0%**	**-50.0%**	**-15.3%**	**-15.3%**	**-4.7%**	**-23.8%**	**-23.8%**	29.2%	29.2%
1	23.5%	**-33.2%**	**-33.2%**	**-8.8%**	**-11.6%**	0.7%	**-9.1%**	**-9.1%**	24.1%	20.1%
2	37.9%	**-16.5%**	**-16.5%**	**-27.7%**	**-27.7%**	1.5%	2.5%	2.5%	**-11.3%**	**-11.3%**

Figure 61. Plot of errors in straining action predictions for (a) AASHTO LLDF, and (b) Proposed LLDF for Culvert Case #2.

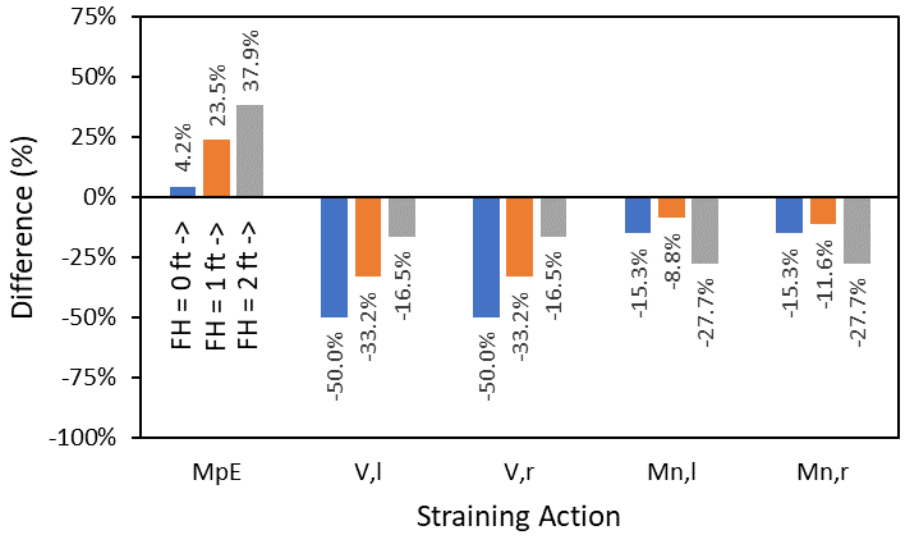

(a) AASHTO LLDF

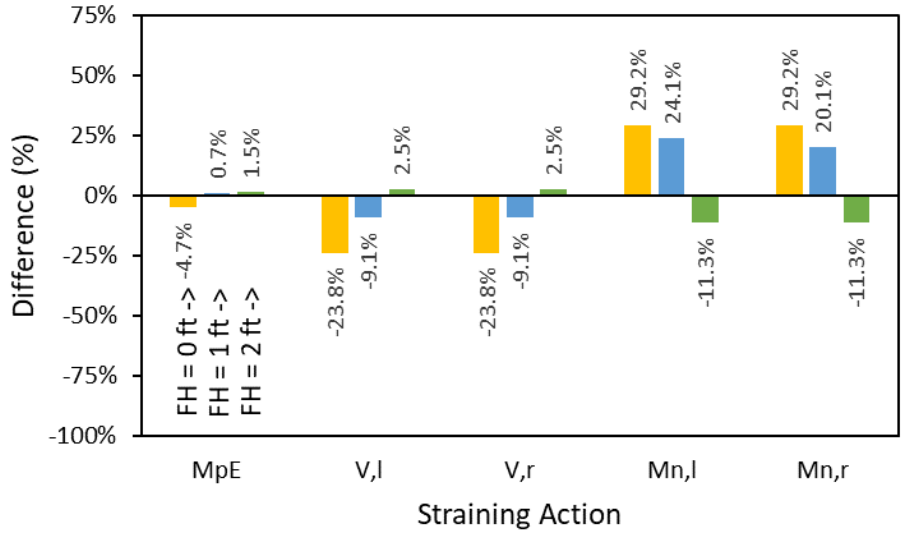

(b) Proposed LLDF

Conclusions

Current Practice

The design and load rating of cast-in-place (CIP) reinforced concrete (RC) box culverts is currently performed using an empirical live load distribution (LLDF) formula to distribute truck wheel loads through earth fill onto the top slab of the culvert, using American Association of State Highway and Transportation Officials (AASHTO) Bridge Design Specifications (BDS). Following this procedure has resulted in challenges to designers all over the country. In Louisiana, this is exacerbated by an old detail that was used for the construction of many culverts that are currently in service. The old detail does not call for top (negative) reinforcement in the outside corners, which releases negative moments in outside corners, and thus increases straining actions in other parts of the culverts. Field inspections have not revealed any distress as predicted by the AASHTO-LRFD BDS, and an earlier study (LTRC Project 16-3ST) on a limited number of culverts revealed that culverts perform well under service conditions despite AASHTO-LRFD BDS data to the contrary.

Project Findings

Based on an extensive parametric study considering 273 culvert configurations covering key parameters known to influence culvert behavior, the following conclusions can be drawn. By comparing results from refined analysis, this study confirms that AASHTO-LRFD BDS predictions using Equation [16] and [17] are inconsistent; they are highly conservative for positive moment starting actions and sometimes unconservative for shear forces and negative moments. Therefore, a new LLDF formula is proposed for predicting straining actions of CIP-RC culverts with Louisiana old details (i.e., those with no top (negative) reinforcement in the outside corners). The proposed formula (Equation [20]) for distributing the wheel load in the direction perpendicular to traffic, along with AASHTO-LRFD BDS Equation [16] for distributing the wheel load in the longitudinal direction, were also used to predict the straining actions. Based on these predictions, a reliability study was conducted to investigate the performance of both LLFD formulas, revealing the following:

- Using the proposed LLDF formula results in more consistent predictions of straining actions for design and load rating of culverts by removing unnecessary conservatism for positive moment straining actions (M_{pE} and M_{pI}) while at the

same time greatly reducing the inconsistency of results for negative moments (V and M_n) and reducing the inconsistency of results for shear forces, albeit to a lesser extent.

- Unlike AASHTO-LRFD BDS LLDF formula, which produces a wide range of reliability index (β) values, including some cases where β is less than β_{target} of 3.5, all predictions using the proposed LLDF formula meet or exceed this β_{target}, and thus conform to AASHTO-LRFD's target safety level.

Recommendations

Based on the findings of this project, the research team recommends the adoption of the proposed formula (Equation [20]) for distributing the wheel load in the direction perpendicular to traffic, along with AASHTO-LRFD BDS Equation [16] for distributing the wheel load in the longitudinal direction for the design and load rating or cast-in-place (CIP) reinforced concrete (RC) box culverts.

$$E = \xi_{SA}(92 + 1.15\,H + 0.3\,S) \quad [20]$$

Where, H is the fill height in inches, S is the barrel span length in inches, and ξ_{SA} is a straining action coefficient equal to 1.0 for positive moment sections (M_{pE} and M_{pI}) and equal to 0.6 for shear and negative moment sections (V and M_n) In the longitudinal direction, it is recommended that the AASHTO-LRFD DBS distribution formula (Equation [16]) be used.

$$E_{span} = L_T + LLDF(H) \quad [16]$$

If the load rating of any culverts does not produce acceptable results, and load posting would be necessary, it is recommended that refined analyses be used while taking advantage of the modeling recommendations from Project 16-3ST [1].

Acronyms, Abbreviations, and Symbols

Term	Description
DOTD	Louisiana Department of Transportation and Development
HWA	Federal Highway Administration
ft.	foot (feet)
in.	inch(es)
LTRC	Louisiana Transportation Research Center
lb.	pound(s)
$COV(X)$	Coefficient of variation of random variable X
E	Distribution width perpendicular to the span (in.)
E_{span}	Distribution width parallel to the span (in.)
H	Depth of fill from top of culvert to top of pavement (in.)
L_T	Length of tire contact area parallel to the span (in.)
$LLDF$	Factor for distribution of live load (1.15 for this study)
Q_{DC}	Random load demand due to component dead loads
Q_{DW}	Random load demand due to wearing surface dead loads
Q_{EF}	Random load demand due to weight of earth fill
Q_{LL+IM}	Random load demand due to live loads plus impact
R_R	Random cross-sectional resistance
S	Clear span (ft for Equation [17] and in. for Equation [20])
η	Parameter for calibration of clear span length term in proposed formula
ξ_{LLDF}	Random variable representing variability due to LLDF formulas
ξ_{SA}	Straining action coefficient
λ_X	Bias of random variable X

References

[1] Okeil, A. M., Ulger, T., and Elshoura, A. "*Live Load Rating of Cast-in-Place Concrete Box Culverts.*" Report No. 593, Louisiana Transportation Research Center, Baton Rouge, LA, 2018.

[2] Federal Highway Administration. *National Bridge Inventory (NBI).* U.S. Department of Transportation. https://www.fhwa.dot.gov/bridge/nbi.cfm. Accessed 02/14/2019.

[3] Petersen, D. L., Nelson, C. R., Li, G., McGrath, T. J., and Kitane, Y. "*Recommended Design Specifications for Live Load Distribution to Buried Structures.*" Report No. National Cooperative Highway Research Program (NCHRP) Report No. 647, Washington, DC, 2010.

[4] AASHTO. *Standard Specifications for Highway Bridges*. American Association of State Highway and Transportation Officials, Washington, D.C., 2002.

[5] AASHTO. *LRFD Bridge Design Specifications*. American Association of State Highway and Transportation Officials, Washington, D.C., 2020.

[6] AASHTO. *Manual for Bridge Evaluation*. American Association of State Highway and Transportation Officials, Washington, D.C., 2018. p. 674.

[7] McGrath, T. J., Liepins, A. A., and Beaver, J. L. "Live Load Distribution Widths for Reinforced Concrete Box Section." *Journal of the Transportation Research Board*, 2005, pp. 99-108.

[8] Kinchen, R. W., Temple, W. H., and Lacinak, H. W. "*Evaluation of Drainage Pipe by field experimentation and supplemental laboratory experimentation.*" Report No. FHWA-LA-101 (Interim Report 1), Louisiana Transportation Research Center, Baton Rouge, LA, 1977.

[9] Kinchen, R. W., Temple, W. H., Lacinak, H. W., and Gueho, B. J. "*Evaluation of Drainage Pipe by field experimentation and supplemental laboratory experimentation.*" Report No. FHWA-LA-78-115 (Interim Report No. 2), Louisiana Transportation Research Center, Baton Rouge, LA, 1978.

[10] Temple, W. H., Rasoulian, M., and Gueho, B. J. "*Evaluation of Drainage Pipe by field experimentation and supplemental laboratory experimentation.*" Report No. 154 (Interim Report 3), Louisiana Transportation Research Center, Baton Rouge, LA, 1981.

[11] Temple, W. H., Cumbaa, S. L., and Gueho, B. J. "*Evaluation of Drainage Pipe by field experimentation and supplemental laboratory experimentation.*" Report No. 174 (Final Report), Louisiana Transportation Research Center, Baton Rouge, LA, 1985.

[12] Garber, J. D., Lin, J. H., and Smith, L. G. "*Feasibility of Applying Cathodic Protection of Culverts to Underground Culverts.*" Report No. FHWA/LA-91/238, Louisiana Transportation Research Center, Baton Rouge, LA, 1991.

[13] Garber, J. D., Lin, J. H., and Smith, L. G. "*Feasibility of Applying Cathodic Protection of Culverts to Underground Culverts.*" Report No. FHWA/LA-94/284 (Final Report), Louisiana Transportation Research Center, Baton Rouge, LA, 1995.

[14] Garber, J. D. and Smith, L. G. "*Cathodic Protection of Culverts - Field Inspection*

and Expert System " Report No. LA-99/324, Louisiana Transportation Research Center, Baton Rouge, LA, 1999.

[15] Abdel-Karim, A. M., Tadros, M. K., and Benak, J. V. "Live Load Distribution on Concrete Box Culverts." *Transportation Research Board*, No. 1288, 1990, pp. 136-151.

[16] Heger, F. J. and McGrath, T. J. "*Design method for reinforced concrete pipe and box sections.*" Report No., Simpson Gumpertz & Heger Inc., Cambridge, MA, 1982.

[17] Frederick, G. R. and Tarhini, K. M. "Model Analysis of Box Culverts Subjected to Highway Loading." *Experimental Mechanics*, Vol. 29, No. 2, 1989, pp. 183-187.

[18] McGrath, T. J., Moore, I. D., Selig, E. T., Webb, M. C., and Taleb, B. "*Recommended Specifications for Large-Span Culverts.*" Report No. NCHRP Report No. 473, Transportation Research Board, Washington, D.C., 2002.

[19] Mlynarski, M., McGrath, T. J., Clancy, C., and Katona, M. G. "*Proposed Modifications to AASHTO Culvert Load Rating Specifications.*" Report No. NCHRP Web-Only Document 268, Transportation Research Board, Washington, D.C., 2019.

[20] Abolmaali, A. and Garg, A. K. "Effect of Wheel Live Load on Shear Behavior of Precast Reinforced Concrete Box Culverts." *Journal of Bridge Engineering*, Vol. 13, No. 1, 2008, pp. 93-99.

[21] Garg, A. K. and Abolmaali, A. "Finite-Element Modeling and Analysis of Reinforced Concrete Box Culverts." *Journal of Transportation Engineering*, Vol. 135, No. 3, 2009, pp. 121-128.

[22] Orton, S. L., Loehr, J. E., Boeckmann, A., and Havens, G. "Live-Load Effect in Reinforced Concrete Box Culverts under Soil Fill." *Journal of Bridge Engineering*, Vol. 20, No. 11, 2015, p. 9.

[23] Wood, T. A., Lawson, W. D., Jayawickrama, P. W., and Newhouse, C. D. "Evaluation of Production Models for Load Rating Reinforced Concrete Box Culverts." *Journal of Bridge Engineering*, Vol. 20, No. 1, 2015.

[24] Wood, T. A., Lawson, W. D., Surles, J. G., Jayawickrama, P. W., and Seo, H. "Improved Load Rating of Reinforced-Concrete Box Culverts Using Depth-Calibrated Live-Load Attenuation." *Journal of Bridge Engineering*, Vol. 21, No. 12, 2016.

[25] Acharya, R., Han, J., and Parsons, R. L. "Numerical Analysis of Low-Fill Box Culvert under Rigid Pavement Subjected to Static Traffic Loading." *International Journal of Geomechanics*, Vol. 16, No. 5, 2016.

[26] Acharya, R., Jie, H., Brennan, J. J., Parsons, R. L., and Khatri, D. K. "Structural Response of a Low-Fill Box Culvert under Static and Traffic Loading." *Journal of Performance of Constructed Facilities*, Vol. 30, No. 1, 2016, pp. 4014184-4014181-4014184-4014187.

[27] Westergaard, H. M. "Computations of stresses in bridge slabs due to wheel loads." *Public Roads*, Vol. 11, No. 1, 1930, pp. 1-23.

[28] ANSYS. Theory Reference. Ver. 17.2, ANSYS, Inc., Canonsburg, PA, 2016.

[29] Han, J., Acharya, R., Parsons, R. L., and Khatri, D. "*Improved load distribution for load rating of low-fill box structures.*" Report No. K-TRAN: KU12-3, Kansas DOT,

Lawrence, KS, 2013.

[30] McGrath, T. J., Liepins, A. A., and Beaver, J. L. "Live load distribution widths for reinforced concrete box sections." *Transportation Research Record: Journal of the Transportation Research Board*, No. CD 11-S, 2005.

[31] Maher, K. T. and Joseph, V. B. "Soil pressure on box culverts." *ACI Structural Journal*, Vol. 86, No. 4, 1989, pp. 439-450.

[32] Abdel-Karim, A. M., Tadros, M. K., and Benak, J. V. "Structural Response of Full-Scale Concrete Box Culvert." *Journal of Structural Engineering*, Vol. 119, No. 11, 1993, pp. 3238-3254.

[33] Yang, M. Z., Drumm, E. C., Bennett, R. M., and Mauldon, M. Measurement of Earth Pressures on Concrete Box Culverts under Highway Embankments.In *Field Instrumentation for Soil and Rock*, ASTM International, West Conshohocken, PA. pp. 87-100.

[34] Holtz, R. D., Kovacs, W. D., and Sheahan, T. C. *An introduction to geotechnical engineering*. Pearson, 2011. p. 853.

[35] Newmark, N. M. "Simplified Computation of Vertical Pressures in Elastic Foundations." *University of Illinois Bulletin*, Circular No. 24, Vol. XXXIII, No. 4, 1935, pp. 1-19.

[36] Nowak, A. S. "*Calibration of LRFD Bridge Design Code.*" Report No. NCHRP Report No. 368, Transportation Research Board, Washington, D.C., 1999.

[37] Kulicki, J. M., Wassef, W. G., Kleinhans, D. D., Yoo, C. H., Nowak, A. S., and Grubb, M. "*Development of LRFD Specifications for Horizontally Curved Steel Girder Bridges.*" Report No. NCHRP Report 563, T. R. Board, Washington, D.C., 2006.

[38] Moses, F. "*Calibration of Load Factors for LRFR Bridge Evaluation.*" Report No. NCHRP Report 454, T. R. Board, Washington, D.C., 2001.

[39] Mlynarski, M., Wassef, W., and Nowak, A. "*A Comparison of AASHTO Bridge Load Rating Methods.*" Report No. NCHRP Report 700, Washington, DC, 2011.

[40] Belarbi, A., Bae, S.-W., Ayoub, A., Kuchma, D., Mirmiran, A., and Okeil, A. M. "*Design of FRP Systems for Strengthening Concrete Girders in Shear.*" Report No. NCHRP Report No. 678, T. R. Board, Washington, D.C., 2011.

[41] Nowak, A. S. and Szerszen, M. M. "Calibration of design code for buildings (ACI 318): Part 1 - Statistical models for resistance." *ACI Structural Journal*, Vol. 100, No. 3, 2003, pp. 377-382.

[42] Okeil, A. M., El-Tawil, S., and Shahawy, M. "Flexural Reliability of RC Bridge Girders Strengthened with CFRP Laminates." *Journal of Bridge Engineering*, Vol. 7, No. 5, 2002, pp. 290-299.

[43] Okeil, A. M., Belarbi, A., and Kuchma, D. A. "Reliability Assessment of FRP-Strengthened Concrete Bridge Girders in Shear." *Journal of Composites for Construction*, Vol. 17, No. 1, 2013, pp. 91-100.

[44] Modjeski and Masters Inc., Univ. of Nebraska-Lincoln, Univ. of Delaware, and NCS Consult. LLC. "*Bridges for Service Life Beyond 100 Years: Service Limit State Design.*" Report No. SHRP 2 Report S2-R19B-RW-1, Washington, D.C., 2015.

[45] Wassef, W. G., Kulicki, J. M., Nassif, H., Mertz, D., and Nowak, A. S. "*Calibration of AASHTO LRFD Concrete Bridge Design Specifications for Serviciability* " Report No. Web-Only Document 201, Transportation Research Board, Washington, DC, 2014.

[46] Modjeski and Masters Inc., University of Nebraska Lincoln, University of Delaware, and NCS Consultants LLC. "*Bridges for Service Life Beyond 100 Years: Service Limit State Design.*" Report No. SHRP 2 Report S2-R19B-RW-1, Washington, D.C., 2015.

[47] Foye, K. C., Salgado, R., and Scott, B. "Assessment of Variable Uncertainties for Reliability-Based Design of Foundations." *Journal of Geotechnical and Geoenvironmental Engineering*, Vol. 132, No. 9, 2006, pp. 1197-1207.

[48] Allen, T. M., Nowak, A. S., and Bathurst, R. J. "Calibration to Determine Load and Resistance Factors for Geotechnical and Structural Design." *Transportation research circular*, 2005.

[49] Ishak, S., Shin, H.-C., and Sridhar, B. "*Characterization and Development of Truck Load Spectra and Growth Factors for Current and Future Pavement Design Practices in Louisiana.*" Report No. 445, Louisiana Transportation Research Center, Baton Rouge, LA, 2011.

[50] Haldar, A. and Mahadaven, S. *Probability, Reliability, and Statistical Methods in Engineering Design*. John Wiley & Sons, USA, 2000.

[51] Ang, A. H.-S. and Tang, W. H. *Probability Concepts in Engineering Planning and Design: Volume 2- Decision, risk and relaibility*. John Wiley & Sons Inc., USA, 1984.

[52] Coles, S., Bawa, J., Trenner, L., and Dorazio, P. *An introduction to statistical modeling of extreme values*. Springer, London, 2001. p. 209.

[53] Nowak, A. S. and Collins, K. R. *Reliability of Structures*. McGraw Hill, USA, 2000.

Appendices

Appendix A
First Order Reliability Method (FORM)

FORM is based on a first order Taylor Series expansion of the limit state function, which approximates the failure surface by a tangent plane at the point of interest. It is not always possible to find a closed form solution for a non-linear limit state function or a function including more than two random variables. Hence, to convert a non-linear limit state function into simple polynomials, Taylor series (Eq. A-1) is used. The expansion of a function, $f(X)$ at a certain point *a* is given by;

$$f(X) = f(a) + (X-a)f'(a) + \frac{(X-a)^2}{2}f''(a) + \ldots\ldots\ldots\ldots + \frac{(X-a)^n}{n!}f^n(a) \qquad \text{(A-1)}$$

FORM uses this expansion to simplify the limit state function $g(Z_1, Z_2, \ldots\ldots, Z_n)$ by considering the expansion of the Taylor series after truncating terms higher than the first order. The expansion is done at the actual design point X^*. The design point is on the failure surface $g(Z_1, Z_2, \ldots\ldots, Z_n)$ as shown in the Figure A62 for the case of two variables in a non-linear limit state function.

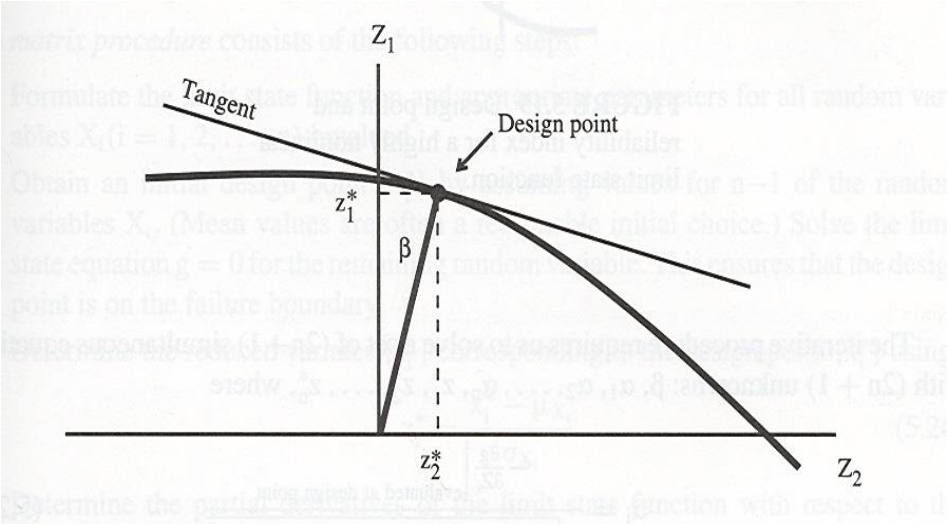

Figure A62. Reliability Index evaluated at design point [53]

To locate this point on the design space of $g(Z_1, Z_2, \ldots\ldots, Z_n) = 0$, an iterative process is needed [53]. For the convergence of a design point through a iterative procedure, it requires solving a set of $(2n + 1)$ simultaneous equations with $(2n + 1)$ unknowns, $\beta, \alpha_1, \alpha_2, \ldots, \alpha_n, Z_1^*, Z_2^*, \cdots, Z_n^*$.

$$\alpha_i = \frac{-\frac{\partial g}{\partial Z_i}\Big|_{\text{evaluated @ design point}}}{\sqrt{\sum_{k=1}^{n}\left(\frac{\partial g}{\partial Z_k}\Big|_{\text{evaluated @ design point}}\right)^2}} \quad \text{(A-2)}$$

$$\frac{\partial g}{\partial Z_i} = \frac{\partial g}{\partial X_i}\frac{\partial X_i}{\partial Z_i} = \frac{\partial g}{\partial X_i}\sigma_{X_i} \quad \text{(A-3)}$$

$$\sum_{i=1}^{n}(\alpha_i)^2 = 1 \quad \text{(A-4)}$$

$$Z_i^* = \beta\alpha_i \quad \text{(A-5)}$$

$$g(Z_1^*, Z_2^*, \cdots, Z_n^*) = 0 \quad \text{(A-6)}$$

Where, α_i is a unit vector in the direction of a design point from the origin and Z_i^* is the design point in transformed space. Equation A-6 is a mathematical statement of the requirement that the design point must be on the failure boundary.

This procedure was derived with the assumption that the involved random variables are normally distributed. When the probability distributions for the variables involved in the limit state function are not normally distributed, it is required to calculate the equivalent normal values of the mean and standard deviation for each non-normal random variable. To obtain the equivalent normal mean (μ_X^e) and standard deviation (σ_X^e), the CDF and PDF of the actual function should be equal to normal CDF and normal PDF at the value of the variable X^*on the failure boundary described by $g = 0$. Mathematically, it can be expressed as:

$$F_X(X^*) = \Phi\left(\frac{X^* - \mu_X^e}{\sigma_X^e}\right) \quad \text{(A-7)}$$

$$f_X(X^*) = \frac{1}{\sigma_X^e}\varphi\left(\frac{X^* - \mu_X^e}{\sigma_X^e}\right) \quad \text{(A-8)}$$

Where, X is a random variable with mean μ_X and standard deviation σ_X and is described by a CDF $F_X(X)$ and a PDF $f_X(X)$, $\Phi(.)$ is the CDF for the standard normal distribution, and $\varphi(.)$ is the PDF for the standard normal distribution. Expressions for μ_X^e and σ_X^e can be obtained as follows:

$$\mu_X^e = X^* - \sigma_X^e\left[\Phi^{-1}\left(F_X(X^*)\right)\right] \quad \text{(A-9)}$$

$$\sigma_X^e = \frac{1}{f_X(X^*)}\varphi\left[\Phi^{-1}\left(F_X(X^*)\right)\right] \quad \text{(A-10)}$$

The basic steps in the iteration procedure [53] to obtain β are as follows:

1. Formulate the limit state function. Determine the probability distributions and appropriate parameters for all random variables $X_i(i = 1,2, \dots, n)$ involved.
2. Obtain an initial design point $\{X_i^*\}$ by assuming values for n-1 of the random variables (mean values are a reasonable choice). Solve the limit state equation $g = 0$ for the remaining random variable, which ensures that the design point is on the failure boundary.
3. Equivalent normal mean (μ_X^e) and standard deviation (σ_X^e) are determined using

Equations A-9 and A-10 for design values corresponding to a non-normal distribution.

Determine the reduced variables $\{Z_i^*\}$ corresponding to the design point $\{X_i^*\}$ using:

$$Z_i^* = \frac{X_i^* - \mu_{X_i}^e}{\sigma_{X_i}^e} \quad \text{(A-11)}$$

4. Determine the partial derivatives of the limit state function with respect to the reduced variables. $\{G\}$ is a column vector whose elements are the partial derivatives (Equation A-3) multiplied by -1.

$$\{G\} = \begin{Bmatrix} G_1 \\ G_2 \\ \vdots \\ G_n \end{Bmatrix} \qquad \text{where, } G_i = -\frac{\partial g}{\partial Z_i}\Big|_{evaluatedatdesignpoint} \quad \text{(A-12)}$$

5. Estimate of $\boldsymbol{\beta}$ is then calculated using the following formula.

$$\beta = \frac{\{G\}^T\{Z^*\}}{\sqrt{\{G\}^T\{G\}}} \qquad \text{where, } \{Z^*\} = \begin{Bmatrix} Z_1^* \\ Z_2^* \\ \vdots \\ Z_n^* \end{Bmatrix} \quad \text{(A-13)}$$

6. The direction cosines for the design point to be used in the subsequent iteration are then calculated using:

$$\{\alpha\} = \frac{\{G\}}{\sqrt{\{G\}^T\{G\}}} \quad \text{(A-14)}$$

7. Determine a new design point for *n*-1 of the variables using:

$$Z_i^* = \alpha_i \beta \quad \text{(A-15)}$$

8. Determine the corresponding design point values in original coordinates for the *n*-1 values in Step 7 by:

$$X_i^* = \mu_{X_i}^e + Z_i^* \sigma_{X_i}^e \quad \text{(A-16)}$$

9. Determine the value of the remaining random variable by solving the limit state function $g = 0$.

10. Repeat Steps 3 to 10 until β and $\{X_i^*\}$ converge.

Appendix B
Chi-Square Statistical Test: "Goodness-of-fit" Test

The Chi-Square test is often used to assess the "goodness-of-fit" between an obtained set of frequencies in a random sample and what is expected under a given statistical hypothesis. In order to decide which distribution is better for a particular random variable, the difference between actual observation values (observed frequencies) and theoretical distribution values (theoretical frequencies) is quantified. The steps required to determine the probability distribution of a random variable are given below.

1. Divide the observed data range into equal intervals.
2. Find the number of observations (Observed Frequency,n_i) within each interval that do not depend on the distribution type.
3. Assume different distribution types that will represent the random variable and find the theoretical distribution values (Theoretical Frequency,e_i) within each interval for the respective distributions. If a random variable, X, lies in an interval a to b such that $a < X \leq b$, then the Theoretical Frequency (e_i) for a certain distribution type is given by:

   $$e_i = P(a < X \leq b) * N \quad \text{(C-1)}$$

4. where, N is the total number of observation (data points), and:

   $$P(a < X \leq b) = P(X \leq b) - P(X < a) \quad \text{(C-2)}$$

5. The probability of X less than a or b, $P(X < a)$ and $P(X \leq b)$ is found using the CDF for the respective distribution. The CDF for different distribution types can be obtained from the literature.
6. For each interval, compute the difference between n_i and e_i (squared) as a ratio of e_i.
7. Compute the summation of differences (squared) as a ratio of e_i which is given as:

   $$\sum_{i=1}^{m} \frac{(n_i - e_i)^2}{e_i} \quad \text{(C-3)}$$

   where, m is the total number of intervals.
8. Calculate the degree of freedom (f) for Chi-Square test which is given by $f = m - 1 - k$, where k is the number of parameters required to describe a particular distribution. In this study, normal and lognormal distribution types are used and for these types $k = 2$.
9. The summation evaluated in Step 5 is compared to the Chi-Square distribution for

a certain significance level,α, which is always taken between 1% and 10 %.

10. If $\sum_{i=1}^{m} \frac{(n_i - e_i)^2}{e_i} < C_{\alpha,f}$, then the assumed distribution fits statistical data sufficiently.
11. $C_{\alpha,f}$ values are given in Table B1.

Table B1. CDF of the Chi-Square Distribution [50]

Table of the CDF of the Chi-Square Distribution with *f* Degrees of Freedom

$$P(C \le c_{\alpha,f}) = \int_0^{c_{\alpha,f}} \frac{1}{2^{f/2}\Gamma(f/2)} s^{(f/2)-1} e^{-s/2} ds$$

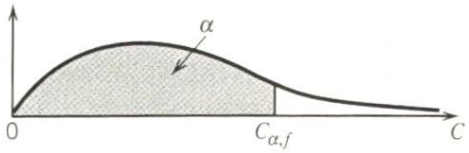

f \ α	0.001	0.005	0.010	0.025	0.050	0.100	0.900	0.950	0.975	0.990	0.995	0.999
1	1.57e–06	3.93e–05	1.57e–04	9.82e–04	3.93e–03	1.58e–02	2.706	3.841	5.024	6.635	7.879	10.83
2	2.00e–03	1.00e–02	0.0201	0.0506	0.1026	0.2107	4.605	5.991	7.378	9.210	10.60	13.82
3	2.43e–02	7.17e–02	0.1148	0.2158	0.3518	0.5844	6.251	7.815	9.348	11.34	12.84	16.27
4	9.08e–02	0.2070	0.2971	0.4844	0.7107	1.064	7.779	9.488	11.14	13.28	14.86	18.47
5	0.2102	0.4118	0.5543	0.8312	1.145	1.610	9.236	11.07	12.83	15.09	16.75	20.51
6	0.3810	0.6757	0.8721	1.237	1.635	2.204	10.64	12.59	14.45	16.81	18.55	22.46
7	0.5985	0.9893	1.239	1.690	2.167	2.833	12.02	14.07	16.01	18.48	20.28	24.32
8	0.8571	1.344	1.647	2.180	2.733	3.490	13.36	15.51	17.53	20.09	21.95	26.12
9	1.152	1.735	2.088	2.700	3.325	4.168	14.68	16.92	19.02	21.67	23.59	27.88
10	1.479	2.156	2.558	3.247	3.940	4.865	15.99	18.31	20.48	23.21	25.19	29.59
11	1.834	2.603	3.053	3.816	4.575	5.578	17.28	19.68	21.92	24.73	26.76	31.26
12	2.214	3.074	3.571	4.404	5.226	6.304	18.55	21.03	23.34	26.22	28.30	32.91
13	2.617	3.565	4.107	5.009	5.892	7.041	19.81	22.36	24.74	27.69	29.82	34.53
14	3.041	4.075	4.660	5.629	6.571	7.790	21.06	23.68	26.12	29.14	31.32	36.12
15	3.483	4.601	5.229	6.262	7.261	8.547	22.31	25.00	27.49	30.58	32.80	37.70
16	3.942	5.142	5.812	6.908	7.962	9.312	23.54	26.30	28.85	32.00	34.27	39.25
17	4.416	5.697	6.408	7.564	8.672	10.09	24.77	27.59	30.19	33.41	35.72	40.79
18	4.905	6.265	7.015	8.231	9.390	10.86	25.99	28.87	31.53	34.81	37.16	42.31
19	5.407	6.844	7.633	8.907	10.12	11.65	27.20	30.14	32.85	36.19	38.58	43.82
20	5.921	7.434	8.260	9.591	10.85	12.44	28.41	31.41	34.17	37.57	40.00	45.31

Appendix C
Distribution Types Used in Current Study

Normal or Gaussian Distribution

If a variable is normally distributed, two quantities have to be specified: the mean (μ_X), which coincides with the peak of the PDF curve, and the standard distribution ($\sigma_{X)}$, which indicates the spread of the bell curve. The PDF for a normal random variable X is given by Equation C-1.

$$f_X(X) = \frac{1}{\sigma_X\sqrt{2\pi}} exp\left[-\frac{1}{2}\left(\frac{X-\mu_X}{\sigma_X}\right)^2\right] \quad \text{(C-1)}$$

There is no closed-form solution for the CDF of a normal random variable, but tables have been developed to provide values of the CDF for the special case in which $\mu_X = 0$ and $\sigma_X = 1$ [53]. These tables can be used to obtain values for any general normal distribution.

Figure C63 Graphical representation of Normal Distribution

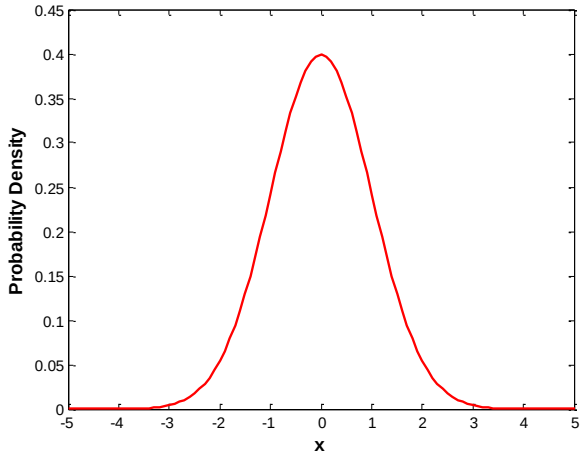

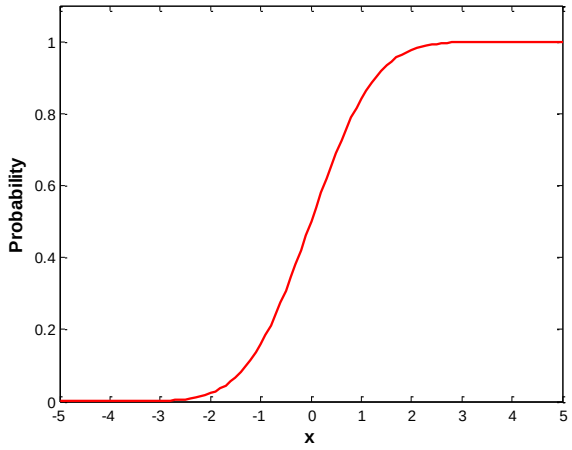

Lognormal Distribution

The random variable X is a lognormal random variable (Figure C64) if Y = ln(X) is normally distributed, $F_X(x) = F_Y(y)$. The mean and standard deviation for Y are given by Equations C-2 and C-3.

$$\sigma_Y = \sigma_{ln(X)} = \sqrt{\ln\left[\left(\frac{\sigma_X}{\mu_X}\right)^2 + 1\right]} \quad \text{(C-2)}$$

$$\mu_Y = \mu_{\ln(X)} = \ln(\mu_X) - \frac{1}{2}\sigma^2_{\ln X} \quad \text{(C-3)}$$

Figure C64 Graphical representation of Lognormal Distribution

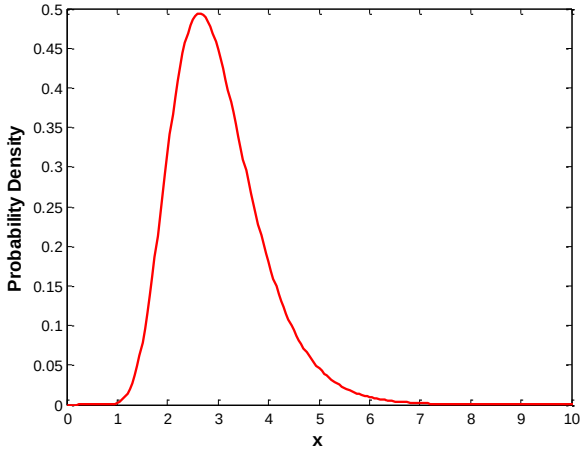

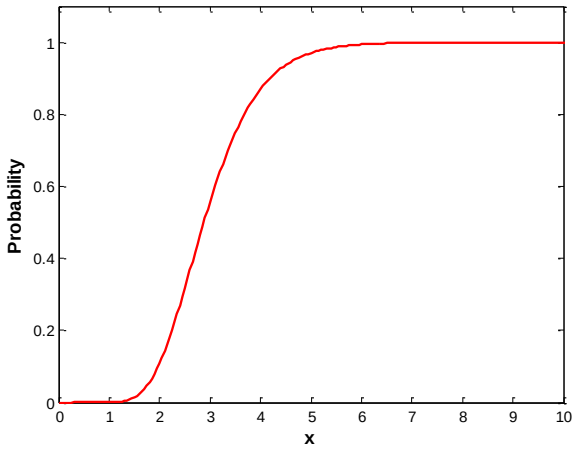

Extreme Type I (Gumbel) Distribution

Extreme Type I is often used to describe maximum periodic event distributions. In this distribution type, the cumulative distribution function (CDF) is given by:

$$F_X(x) = e^{-e^{-\alpha(x-u)}} \tag{C-4}$$

and the probability density function (PDF) is given by:

$$f_X(x) = \alpha\, e^{-e^{-\alpha(x-u)}} e^{-\alpha(x-u)} \tag{C-5}$$

Approximate expressions that relate the mean and standard deviation to the scale and shape parameters of the distribution can be found in the literature (Benjamin and Cornell 1970).

$$\mu_X \approx u + \frac{0.577}{\alpha} \tag{C-6}$$

$$\sigma_X \approx \frac{1.282}{\alpha} \tag{C-7}$$

Figure C65 Graphical representation of Extreme Type I Distribution

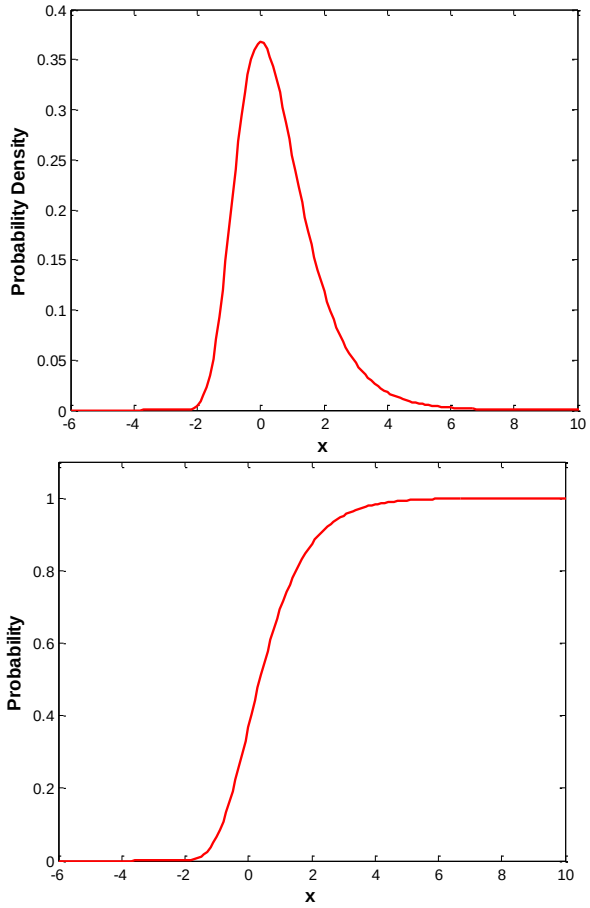

Appendix D
Details of Culverts in Parametric Study

This appendix provides the full details of the properties of the 273 culverts considered in this study.

Table D1. List of parametric study cases (1-barrel culverts)

#	Case	Barrel Dimensions (ft. x ft.)	Slab Thickness (in.)	Wall Thickness (in.)	Fill Height (ft.)	Concrete Strength (psi)
1	B1W6H6ST7WT6H0C3	6 x 6	7.0	6.0	0	3000
2	B1W6H6ST7WT6H1C3				1	
3	B1W6H6ST7WT6H2C3				2	
4	B1W6H6ST8WT6H0C3		8.0		0	
5	B1W6H6ST8WT6H1C3				1	
6	B1W6H6ST8WT6H2C3				2	
7	B1W6H6ST9WT6H0C3		9.0		0	
8	B1W6H6ST9WT6H1C3				1	
9	B1W6H6ST9WT6H2C3				2	
10	B1W6H6ST7WT6H0C4		7.0		0	4000
11	B1W6H6ST7WT6H1C4				1	
12	B1W6H6ST7WT6H2C4				2	
13	B1W6H6ST8WT6H0C4		8.0		0	
14	B1W6H6ST8WT6H1C4				1	
15	B1W6H6ST8WT6H2C4				2	
16	B1W6H6ST9WT6H0C4		9.0		0	
17	B1W6H6ST9WT6H1C4				1	
18	B1W6H6ST9WT6H2C4				2	
19	B1W6H6ST7WT6H0C5		7.0		0	5000
20	B1W6H6ST7WT6H1C5				1	
21	B1W6H6ST7WT6H2C5				2	
22	B1W6H6ST8WT6H0C5		8.0		0	
23	B1W6H6ST8WT6H1C5				1	
24	B1W6H6ST8WT6H2C5				2	
25	B1W6H6ST9WT6H0C5		9.0		0	
26	B1W6H6ST9WT6H1C5				1	
27	B1W6H6ST9WT6H2C5				2	

#	Case	Barrel Dimensions (ft. x ft.)	Slab Thickness (in.)	Wall Thickness (in.)	Fill Height (ft.)	Concrete Strength (psi)
28	B1W7H7ST7.5WT7H0C3	7 x 7	7.5	7.0	0	3000
29	B1W7H7ST7.5WT7H1C3				1	
30	B1W7H7ST7.5WT7H2C3				2	
31	B1W7H7ST8.5WT7H0C3		8.5		0	
32	B1W7H7ST8.5WT7H1C3				1	
33	B1W7H7ST8.5WT7H2C3				2	
34	B1W7H7ST9.5WT7H0C3		9.5		0	
35	B1W7H7ST9.5WT7H1C3				1	
36	B1W7H7ST9.5WT7H2C3				2	
37	B1W7H7ST7.5WT7H0C4		7.5		0	4000
38	B1W7H7ST7.5WT7H1C4				1	
39	B1W7H7ST7.5WT7H2C4				2	
40	B1W7H7ST8.5WT7H0C4		8.5		0	
41	B1W7H7ST8.5WT7H1C4				1	
42	B1W7H7ST8.5WT7H2C4				2	
43	B1W7H7ST9.5WT7H0C4		9.5		0	
44	B1W7H7ST9.5WT7H1C4				1	
45	B1W7H7ST9.5WT7H2C4				2	
46	B1W7H7ST7.5WT7H0C5		7.5		0	5000
47	B1W7H7ST7.5WT7H1C5				1	
48	B1W7H7ST7.5WT7H2C5				2	
49	B1W7H7ST8.5WT7H0C5		8.5		0	
50	B1W7H7ST8.5WT7H1C5				1	
51	B1W7H7ST8.5WT7H2C5				2	
52	B1W7H7ST9.5WT7H0C5		9.5		0	
53	B1W7H7ST9.5WT7H1C5				1	
54	B1W7H7ST9.5WT7H2C5				2	

#	Case	Barrel Dimensions (ft. x ft.)	Slab Thickness (in.)	Wall Thickness (in.)	Fill Height (ft.)	Concrete Strength (psi)
55	B1W8H8ST8WT8H0C3	8 x 8	8.0	8.0	0	3000
56	B1W8H8ST8WT8H1C3				1	
57	B1W8H8ST8WT8H2C3				2	
58	B1W8H8ST9WT8H0C3		9.0		0	
59	B1W8H8ST9WT8H1C3				1	
60	B1W8H8ST9WT8H2C3				2	
61	B1W8H8ST10WT8H0C3		10.0		0	
62	B1W8H8ST10WT8H1C3				1	
63	B1W8H8ST10WT8H2C3				2	
64	B1W8H8ST8WT8H0C4		8.0		0	4000
65	B1W8H8ST8WT8H1C4				1	
66	B1W8H8ST8WT8H2C4				2	
67	B1W8H8ST9WT8H0C4		9.0		0	
68	B1W8H8ST9WT8H1C4				1	
69	B1W8H8ST9WT8H2C4				2	
70	B1W8H8ST10WT8H0C4		10.0		0	
71	B1W8H8ST10WT8H1C4				1	
72	B1W8H8ST10WT8H2C4				2	
73	B1W8H8ST8WT8H0C5		8.0		0	5000
74	B1W8H8ST8WT8H1C5				1	
75	B1W8H8ST8WT8H2C5				2	
76	B1W8H8ST9WT8H0C5		9.0		0	
77	B1W8H8ST9WT8H1C5				1	
78	B1W8H8ST9WT8H2C5				2	
79	B1W8H8ST10WT8H0C5		10.0		0	
80	B1W8H8ST10WT8H1C5				1	
81	B1W8H8ST10WT8H2C5				2	

#	Case	Barrel Dimensions (ft. x ft.)	Slab Thickness (in.)	Wall Thickness (in.)	Fill Height (ft.)	Concrete Strength (psi)
82	B1W9H9ST8.5WT9H0C3	9 x 9	8.5	9.0	0	3000
83	B1W9H9ST8.5WT9H1C3				1	
84	B1W9H9ST8.5WT9H2C3				2	
85	B1W9H9ST9.5WT9H0C3		9.5		0	
86	B1W9H9ST9.5WT9H1C3				1	
87	B1W9H9ST9.5WT9H2C3				2	
88	B1W9H9ST10.5WT9H0C3		10.5		0	
89	B1W9H9ST10.5WT9H1C3				1	
90	B1W9H9ST10.5WT9H2C3				2	
91	B1W9H9ST8.5WT9H0C4		8.5		0	4000
92	B1W9H9ST8.5WT9H1C4				1	
93	B1W9H9ST8.5WT9H2C4				2	
94	B1W9H9ST9.5WT9H0C4		9.5		0	
95	B1W9H9ST9.5WT9H1C4				1	
96	B1W9H9ST9.5WT9H2C4				2	
97	B1W9H9ST10.5WT9H0C4		10.5		0	
98	B1W9H9ST10.5WT9H1C4				1	
99	B1W9H9ST10.5WT9H2C4				2	
100	B1W9H9ST8.5WT9H0C5		8.5		0	5000
101	B1W9H9ST8.5WT9H1C5				1	
102	B1W9H9ST8.5WT9H2C5				2	
103	B1W9H9ST9.5WT9H0C5		9.5		0	
104	B1W9H9ST9.5WT9H1C5				1	
105	B1W9H9ST9.5WT9H2C5				2	
106	B1W9H9ST10.5WT9H0C5		10.5		0	
107	B1W9H9ST10.5WT9H1C5				1	
108	B1W9H9ST10.5WT9H2C5				2	

#	Case	Barrel Dimensions (ft. x ft.)	Slab Thickness (in.)	Wall Thickness (in.)	Fill Height (ft.)	Concrete Strength (psi)
109	B1W10H10ST9WT10H0C3	10 x 10	9.0	10.0	0	3000
110	B1W10H10ST9WT10H1C3				1	
111	B1W10H10ST9WT10H2C3				2	
112	B1W10H10ST10WT10H0C3		10.0		0	
113	B1W10H10ST10WT10H1C3				1	
114	B1W10H10ST10WT10H2C3				2	
115	B1W10H10ST11WT10H0C3		11.0		0	
116	B1W10H10ST11WT10H1C3				1	
117	B1W10H10ST11WT10H2C3				2	
118	B1W10H10ST9WT10H0C4		9.0		0	4000
119	B1W10H10ST9WT10H1C4				1	
120	B1W10H10ST9WT10H2C4				2	
121	B1W10H10ST10WT10H0C4		10.0		0	
122	B1W10H10ST10WT10H1C4				1	
123	B1W10H10ST10WT10H2C4				2	
124	B1W10H10ST11WT10H0C4		11.0		0	
125	B1W10H10ST11WT10H1C4				1	
126	B1W10H10ST11WT10H2C4				2	
127	B1W10H10ST9WT10H0C5		9.0		0	5000
128	B1W10H10ST9WT10H1C5				1	
129	B1W10H10ST9WT10H2C5				2	
130	B1W10H10ST10WT10H0C5		10.0		0	
131	B1W10H10ST10WT10H1C5				1	
132	B1W10H10ST10WT10H2C5				2	
133	B1W10H10ST11WT10H0C5		11.0		0	
134	B1W10H10ST11WT10H1C5				1	
135	B1W10H10ST11WT10H2C5				2	

#	Case	Barrel Dimensions (ft. x ft.)	Slab Thickness (in.)	Wall Thickness (in.)	Fill Height (ft.)	Concrete Strength (psi)
136	B1W11H11ST9.5WT11H0C3	11 x 11	9.5	11.0	0	3000
137	B1W11H11ST9.5WT11H1C3				1	
138	B1W11H11ST9.5WT11H2C3				2	
139	B1W11H11ST10.5WT11H0C3		10.5		0	
140	B1W11H11ST10.5WT11H1C3				1	
141	B1W11H11ST10.5WT11H2C3				2	
142	B1W11H11ST11.5WT11H0C3		11.5		0	
143	B1W11H11ST11.5WT11H1C3				1	
144	B1W11H11ST11.5WT11H2C3				2	
145	B1W11H11ST9.5WT11H0C4		9.5		0	4000
146	B1W11H11ST9.5WT11H1C4				1	
147	B1W11H11ST9.5WT11H2C4				2	
148	B1W11H11ST10.5WT11H0C4		10.5		0	
149	B1W11H11ST10.5WT11H1C4				1	
150	B1W11H11ST10.5WT11H2C4				2	
151	B1W11H11ST11.5WT11H0C4		11.5		0	
152	B1W11H11ST11.5WT11H1C4				1	
153	B1W11H11ST11.5WT11H2C4				2	
154	B1W11H11ST9.5WT11H0C5		9.5		0	5000
155	B1W11H11ST9.5WT11H1C5				1	
156	B1W11H11ST9.5WT11H2C5				2	
157	B1W11H11ST10.5WT11H0C5		10.5		0	
158	B1W11H11ST10.5WT11H1C5				1	
159	B1W11H11ST10.5WT11H2C5				2	
160	B1W11H11ST11.5WT11H0C5		11.5		0	
161	B1W11H11ST11.5WT11H1C5				1	
162	B1W11H11ST11.5WT11H2C5				2	

#	Case	Barrel Dimensions (ft. x ft.)	Slab Thickness (in.)	Wall Thickness (in.)	Fill Height (ft.)	Concrete Strength (psi)
163	B1W12H12ST10WT12H0C3	12 x 12	10.0	12.0	0	3000
164	B1W12H12ST10WT12H1C3				1	
165	B1W12H12ST10WT12H2C3				2	
166	B1W12H12ST11WT12H0C3		11.0		0	
167	B1W12H12ST11WT12H1C3				1	
168	B1W12H12ST11WT12H2C3				2	
169	B1W12H12ST12WT12H0C3		12.0		0	
170	B1W12H12ST12WT12H1C3				1	
171	B1W12H12ST12WT12H2C3				2	
172	B1W12H12ST10WT12H0C4		10.0		0	4000
173	B1W12H12ST10WT12H1C4				1	
174	B1W12H12ST10WT12H2C4				2	
175	B1W12H12ST11WT12H0C4		11.0		0	
176	B1W12H12ST11WT12H1C4				1	
177	B1W12H12ST11WT12H2C4				2	
178	B1W12H12ST12WT12H0C4		12.0		0	
179	B1W12H12ST12WT12H1C4				1	
180	B1W12H12ST12WT12H2C4				2	
181	B1W12H12ST10WT12H0C5		10.0		0	5000
182	B1W12H12ST10WT12H1C5				1	
183	B1W12H12ST10WT12H2C5				2	
184	B1W12H12ST11WT12H0C5		11.0		0	
185	B1W12H12ST11WT12H1C5				1	
186	B1W12H12ST11WT12H2C5				2	
187	B1W12H12ST12WT12H0C5		12.0		0	
188	B1W12H12ST12WT12H1C5				1	
189	B1W12H12ST12WT12H2C5				2	

Table D2. List of parametric study cases (2-barrel culverts— $f'_c = 4000$ psi)

#	Case	Barrel Dimensions (ft. x ft.)	Slab Thickness (in.)	Wall Thickness (in.)	Fill Height (ft.)
1	B2W6H6ST7WT6H0C4	6 x 6	7.0	6.0	0
2	B2W6H6ST7WT6H1C4				1
3	B2W6H6ST7WT6H2C4				2
4	B2W6H6ST8WT6H0C4		8.0		0
5	B2W6H6ST8WT6H1C4				1
6	B2W6H6ST8WT6H2C4				2
7	B2W6H6ST9WT6H0C4		9.0		0
8	B2W6H6ST9WT6H1C4				1
9	B2W6H6ST9WT6H2C4				2
10	B2W7H7ST7.5WT7H0C4	7 x 7	7.5	7.0	0
11	B2W7H7ST7.5WT7H1C4				1
12	B2W7H7ST7.5WT7H2C4				2
13	B2W7H7ST8.5WT7H0C4		8.5		0
14	B2W7H7ST8.5WT7H1C4				1
15	B2W7H7ST8.5WT7H2C4				2
16	B2W7H7ST9.5WT7H0C4		9.5		0
17	B2W7H7ST9.5WT7H1C4				1
18	B2W7H7ST9.5WT7H2C4				2
19	B2W8H8ST8WT8H0C4	8 x 8	8.0	8.0	0
20	B2W8H8ST8WT8H1C4				1
21	B2W8H8ST8WT8H2C4				2
22	B2W8H8ST9WT8H0C4		9.0		0
23	B2W8H8ST9WT8H1C4				1
24	B2W8H8ST9WT8H2C4				2
25	B2W8H8ST10WT8H0C4		10.0		0
26	B2W8H8ST10WT8H1C4				1
27	B2W8H8ST10WT8H2C4				2
28	B2W9H9ST8.5WT9H0C4	9 x 9	8.5	9.0	0
29	B2W9H9ST8.5WT9H1C4				1
30	B2W9H9ST8.5WT9H2C4				2
31	B2W9H9ST9.5WT9H0C4		9.5		0
32	B2W9H9ST9.5WT9H1C4				1
33	B2W9H9ST9.5WT9H2C4				2
34	B2W9H9ST10.5WT9H0C4		10.5		0
35	B2W9H9ST10.5WT9H1C4				1
36	B2W9H9ST10.5WT9H2C4				2

#	Case	Barrel Dimensions (ft. x ft.)	Slab Thickness (in.)	Wall Thickness (in.)	Fill Height (ft.)
37	B2W10H10ST9WT10H0C4	10 x 10	9.0	10.0	0
38	B2W10H10ST9WT10H1C4				1
39	B2W10H10ST9WT10H2C4				2
40	B2W10H10ST10WT10H0C4		10.0		0
41	B2W10H10ST10WT10H1C4				1
42	B2W10H10ST10WT10H2C4				2
43	B2W10H10ST11WT10H0C4		11.0		0
44	B2W10H10ST11WT10H1C4				1
45	B2W10H10ST11WT10H2C4				2

46	B2W11H11ST9.5WT11H0C4	11 x 11	9.5	11.0	0
47	B2W11H11ST9.5WT11H1C4				1
48	B2W11H11ST9.5WT11H2C4				2
49	B2W11H11ST10.5WT11H0C4		10.5		0
50	B2W11H11ST10.5WT11H1C4				1
51	B2W11H11ST10.5WT11H2C4				2
52	B2W11H11ST11.5WT11H0C4		11.5		0
53	B2W11H11ST11.5WT11H1C4				1
54	B2W11H11ST11.5WT11H2C4				2

55	B2W12H12ST10WT12H0C4	12 x 12	10.0	12.0	0
56	B2W12H12ST10WT12H1C4				1
57	B2W12H12ST10WT12H2C4				2
58	B2W12H12ST11WT12H0C4		11.0		0
59	B2W12H12ST11WT12H1C4				1
60	B2W12H12ST11WT12H2C4				2
61	B2W12H12ST12WT12H0C4		12.0		0
62	B2W12H12ST12WT12H1C4				1
63	B2W12H12ST12WT12H2C4				2

Table D3. List of parametric study cases (3-barrel culverts— $f'_c = 4000$ psi)

#	Case	Barrel Dimensions (ft. x ft.)	Slab Thickness (in.)	Wall Thickness (in.)	Fill Height (ft.)
1	B3W6H6ST8WT6H0C4	6 x 6	8.0	6.0	0
2	B3W6H6ST8WT6H1C4				1
3	B3W6H6ST8WT6H2C4				2
4	B3W7H7ST8.5WT7H0C4	7 x 7	8.5	7.0	0
5	B3W7H7ST8.5WT7H1C4				1
6	B3W7H7ST8.5WT7H2C4				2
7	B3W8H8ST9WT8H0C4	8 x 8	9.0	8.0	0
8	B3W8H8ST9WT8H1C4				1
9	B3W8H8ST9WT8H2C4				2
10	B3W9H9ST9.5WT9H0C4	9 x 9	9.5	9.0	0
11	B3W9H9ST9.5WT9H1C4				1
12	B3W9H9ST9.5WT9H2C4				2
13	B3W10H10ST10WT10H0C4	10 x 10	10.0	10.0	0
14	B3W10H10ST10WT10H1C4				1
15	B3W10H10ST10WT10H2C4				2
16	B3W11H11ST10.5WT11H0C4	11 x 11	10.5	11.0	0
17	B3W11H11ST10.5WT11H1C4				1
18	B3W11H11ST10.5WT11H2C4				2
19	B3W12H12ST11WT12H0C4	12 x 12	11.0	12.0	0
20	B3W12H12ST11WT12H1C4				1
21	B3W12H12ST11WT12H2C4				2

Appendix E
Results from Parametric Study

This appendix provides the results from the parametric study of the 273 culverts considered in this study. The first set of results was obtained from the 3D shell element model. Following this set, results from the 2D model using the AASHTO-LRFD BDS live load distribution formula are presented.

The reported results are:

M_{pE}^{DC} =	positive moment at 1st exterior midspan due to component weight	V_L^{DC} =	shear force left of 1st interior wall due to component weight
M_{pE}^{EF} =	positive moment at 1st exterior midspan due to earth fill weight	V_L^{EF} =	shear force left of 1st interior wall due to earth fill weight
M_{pE}^{DW} =	positive moment at 1st exterior midspan due to wearing surface	V_L^{DW} =	shear force left of 1st interior wall due to wearing surface load
M_{pE}^{LL} =	positive moment at 1st exterior midspan due to live load	V_L^{LL} =	shear force left of 1st interior wall due to live load
M_{nL}^{DC} =	negative moment at left of 1st interior wall due to component weight	V_R^{DC} =	shear force right of 1st interior wall due to component weight
M_{nL}^{EF} =	negative moment at left of 1st interior wall due to earth fill weight	V_R^{EF} =	shear force right of 1st interior wall due to earth fill weight
M_{nL}^{DW} =	negative moment left of 1st interior wall due to wearing surface	V_R^{DW} =	shear force right of 1st interior wall due to wearing surface
M_{nL}^{LL} =	negative moment left of 1st interior wall due to live load	V_R^{LL} =	shear force right of 1st interior wall due to live load
M_{nR}^{DC} =	negative moment at right of 1st interior wall due to component weight	M_{pI}^{DC} =	positive moment at 1st interior midspan due to component weight
M_{nR}^{EF} =	negative moment at right of 1st interior wall due to earth fill weight	M_{pI}^{EF} =	positive moment at 1st interior midspan due to earth fill weight
M_{nR}^{DW} =	negative moment right of 1st interior wall due to wearing surface	M_{pI}^{DW} =	positive moment at 1st interior midspan due to wearing surface
M_{nR}^{LL} =	negative moment right of 1st interior wall due to live load	M_{pI}^{LL} =	positive moment at 1st interior midspan due to live load

Table E1. Bending moment and shear force values (3D model; 1-barrel culverts)

#	Case	NLS	V_L^{DC}	V_L^{EF}	V_L^{DW}	V_L^{LL}	M_{pE}^{DC}	M_{pE}^{EF}	M_{pE}^{DW}	M_{pE}^{LL}
1	B1W6H6ST7WT6H0C3	18	-18.2	0.0	-6.0	-454	-273	0	-90.6	-3882
2	B1W6H6ST7WT6H1C3	16	-18.2	-25.0	-6.0	-309	-273	-375	-90.6	-2977
3	B1W6H6ST7WT6H2C3	12	-18.2	-50.0	-6.0	-206	-273	-750	-90.6	-2399
4	B1W6H6ST8WT6H0C3	18	-20.8	0.0	-6.0	-453	-312	0	-90.6	-3886
5	B1W6H6ST8WT6H1C3	16	-20.8	-25.0	-6.0	-308	-312	-375	-90.6	-2981
6	B1W6H6ST8WT6H2C3	12	-20.8	-50.0	-6.0	-206	-312	-750	-90.6	-2403
7	B1W6H6ST9WT6H0C3	18	-23.4	0.0	-6.0	-451	-352	0	-90.6	-3890
8	B1W6H6ST9WT6H1C3	16	-23.4	-25.0	-6.0	-307	-352	-375	-90.6	-2985
9	B1W6H6ST9WT6H2C3	12	-23.4	-50.0	-6.0	-206	-352	-750	-90.6	-2407
10	B1W6H6ST7WT6H0C4	18	-18.2	0.0	-6.0	-454	-273	0	-90.6	-3882
11	B1W6H6ST7WT6H1C4	16	-18.2	-25.0	-6.0	-309	-273	-375	-90.6	-2977
12	B1W6H6ST7WT6H2C4	12	-18.2	-50.0	-6.0	-206	-273	-750	-90.6	-2399
13	B1W6H6ST8WT6H0C4	18	-20.8	0.0	-6.0	-453	-312	0	-90.6	-3886
14	B1W6H6ST8WT6H1C4	16	-20.8	-25.0	-6.0	-308	-312	-375	-90.6	-2981
15	B1W6H6ST8WT6H2C4	12	-20.8	-50.0	-6.0	-206	-312	-750	-90.6	-2403
16	B1W6H6ST9WT6H0C4	18	-23.4	0.0	-6.0	-451	-352	0	-90.6	-3890
17	B1W6H6ST9WT6H1C4	16	-23.4	-25.0	-6.0	-307	-352	-375	-90.6	-2985
18	B1W6H6ST9WT6H2C4	12	-23.4	-50.0	-6.0	-206	-352	-750	-90.6	-2407
19	B1W6H6ST7WT6H0C5	18	-18.2	0.0	-6.0	-454	-273	0	-90.6	-3882
20	B1W6H6ST7WT6H1C5	16	-18.2	-25.0	-6.0	-309	-273	-375	-90.6	-2977
21	B1W6H6ST7WT6H2C5	12	-18.2	-50.0	-6.0	-206	-273	-750	-90.6	-2399
22	B1W6H6ST8WT6H0C5	18	-20.8	0.0	-6.0	-453	-312	0	-90.6	-3886
23	B1W6H6ST8WT6H1C5	16	-20.8	-25.0	-6.0	-308	-312	-375	-90.6	-2981
24	B1W6H6ST8WT6H2C5	12	-20.8	-50.0	-6.0	-206	-312	-750	-90.6	-2403
25	B1W6H6ST9WT6H0C5	18	-23.4	0.0	-6.0	-451	-352	0	-90.6	-3890
26	B1W6H6ST9WT6H1C5	16	-23.4	-25.0	-6.0	-307	-352	-375	-90.6	-2985
27	B1W6H6ST9WT6H2C5	12	-23.4	-50.0	-6.0	-206	-352	-750	-90.6	-2407

Units: lb./in. for shear; lb.-in./in. for bending moment

#	Case	NLS	V_L^{DC}	V_L^{EF}	V_L^{DW}	V_L^{LL}	M_{pE}^{DC}	M_{pE}^{EF}	M_{pE}^{DW}	M_{pE}^{LL}
28	B1W7H7ST7.5WT7H0C3	25	-23.1	0.0	-7.1	-499	-410	0	-126.9	-4291
29	B1W7H7ST7.5WT7H1C3	18	-23.1	-29.6	-7.1	-279	-410	-525	-126.9	-3402
30	B1W7H7ST7.5WT7H2C3	14	-23.1	-59.2	-7.1	-196	-410	-1050	-126.9	-2838
31	B1W7H7ST8.5WT7H0C3	25	-26.2	0.0	-7.1	-497	-465	0	-126.9	-4295
32	B1W7H7ST8.5WT7H1C3	18	-26.2	-29.6	-7.1	-279	-465	-525	-126.9	-3406
33	B1W7H7ST8.5WT7H2C3	14	-26.2	-59.2	-7.1	-196	-465	-1050	-126.9	-2842
34	B1W7H7ST9.5WT7H0C3	25	-29.3	0.0	-7.1	-495	-520	0	-126.9	-4299
35	B1W7H7ST9.5WT7H1C3	18	-29.3	-29.6	-7.1	-279	-520	-525	-126.9	-3410
36	B1W7H7ST9.5WT7H2C3	14	-29.3	-59.2	-7.1	-196	-520	-1050	-126.9	-2846
37	B1W7H7ST7.5WT7H0C4	25	-23.1	0.0	-7.1	-499	-410	0	-126.9	-4291
38	B1W7H7ST7.5WT7H1C4	18	-23.1	-29.6	-7.1	-279	-410	-525	-126.9	-3402
39	B1W7H7ST7.5WT7H2C4	14	-23.1	-59.2	-7.1	-196	-410	-1050	-126.9	-2838
40	B1W7H7ST8.5WT7H0C4	25	-26.2	0.0	-7.1	-497	-465	0	-126.9	-4295
41	B1W7H7ST8.5WT7H1C4	18	-26.2	-29.6	-7.1	-279	-465	-525	-126.9	-3406
42	B1W7H7ST8.5WT7H2C4	14	-26.2	-59.2	-7.1	-196	-465	-1050	-126.9	-2842
43	B1W7H7ST9.5WT7H0C4	25	-29.3	0.0	-7.1	-495	-520	0	-126.9	-4299
44	B1W7H7ST9.5WT7H1C4	18	-29.3	-29.6	-7.1	-279	-520	-525	-126.9	-3410
45	B1W7H7ST9.5WT7H2C4	14	-29.3	-59.2	-7.1	-196	-520	-1050	-126.9	-2846
46	B1W7H7ST7.5WT7H0C5	25	-23.1	0.0	-7.1	-499	-410	0	-126.9	-4291
47	B1W7H7ST7.5WT7H1C5	18	-23.1	-29.6	-7.1	-279	-410	-525	-126.9	-3402
48	B1W7H7ST7.5WT7H2C5	14	-23.1	-59.2	-7.1	-196	-410	-1050	-126.9	-2838
49	B1W7H7ST8.5WT7H0C5	25	-26.2	0.0	-7.1	-497	-465	0	-126.9	-4295
50	B1W7H7ST8.5WT7H1C5	18	-26.2	-29.6	-7.1	-279	-465	-525	-126.9	-3406
51	B1W7H7ST8.5WT7H2C5	14	-26.2	-59.2	-7.1	-196	-465	-1050	-126.9	-2842
52	B1W7H7ST9.5WT7H0C5	25	-29.3	0.0	-7.1	-495	-520	0	-126.9	-4299
53	B1W7H7ST9.5WT7H1C5	18	-29.3	-29.6	-7.1	-279	-520	-525	-126.9	-3410
54	B1W7H7ST9.5WT7H2C5	14	-29.3	-59.2	-7.1	-196	-520	-1050	-126.9	-2846

Units: lb./in. for shear; lb.-in./in. for bending moment

#	Case	NLS	V_L^{DC}	V_L^{EF}	V_L^{DW}	V_L^{LL}	M_{pE}^{DC}	M_{pE}^{EF}	M_{pE}^{DW}	M_{pE}^{LL}
55	B1W8H8ST8WT8H0C3	28	-28.5	0.0	-8.3	-429	-584	0	-169.2	-4671
56	B1W8H8ST8WT8H1C3	23	-28.5	-34.2	-8.3	-295	-584	-700	-169.2	-3800
57	B1W8H8ST8WT8H2C3	18	-28.5	-68.3	-8.3	-208	-584	-1401	-169.2	-3241
58	B1W8H8ST9WT8H0C3	28	-32.0	0.0	-8.3	-428	-657	0	-169.2	-4675
59	B1W8H8ST9WT8H1C3	23	-32.0	-34.2	-8.3	-295	-657	-700	-169.2	-3804
60	B1W8H8ST9WT8H2C3	18	-32.0	-68.3	-8.3	-208	-657	-1401	-169.2	-3245
61	B1W8H8ST10WT8H0C3	28	-35.6	0.0	-8.3	-427	-729	0	-169.2	-4679
62	B1W8H8ST10WT8H1C3	23	-35.6	-34.2	-8.3	-294	-730	-700	-169.2	-3808
63	B1W8H8ST10WT8H2C3	18	-35.6	-68.3	-8.3	-208	-730	-1401	-169.2	-3249
64	B1W8H8ST8WT8H0C4	28	-28.5	0.0	-8.3	-429	-584	0	-169.2	-4671
65	B1W8H8ST8WT8H1C4	23	-28.5	-34.2	-8.3	-295	-584	-700	-169.2	-3800
66	B1W8H8ST8WT8H2C4	18	-28.5	-68.3	-8.3	-208	-584	-1401	-169.2	-3241
67	B1W8H8ST9WT8H0C4	28	-32.0	0.0	-8.3	-428	-657	0	-169.2	-4675
68	B1W8H8ST9WT8H1C4	23	-32.0	-34.2	-8.3	-295	-657	-700	-169.2	-3804
69	B1W8H8ST9WT8H2C4	18	-32.0	-68.3	-8.3	-208	-657	-1401	-169.2	-3245
70	B1W8H8ST10WT8H0C4	28	-35.6	0.0	-8.3	-427	-729	0	-169.2	-4679
71	B1W8H8ST10WT8H1C4	23	-35.6	-34.2	-8.3	-294	-730	-700	-169.2	-3808
72	B1W8H8ST10WT8H2C4	18	-35.6	-68.3	-8.3	-208	-730	-1401	-169.2	-3249
73	B1W8H8ST8WT8H0C5	28	-28.5	0.0	-8.3	-429	-584	0	-169.2	-4671
74	B1W8H8ST8WT8H1C5	23	-28.5	-34.2	-8.3	-295	-584	-700	-169.2	-3800
75	B1W8H8ST8WT8H2C5	18	-28.5	-68.3	-8.3	-208	-584	-1401	-169.2	-3241
76	B1W8H8ST9WT8H0C5	28	-32.0	0.0	-8.3	-428	-657	0	-169.2	-4675
77	B1W8H8ST9WT8H1C5	23	-32.0	-34.2	-8.3	-295	-657	-700	-169.2	-3804
78	B1W8H8ST9WT8H2C5	18	-32.0	-68.3	-8.3	-208	-657	-1401	-169.2	-3245
79	B1W8H8ST10WT8H0C5	28	-35.6	0.0	-8.3	-427	-729	0	-169.2	-4679
80	B1W8H8ST10WT8H1C5	23	-35.6	-34.2	-8.3	-294	-730	-700	-169.2	-3808
81	B1W8H8ST10WT8H2C5	18	-35.6	-68.3	-8.3	-208	-730	-1401	-169.2	-3249

Units: lb./in. for shear; lb.-in./in. for bending moment

#	Case	NLS	V_L^{DC}	V_L^{EF}	V_L^{DW}	V_L^{LL}	M_{pE}^{DC}	M_{pE}^{EF}	M_{pE}^{DW}	M_{pE}^{LL}
82	B1W9H9ST8.5WT9H0C3	35	-34.3	0.0	-9.4	-466	-797	0	-217.6	-5024
83	B1W9H9ST8.5WT9H1C3	31	-34.3	-38.8	-9.4	-310	-797	-901	-217.7	-4164
84	B1W9H9ST8.5WT9H2C3	22	-34.3	-77.5	-9.4	-219	-797	-1801	-217.7	-3616
85	B1W9H9ST9.5WT9H0C3	35	-38.3	0.0	-9.4	-465	-891	0	-217.6	-5028
86	B1W9H9ST9.5WT9H1C3	31	-38.3	-38.8	-9.4	-309	-891	-901	-217.7	-4168
87	B1W9H9ST9.5WT9H2C3	22	-38.3	-77.5	-9.4	-218	-891	-1801	-217.7	-3621
88	B1W9H9ST10.5WT9H0C3	35	-42.4	0.0	-9.4	-464	-985	0	-217.6	-5031
89	B1W9H9ST10.5WT9H1C3	31	-42.4	-38.8	-9.4	-308	-985	-901	-217.7	-4172
90	B1W9H9ST10.5WT9H2C3	22	-42.4	-77.5	-9.4	-218	-985	-1801	-217.7	-3625
91	B1W9H9ST8.5WT9H0C4	35	-34.3	0.0	-9.4	-466	-797	0	-217.6	-5024
92	B1W9H9ST8.5WT9H1C4	31	-34.3	-38.8	-9.4	-310	-797	-901	-217.7	-4164
93	B1W9H9ST8.5WT9H2C4	22	-34.3	-77.5	-9.4	-219	-797	-1801	-217.7	-3616
94	B1W9H9ST9.5WT9H0C4	35	-38.3	0.0	-9.4	-465	-891	0	-217.6	-5028
95	B1W9H9ST9.5WT9H1C4	31	-38.3	-38.8	-9.4	-309	-891	-901	-217.7	-4168
96	B1W9H9ST9.5WT9H2C4	22	-38.3	-77.5	-9.4	-218	-891	-1801	-217.7	-3621
97	B1W9H9ST10.5WT9H0C4	35	-42.4	0.0	-9.4	-464	-985	0	-217.6	-5031
98	B1W9H9ST10.5WT9H1C4	31	-42.4	-38.8	-9.4	-308	-985	-901	-217.7	-4172
99	B1W9H9ST10.5WT9H2C4	22	-42.4	-77.5	-9.4	-218	-985	-1801	-217.7	-3625
100	B1W9H9ST8.5WT9H0C5	35	-34.3	0.0	-9.4	-466	-797	0	-217.6	-5024
101	B1W9H9ST8.5WT9H1C5	31	-34.3	-38.8	-9.4	-310	-797	-901	-217.7	-4164
102	B1W9H9ST8.5WT9H2C5	22	-34.3	-77.5	-9.4	-219	-797	-1801	-217.7	-3616
103	B1W9H9ST9.5WT9H0C5	35	-38.3	0.0	-9.4	-465	-891	0	-217.6	-5028
104	B1W9H9ST9.5WT9H1C5	31	-38.3	-38.8	-9.4	-309	-891	-901	-217.7	-4168
105	B1W9H9ST9.5WT9H2C5	22	-38.3	-77.5	-9.4	-218	-891	-1801	-217.7	-3621
106	B1W9H9ST10.5WT9H0C5	35	-42.4	0.0	-9.4	-464	-985	0	-217.6	-5031
107	B1W9H9ST10.5WT9H1C5	31	-42.4	-38.8	-9.4	-308	-985	-901	-217.7	-4172
108	B1W9H9ST10.5WT9H2C5	22	-42.4	-77.5	-9.4	-218	-985	-1801	-217.7	-3625

Units: lb./in. for shear; lb.-in./in. for bending moment

#	Case	NLS	V_L^{DC}	V_L^{EF}	V_L^{DW}	V_L^{LL}	M_{pE}^{DC}	M_{pE}^{EF}	M_{pE}^{DW}	M_{pE}^{LL}
109	B1W10H10ST9WT10H0C3	44	-40.6	0.0	-10.5	-508	-1055	0	-272.1	-5348
110	B1W10H10ST9WT10H1C3	38	-40.6	-43.3	-10.5	-324	-1056	-1126	-272.1	-4496
111	B1W10H10ST9WT10H2C3	30	-40.6	-86.7	-10.5	-229	-1056	-2252	-272.1	-3957
112	B1W10H10ST10WT10H0C3	44	-45.1	0.0	-10.5	-506	-1173	0	-272.1	-5352
113	B1W10H10ST10WT10H1C3	38	-45.1	-43.3	-10.5	-322	-1173	-1126	-272.1	-4500
114	B1W10H10ST10WT10H2C3	30	-45.1	-86.7	-10.5	-229	-1173	-2252	-272.1	-3961
115	B1W10H10ST11WT10H0C3	44	-49.7	0.0	-10.5	-504	-1290	0	-272.1	-5356
116	B1W10H10ST11WT10H1C3	38	-49.7	-43.3	-10.5	-321	-1290	-1126	-272.1	-4504
117	B1W10H10ST11WT10H2C3	30	-49.7	-86.7	-10.5	-229	-1290	-2252	-272.1	-3965
118	B1W10H10ST9WT10H0C4	44	-40.6	0.0	-10.5	-508	-1055	0	-272.1	-5348
119	B1W10H10ST9WT10H1C4	38	-40.6	-43.3	-10.5	-324	-1056	-1126	-272.1	-4496
120	B1W10H10ST9WT10H2C4	30	-40.6	-86.7	-10.5	-229	-1056	-2252	-272.1	-3957
121	B1W10H10ST10WT10H0C4	44	-45.1	0.0	-10.5	-506	-1173	0	-272.1	-5352
122	B1W10H10ST10WT10H1C4	38	-45.1	-43.3	-10.5	-322	-1173	-1126	-272.1	-4500
123	B1W10H10ST10WT10H2C4	30	-45.1	-86.7	-10.5	-229	-1173	-2252	-272.1	-3961
124	B1W10H10ST11WT10H0C4	44	-49.7	0.0	-10.5	-504	-1290	0	-272.1	-5356
125	B1W10H10ST11WT10H1C4	38	-49.7	-43.3	-10.5	-321	-1290	-1126	-272.1	-4504
126	B1W10H10ST11WT10H2C4	30	-49.7	-86.7	-10.5	-229	-1290	-2252	-272.1	-3965
127	B1W10H10ST9WT10H0C5	44	-40.6	0.0	-10.5	-508	-1055	0	-272.1	-5348
128	B1W10H10ST9WT10H1C5	38	-40.6	-43.3	-10.5	-324	-1056	-1126	-272.1	-4496
129	B1W10H10ST9WT10H2C5	30	-40.6	-86.7	-10.5	-229	-1056	-2252	-272.1	-3957
130	B1W10H10ST10WT10H0C5	44	-45.1	0.0	-10.5	-506	-1173	0	-272.1	-5352
131	B1W10H10ST10WT10H1C5	38	-45.1	-43.3	-10.5	-322	-1173	-1126	-272.1	-4500
132	B1W10H10ST10WT10H2C5	30	-45.1	-86.7	-10.5	-229	-1173	-2252	-272.1	-3961
133	B1W10H10ST11WT10H0C5	44	-49.7	0.0	-10.5	-504	-1290	0	-272.1	-5356
134	B1W10H10ST11WT10H1C5	38	-49.7	-43.3	-10.5	-321	-1290	-1126	-272.1	-4504
135	B1W10H10ST11WT10H2C5	30	-49.7	-86.7	-10.5	-229	-1290	-2252	-272.1	-3965

Units: lb./in. for shear; lb.-in./in. for bending moment

#	Case	NLS	V_L^{DC}	V_L^{EF}	V_L^{DW}	V_L^{LL}	M_{pE}^{DC}	M_{pE}^{EF}	M_{pE}^{DW}	M_{pE}^{LL}
136	B1W11H11ST9.5WT11H0C3	47	-47.4	0.0	-11.6	-437	-1362	0	-332.5	-5648
137	B1W11H11ST9.5WT11H1C3	42	-47.4	-47.9	-11.6	-297	-1362	-1376	-332.5	-4800
138	B1W11H11ST9.5WT11H2C3	37	-47.4	-95.8	-11.6	-245	-1346	-2721	-328.7	-4322
139	B1W11H11ST10.5WT11H0C3	47	-52.4	0.0	-11.6	-436	-1505	0	-332.5	-5651
140	B1W11H11ST10.5WT11H1C3	42	-52.4	-47.9	-11.6	-297	-1505	-1376	-332.5	-4805
141	B1W11H11ST10.5WT11H2C3	37	-52.4	-95.8	-11.6	-244	-1488	-2721	-328.7	-4328
142	B1W11H11ST11.5WT11H0C3	47	-57.4	0.0	-11.6	-435	-1648	0	-332.5	-5655
143	B1W11H11ST11.5WT11H1C3	42	-57.4	-47.9	-11.6	-297	-1648	-1376	-332.5	-4809
144	B1W11H11ST11.5WT11H2C3	37	-57.4	-95.8	-11.6	-244	-1629	-2721	-328.7	-4334
145	B1W11H11ST9.5WT11H0C4	47	-47.4	0.0	-11.6	-437	-1362	0	-332.5	-5648
146	B1W11H11ST9.5WT11H1C4	42	-47.4	-47.9	-11.6	-297	-1362	-1376	-332.5	-4800
147	B1W11H11ST9.5WT11H2C4	37	-47.4	-95.8	-11.6	-245	-1346	-2721	-328.7	-4322
148	B1W11H11ST10.5WT11H0C4	47	-52.4	0.0	-11.6	-436	-1505	0	-332.5	-5651
149	B1W11H11ST10.5WT11H1C4	42	-52.4	-47.9	-11.6	-297	-1505	-1376	-332.5	-4805
150	B1W11H11ST10.5WT11H2C4	37	-52.4	-95.8	-11.6	-244	-1488	-2721	-328.7	-4328
151	B1W11H11ST11.5WT11H0C4	47	-57.4	0.0	-11.6	-435	-1648	0	-332.5	-5655
152	B1W11H11ST11.5WT11H1C4	42	-57.4	-47.9	-11.6	-297	-1648	-1376	-332.5	-4809
153	B1W11H11ST11.5WT11H2C4	37	-57.4	-95.8	-11.6	-244	-1629	-2721	-328.7	-4334
154	B1W11H11ST9.5WT11H0C5	47	-47.4	0.0	-11.6	-437	-1362	0	-332.5	-5648
155	B1W11H11ST9.5WT11H1C5	42	-47.4	-47.9	-11.6	-297	-1362	-1376	-332.5	-4800
156	B1W11H11ST9.5WT11H2C5	37	-47.4	-95.8	-11.6	-245	-1346	-2721	-328.7	-4322
157	B1W11H11ST10.5WT11H0C5	47	-52.4	0.0	-11.6	-436	-1505	0	-332.5	-5651
158	B1W11H11ST10.5WT11H1C5	42	-52.4	-47.9	-11.6	-297	-1505	-1376	-332.5	-4805
159	B1W11H11ST10.5WT11H2C5	37	-52.4	-95.8	-11.6	-244	-1488	-2721	-328.7	-4328
160	B1W11H11ST11.5WT11H0C5	47	-57.4	0.0	-11.6	-435	-1648	0	-332.5	-5655
161	B1W11H11ST11.5WT11H1C5	42	-57.4	-47.9	-11.6	-297	-1648	-1376	-332.5	-4809
162	B1W11H11ST11.5WT11H2C5	37	-57.4	-95.8	-11.6	-244	-1629	-2721	-328.7	-4334

Units: lb./in. for shear; lb.-in./in. for bending moment

#	Case	NLS	V_L^{DC}	V_L^{EF}	V_L^{DW}	V_L^{LL}	M_{pE}^{DC}	M_{pE}^{EF}	M_{pE}^{DW}	M_{pE}^{LL}
163	B1W12H12ST10WT12H0C3	54	-54.7	0.0	-12.7	-473	-1719	0	-398.9	-5925
164	B1W12H12ST10WT12H1C3	49	-54.7	-52.5	-12.7	-314	-1681	-1614	-390.0	-5142
165	B1W12H12ST10WT12H2C3	40	-54.7	-105.0	-12.7	-234	-1716	-3295	-398.1	-4802
166	B1W12H12ST11WT12H0C3	54	-60.1	0.0	-12.7	-472	-1891	0	-398.9	-5929
167	B1W12H12ST11WT12H1C3	49	-60.1	-52.5	-12.7	-313	-1849	-1614	-390.0	-5148
168	B1W12H12ST11WT12H2C3	40	-60.1	-105.0	-12.7	-234	-1887	-3294	-398.1	-4809
169	B1W12H12ST12WT12H0C3	54	-65.6	0.0	-12.7	-470	-2063	0	-398.9	-5932
170	B1W12H12ST12WT12H1C3	49	-65.6	-52.5	-12.7	-313	-2017	-1614	-390.0	-5153
171	B1W12H12ST12WT12H2C3	40	-65.6	-105.0	-12.7	-234	-2059	-3294	-398.1	-4815
172	B1W12H12ST10WT12H0C4	54	-54.7	0.0	-12.7	-473	-1719	0	-398.9	-5925
173	B1W12H12ST10WT12H1C4	49	-54.7	-52.5	-12.7	-314	-1681	-1614	-390.0	-5142
174	B1W12H12ST10WT12H2C4	40	-54.7	-105.0	-12.7	-234	-1716	-3295	-398.1	-4802
175	B1W12H12ST11WT12H0C4	54	-60.1	0.0	-12.7	-472	-1891	0	-398.9	-5929
176	B1W12H12ST11WT12H1C4	49	-60.1	-52.5	-12.7	-313	-1849	-1614	-390.0	-5148
177	B1W12H12ST11WT12H2C4	40	-60.1	-105.0	-12.7	-234	-1887	-3294	-398.1	-4809
178	B1W12H12ST12WT12H0C4	54	-65.6	0.0	-12.7	-470	-2063	0	-398.9	-5932
179	B1W12H12ST12WT12H1C4	49	-65.6	-52.5	-12.7	-313	-2017	-1614	-390.0	-5153
180	B1W12H12ST12WT12H2C4	40	-65.6	-105.0	-12.7	-234	-2059	-3294	-398.1	-4815
181	B1W12H12ST10WT12H0C5	54	-54.7	0.0	-12.7	-473	-1719	0	-398.9	-5925
182	B1W12H12ST10WT12H1C5	49	-54.7	-52.5	-12.7	-314	-1681	-1614	-390.0	-5142
183	B1W12H12ST10WT12H2C5	40	-54.7	-105.0	-12.7	-234	-1716	-3295	-398.1	-4802
184	B1W12H12ST11WT12H0C5	54	-60.1	0.0	-12.7	-472	-1891	0	-398.9	-5929
185	B1W12H12ST11WT12H1C5	49	-60.1	-52.5	-12.7	-313	-1849	-1614	-390.0	-5148
186	B1W12H12ST11WT12H2C5	40	-60.1	-105.0	-12.7	-234	-1887	-3294	-398.1	-4809
187	B1W12H12ST12WT12H0C5	54	-65.6	0.0	-12.7	-470	-2063	0	-398.9	-5932
188	B1W12H12ST12WT12H1C5	49	-65.6	-52.5	-12.7	-313	-2017	-1614	-390.0	-5153
189	B1W12H12ST12WT12H2C5	40	-65.6	-105.0	-12.7	-234	-2059	-3294	-398.1	-4815

Units: lb./in. for shear; lb.-in./in. for bending moment

Table E2. Bending moment and shear force values (3D model; 2-barrel culverts)

#	Case	NLS	V_L^{DC}	V_L^{EF}	V_L^{DW}	V_L^{LL}	V_R^{DC}	V_R^{EF}	V_R^{DW}	V_R^{LL}
1	B2W6H6ST7WT6H0C4	44	-25.3	0	-7.6	-558	-25	0	-7.6	-558
2	B2W6H6ST7WT6H1C4	38	-25.3	-32	-7.6	-377	-25	-32	-7.6	-377
3	B2W6H6ST7WT6H2C4	26	-25.3	-63	-7.6	-259	-25	-63	-7.6	-259
4	B2W6H6ST8WT6H0C4	44	-29.6	0	-7.7	-548	-30	0	-7.7	-548
5	B2W6H6ST8WT6H1C4	38	-29.5	-32	-7.7	-372	-30	-32	-7.7	-372
6	B2W6H6ST8WT6H2C4	26	-29.5	-63	-7.7	-256	-30	-63	-7.7	-256
7	B2W6H6ST9WT6H0C4	44	-33.9	0	-7.7	-539	-34	0	-7.7	-539
8	B2W6H6ST9WT6H1C4	38	-33.9	-32	-7.7	-367	-34	-32	-7.7	-367
9	B2W6H6ST9WT6H2C4	26	-33.9	-64	-7.7	-253	-34	-64	-7.7	-253
10	B2W7H7ST7.5WT7H0C4	59	-31.3	0	-9.0	-587	-31	0	-9.0	-587
11	B2W7H7ST7.5WT7H1C4	44	-31.3	-37	-9.0	-356	-31	-37	-9.0	-356
12	B2W7H7ST7.5WT7H2C4	32	-31.3	-74	-9.0	-253	-31	-74	-9.0	-253
13	B2W7H7ST8.5WT7H0C4	59	-36.0	0	-9.0	-577	-36	0	-9.0	-577
14	B2W7H7ST8.5WT7H1C4	44	-36.0	-37	-9.0	-351	-36	-37	-9.0	-351
15	B2W7H7ST8.5WT7H2C4	32	-36.1	-75	-9.0	-250	-36	-75	-9.0	-250
16	B2W7H7ST9.5WT7H0C4	59	-41.0	0	-9.0	-569	-41	0	-9.0	-569
17	B2W7H7ST9.5WT7H1C4	44	-41.0	-37	-9.0	-346	-41	-37	-9.0	-346
18	B2W7H7ST9.5WT7H2C4	32	-41.0	-75	-9.0	-248	-41	-75	-9.0	-248
19	B2W8H8ST8WT8H0C4	66	-37.8	0	-10.4	-530	-38	0	-10.4	-530
20	B2W8H8ST8WT8H1C4	57	-37.8	-43	-10.4	-366	-38	-43	-10.4	-366
21	B2W8H8ST8WT8H2C4	44	-37.8	-86	-10.4	-263	-38	-86	-10.4	-263
22	B2W8H8ST9WT8H0C4	66	-43.2	0	-10.4	-522	-43	0	-10.4	-522
23	B2W8H8ST9WT8H1C4	57	-43.1	-43	-10.4	-361	-43	-43	-10.4	-361
24	B2W8H8ST9WT8H2C4	44	-43.1	-86	-10.4	-261	-43	-86	-10.4	-261
25	B2W8H8ST10WT8H0C4	66	-48.6	0	-10.4	-513	-49	0	-10.4	-513
26	B2W8H8ST10WT8H1C4	57	-48.6	-43	-10.4	-357	-49	-43	-10.4	-357
27	B2W8H8ST10WT8H2C4	44	-48.6	-86	-10.4	-258	-49	-86	-10.4	-258

Units: lb./in. for shear

#	Case	M_{pE}^{DC}	M_{pE}^{EF}	M_{pE}^{DW}	M_{pE}^{LL}	M_{nL}^{DC}	M_{nL}^{EF}	M_{nL}^{DW}	M_{nL}^{LL}	M_{nR}^{DC}	M_{nR}^{EF}	M_{nR}^{DW}	M_{nR}^{LL}
1	B2W6H6ST7WT6H0C4	-94	0	-49	-3230	426	0	95	3064	-426	0	-95	-3064
2	B2W6H6ST7WT6H1C4	-94	-203	-49	-2339	423	393	95	2641	-423	-393	-95	-2641
3	B2W6H6ST7WT6H2C4	-94	-406	-49	-1763	424	786	95	2194	-424	-786	-95	-2194
4	B2W6H6ST8WT6H0C4	-93	0	-48	-3238	525	0	97	2965	-525	0	-97	-2965
5	B2W6H6ST8WT6H1C4	-92	-200	-48	-2346	522	401	97	2567	-522	-401	-97	-2567
6	B2W6H6ST8WT6H2C4	-92	-400	-48	-1768	523	802	97	2142	-523	-802	-97	-2142
7	B2W6H6ST9WT6H0C4	-89	0	-48	-3243	630	0	99	2871	-630	0	-99	-2871
8	B2W6H6ST9WT6H1C4	-89	-197	-48	-2351	626	409	99	2497	-626	-409	-99	-2497
9	B2W6H6ST9WT6H2C4	-88	-394	-48	-1773	627	818	99	2094	-627	-818	-99	-2094
10	B2W7H7ST7.5WT7H0C4	-170	0	-70	-3574	578	0	131	3260	-578	0	-131	-3260
11	B2W7H7ST7.5WT7H1C4	-169	-290	-70	-2684	578	541	131	2892	-578	-541	-131	-2892
12	B2W7H7ST7.5WT7H2C4	-168	-579	-70	-2117	579	1081	131	2508	-579	-1081	-131	-2508
13	B2W7H7ST8.5WT7H0C4	-177	0	-69	-3580	699	0	132	3199	-699	0	-132	-3199
14	B2W7H7ST8.5WT7H1C4	-175	-287	-69	-2690	700	548	132	2815	-700	-548	-132	-2815
15	B2W7H7ST8.5WT7H2C4	-162	-566	-68	-2125	700	1096	132	2449	-700	-1096	-132	-2449
16	B2W7H7ST9.5WT7H0C4	-181	0	-69	-3585	829	0	134	3146	-829	0	-134	-3146
17	B2W7H7ST9.5WT7H1C4	-178	-284	-69	-2695	830	555	134	2743	-830	-555	-134	-2743
18	B2W7H7ST9.5WT7H2C4	-161	-560	-68	-2132	831	1111	134	2401	-831	-1111	-134	-2401
19	B2W8H8ST8WT8H0C4	-258	0	-94	-3903	769	0	172	3864	-769	0	-172	-3864
20	B2W8H8ST8WT8H1C4	-258	-389	-94	-3013	766	713	172	3346	-766	-713	-172	-3385
21	B2W8H8ST8WT8H2C4	-257	-777	-94	-2466	767	1427	172	2803	-767	-1427	-172	-2803
22	B2W8H8ST9WT8H0C4	-272	0	-93	-3912	913	0	174	3776	-913	0	-174	-3776
23	B2W8H8ST9WT8H1C4	-272	-386	-93	-3022	910	720	174	3280	-910	-720	-174	-3325
24	B2W8H8ST9WT8H2C4	-271	-772	-93	-2474	911	1440	174	2746	-911	-1440	-174	-2746
25	B2W8H8ST10WT8H0C4	-282	0	-93	-3918	1069	0	176	3705	-1069	0	-176	-3705
26	B2W8H8ST10WT8H1C4	-281	-384	-93	-3029	1065	727	176	3221	-1065	-727	-176	-3273
27	B2W8H8ST10WT8H2C4	-280	-767	-93	-2481	1065	1453	176	2693	-1065	-1453	-176	-2693

Units: lb.-in./in. for bending moment

#	Case	NLS	V_L^{DC}	V_L^{EF}	V_L^{DW}	V_L^{LL}	V_R^{DC}	V_R^{EF}	V_R^{DW}	V_R^{LL}
28	B2W9H9ST8.5WT9H0C4	79	-45.0	0	-11.7	-556	-45	0	-11.7	-556
29	B2W9H9ST8.5WT9H1C4	71	-45.0	-49	-11.7	-376	-45	-49	-11.7	-376
30	B2W9H9ST8.5WT9H2C4	54	-45.0	-97	-11.7	-271	-45	-97	-11.7	-271
31	B2W9H9ST9.5WT9H0C4	79	-50.9	0	-11.7	-547	-51	0	-11.7	-547
32	B2W9H9ST9.5WT9H1C4	71	-50.9	-49	-11.7	-371	-51	-49	-11.7	-371
33	B2W9H9ST9.5WT9H2C4	54	-50.9	-97	-11.7	-268	-51	-97	-11.7	-268
34	B2W9H9ST10.5WT9H0C4	79	-56.9	0	-11.8	-540	-57	0	-11.8	-540
35	B2W9H9ST10.5WT9H1C4	71	-56.8	-49	-11.8	-367	-57	-49	-11.8	-367
36	B2W9H9ST10.5WT9H2C4	54	-56.8	-97	-11.8	-265	-57	-97	-11.8	-265
37	B2W10H10ST9WT10H0C4	96	-52.9	0	-13.1	-583	-53	0	-13.1	-583
38	B2W10H10ST9WT10H1C4	84	-52.9	-54	-13.1	-395	-53	-54	-13.1	-395
39	B2W10H10ST9WT10H2C4	70	-52.9	-109	-13.1	-290	-53	-109	-13.1	-290
40	B2W10H10ST10WT10H0C4	96	-59.3	0	-13.1	-575	-59	0	-13.1	-575
41	B2W10H10ST10WT10H1C4	84	-59.2	-54	-13.1	-391	-59	-54	-13.1	-391
42	B2W10H10ST10WT10H2C4	70	-59.3	-109	-13.1	-288	-59	-109	-13.1	-288
43	B2W10H10ST11WT10H0C4	96	-65.8	0	-13.1	-568	-66	0	-13.1	-568
44	B2W10H10ST11WT10H1C4	84	-65.7	-54	-13.1	-387	-66	-54	-13.1	-387
45	B2W10H10ST11WT10H2C4	70	-65.8	-109	-13.1	-285	-66	-109	-13.1	-285
46	B2W11H11ST9.5WT11H0C4	103	-61.4	0	-14.5	-527	-61	0	-14.5	-527
47	B2W11H11ST9.5WT11H1C4	94	-61.4	-60	-14.5	-381	-61	-60	-14.5	-381
48	B2W11H11ST9.5WT11H2C4	83	-61.3	-120	-14.5	-306	-61	-120	-14.5	-306
49	B2W11H11ST10.5WT11H0C4	103	-68.3	0	-14.5	-520	-68	0	-14.5	-520
50	B2W11H11ST10.5WT11H1C4	94	-68.3	-60	-14.5	-376	-68	-60	-14.5	-376
51	B2W11H11ST10.5WT11H2C4	83	-68.3	-120	-14.5	-303	-68	-120	-14.5	-303
52	B2W11H11ST11.5WT11H0C4	103	-75.4	0	-14.5	-513	-75	0	-14.5	-513
53	B2W11H11ST11.5WT11H1C4	94	-75.4	-60	-14.5	-372	-75	-60	-14.5	-372
54	B2W11H11ST11.5WT11H2C4	83	-75.3	-120	-14.5	-300	-75	-120	-14.5	-300

Units: lb./in. for shear

#	Case	M_{pE}^{DC}	M_{pE}^{EF}	M_{pE}^{DW}	M_{pE}^{LL}	M_{nL}^{DC}	M_{nL}^{EF}	M_{nL}^{DW}	M_{nL}^{LL}	M_{nR}^{DC}	M_{nR}^{EF}	M_{nR}^{DW}	M_{nR}^{LL}
28	B2W9H9ST8.5WT9H0C4	-369	0	-121	-4211	998	0	220	4362	-998	0	-220	-4362
29	B2W9H9ST8.5WT9H1C4	-368	-501	-121	-3328	996	912	220	3940	-996	-912	-220	-3940
30	B2W9H9ST8.5WT9H2C4	-367	-1000	-121	-2787	996	1823	220	3439	-996	-1823	-220	-3358
31	B2W9H9ST9.5WT9H0C4	-392	0	-121	-4222	1167	0	222	4263	-1167	0	-222	-4263
32	B2W9H9ST9.5WT9H1C4	-391	-498	-120	-3339	1163	917	222	3868	-1163	-917	-222	-3868
33	B2W9H9ST9.5WT9H2C4	-390	-996	-120	-2798	1164	1835	222	3384	-1164	-1835	-222	-3301
34	B2W9H9ST10.5WT9H0C4	-411	0	-120	-4231	1348	0	223	4172	-1348	0	-223	-4172
35	B2W9H9ST10.5WT9H1C4	-409	-496	-120	-3348	1343	924	223	3805	-1343	-924	-223	-3805
36	B2W9H9ST10.5WT9H2C4	-408	-991	-120	-2807	1344	1847	223	3335	-1344	-1847	-223	-3252
37	B2W10H10ST9WT10H0C4	-513	0	-152	-4506	1275	0	274	4786	-1275	0	-274	-4786
38	B2W10H10ST9WT10H1C4	-512	-630	-152	-3636	1272	1136	274	4454	-1272	-1136	-274	-4454
39	B2W10H10ST9WT10H2C4	-511	-1260	-152	-3092	1273	2271	274	4013	-1273	-2271	-274	-4013
40	B2W10H10ST10WT10H0C4	-550	0	-152	-4517	1470	0	276	4679	-1470	0	-276	-4679
41	B2W10H10ST10WT10H1C4	-549	-628	-152	-3648	1467	1141	276	4372	-1467	-1141	-276	-4372
42	B2W10H10ST10WT10H2C4	-548	-1256	-152	-3104	1467	2282	276	3949	-1467	-2282	-276	-3949
43	B2W10H10ST11WT10H0C4	-582	0	-151	-4526	1678	0	277	4581	-1678	0	-277	-4581
44	B2W10H10ST11WT10H1C4	-581	-626	-151	-3657	1674	1147	277	4298	-1674	-1147	-277	-4298
45	B2W10H10ST11WT10H2C4	-580	-1252	-151	-3113	1675	2294	277	3893	-1675	-2294	-277	-3893
46	B2W11H11ST9.5WT11H0C4	-673	0	-186	-4786	1605	0	335	5176	-1605	0	-335	-5176
47	B2W11H11ST9.5WT11H1C4	-672	-770	-186	-3921	1602	1385	335	4917	-1602	-1385	-335	-4917
48	B2W11H11ST9.5WT11H2C4	-672	-1540	-186	-3379	1600	2770	335	4528	-1600	-2770	-335	-4528
49	B2W11H11ST10.5WT11H0C4	-723	0	-186	-4799	1830	0	336	5076	-1830	0	-336	-5076
50	B2W11H11ST10.5WT11H1C4	-721	-768	-186	-3935	1827	1390	336	4826	-1827	-1390	-336	-4826
51	B2W11H11ST10.5WT11H2C4	-721	-1536	-186	-3393	1824	2780	336	4457	-1824	-2780	-336	-4457
52	B2W11H11ST11.5WT11H0C4	-766	0	-185	-4809	2070	0	337	4986	-2070	0	-337	-4986
53	B2W11H11ST11.5WT11H1C4	-764	-766	-185	-3946	2065	1396	337	4746	-2065	-1396	-337	-4746
54	B2W11H11ST11.5WT11H2C4	-765	-1532	-185	-3404	2062	2791	337	4394	-2062	-2791	-337	-4394

Units: lb.-in./in. for bending moment

#	Case	NLS	V_L^{DC}	V_L^{EF}	V_L^{DW}	V_L^{LL}	V_R^{DC}	V_R^{EF}	V_R^{DW}	V_R^{LL}
55	B2W12H12ST10WT12H0C4	116	-70.5	0	-15.9	-554	-70	0	-15.9	-554
56	B2W12H12ST10WT12H1C4	107	-70.4	-66	-15.9	-394	-70	-66	-15.9	-394
57	B2W12H12ST10WT12H2C4	90	-70.4	-131	-15.9	-301	-70	-131	-15.9	-301
58	B2W12H12ST11WT12H0C4	116	-78.0	0	-15.9	-548	-78	0	-15.9	-548
59	B2W12H12ST11WT12H1C4	107	-78.0	-66	-15.9	-390	-78	-66	-15.9	-390
60	B2W12H12ST11WT12H2C4	90	-78.0	-131	-15.9	-298	-78	-131	-15.9	-298
61	B2W12H12ST12WT12H0C4	116	-85.6	0	-15.9	-541	-86	0	-15.9	-541
62	B2W12H12ST12WT12H1C4	107	-85.6	-66	-15.9	-386	-86	-66	-15.9	-386
63	B2W12H12ST12WT12H2C4	90	-85.6	-132	-15.9	-296	-86	-132	-15.9	-296

Units: lb./in. for shear

#	Case	M_{pE}^{DC}	M_{pE}^{EF}	M_{pE}^{DW}	M_{pE}^{LL}	M_{nL}^{DC}	M_{nL}^{EF}	M_{nL}^{DW}	M_{nL}^{LL}	M_{nR}^{DC}	M_{nR}^{EF}	M_{nR}^{DW}	M_{nR}^{LL}
55	B2W12H12ST10WT12H0C4	-862	0	-223	-5046	1987	0	401	5540	-1987	0	-401	-5540
56	B2W12H12ST10WT12H1C4	-870	-927	-224	-4189	1985	1660	401	5318	-1985	-1660	-401	-5318
57	B2W12H12ST10WT12H2C4	-869	-1855	-224	-3651	1985	3320	401	5010	-1985	-3320	-401	-5010
58	B2W12H12ST11WT12H0C4	-925	0	-223	-5060	2245	0	402	5434	-2245	0	-402	-5434
59	B2W12H12ST11WT12H1C4	-935	-925	-224	-4202	2242	1665	402	5221	-2242	-1665	-402	-5221
60	B2W12H12ST11WT12H2C4	-939	-1845	-223	-3667	2243	3330	402	4930	-2243	-3330	-402	-4930
61	B2W12H12ST12WT12H0C4	-982	0	-222	-5073	2517	0	404	5338	-2517	0	-404	-5338
62	B2W12H12ST12WT12H1C4	-979	-919	-222	-4214	2513	1670	404	5134	-2513	-1670	-404	-5134
63	B2W12H12ST12WT12H2C4	-994	-1847	-223	-3687	2514	3341	404	4859	-2514	-3341	-404	-4859

Units: lb.-in./in. for bending moment

Table E3. Bending moment and shear force values (3D model; 3-barrel culverts)

#	Case	NLS	V_L^{DC}	V_L^{EF}	V_L^{DW}	V_L^{LL}	V_R^{DC}	V_R^{EF}	V_R^{DW}	V_R^{LL}
1	B3W6H6ST8WT6H0C4	44	-27.2	0.0	-7.4	-548.6	-27.2	0.0	-7.4	-530.8
2	B3W6H6ST8WT6H1C4	38	-27.1	-30.5	-7.4	-372.4	-27.1	-30.5	-7.4	-344.2
3	B3W6H6ST8WT6H2C4	26	-27.2	-61.0	-7.4	-256.6	-27.2	-61.0	-7.4	-216.3
4	B3W7H7ST8.5WT7H0C4	59	-33.6	0.0	-8.7	-577.9	-33.6	0.0	-8.7	-561.9
5	B3W7H7ST8.5WT7H1C4	44	-33.7	-36.1	-8.7	-352.0	-33.7	-36.1	-8.7	-322.8
6	B3W7H7ST8.5WT7H2C4	32	-33.7	-72.1	-8.7	-251.4	-33.7	-72.1	-8.7	-210.1
7	B3W8H8ST9WT8H0C4	66	-40.8	0.0	-10.1	-522.1	-40.8	0.0	-10.1	-504.6
8	B3W8H8ST9WT8H1C4	57	-40.8	-41.7	-10.1	-362.1	-40.8	-41.7	-10.1	-333.6
9	B3W8H8ST9WT8H2C4	44	-40.8	-83.3	-10.1	-261.4	-40.8	-83.3	-10.1	-220.5
10	B3W9H9ST9.5WT9H0C4	79	-48.5	0.0	-11.4	-547.8	-48.5	0.0	-11.4	-530.3
11	B3W9H9ST9.5WT9H1C4	71	-48.5	-47.3	-11.4	-372.7	-48.5	-47.3	-11.4	-341.5
12	B3W9H9ST9.5WT9H2C4	54	-48.5	-94.6	-11.4	-268.7	-48.5	-94.6	-11.4	-226.9
13	B3W10H10ST10WT10H0C4	96	-56.9	0.0	-12.8	-575.4	-56.9	0.0	-12.8	-557.2
14	B3W10H10ST10WT10H1C4	84	-56.8	-52.9	-12.8	-392.1	-56.8	-52.9	-12.8	-347.6
15	B3W10H10ST10WT10H2C4	70	-56.9	-105.9	-12.8	-289.0	-56.9	-105.9	-12.8	-230.7
16	B3W11H11ST10.5WT11H0C4	103	-65.9	0.0	-14.2	-521.2	-65.9	0.0	-14.2	-498.5
17	B3W11H11ST10.5WT11H1C4	94	-65.8	-58.6	-14.2	-377.9	-65.8	-58.6	-14.2	-324.2
18	B3W11H11ST10.5WT11H2C4	83	-65.8	-117.2	-14.2	-304.4	-65.8	-117.2	-14.2	-238.3
19	B3W12H12ST11WT12H0C4	116	-75.4	0.0	-15.5	-549.0	-75.4	0.0	-15.5	-522.3
20	B3W12H12ST11WT12H1C4	107	-75.4	-64.3	-15.5	-391.3	-75.4	-64.3	-15.5	-337.6
21	B3W12H12ST11WT12H2C4	90	-75.4	-128.5	-15.5	-300.0	-75.4	-128.5	-15.5	-231.0

Units: lb./in. for shear

#	Case	M_{pE}^{DC}	M_{pE}^{EF}	M_{pE}^{DW}	M_{pE}^{LL}	M_{nL}^{DC}	M_{nL}^{EF}	M_{nL}^{DW}	M_{nL}^{LL}	M_{nR}^{DC}	M_{nR}^{EF}	M_{nR}^{DW}	M_{nR}^{LL}	M_{pI}^{DC}	M_{pI}^{EF}	M_{pI}^{DW}	M_{pI}^{LL}
1	B3W6H6ST8WT6H0C4	-149	0	-55	-3216	381	0	80	3021	-317	0	-75	-2678	5	0	-16	-2727
2	B3W6H6ST8WT6H1C4	-149	-229	-55	-2324	379	329	80	2623	-316	-309	-75	-2212	4	-66	-16	-1873
3	B3W6H6ST8WT6H2C4	-149	-457	-55	-1747	379	658	80	2196	-317	-618	-75	-1732	4	-132	-16	-1353
4	B3W7H7ST8.5WT7H0C4	-238	0	-77	-3557	529	0	111	3273	-433	0	-101	-2859	-32	0	-26	-3005
5	B3W7H7ST8.5WT7H1C4	-238	-319	-77	-2667	530	460	111	2885	-433	-419	-101	-2472	-32	-106	-26	-2143
6	B3W7H7ST8.5WT7H2C4	-237	-639	-77	-2100	530	920	111	2517	-434	-839	-101	-2044	-31	-211	-26	-1610
7	B3W8H8ST9WT8H0C4	-346	0	-103	-3881	717	0	149	3876	-577	0	-132	-3106	-79	0	-37	-3267
8	B3W8H8ST9WT8H1C4	-346	-427	-103	-2992	715	615	149	3376	-576	-547	-132	-2685	-80	-153	-37	-2400
9	B3W8H8ST9WT8H2C4	-346	-853	-103	-2445	716	1230	149	2831	-576	-1094	-132	-2312	-80	-307	-37	-1863
10	B3W9H9ST9.5WT9H0C4	-479	0	-132	-4185	945	0	192	4389	-750	0	-167	-3557	-141	0	-50	-3518
11	B3W9H9ST9.5WT9H1C4	-482	-545	-132	-3303	943	795	192	3993	-750	-692	-167	-3125	-142	-209	-51	-2648
12	B3W9H9ST9.5WT9H2C4	-478	-1094	-132	-2761	943	1589	192	3501	-750	-1384	-167	-2577	-142	-418	-50	-2116
13	B3W10H10ST10WT10H0C4	-643	0	-165	-4478	1219	0	241	4833	-957	0	-207	-3962	-212	0	-65	-3705
14	B3W10H10ST10WT10H1C4	-644	-682	-165	-3607	1217	999	241	4525	-956	-854	-207	-3579	-213	-268	-65	-2876
15	B3W10H10ST10WT10H2C4	-643	-1365	-165	-3064	1217	1998	241	4095	-957	-1709	-207	-3141	-217	-544	-66	-2360
16	B3W11H11ST10.5WT11H0C4	-832	0	-201	-4752	1546	0	297	5261	-1201	0	-250	-4355	-306	0	-83	-3880
17	B3W11H11ST10.5WT11H1C4	-832	-832	-201	-3887	1544	1228	297	5009	-1200	-1035	-250	-4021	-306	-343	-83	-2999
18	B3W11H11ST10.5WT11H2C4	-832	-1664	-201	-3346	1542	2455	297	4632	-1200	-2069	-250	-3610	-307	-686	-83	-2494
19	B3W12H12ST11WT12H0C4	-1054	0	-240	-5008	1924	0	358	5645	-1483	0	-298	-4691	-411	0	-102	-4056
20	B3W12H12ST11WT12H1C4	-1055	-995	-240	-4152	1922	1481	358	5431	-1483	-1232	-298	-4425	-412	-422	-102	-3191
21	B3W12H12ST11WT12H2C4	-1055	-1990	-240	-3615	1923	2962	358	5134	-1483	-2465	-298	-4053	-407	-835	-101	-2674

Units: lb.-in./in. for bending moment

Table E4. Bending moment and shear force values (2D model; AASHTO-LRFD BDS; 1-barrel culverts)

#	Case	NLS	V_L^{DC}	V_L^{EF}	V_L^{DW}	V_L^{LL}	M_{pE}^{DC}	M_{pE}^{EF}	M_{pE}^{DW}	M_{pE}^{LL}
1	B1W6H6ST7WT6H0C3	16	-20.1	0.0	-6.6	-270.6	-331	0	-110	-4653
2	B1W6H6ST7WT6H1C3	11	-20.1	-27.5	-6.6	-237.2	-331	-454	-110	-4165
3	B1W6H6ST7WT6H2C3	21	-20.1	-55.0	-6.6	-201.2	-331	-908	-110	-3625
4	B1W6H6ST8WT6H0C3	16	-22.9	0.0	-6.6	-270.6	-378	0	-110	-4653
5	B1W6H6ST8WT6H1C3	11	-22.9	-27.5	-6.6	-237.2	-378	-454	-110	-4165
6	B1W6H6ST8WT6H2C3	21	-22.9	-55.0	-6.6	-201.2	-378	-908	-110	-3625
7	B1W6H6ST9WT6H0C3	16	-25.8	0.0	-6.6	-270.6	-425	0	-110	-4653
8	B1W6H6ST9WT6H1C3	11	-25.8	-27.5	-6.6	-237.2	-425	-454	-110	-4165
9	B1W6H6ST9WT6H2C3	21	-25.8	-55.0	-6.6	-201.2	-425	-908	-110	-3625
10	B1W6H6ST7WT6H0C4	16	-20.1	0.0	-6.6	-270.6	-331	0	-110	-4653
11	B1W6H6ST7WT6H1C4	11	-20.1	-27.5	-6.6	-237.2	-331	-454	-110	-4165
12	B1W6H6ST7WT6H2C4	21	-20.1	-55.0	-6.6	-201.2	-331	-908	-110	-3625
13	B1W6H6ST8WT6H0C4	16	-22.9	0.0	-6.6	-270.6	-378	0	-110	-4653
14	B1W6H6ST8WT6H1C4	11	-22.9	-27.5	-6.6	-237.2	-378	-454	-110	-4165
15	B1W6H6ST8WT6H2C4	21	-22.9	-55.0	-6.6	-201.2	-378	-908	-110	-3625
16	B1W6H6ST9WT6H0C4	16	-25.8	0.0	-6.6	-270.6	-425	0	-110	-4653
17	B1W6H6ST9WT6H1C4	11	-25.8	-27.5	-6.6	-237.2	-425	-454	-110	-4165
18	B1W6H6ST9WT6H2C4	21	-25.8	-55.0	-6.6	-201.2	-425	-908	-110	-3625
19	B1W6H6ST7WT6H0C5	16	-20.1	0.0	-6.6	-270.6	-331	0	-110	-4653
20	B1W6H6ST7WT6H1C5	11	-20.1	-27.5	-6.6	-237.2	-331	-454	-110	-4165
21	B1W6H6ST7WT6H2C5	21	-20.1	-55.0	-6.6	-201.2	-331	-908	-110	-3625
22	B1W6H6ST8WT6H0C5	16	-22.9	0.0	-6.6	-270.6	-378	0	-110	-4653
23	B1W6H6ST8WT6H1C5	11	-22.9	-27.5	-6.6	-237.2	-378	-454	-110	-4165
24	B1W6H6ST8WT6H2C5	21	-22.9	-55.0	-6.6	-201.2	-378	-908	-110	-3625
25	B1W6H6ST9WT6H0C5	16	-25.8	0.0	-6.6	-270.6	-425	0	-110	-4653
26	B1W6H6ST9WT6H1C5	11	-25.8	-27.5	-6.6	-237.2	-425	-454	-110	-4165
27	B1W6H6ST9WT6H2C5	16	-25.8	-55.0	-6.6	-201.2	-425	-908	-110	-3625

Units: lb./in. for shear; lb.-in./in. for bending moment

#	Case	NLS	V_L^{DC}	V_L^{EF}	V_L^{DW}	V_L^{LL}	M_{pE}^{DC}	M_{pE}^{EF}	M_{pE}^{DW}	M_{pE}^{LL}
28	B1W7H7ST7.5WT7H0C3	29	-25.1	0.0	-7.8	-289.0	-483	0	-149	-5431
29	B1W7H7ST7.5WT7H1C3	21	-25.1	-32.1	-7.8	-246.0	-483	-618	-149	-4949
30	B1W7H7ST7.5WT7H2C3	15	-25.1	-64.2	-7.8	-214.9	-483	-1235	-149	-4416
31	B1W7H7ST8.5WT7H0C3	29	-28.4	0.0	-7.8	-289.0	-547	0	-149	-5431
32	B1W7H7ST8.5WT7H1C3	21	-28.4	-32.1	-7.8	-246.0	-547	-618	-149	-4949
33	B1W7H7ST8.5WT7H2C3	15	-28.4	-64.2	-7.8	-214.9	-547	-1235	-149	-4416
34	B1W7H7ST9.5WT7H0C3	29	-31.7	0.0	-7.8	-289.0	-611	0	-149	-5431
35	B1W7H7ST9.5WT7H1C3	21	-31.7	-32.1	-7.8	-246.0	-611	-618	-149	-4949
36	B1W7H7ST9.5WT7H2C3	15	-31.7	-64.2	-7.8	-214.9	-611	-1235	-149	-4416
37	B1W7H7ST7.5WT7H0C4	29	-25.1	0.0	-7.8	-289.0	-483	0	-149	-5431
38	B1W7H7ST7.5WT7H1C4	21	-25.1	-32.1	-7.8	-246.0	-483	-618	-149	-4949
39	B1W7H7ST7.5WT7H2C4	15	-25.1	-64.2	-7.8	-214.9	-483	-1235	-149	-4416
40	B1W7H7ST8.5WT7H0C4	29	-28.4	0.0	-7.8	-289.0	-547	0	-149	-5431
41	B1W7H7ST8.5WT7H1C4	21	-28.4	-32.1	-7.8	-246.0	-547	-618	-149	-4949
42	B1W7H7ST8.5WT7H2C4	15	-28.4	-64.2	-7.8	-214.9	-547	-1235	-149	-4416
43	B1W7H7ST9.5WT7H0C4	29	-31.7	0.0	-7.8	-289.0	-611	0	-149	-5431
44	B1W7H7ST9.5WT7H1C4	21	-31.7	-32.1	-7.8	-246.0	-611	-618	-149	-4949
45	B1W7H7ST9.5WT7H2C4	15	-31.7	-64.2	-7.8	-214.9	-611	-1235	-149	-4416
46	B1W7H7ST7.5WT7H0C5	29	-25.1	0.0	-7.8	-289.0	-483	0	-149	-5431
47	B1W7H7ST7.5WT7H1C5	21	-25.1	-32.1	-7.8	-246.0	-483	-618	-149	-4949
48	B1W7H7ST7.5WT7H2C5	15	-25.1	-64.2	-7.8	-214.9	-483	-1235	-149	-4416
49	B1W7H7ST8.5WT7H0C5	29	-28.4	0.0	-7.8	-289.0	-547	0	-149	-5431
50	B1W7H7ST8.5WT7H1C5	21	-28.4	-32.1	-7.8	-246.0	-547	-618	-149	-4949
51	B1W7H7ST8.5WT7H2C5	15	-28.4	-64.2	-7.8	-214.9	-547	-1235	-149	-4416
52	B1W7H7ST9.5WT7H0C5	29	-31.7	0.0	-7.8	-289.0	-611	0	-149	-5431
53	B1W7H7ST9.5WT7H1C5	21	-31.7	-32.1	-7.8	-246.0	-611	-618	-149	-4949
54	B1W7H7ST9.5WT7H2C5	15	-31.7	-64.2	-7.8	-214.9	-611	-1235	-149	-4416

Units: lb./in. for shear; lb.-in./in. for bending moment

#	Case	NLS	V_L^{DC}	V_L^{EF}	V_L^{DW}	V_L^{LL}	M_{pE}^{DC}	M_{pE}^{EF}	M_{pE}^{DW}	M_{pE}^{LL}
55	B1W8H8ST8WT8H0C3	32	-30.6	0.0	-8.9	-296.8	-672	0	-195	-6190
56	B1W8H8ST8WT8H1C3	29	-30.6	-36.7	-8.9	-266.3	-672	-807	-195	-5713
57	B1W8H8ST8WT8H2C3	19	-30.6	-73.3	-8.9	-224.2	-672	-1613	-195	-5187
58	B1W8H8ST9WT8H0C3	32	-34.4	0.0	-8.9	-296.8	-756	0	-195	-6190
59	B1W8H8ST9WT8H1C3	29	-34.4	-36.7	-8.9	-266.3	-756	-807	-195	-5713
60	B1W8H8ST9WT8H2C3	19	-34.4	-73.3	-8.9	-224.2	-756	-1613	-195	-5187
61	B1W8H8ST10WT8H0C3	32	-38.2	0.0	-8.9	-296.8	-840	0	-195	-6190
62	B1W8H8ST10WT8H1C3	29	-38.2	-36.7	-8.9	-266.3	-840	-807	-195	-5713
63	B1W8H8ST10WT8H2C3	19	-38.2	-73.3	-8.9	-224.2	-840	-1613	-195	-5187
64	B1W8H8ST8WT8H0C4	32	-30.6	0.0	-8.9	-296.8	-672	0	-195	-6190
65	B1W8H8ST8WT8H1C4	29	-30.6	-36.7	-8.9	-266.3	-672	-807	-195	-5713
66	B1W8H8ST8WT8H2C4	19	-30.6	-73.3	-8.9	-224.2	-672	-1613	-195	-5187
67	B1W8H8ST9WT8H0C4	32	-34.4	0.0	-8.9	-296.8	-756	0	-195	-6190
68	B1W8H8ST9WT8H1C4	29	-34.4	-36.7	-8.9	-266.3	-756	-807	-195	-5713
69	B1W8H8ST9WT8H2C4	19	-34.4	-73.3	-8.9	-224.2	-756	-1613	-195	-5187
70	B1W8H8ST10WT8H0C4	32	-38.2	0.0	-8.9	-296.8	-840	0	-195	-6190
71	B1W8H8ST10WT8H1C4	29	-38.2	-36.7	-8.9	-266.3	-840	-807	-195	-5713
72	B1W8H8ST10WT8H2C4	19	-38.2	-73.3	-8.9	-224.2	-840	-1613	-195	-5187
73	B1W8H8ST8WT8H0C5	32	-30.6	0.0	-8.9	-296.8	-672	0	-195	-6190
74	B1W8H8ST8WT8H1C5	29	-30.6	-36.7	-8.9	-266.3	-672	-807	-195	-5713
75	B1W8H8ST8WT8H2C5	19	-30.6	-73.3	-8.9	-224.2	-672	-1613	-195	-5187
76	B1W8H8ST9WT8H0C5	32	-34.4	0.0	-8.9	-296.8	-756	0	-195	-6190
77	B1W8H8ST9WT8H1C5	29	-34.4	-36.7	-8.9	-266.3	-756	-807	-195	-5713
78	B1W8H8ST9WT8H2C5	19	-34.4	-73.3	-8.9	-224.2	-756	-1613	-195	-5187
79	B1W8H8ST10WT8H0C5	32	-38.2	0.0	-8.9	-296.8	-840	0	-195	-6190
80	B1W8H8ST10WT8H1C5	29	-38.2	-36.7	-8.9	-266.3	-840	-807	-195	-5713
81	B1W8H8ST10WT8H2C5	19	-38.2	-73.3	-8.9	-224.2	-840	-1613	-195	-5187

Units: lb./in. for shear; lb.-in./in. for bending moment

#	Case	NLS	V_L^{DC}	V_L^{EF}	V_L^{DW}	V_L^{LL}	M_{pE}^{DC}	M_{pE}^{EF}	M_{pE}^{DW}	M_{pE}^{LL}
82	B1W9H9ST8.5WT9H0C3	40	-36.5	0.0	-10.0	-317.6	-904	0	-247	-6930
83	B1W9H9ST8.5WT9H1C3	37	-36.5	-41.3	-10.0	-287.5	-904	-1021	-247	-6459
84	B1W9H9ST8.5WT9H2C3	26	-36.5	-82.5	-10.0	-245.3	-904	-2042	-247	-5939
85	B1W9H9ST9.5WT9H0C3	40	-40.8	0.0	-10.0	-317.6	-1010	0	-247	-6930
86	B1W9H9ST9.5WT9H1C3	37	-40.8	-41.3	-10.0	-287.5	-1010	-1021	-247	-6459
87	B1W9H9ST9.5WT9H2C3	26	-40.8	-82.5	-10.0	-245.3	-1010	-2042	-247	-5939
88	B1W9H9ST10.5WT9H0C3	40	-45.1	0.0	-10.0	-317.6	-1117	0	-247	-6930
89	B1W9H9ST10.5WT9H1C3	37	-45.1	-41.3	-10.0	-287.5	-1117	-1021	-247	-6459
90	B1W9H9ST10.5WT9H2C3	26	-45.1	-82.5	-10.0	-245.3	-1117	-2042	-247	-5939
91	B1W9H9ST8.5WT9H0C4	40	-36.5	0.0	-10.0	-317.6	-904	0	-247	-6930
92	B1W9H9ST8.5WT9H1C4	37	-36.5	-41.3	-10.0	-287.5	-904	-1021	-247	-6459
93	B1W9H9ST8.5WT9H2C4	26	-36.5	-82.5	-10.0	-245.3	-904	-2042	-247	-5939
94	B1W9H9ST9.5WT9H0C4	40	-40.8	0.0	-10.0	-317.6	-1010	0	-247	-6930
95	B1W9H9ST9.5WT9H1C4	37	-40.8	-41.3	-10.0	-287.5	-1010	-1021	-247	-6459
96	B1W9H9ST9.5WT9H2C4	26	-40.8	-82.5	-10.0	-245.3	-1010	-2042	-247	-5939
97	B1W9H9ST10.5WT9H0C4	40	-45.1	0.0	-10.0	-317.6	-1117	0	-247	-6930
98	B1W9H9ST10.5WT9H1C4	37	-45.1	-41.3	-10.0	-287.5	-1117	-1021	-247	-6459
99	B1W9H9ST10.5WT9H2C4	26	-45.1	-82.5	-10.0	-245.3	-1117	-2042	-247	-5939
100	B1W9H9ST8.5WT9H0C5	40	-36.5	0.0	-10.0	-317.6	-904	0	-247	-6930
101	B1W9H9ST8.5WT9H1C5	37	-36.5	-41.3	-10.0	-287.5	-904	-1021	-247	-6459
102	B1W9H9ST8.5WT9H2C5	26	-36.5	-82.5	-10.0	-245.3	-904	-2042	-247	-5939
103	B1W9H9ST9.5WT9H0C5	40	-40.8	0.0	-10.0	-317.6	-1010	0	-247	-6930
104	B1W9H9ST9.5WT9H1C5	37	-40.8	-41.3	-10.0	-287.5	-1010	-1021	-247	-6459
105	B1W9H9ST9.5WT9H2C5	26	-40.8	-82.5	-10.0	-245.3	-1010	-2042	-247	-5939
106	B1W9H9ST10.5WT9H0C5	40	-45.1	0.0	-10.0	-317.6	-1117	0	-247	-6930
107	B1W9H9ST10.5WT9H1C5	37	-45.1	-41.3	-10.0	-287.5	-1117	-1021	-247	-6459
108	B1W9H9ST10.5WT9H2C5	26	-45.1	-82.5	-10.0	-245.3	-1117	-2042	-247	-5939

Units: lb./in. for shear; lb.-in./in. for bending moment

#	Case	NLS	V_L^{DC}	V_L^{EF}	V_L^{DW}	V_L^{LL}	M_{pE}^{DC}	M_{pE}^{EF}	M_{pE}^{DW}	M_{pE}^{LL}
109	B1W10H10ST9WT10H0C3	44	-43.0	0.0	-11.1	-319.1	-1182	0	-305	-7652
110	B1W10H10ST9WT10H1C3	40	-43.0	-45.8	-11.1	-290.9	-1168	-1246	-301	-7321
111	B1W10H10ST9WT10H2C3	34	-43.0	-91.7	-11.1	-265.1	-1178	-2514	-304	-7007
112	B1W10H10ST10WT10H0C3	44	-47.7	0.0	-11.1	-319.1	-1313	0	-305	-7652
113	B1W10H10ST10WT10H1C3	40	-47.7	-45.8	-11.1	-290.9	-1278	-1227	-297	-7321
114	B1W10H10ST10WT10H2C3	34	-47.7	-91.7	-11.1	-265.1	-1298	-2493	-301	-7007
115	B1W10H10ST11WT10H0C3	44	-52.5	0.0	-11.1	-319.1	-1444	0	-305	-7652
116	B1W10H10ST11WT10H1C3	40	-52.5	-45.8	-11.1	-290.9	-1427	-1246	-301	-7321
117	B1W10H10ST11WT10H2C3	34	-52.5	-91.7	-11.1	-265.1	-1440	-2514	-304	-7007
118	B1W10H10ST9WT10H0C4	44	-43.0	0.0	-11.1	-319.1	-1182	0	-305	-7652
119	B1W10H10ST9WT10H1C4	40	-43.0	-45.8	-11.1	-290.9	-1168	-1246	-301	-7321
120	B1W10H10ST9WT10H2C4	34	-43.0	-91.7	-11.1	-265.1	-1178	-2514	-304	-7007
121	B1W10H10ST10WT10H0C4	44	-47.7	0.0	-11.1	-319.1	-1313	0	-305	-7652
122	B1W10H10ST10WT10H1C4	40	-47.7	-45.8	-11.1	-290.9	-1278	-1227	-297	-7321
123	B1W10H10ST10WT10H2C4	34	-47.7	-91.7	-11.1	-265.1	-1298	-2493	-301	-7007
124	B1W10H10ST11WT10H0C4	44	-52.5	0.0	-11.1	-319.1	-1444	0	-305	-7652
125	B1W10H10ST11WT10H1C4	40	-52.5	-45.8	-11.1	-290.9	-1427	-1246	-301	-7321
126	B1W10H10ST11WT10H2C4	34	-52.5	-91.7	-11.1	-265.1	-1440	-2514	-304	-7007
127	B1W10H10ST9WT10H0C5	44	-43.0	0.0	-11.1	-319.1	-1182	0	-305	-7652
128	B1W10H10ST9WT10H1C5	40	-43.0	-45.8	-11.1	-290.9	-1168	-1246	-301	-7321
129	B1W10H10ST9WT10H2C5	34	-43.0	-91.7	-11.1	-265.1	-1178	-2514	-304	-7007
130	B1W10H10ST10WT10H0C5	44	-47.7	0.0	-11.1	-319.1	-1313	0	-305	-7652
131	B1W10H10ST10WT10H1C5	40	-47.7	-45.8	-11.1	-290.9	-1278	-1227	-297	-7321
132	B1W10H10ST10WT10H2C5	34	-47.7	-91.7	-11.1	-265.1	-1298	-2493	-301	-7007
133	B1W10H10ST11WT10H0C5	44	-52.5	0.0	-11.1	-319.1	-1444	0	-305	-7652
134	B1W10H10ST11WT10H1C5	40	-52.5	-45.8	-11.1	-290.9	-1427	-1246	-301	-7321
135	B1W10H10ST11WT10H2C5	34	-52.5	-91.7	-11.1	-265.1	-1440	-2514	-304	-7007

Units: lb./in. for shear; lb.-in./in. for bending moment

#	Case	NLS	V_L^{DC}	V_L^{EF}	V_L^{DW}	V_L^{LL}	M_{pE}^{DC}	M_{pE}^{EF}	M_{pE}^{DW}	M_{pE}^{LL}
136	B1W11H11ST9.5WT11H0C3	52	-49.9	0.0	-12.2	-332.1	-1468	0	-358	-8719
137	B1W11H11ST9.5WT11H1C3	48	-49.9	-50.4	-12.2	-304.1	-1495	-1510	-365	-8458
138	B1W11H11ST9.5WT11H2C3	41	-49.9	-100.8	-12.2	-280.3	-1495	-3022	-365	-8162
139	B1W11H11ST10.5WT11H0C3	52	-55.1	0.0	-12.2	-332.1	-1623	0	-358	-8719
140	B1W11H11ST10.5WT11H1C3	48	-55.1	-50.4	-12.2	-304.1	-1652	-1510	-365	-8458
141	B1W11H11ST10.5WT11H2C3	41	-55.1	-100.8	-12.2	-280.3	-1664	-3043	-368	-8162
142	B1W11H11ST11.5WT11H0C3	52	-60.4	0.0	-12.2	-332.1	-1777	0	-358	-8719
143	B1W11H11ST11.5WT11H1C3	48	-60.4	-50.4	-12.2	-304.1	-1809	-1510	-365	-8458
144	B1W11H11ST11.5WT11H2C3	41	-60.4	-100.8	-12.2	-280.3	-1810	-3022	-365	-8162
145	B1W11H11ST9.5WT11H0C4	52	-49.9	0.0	-12.2	-332.1	-1468	0	-358	-8719
146	B1W11H11ST9.5WT11H1C4	48	-49.9	-50.4	-12.2	-304.1	-1495	-1510	-365	-8458
147	B1W11H11ST9.5WT11H2C4	41	-49.9	-100.8	-12.2	-280.3	-1495	-3022	-365	-8162
148	B1W11H11ST10.5WT11H0C4	52	-55.1	0.0	-12.2	-332.1	-1623	0	-358	-8719
149	B1W11H11ST10.5WT11H1C4	48	-55.1	-50.4	-12.2	-304.1	-1652	-1510	-365	-8458
150	B1W11H11ST10.5WT11H2C4	41	-55.1	-100.8	-12.2	-280.3	-1664	-3043	-368	-8162
151	B1W11H11ST11.5WT11H0C4	52	-60.4	0.0	-12.2	-332.1	-1777	0	-358	-8719
152	B1W11H11ST11.5WT11H1C4	48	-60.4	-50.4	-12.2	-304.1	-1809	-1510	-365	-8458
153	B1W11H11ST11.5WT11H2C4	41	-60.4	-100.8	-12.2	-280.3	-1810	-3022	-365	-8162
154	B1W11H11ST9.5WT11H0C5	52	-49.9	0.0	-12.2	-332.1	-1468	0	-358	-8719
155	B1W11H11ST9.5WT11H1C5	48	-49.9	-50.4	-12.2	-304.1	-1495	-1510	-365	-8458
156	B1W11H11ST9.5WT11H2C5	41	-49.9	-100.8	-12.2	-280.3	-1495	-3022	-365	-8162
157	B1W11H11ST10.5WT11H0C5	52	-55.1	0.0	-12.2	-332.1	-1623	0	-358	-8719
158	B1W11H11ST10.5WT11H1C5	48	-55.1	-50.4	-12.2	-304.1	-1652	-1510	-365	-8458
159	B1W11H11ST10.5WT11H2C5	41	-55.1	-100.8	-12.2	-280.3	-1664	-3043	-368	-8162
160	B1W11H11ST11.5WT11H0C5	52	-60.4	0.0	-12.2	-332.1	-1777	0	-358	-8719
161	B1W11H11ST11.5WT11H1C5	48	-60.4	-50.4	-12.2	-304.1	-1809	-1510	-365	-8458
162	B1W11H11ST11.5WT11H2C5	41	-60.4	-100.8	-12.2	-280.3	-1810	-3022	-365	-8162

Units: lb./in. for shear; lb.-in./in. for bending moment

#	Case	NLS	V_L^{DC}	V_L^{EF}	V_L^{DW}	V_L^{LL}	M_{pE}^{DC}	M_{pE}^{EF}	M_{pE}^{DW}	M_{pE}^{LL}
163	B1W12H12ST10WT12H0C3	59	-57.3	0.0	-13.3	-342.1	-1847	0	-429	-9820
164	B1W12H12ST10WT12H1C3	55	-57.3	-55.0	-13.3	-314.2	-1856	-1782	-431	-9571
165	B1W12H12ST10WT12H2C3	49	-57.3	-110.0	-13.3	-292.1	-1887	-3623	-438	-9290
166	B1W12H12ST11WT12H0C3	59	-63.0	0.0	-13.3	-342.1	-2032	0	-429	-9820
167	B1W12H12ST11WT12H1C3	55	-63.0	-55.0	-13.3	-314.2	-2063	-1800	-435	-9571
168	B1W12H12ST11WT12H2C3	49	-63.0	-110.0	-13.3	-292.1	-2076	-3623	-438	-9290
169	B1W12H12ST12WT12H0C3	59	-68.8	0.0	-13.3	-342.1	-2217	0	-429	-9820
170	B1W12H12ST12WT12H1C3	55	-68.8	-55.0	-13.3	-314.2	-2250	-1800	-435	-9571
171	B1W12H12ST12WT12H2C3	49	-68.8	-110.0	-13.3	-292.1	-2264	-3623	-438	-9290
172	B1W12H12ST10WT12H0C4	59	-57.3	0.0	-13.3	-342.1	-1847	0	-429	-9820
173	B1W12H12ST10WT12H1C4	55	-57.3	-55.0	-13.3	-314.2	-1856	-1782	-431	-9571
174	B1W12H12ST10WT12H2C4	49	-57.3	-110.0	-13.3	-292.1	-1887	-3623	-438	-9290
175	B1W12H12ST11WT12H0C4	59	-63.0	0.0	-13.3	-342.1	-2032	0	-429	-9820
176	B1W12H12ST11WT12H1C4	55	-63.0	-55.0	-13.3	-314.2	-2063	-1800	-435	-9571
177	B1W12H12ST11WT12H2C4	49	-63.0	-110.0	-13.3	-292.1	-2076	-3623	-438	-9290
178	B1W12H12ST12WT12H0C4	59	-68.8	0.0	-13.3	-342.1	-2217	0	-429	-9820
179	B1W12H12ST12WT12H1C4	55	-68.8	-55.0	-13.3	-314.2	-2250	-1800	-435	-9571
180	B1W12H12ST12WT12H2C4	49	-68.8	-110.0	-13.3	-292.1	-2264	-3623	-438	-9290
181	B1W12H12ST10WT12H0C5	59	-57.3	0.0	-13.3	-342.1	-1847	0	-429	-9820
182	B1W12H12ST10WT12H1C5	55	-57.3	-55.0	-13.3	-314.2	-1856	-1782	-431	-9571
183	B1W12H12ST10WT12H2C5	49	-57.3	-110.0	-13.3	-292.1	-1887	-3623	-438	-9290
184	B1W12H12ST11WT12H0C5	59	-63.0	0.0	-13.3	-342.1	-2032	0	-429	-9820
185	B1W12H12ST11WT12H1C5	55	-63.0	-55.0	-13.3	-314.2	-2063	-1800	-435	-9571
186	B1W12H12ST11WT12H2C5	49	-63.0	-110.0	-13.3	-292.1	-2076	-3623	-438	-9290
187	B1W12H12ST12WT12H0C5	59	-68.8	0.0	-13.3	-342.1	-2217	0	-429	-9820
188	B1W12H12ST12WT12H1C5	55	-68.8	-55.0	-13.3	-314.2	-2250	-1800	-435	-9571
189	B1W12H12ST12WT12H2C5	49	-68.8	-110.0	-13.3	-292.1	-2264	-3623	-438	-9290

Units: lb./in. for shear; lb.-in./in. for bending moment

Table E5. Bending moment and shear force values (2D model; AASHTO-LRFD BDS; 2-barrel culverts)

#	Case	NLS	V_L^{DC}	V_L^{EF}	V_L^{DW}	V_L^{LL}	V_R^{DC}	V_R^{EF}	V_R^{DW}	V_R^{LL}
1	B2W6H6ST7WT6H0C4	51	-24.8	0.0	-8.3	-282.1	-24.8	0.0	-8.3	-282.1
2	B2W6H6ST7WT6H1C4	40	-24.9	-34.2	-8.3	-257.9	-24.9	-34.2	-8.3	-257.9
3	B2W6H6ST7WT6H2C4	25	-24.9	-68.4	-8.3	-226.0	-24.9	-68.4	-8.3	-226.0
4	B2W6H6ST8WT6H0C4	51	-28.3	0.0	-8.2	-280.8	-28.3	0.0	-8.2	-280.8
5	B2W6H6ST8WT6H1C4	40	-28.3	-34.1	-8.2	-256.5	-28.3	-34.1	-8.2	-256.5
6	B2W6H6ST8WT6H2C4	25	-28.3	-68.3	-8.2	-224.6	-28.3	-68.3	-8.2	-224.6
7	B2W6H6ST9WT6H0C4	51	-31.7	0.0	-8.2	-279.8	-31.7	0.0	-8.2	-279.8
8	B2W6H6ST9WT6H1C4	40	-31.7	-34.0	-8.2	-255.3	-31.7	-34.0	-8.2	-255.3
9	B2W6H6ST9WT6H2C4	25	-31.7	-68.1	-8.2	-223.5	-31.7	-68.1	-8.2	-223.5
10	B2W7H7ST7.5WT7H0C4	67	-31.1	0.0	-9.7	-314.5	-31.1	0.0	-9.7	-314.5
11	B2W7H7ST7.5WT7H1C4	53	-31.1	-39.9	-9.7	-265.6	-31.1	-39.9	-9.7	-264.5
12	B2W7H7ST7.5WT7H2C4	37	-31.1	-79.9	-9.7	-238.9	-31.1	-79.9	-9.7	-238.9
13	B2W7H7ST8.5WT7H0C4	67	-35.2	0.0	-9.6	-313.0	-35.2	0.0	-9.6	-313.0
14	B2W7H7ST8.5WT7H1C4	53	-35.2	-39.9	-9.6	-264.3	-35.2	-39.9	-9.6	-263.2
15	B2W7H7ST8.5WT7H2C4	37	-35.2	-79.8	-9.6	-237.5	-35.2	-79.8	-9.6	-237.5
16	B2W7H7ST9.5WT7H0C4	67	-39.2	0.0	-9.6	-311.9	-39.2	0.0	-9.6	-311.9
17	B2W7H7ST9.5WT7H1C4	53	-39.2	-39.8	-9.6	-263.3	-39.2	-39.8	-9.6	-262.1
18	B2W7H7ST9.5WT7H2C4	37	-39.2	-79.6	-9.6	-236.4	-39.2	-79.6	-9.6	-236.4
19	B2W8H8ST8WT8H0C4	74	-38.0	0.0	-11.0	-326.9	-38.0	0.0	-11.0	-326.9
20	B2W8H8ST8WT8H1C4	69	-38.0	-45.7	-11.0	-298.1	-38.0	-45.7	-11.0	-298.1
21	B2W8H8ST8WT8H2C4	49	-38.0	-91.4	-11.0	-247.1	-38.0	-91.4	-11.0	-247.1
22	B2W8H8ST9WT8H0C4	74	-42.6	0.0	-11.0	-325.2	-42.6	0.0	-11.0	-325.2
23	B2W8H8ST9WT8H1C4	69	-42.6	-45.6	-11.0	-296.5	-42.6	-45.6	-11.0	-296.5
24	B2W8H8ST9WT8H2C4	49	-42.6	-91.3	-11.0	-245.7	-42.6	-91.3	-11.0	-245.7
25	B2W8H8ST10WT8H0C4	74	-47.3	0.0	-11.0	-323.8	-47.3	0.0	-11.0	-323.8
26	B2W8H8ST10WT8H1C4	69	-47.3	-45.6	-11.0	-295.2	-47.3	-45.6	-11.0	-295.2
27	B2W8H8ST10WT8H2C4	49	-47.3	-91.1	-11.0	-244.6	-47.3	-91.1	-11.0	-244.6

Units: lb./in. for shear

#	Case	M_{pE}^{DC}	M_{pE}^{EF}	M_{pE}^{DW}	M_{pE}^{LL}	M_{nL}^{DC}	M_{nL}^{EF}	M_{nL}^{DW}	M_{nL}^{LL}	M_{nR}^{DC}	M_{nR}^{EF}	M_{nR}^{DW}	M_{nR}^{LL}
1	B2W6H6ST7WT6H0C4	-191	0	-63	-3727	317	0	107	2804	-317	0	-107	-2804
2	B2W6H6ST7WT6H1C4	-184	-249	-60	-3253	317	442	107	2655	-317	-442	-107	-2655
3	B2W6H6ST7WT6H2C4	-184	-497	-60	-2782	317	884	107	1818	-317	-884	-107	-1818
4	B2W6H6ST8WT6H0C4	-214	0	-61	-3763	356	0	106	2760	-356	0	-106	-2760
5	B2W6H6ST8WT6H1C4	-213	-251	-61	-3289	356	438	106	2611	-356	-438	-106	-2611
6	B2W6H6ST8WT6H2C4	-213	-501	-61	-2817	356	875	106	1735	-356	-875	-106	-1735
7	B2W6H6ST9WT6H0C4	-244	0	-62	-3793	393	0	104	2707	-393	0	-104	-2707
8	B2W6H6ST9WT6H1C4	-243	-254	-61	-3317	393	432	104	2560	-393	-432	-104	-2560
9	B2W6H6ST9WT6H2C4	-243	-506	-61	-2844	393	864	104	1669	-393	-864	-104	-1669
10	B2W7H7ST7.5WT7H0C4	-276	0	-84	-4340	465	0	146	2992	-465	0	-146	-2992
11	B2W7H7ST7.5WT7H1C4	-274	-347	-84	-3864	466	605	146	2898	-466	-605	-146	-2898
12	B2W7H7ST7.5WT7H2C4	-274	-693	-84	-3394	466	1210	146	2240	-466	-1210	-146	-2240
13	B2W7H7ST8.5WT7H0C4	-315	0	-85	-4380	521	0	145	2946	-521	0	-145	-2946
14	B2W7H7ST8.5WT7H1C4	-313	-349	-84	-3902	521	600	145	2854	-521	-600	-145	-2854
15	B2W7H7ST8.5WT7H2C4	-313	-697	-84	-3433	521	1201	145	2137	-521	-1201	-145	-2137
16	B2W7H7ST9.5WT7H0C4	-355	0	-85	-4410	575	0	144	2894	-575	0	-144	-2894
17	B2W7H7ST9.5WT7H1C4	-354	-351	-85	-3932	575	595	144	2804	-575	-595	-144	-2804
18	B2W7H7ST9.5WT7H2C4	-353	-702	-85	-3462	575	1190	144	2058	-575	-1190	-144	-2058
19	B2W8H8ST8WT8H0C4	-380	0	-109	-4926	652	0	192	3226	-652	0	-192	-3226
20	B2W8H8ST8WT8H1C4	-378	-449	-109	-4454	652	793	192	3068	-652	-793	-192	-3057
21	B2W8H8ST8WT8H2C4	-377	-897	-108	-3982	652	1586	192	2656	-652	-1586	-192	-2656
22	B2W8H8ST9WT8H0C4	-431	0	-110	-4975	727	0	190	3176	-727	0	-190	-3176
23	B2W8H8ST9WT8H1C4	-428	-451	-109	-4502	727	788	191	3015	-727	-788	-191	-3013
24	B2W8H8ST9WT8H2C4	-428	-901	-109	-4029	727	1577	191	2535	-727	-1577	-191	-2535
25	B2W8H8ST10WT8H0C4	-482	0	-110	-5012	799	0	189	3124	-799	0	-189	-3124
26	B2W8H8ST10WT8H1C4	-480	-453	-110	-4538	799	783	189	2965	-799	-783	-189	-2965
27	B2W8H8ST10WT8H2C4	-479	-906	-109	-4066	799	1566	189	2441	-799	-1566	-189	-2441

Units: lb.-in./in. for bending moment

#	Case	NLS	V_L^{DC}	V_L^{EF}	V_L^{DW}	V_L^{LL}	V_R^{DC}	V_R^{EF}	V_R^{DW}	V_R^{LL}
28	B2W9H9ST8.5WT9H0C4	90	-45.4	0.0	-12.4	-347.9	-45.4	0.0	-12.4	-347.9
29	B2W9H9ST8.5WT9H1C4	85	-45.4	-51.4	-12.4	-321.2	-45.4	-51.4	-12.4	-321.2
30	B2W9H9ST8.5WT9H2C4	64	-45.4	-102.8	-12.4	-280.0	-45.4	-102.8	-12.4	-280.0
31	B2W9H9ST9.5WT9H0C4	90	-50.7	0.0	-12.4	-346.2	-50.7	0.0	-12.4	-346.2
32	B2W9H9ST9.5WT9H1C4	85	-50.7	-51.4	-12.4	-319.4	-50.7	-51.4	-12.4	-319.4
33	B2W9H9ST9.5WT9H2C4	64	-50.7	-102.7	-12.4	-278.4	-50.7	-102.7	-12.4	-278.4
34	B2W9H9ST10.5WT9H0C4	90	-55.9	0.0	-12.4	-344.8	-55.9	0.0	-12.4	-344.8
35	B2W9H9ST10.5WT9H1C4	85	-55.9	-51.3	-12.4	-318.0	-55.9	-51.3	-12.4	-318.0
36	B2W9H9ST10.5WT9H2C4	64	-55.9	-102.6	-12.4	-277.1	-55.9	-102.6	-12.4	-277.1
37	B2W10H10ST9WT10H0C4	98	-53.5	0.0	-13.8	-352.0	-53.5	0.0	-13.8	-352.0
38	B2W10H10ST9WT10H1C4	92	-53.5	-57.1	-13.8	-327.2	-53.5	-57.1	-13.8	-327.2
39	B2W10H10ST9WT10H2C4	80	-53.5	-114.3	-13.8	-302.0	-53.5	-114.3	-13.8	-302.0
40	B2W10H10ST10WT10H0C4	98	-59.3	0.0	-13.8	-350.1	-59.3	0.0	-13.8	-350.1
41	B2W10H10ST10WT10H1C4	92	-59.3	-57.1	-13.8	-325.4	-59.3	-57.1	-13.8	-325.4
42	B2W10H10ST10WT10H2C4	80	-59.3	-114.2	-13.8	-300.2	-59.3	-114.2	-13.8	-300.2
43	B2W10H10ST11WT10H0C4	98	-65.2	0.0	-13.8	-348.7	-65.2	0.0	-13.8	-348.7
44	B2W10H10ST11WT10H1C4	92	-65.2	-57.1	-13.8	-323.8	-65.2	-57.1	-13.8	-323.8
45	B2W10H10ST11WT10H2C4	80	-65.2	-114.1	-13.8	-298.8	-65.2	-114.1	-13.8	-298.8
46	B2W11H11ST9.5WT11H0C4	114	-62.1	0.0	-15.2	-363.8	-62.1	0.0	-15.2	-363.8
47	B2W11H11ST9.5WT11H1C4	108	-62.1	-62.9	-15.2	-340.6	-62.1	-62.9	-15.2	-340.6
48	B2W11H11ST9.5WT11H2C4	93	-62.1	-125.8	-15.2	-318.3	-62.1	-125.8	-15.2	-318.3
49	B2W11H11ST10.5WT11H0C4	114	-68.6	0.0	-15.2	-362.0	-68.6	0.0	-15.2	-362.0
50	B2W11H11ST10.5WT11H1C4	108	-68.6	-62.8	-15.2	-338.7	-68.6	-62.8	-15.2	-338.7
51	B2W11H11ST10.5WT11H2C4	93	-68.6	-125.7	-15.2	-316.4	-68.6	-125.7	-15.2	-316.4
52	B2W11H11ST11.5WT11H0C4	114	-75.0	0.0	-15.2	-360.6	-75.0	0.0	-15.2	-360.6
53	B2W11H11ST11.5WT11H1C4	108	-75.0	-62.8	-15.2	-337.2	-75.0	-62.8	-15.2	-337.2
54	B2W11H11ST11.5WT11H2C4	93	-75.0	-125.6	-15.2	-314.9	-75.0	-125.6	-15.2	-314.9

Units: lb./in. for shear

#	Case	M_{pE}^{DC}	M_{pE}^{EF}	M_{pE}^{DW}	M_{pE}^{LL}	M_{nL}^{DC}	M_{nL}^{EF}	M_{nL}^{DW}	M_{nL}^{LL}	M_{nR}^{DC}	M_{nR}^{EF}	M_{nR}^{DW}	M_{nR}^{LL}
28	B2W9H9ST8.5WT9H0C4	-507	0	-137	-5488	880	0	243	3843	-880	0	-243	-3843
29	B2W9H9ST8.5WT9H1C4	-504	-564	-136	-5021	880	1006	243	3717	-880	-1006	-243	-3717
30	B2W9H9ST8.5WT9H2C4	-513	-1149	-139	-4552	880	2012	243	3496	-880	-2012	-243	-3487
31	B2W9H9ST9.5WT9H0C4	-570	0	-138	-5545	976	0	242	3673	-976	0	-242	-3673
32	B2W9H9ST9.5WT9H1C4	-566	-566	-137	-5077	976	1001	242	3549	-976	-1001	-242	-3549
33	B2W9H9ST9.5WT9H2C4	-565	-1130	-136	-4603	976	2003	242	3341	-976	-2003	-242	-3327
34	B2W9H9ST10.5WT9H0C4	-634	0	-138	-5589	1070	0	241	3538	-1070	0	-241	-3538
35	B2W9H9ST10.5WT9H1C4	-630	-568	-137	-5121	1070	996	241	3421	-1070	-996	-241	-3421
36	B2W9H9ST10.5WT9H2C4	-629	-1135	-137	-4647	1070	1992	241	3220	-1070	-1992	-241	-3201
37	B2W10H10ST9WT10H0C4	-671	0	-172	-6043	1154	0	301	4563	-1154	0	-301	-4563
38	B2W10H10ST9WT10H1C4	-667	-706	-171	-5580	1154	1244	301	4446	-1154	-1244	-301	-4446
39	B2W10H10ST9WT10H2C4	-674	-1427	-172	-5210	1154	2489	301	4237	-1154	-2489	-301	-4237
40	B2W10H10ST10WT10H0C4	-748	0	-172	-6099	1274	0	300	4358	-1274	0	-300	-4358
41	B2W10H10ST10WT10H1C4	-745	-708	-171	-5637	1274	1240	300	4249	-1274	-1240	-300	-4249
42	B2W10H10ST10WT10H2C4	-752	-1430	-173	-5286	1274	2479	300	4048	-1274	-2479	-300	-4048
43	B2W10H10ST11WT10H0C4	-812	0	-169	-6145	1391	0	298	4230	-1391	0	-298	-4230
44	B2W10H10ST11WT10H1C4	-832	-718	-174	-5695	1391	1234	298	4138	-1391	-1234	-298	-4138
45	B2W10H10ST11WT10H2C4	-831	-1435	-173	-5347	1391	2468	298	3979	-1391	-2468	-298	-3979
46	B2W11H11ST9.5WT11H0C4	-860	0	-209	-6692	1477	0	364	5344	-1477	0	-364	-5344
47	B2W11H11ST9.5WT11H1C4	-861	-864	-209	-6357	1477	1508	364	5335	-1477	-1508	-364	-5335
48	B2W11H11ST9.5WT11H2C4	-857	-1719	-208	-6021	1477	3016	364	5285	-1477	-3016	-364	-5285
49	B2W11H11ST10.5WT11H0C4	-953	0	-209	-6777	1623	0	363	5319	-1623	0	-363	-5319
50	B2W11H11ST10.5WT11H1C4	-955	-866	-209	-6442	1624	1503	363	5313	-1624	-1503	-363	-5313
51	B2W11H11ST10.5WT11H2C4	-951	-1723	-208	-6109	1624	3006	363	5266	-1624	-3006	-363	-5266
52	B2W11H11ST11.5WT11H0C4	-1048	0	-210	-6846	1767	0	362	5307	-1767	0	-362	-5307
53	B2W11H11ST11.5WT11H1C4	-1050	-868	-210	-6512	1767	1497	362	5301	-1767	-1497	-362	-5301
54	B2W11H11ST11.5WT11H2C4	-1045	-1728	-209	-6182	1767	2994	362	5252	-1767	-2994	-362	-5252

Units: lb.-in./in. for bending moment

#	Case	NLS	V_L^{DC}	V_L^{EF}	V_L^{DW}	V_L^{LL}	V_R^{DC}	V_R^{EF}	V_R^{DW}	V_R^{LL}
55	B2W12H12ST10WT12H0C4	127	-71.3	0.0	-16.6	-372.1	-71.3	0.0	-16.6	-372.1
56	B2W12H12ST10WT12H1C4	121	-71.3	-68.6	-16.6	-350.3	-71.3	-68.6	-16.6	-350.3
57	B2W12H12ST10WT12H2C4	109	-71.3	-137.2	-16.6	-330.4	-71.3	-137.2	-16.6	-330.4
58	B2W12H12ST11WT12H0C4	127	-78.4	0.0	-16.6	-370.4	-78.4	0.0	-16.6	-370.4
59	B2W12H12ST11WT12H1C4	121	-78.4	-68.6	-16.6	-348.4	-78.4	-68.6	-16.6	-348.4
60	B2W12H12ST11WT12H2C4	109	-78.4	-137.1	-16.6	-328.6	-78.4	-137.1	-16.6	-328.6
61	B2W12H12ST12WT12H0C4	127	-85.4	0.0	-16.6	-369.0	-85.4	0.0	-16.6	-369.0
62	B2W12H12ST12WT12H1C4	121	-85.4	-68.5	-16.6	-346.9	-85.4	-68.5	-16.6	-346.9
63	B2W12H12ST12WT12H2C4	109	-85.4	-137.1	-16.6	-327.0	-85.4	-137.1	-16.6	-327.0

Units: lb./in. for shear

#	Case	M_{pE}^{DC}	M_{pE}^{EF}	M_{pE}^{DW}	M_{pE}^{LL}	M_{nL}^{DC}	M_{nL}^{EF}	M_{nL}^{DW}	M_{nL}^{LL}	M_{nR}^{DC}	M_{nR}^{EF}	M_{nR}^{DW}	M_{nR}^{LL}
55	B2W12H12ST10WT12H0C4	-1077	0	-248	-7475	1853	0	434	6404	-1853	0	-434	-6404
56	B2W12H12ST10WT12H1C4	-1077	-1027	-248	-7153	1854	1796	434	6338	-1854	-1796	-434	-6338
57	B2W12H12ST10WT12H2C4	-1068	-2037	-246	-6826	1854	3593	434	6265	-1854	-3593	-434	-6265
58	B2W12H12ST11WT12H0C4	-1189	0	-249	-7571	2029	0	433	6386	-2029	0	-433	-6386
59	B2W12H12ST11WT12H1C4	-1188	-1029	-249	-7250	2029	1791	433	6319	-2029	-1791	-433	-6319
60	B2W12H12ST11WT12H2C4	-1179	-2041	-247	-6924	2029	3582	433	6247	-2029	-3582	-433	-6247
61	B2W12H12ST12WT12H0C4	-1301	0	-249	-7650	2202	0	431	6372	-2202	0	-431	-6372
62	B2W12H12ST12WT12H1C4	-1301	-1031	-249	-7330	2202	1785	431	6306	-2202	-1785	-431	-6306
63	B2W12H12ST12WT12H2C4	-1291	-2046	-247	-7005	2202	3571	431	6234	-2202	-3571	-431	-6234

Units: lb.-in./in. for bending moment

Table E6. Bending moment and shear force values (2D model; AASHTO-LRFD BDS; 3-barrel culverts)

#	Case	NLS	V_L^{DC}	V_L^{EF}	V_L^{DW}	V_L^{LL}	V_R^{DC}	V_R^{EF}	V_R^{DW}	V_R^{LL}
1	B3W6H6ST8WT6H0C4	51	-27.7	0.0	-8.0	-282.7	-22.9	0.0	-6.6	-270.4
2	B3W6H6ST8WT6H1C4	40	-27.7	-33.1	-8.0	-259.0	-22.9	-27.5	-6.6	-239.6
3	B3W6H6ST8WT6H2C4	25	-27.7	-66.2	-8.0	-227.2	-22.9	-55.0	-6.6	-202.6
4	B3W7H7ST8.5WT7H0C4	67	-34.4	0.0	-9.4	-315.8	-28.4	0.0	-7.8	-284.0
5	B3W7H7ST8.5WT7H1C4	53	-34.4	-38.7	-9.4	-266.9	-28.4	-32.1	-7.8	-248.6
6	B3W7H7ST8.5WT7H2C4	37	-34.4	-77.5	-9.4	-240.5	-28.4	-64.2	-7.8	-217.4
7	B3W8H8ST9WT8H0C4	74	-41.7	0.0	-10.7	-328.9	-34.4	0.0	-8.9	-293.7
8	B3W8H8ST9WT8H1C4	69	-41.7	-44.4	-10.7	-300.1	-34.4	-36.7	-8.9	-264.5
9	B3W8H8ST9WT8H2C4	49	-41.7	-88.8	-10.7	-248.8	-34.4	-73.3	-8.9	-227.4
10	B3W9H9ST9.5WT9H0C4	90	-49.7	0.0	-12.1	-350.4	-40.8	0.0	-10.0	-315.4
11	B3W9H9ST9.5WT9H1C4	85	-49.7	-50.0	-12.1	-323.6	-40.8	-41.3	-10.0	-286.1
12	B3W9H9ST9.5WT9H2C4	64	-49.7	-100.1	-12.1	-282.3	-40.8	-82.5	-10.0	-244.8
13	B3W10H10ST10WT10H0C4	98	-58.2	0.0	-13.5	-354.8	-47.7	0.0	-11.1	-319.1
14	B3W10H10ST10WT10H1C4	92	-58.2	-55.7	-13.5	-330.1	-47.7	-45.8	-11.1	-291.1
15	B3W10H10ST10WT10H2C4	80	-58.2	-111.4	-13.5	-304.8	-47.7	-91.7	-11.1	-264.8
16	B3W11H11ST10.5WT11H0C4	114	-67.3	0.0	-14.8	-366.8	-55.1	0.0	-12.2	-333.1
17	B3W11H11ST10.5WT11H1C4	108	-67.3	-61.3	-14.8	-343.7	-55.1	-50.4	-12.2	-305.6
18	B3W11H11ST10.5WT11H2C4	93	-67.3	-122.7	-14.8	-321.4	-55.1	-100.8	-12.2	-281.0
19	B3W12H12ST11WT12H0C4	127	-77.0	0.0	-16.2	-375.2	-63.0	0.0	-13.3	-343.8
20	B3W12H12ST11WT12H1C4	121	-77.0	-67.0	-16.2	-353.6	-63.0	-55.0	-13.3	-316.9
21	B3W12H12ST11WT12H2C4	109	-77.0	-134.0	-16.2	-333.8	-63.0	-110.0	-13.3	-294.1

Units: lb./in. for shear

#	Case	M_{pE}^{DC}	M_{pE}^{EF}	M_{pE}^{DW}	M_{pE}^{LL}	M_{nL}^{DC}	M_{nL}^{EF}	M_{nL}^{DW}	M_{nL}^{LL}	M_{nR}^{DC}	M_{nR}^{EF}	M_{nR}^{DW}	M_{nR}^{LL}	M_{pI}^{DC}	M_{pI}^{EF}	M_{pI}^{DW}	M_{pI}^{LL}
1	B3W6H6ST8WT6H0C4	-238	0	-69	-3696	313	0	89	2648	-280	0	-84	-2617	-98	0	-26	-3000
2	B3W6H6ST8WT6H1C4	-232	-282	-68	-3217	313	370	89	2498	-280	-347	-84	-2470	-98	-106	-26	-2571
3	B3W6H6ST8WT6H2C4	-237	-574	-69	-2753	313	741	89	1897	-280	-695	-84	-1637	-98	-213	-26	-2153
4	B3W7H7ST8.5WT7H0C4	-340	0	-94	-4292	462	0	124	2873	-403	0	-114	-2810	-143	0	-36	-3450
5	B3W7H7ST8.5WT7H1C4	-339	-386	-93	-3817	462	512	124	2777	-404	-470	-114	-2718	-143	-148	-36	-3019
6	B3W7H7ST8.5WT7H2C4	-338	-772	-93	-3348	462	1025	124	2363	-404	-940	-114	-1908	-143	-295	-36	-2592
7	B3W8H8ST9WT8H0C4	-464	0	-121	-4859	648	0	164	3285	-555	0	-147	-3034	-201	0	-48	-3880
8	B3W8H8ST9WT8H1C4	-462	-499	-120	-4389	648	678	164	3136	-556	-610	-147	-2884	-201	-197	-48	-3449
9	B3W8H8ST9WT8H2C4	-462	-996	-120	-3916	648	1357	164	2828	-556	-1220	-147	-2206	-201	-393	-48	-3016
10	B3W9H9ST9.5WT9H0C4	-620	0	-153	-5409	876	0	210	4090	-739	0	-185	-3143	-272	0	-61	-4293
11	B3W9H9ST9.5WT9H1C4	-618	-632	-153	-4944	876	869	210	3956	-739	-767	-185	-3038	-271	-254	-61	-3864
12	B3W9H9ST9.5WT9H2C4	-618	-1263	-153	-4477	876	1738	210	3709	-739	-1535	-185	-2844	-271	-507	-61	-3427
13	B3W10H10ST10WT10H0C4	-799	0	-187	-5950	1149	0	262	4887	-956	0	-228	-3754	-352	0	-76	-4615
14	B3W10H10ST10WT10H1C4	-797	-773	-187	-5488	1149	1083	262	4755	-956	-942	-228	-3672	-353	-315	-76	-4246
15	B3W10H10ST10WT10H2C4	-801	-1554	-188	-5092	1149	2167	262	4529	-956	-1884	-228	-3536	-357	-636	-77	-3825
16	B3W11H11ST10.5WT11H0C4	-1008	0	-225	-6546	1472	0	320	5657	-1210	0	-274	-4771	-458	0	-94	-4698
17	B3W11H11ST10.5WT11H1C4	-1012	-934	-226	-6211	1472	1322	320	5538	-1211	-1134	-274	-4773	-453	-387	-94	-4397
18	B3W11H11ST10.5WT11H2C4	-1013	-1870	-226	-5873	1472	2645	320	5322	-1211	-2269	-274	-4741	-454	-775	-94	-4157
19	B3W12H12ST11WT12H0C4	-1257	0	-267	-7300	1847	0	383	6411	-1504	0	-325	-5797	-570	0	-113	-5205
20	B3W12H12ST11WT12H1C4	-1254	-1104	-267	-6977	1847	1586	383	6299	-1504	-1344	-325	-5735	-571	-468	-113	-4924
21	B3W12H12ST11WT12H2C4	-1259	-2217	-268	-6658	1847	3172	383	6101	-1504	-2687	-325	-5675	-571	-936	-113	-4696

Units: lb.-in./in. for bending moment

Table E7. Bending moment and shear force values (2D model; AASHTO-LRFD BDS with rigid joints; 1-barrel culverts)

#	Case	NLS	V_L^{DC}	V_L^{EF}	V_L^{DW}	V_L^{LL}	M_{pE}^{DC}	M_{pE}^{EF}	M_{pE}^{DW}	M_{pE}^{LL}
1	B1W6H6ST7WT6H0C3	17	-18.2	0.0	-6.0	-265	-273	0	-90.6	-4191
2	B1W6H6ST7WT6H1C3	14	-18.2	-25.0	-6.0	-230	-273	-375	-90.6	-3703
3	B1W6H6ST7WT6H2C3	9	-18.2	-50.0	-6.0	-191	-273	-750	-90.6	-3163
4	B1W6H6ST8WT6H0C3	17	-20.8	0.0	-6.0	-265	-313	0	-90.6	-4191
5	B1W6H6ST8WT6H1C3	14	-20.8	-25.0	-6.0	-230	-313	-375	-90.6	-3703
6	B1W6H6ST8WT6H2C3	9	-20.8	-50.0	-6.0	-191	-313	-750	-90.6	-3163
7	B1W6H6ST9WT6H0C3	17	-23.4	0.0	-6.0	-265	-352	0	-90.6	-4191
8	B1W6H6ST9WT6H1C3	14	-23.4	-25.0	-6.0	-230	-352	-375	-90.6	-3703
9	B1W6H6ST9WT6H2C3	9	-23.4	-50.0	-6.0	-191	-352	-750	-90.6	-3163
10	B1W6H6ST7WT6H0C4	17	-18.2	0.0	-6.0	-265	-273	0	-90.6	-4191
11	B1W6H6ST7WT6H1C4	14	-18.2	-25.0	-6.0	-230	-273	-375	-90.6	-3703
12	B1W6H6ST7WT6H2C4	9	-18.2	-50.0	-6.0	-191	-273	-750	-90.6	-3163
13	B1W6H6ST8WT6H0C4	17	-20.8	0.0	-6.0	-265	-313	0	-90.6	-4191
14	B1W6H6ST8WT6H1C4	14	-20.8	-25.0	-6.0	-230	-313	-375	-90.6	-3703
15	B1W6H6ST8WT6H2C4	9	-20.8	-50.0	-6.0	-191	-313	-750	-90.6	-3163
16	B1W6H6ST9WT6H0C4	17	-23.4	0.0	-6.0	-265	-352	0	-90.6	-4191
17	B1W6H6ST9WT6H1C4	14	-23.4	-25.0	-6.0	-230	-352	-375	-90.6	-3703
18	B1W6H6ST9WT6H2C4	9	-23.4	-50.0	-6.0	-191	-352	-750	-90.6	-3163
19	B1W6H6ST7WT6H0C5	17	-18.2	0.0	-6.0	-265	-273	0	-90.6	-4191
20	B1W6H6ST7WT6H1C5	14	-18.2	-25.0	-6.0	-230	-273	-375	-90.6	-3703
21	B1W6H6ST7WT6H2C5	9	-18.2	-50.0	-6.0	-191	-273	-750	-90.6	-3163
22	B1W6H6ST8WT6H0C5	17	-20.8	0.0	-6.0	-265	-313	0	-90.6	-4191
23	B1W6H6ST8WT6H1C5	14	-20.8	-25.0	-6.0	-230	-313	-375	-90.6	-3703
24	B1W6H6ST8WT6H2C5	9	-20.8	-50.0	-6.0	-191	-313	-750	-90.6	-3163
25	B1W6H6ST9WT6H0C5	17	-23.4	0.0	-6.0	-265	-352	0	-90.6	-4191
26	B1W6H6ST9WT6H1C5	14	-23.4	-25.0	-6.0	-230	-352	-375	-90.6	-3703
27	B1W6H6ST9WT6H2C5	9	-23.4	-50.0	-6.0	-191	-352	-750	-90.6	-3163

Units: lb./in. for shear; lb.-in./in. for bending moment

#	Case	NLS	V_L^{DC}	V_L^{EF}	V_L^{DW}	V_L^{LL}	M_{pE}^{DC}	M_{pE}^{EF}	M_{pE}^{DW}	M_{pE}^{LL}
28	B1W7H7ST7.5WT7H0C3	24	-23.1	0.0	-7.1	-273	-410	0	-126.9	-4975
29	B1W7H7ST7.5WT7H1C3	18	-23.1	-29.6	-7.1	-241	-410	-525	-126.9	-4493
30	B1W7H7ST7.5WT7H2C3	13	-23.1	-59.2	-7.1	-208	-410	-1050	-126.9	-3960
31	B1W7H7ST8.5WT7H0C3	24	-26.2	0.0	-7.1	-273	-465	0	-126.9	-4975
32	B1W7H7ST8.5WT7H1C3	18	-26.2	-29.6	-7.1	-241	-465	-525	-126.9	-4493
33	B1W7H7ST8.5WT7H2C3	13	-26.2	-59.2	-7.1	-208	-465	-1050	-126.9	-3960
34	B1W7H7ST9.5WT7H0C3	24	-29.3	0.0	-7.1	-273	-520	0	-126.9	-4975
35	B1W7H7ST9.5WT7H1C3	18	-29.3	-29.6	-7.1	-241	-520	-525	-126.9	-4493
36	B1W7H7ST9.5WT7H2C3	13	-29.3	-59.2	-7.1	-208	-520	-1050	-126.9	-3960
37	B1W7H7ST7.5WT7H0C4	24	-23.1	0.0	-7.1	-273	-410	0	-126.9	-4975
38	B1W7H7ST7.5WT7H1C4	18	-23.1	-29.6	-7.1	-241	-410	-525	-126.9	-4493
39	B1W7H7ST7.5WT7H2C4	13	-23.1	-59.2	-7.1	-208	-410	-1050	-126.9	-3960
40	B1W7H7ST8.5WT7H0C4	24	-26.2	0.0	-7.1	-273	-465	0	-126.9	-4975
41	B1W7H7ST8.5WT7H1C4	18	-26.2	-29.6	-7.1	-241	-465	-525	-126.9	-4493
42	B1W7H7ST8.5WT7H2C4	13	-26.2	-59.2	-7.1	-208	-465	-1050	-126.9	-3960
43	B1W7H7ST9.5WT7H0C4	24	-29.3	0.0	-7.1	-273	-520	0	-126.9	-4975
44	B1W7H7ST9.5WT7H1C4	18	-29.3	-29.6	-7.1	-241	-520	-525	-126.9	-4493
45	B1W7H7ST9.5WT7H2C4	13	-29.3	-59.2	-7.1	-208	-520	-1050	-126.9	-3960
46	B1W7H7ST7.5WT7H0C5	24	-23.1	0.0	-7.1	-273	-410	0	-126.9	-4975
47	B1W7H7ST7.5WT7H1C5	18	-23.1	-29.6	-7.1	-241	-410	-525	-126.9	-4493
48	B1W7H7ST7.5WT7H2C5	13	-23.1	-59.2	-7.1	-208	-410	-1050	-126.9	-3960
49	B1W7H7ST8.5WT7H0C5	24	-26.2	0.0	-7.1	-273	-465	0	-126.9	-4975
50	B1W7H7ST8.5WT7H1C5	18	-26.2	-29.6	-7.1	-241	-465	-525	-126.9	-4493
51	B1W7H7ST8.5WT7H2C5	13	-26.2	-59.2	-7.1	-208	-465	-1050	-126.9	-3960
52	B1W7H7ST9.5WT7H0C5	24	-29.3	0.0	-7.1	-273	-520	0	-126.9	-4975
53	B1W7H7ST9.5WT7H1C5	18	-29.3	-29.6	-7.1	-241	-520	-525	-126.9	-4493
54	B1W7H7ST9.5WT7H2C5	13	-29.3	-59.2	-7.1	-208	-520	-1050	-126.9	-3960

Units: lb./in. for shear; lb.-in./in. for bending moment

#	Case	NLS	V_L^{DC}	V_L^{EF}	V_L^{DW}	V_L^{LL}	M_{pE}^{DC}	M_{pE}^{EF}	M_{pE}^{DW}	M_{pE}^{LL}
55	B1W8H8ST8WT8H0C3	27	-28.5	0.0	-8.3	-282	-584	0	-169.3	-5739
56	B1W8H8ST8WT8H1C3	24	-28.5	-34.2	-8.3	-252	-584	-700	-169.3	-5263
57	B1W8H8ST8WT8H2C3	17	-28.5	-68.3	-8.3	-219	-584	-1401	-169.3	-4736
58	B1W8H8ST9WT8H0C3	27	-32.0	0.0	-8.3	-282	-657	0	-169.3	-5739
59	B1W8H8ST9WT8H1C3	24	-32.0	-34.2	-8.3	-252	-657	-700	-169.3	-5263
60	B1W8H8ST9WT8H2C3	17	-32.0	-68.3	-8.3	-219	-657	-1401	-169.3	-4736
61	B1W8H8ST10WT8H0C3	27	-35.6	0.0	-8.3	-282	-730	0	-169.3	-5739
62	B1W8H8ST10WT8H1C3	24	-35.6	-34.2	-8.3	-252	-730	-700	-169.3	-5263
63	B1W8H8ST10WT8H2C3	17	-35.6	-68.3	-8.3	-219	-730	-1401	-169.3	-4736
64	B1W8H8ST8WT8H0C4	27	-28.5	0.0	-8.3	-282	-584	0	-169.3	-5739
65	B1W8H8ST8WT8H1C4	24	-28.5	-34.2	-8.3	-252	-584	-700	-169.3	-5263
66	B1W8H8ST8WT8H2C4	17	-28.5	-68.3	-8.3	-219	-584	-1401	-169.3	-4736
67	B1W8H8ST9WT8H0C4	27	-32.0	0.0	-8.3	-282	-657	0	-169.3	-5739
68	B1W8H8ST9WT8H1C4	24	-32.0	-34.2	-8.3	-252	-657	-700	-169.3	-5263
69	B1W8H8ST9WT8H2C4	17	-32.0	-68.3	-8.3	-219	-657	-1401	-169.3	-4736
70	B1W8H8ST10WT8H0C4	27	-35.6	0.0	-8.3	-282	-730	0	-169.3	-5739
71	B1W8H8ST10WT8H1C4	24	-35.6	-34.2	-8.3	-252	-730	-700	-169.3	-5263
72	B1W8H8ST10WT8H2C4	17	-35.6	-68.3	-8.3	-219	-730	-1401	-169.3	-4736
73	B1W8H8ST8WT8H0C5	27	-28.5	0.0	-8.3	-282	-584	0	-169.3	-5739
74	B1W8H8ST8WT8H1C5	24	-28.5	-34.2	-8.3	-252	-584	-700	-169.3	-5263
75	B1W8H8ST8WT8H2C5	17	-28.5	-68.3	-8.3	-219	-584	-1401	-169.3	-4736
76	B1W8H8ST9WT8H0C5	27	-32.0	0.0	-8.3	-282	-657	0	-169.3	-5739
77	B1W8H8ST9WT8H1C5	24	-32.0	-34.2	-8.3	-252	-657	-700	-169.3	-5263
78	B1W8H8ST9WT8H2C5	17	-32.0	-68.3	-8.3	-219	-657	-1401	-169.3	-4736
79	B1W8H8ST10WT8H0C5	27	-35.6	0.0	-8.3	-282	-730	0	-169.3	-5739
80	B1W8H8ST10WT8H1C5	24	-35.6	-34.2	-8.3	-252	-730	-700	-169.3	-5263
81	B1W8H8ST10WT8H2C5	17	-35.6	-68.3	-8.3	-219	-730	-1401	-169.3	-4736

Units: lb./in. for shear; lb.-in./in. for bending moment

#	Case	NLS	V_L^{DC}	V_L^{EF}	V_L^{DW}	V_L^{LL}	M_{pE}^{DC}	M_{pE}^{EF}	M_{pE}^{DW}	M_{pE}^{LL}
82	B1W9H9ST8.5WT9H0C3	35	-34.3	0.0	-9.4	-306	-798	0	-217.7	-6485
83	B1W9H9ST8.5WT9H1C3	32	-34.3	-38.8	-9.4	-276	-798	-901	-217.7	-6014
84	B1W9H9ST8.5WT9H2C3	21	-34.3	-77.5	-9.4	-227	-798	-1802	-217.7	-5494
85	B1W9H9ST9.5WT9H0C3	35	-38.3	0.0	-9.4	-306	-892	0	-217.7	-6485
86	B1W9H9ST9.5WT9H1C3	32	-38.3	-38.8	-9.4	-276	-892	-901	-217.7	-6014
87	B1W9H9ST9.5WT9H2C3	21	-38.3	-77.5	-9.4	-227	-892	-1802	-217.7	-5494
88	B1W9H9ST10.5WT9H0C3	35	-42.4	0.0	-9.4	-306	-985	0	-217.7	-6485
89	B1W9H9ST10.5WT9H1C3	32	-42.4	-38.8	-9.4	-276	-985	-901	-217.7	-6014
90	B1W9H9ST10.5WT9H2C3	21	-42.4	-77.5	-9.4	-227	-985	-1802	-217.7	-5494
91	B1W9H9ST8.5WT9H0C4	35	-34.3	0.0	-9.4	-306	-798	0	-217.7	-6485
92	B1W9H9ST8.5WT9H1C4	32	-34.3	-38.8	-9.4	-276	-798	-901	-217.7	-6014
93	B1W9H9ST8.5WT9H2C4	21	-34.3	-77.5	-9.4	-227	-798	-1802	-217.7	-5494
94	B1W9H9ST9.5WT9H0C4	35	-38.3	0.0	-9.4	-306	-892	0	-217.7	-6485
95	B1W9H9ST9.5WT9H1C4	32	-38.3	-38.8	-9.4	-276	-892	-901	-217.7	-6014
96	B1W9H9ST9.5WT9H2C4	21	-38.3	-77.5	-9.4	-227	-892	-1802	-217.7	-5494
97	B1W9H9ST10.5WT9H0C4	35	-42.4	0.0	-9.4	-306	-985	0	-217.7	-6485
98	B1W9H9ST10.5WT9H1C4	32	-42.4	-38.8	-9.4	-276	-985	-901	-217.7	-6014
99	B1W9H9ST10.5WT9H2C4	21	-42.4	-77.5	-9.4	-227	-985	-1802	-217.7	-5494
100	B1W9H9ST8.5WT9H0C5	35	-34.3	0.0	-9.4	-306	-798	0	-217.7	-6485
101	B1W9H9ST8.5WT9H1C5	32	-34.3	-38.8	-9.4	-276	-798	-901	-217.7	-6014
102	B1W9H9ST8.5WT9H2C5	21	-34.3	-77.5	-9.4	-227	-798	-1802	-217.7	-5494
103	B1W9H9ST9.5WT9H0C5	35	-38.3	0.0	-9.4	-306	-892	0	-217.7	-6485
104	B1W9H9ST9.5WT9H1C5	32	-38.3	-38.8	-9.4	-276	-892	-901	-217.7	-6014
105	B1W9H9ST9.5WT9H2C5	21	-38.3	-77.5	-9.4	-227	-892	-1802	-217.7	-5494
106	B1W9H9ST10.5WT9H0C5	35	-42.4	0.0	-9.4	-306	-985	0	-217.7	-6485
107	B1W9H9ST10.5WT9H1C5	32	-42.4	-38.8	-9.4	-276	-985	-901	-217.7	-6014
108	B1W9H9ST10.5WT9H2C5	21	-42.4	-77.5	-9.4	-227	-985	-1802	-217.7	-5494

Units: lb./in. for shear; lb.-in./in. for bending moment

#	Case	NLS	V_L^{DC}	V_L^{EF}	V_L^{DW}	V_L^{LL}	M_{pE}^{DC}	M_{pE}^{EF}	M_{pE}^{DW}	M_{pE}^{LL}
109	B1W10H10ST9WT10H0C3	44	-40.6	0.0	-10.5	-324	-1056	0	-272.3	-7212
110	B1W10H10ST9WT10H1C3	35	-40.6	-43.3	-10.5	-281	-1056	-1127	-272.3	-6747
111	B1W10H10ST9WT10H2C3	29	-40.6	-86.7	-10.5	-254	-1053	-2246	-271.4	-6325
112	B1W10H10ST10WT10H0C3	44	-45.1	0.0	-10.5	-324	-1174	0	-272.3	-7212
113	B1W10H10ST10WT10H1C3	35	-45.1	-43.3	-10.5	-281	-1174	-1127	-272.3	-6747
114	B1W10H10ST10WT10H2C3	29	-45.1	-86.7	-10.5	-254	-1170	-2246	-271.4	-6325
115	B1W10H10ST11WT10H0C3	44	-49.7	0.0	-10.5	-324	-1291	0	-272.3	-7212
116	B1W10H10ST11WT10H1C3	35	-49.7	-43.3	-10.5	-281	-1291	-1127	-272.3	-6747
117	B1W10H10ST11WT10H2C3	29	-49.7	-86.7	-10.5	-254	-1287	-2246	-271.4	-6325
118	B1W10H10ST9WT10H0C4	44	-40.6	0.0	-10.5	-324	-1056	0	-272.3	-7212
119	B1W10H10ST9WT10H1C4	35	-40.6	-43.3	-10.5	-281	-1056	-1127	-272.3	-6747
120	B1W10H10ST9WT10H2C4	29	-40.6	-86.7	-10.5	-254	-1053	-2246	-271.4	-6325
121	B1W10H10ST10WT10H0C4	44	-45.1	0.0	-10.5	-324	-1174	0	-272.3	-7212
122	B1W10H10ST10WT10H1C4	35	-45.1	-43.3	-10.5	-281	-1174	-1127	-272.3	-6747
123	B1W10H10ST10WT10H2C4	29	-45.1	-86.7	-10.5	-254	-1170	-2246	-271.4	-6325
124	B1W10H10ST11WT10H0C4	44	-49.7	0.0	-10.5	-324	-1291	0	-272.3	-7212
125	B1W10H10ST11WT10H1C4	35	-49.7	-43.3	-10.5	-281	-1291	-1127	-272.3	-6747
126	B1W10H10ST11WT10H2C4	29	-49.7	-86.7	-10.5	-254	-1287	-2246	-271.4	-6325
127	B1W10H10ST9WT10H0C5	44	-40.6	0.0	-10.5	-324	-1056	0	-272.3	-7212
128	B1W10H10ST9WT10H1C5	35	-40.6	-43.3	-10.5	-281	-1056	-1127	-272.3	-6747
129	B1W10H10ST9WT10H2C5	29	-40.6	-86.7	-10.5	-254	-1053	-2246	-271.4	-6325
130	B1W10H10ST10WT10H0C5	44	-45.1	0.0	-10.5	-324	-1174	0	-272.3	-7212
131	B1W10H10ST10WT10H1C5	35	-45.1	-43.3	-10.5	-281	-1174	-1127	-272.3	-6747
132	B1W10H10ST10WT10H2C5	29	-45.1	-86.7	-10.5	-254	-1170	-2246	-271.4	-6325
133	B1W10H10ST11WT10H0C5	44	-49.7	0.0	-10.5	-324	-1291	0	-272.3	-7212
134	B1W10H10ST11WT10H1C5	35	-49.7	-43.3	-10.5	-281	-1291	-1127	-272.3	-6747
135	B1W10H10ST11WT10H2C5	29	-49.7	-86.7	-10.5	-254	-1287	-2246	-271.4	-6325

Units: lb./in. for shear; lb.-in./in. for bending moment

#	Case	NLS	V_L^{DC}	V_L^{EF}	V_L^{DW}	V_L^{LL}	M_{pE}^{DC}	M_{pE}^{EF}	M_{pE}^{DW}	M_{pE}^{LL}
136	B1W11H11ST9.5WT11H0C3	47	-47.4	0.0	-11.6	-325	-1322	0	-322.9	-8062
137	B1W11H11ST9.5WT11H1C3	43	-47.4	-47.9	-11.6	-296	-1349	-1363	-329.4	-7790
138	B1W11H11ST9.5WT11H2C3	37	-47.4	-95.8	-11.6	-272	-1349	-2727	-329.6	-7486
139	B1W11H11ST10.5WT11H0C3	47	-52.4	0.0	-11.6	-325	-1461	0	-322.9	-8062
140	B1W11H11ST10.5WT11H1C3	43	-52.4	-47.9	-11.6	-296	-1491	-1363	-329.4	-7790
141	B1W11H11ST10.5WT11H2C3	37	-52.4	-95.8	-11.6	-272	-1503	-2748	-332.1	-7486
142	B1W11H11ST11.5WT11H0C3	47	-57.4	0.0	-11.6	-325	-1600	0	-322.9	-8062
143	B1W11H11ST11.5WT11H1C3	43	-57.4	-47.9	-11.6	-296	-1610	-1344	-324.9	-7790
144	B1W11H11ST11.5WT11H2C3	37	-57.4	-95.8	-11.6	-272	-1646	-2748	-332.1	-7486
145	B1W11H11ST9.5WT11H0C4	47	-47.4	0.0	-11.6	-325	-1322	0	-322.9	-8062
146	B1W11H11ST9.5WT11H1C4	43	-47.4	-47.9	-11.6	-296	-1349	-1363	-329.4	-7790
147	B1W11H11ST9.5WT11H2C4	37	-47.4	-95.8	-11.6	-272	-1349	-2727	-329.6	-7486
148	B1W11H11ST10.5WT11H0C4	47	-52.4	0.0	-11.6	-325	-1461	0	-322.9	-8062
149	B1W11H11ST10.5WT11H1C4	43	-52.4	-47.9	-11.6	-296	-1491	-1363	-329.4	-7790
150	B1W11H11ST10.5WT11H2C4	37	-52.4	-95.8	-11.6	-272	-1503	-2748	-332.1	-7486
151	B1W11H11ST11.5WT11H0C4	47	-57.4	0.0	-11.6	-325	-1600	0	-322.9	-8062
152	B1W11H11ST11.5WT11H1C4	43	-57.4	-47.9	-11.6	-296	-1610	-1344	-324.9	-7790
153	B1W11H11ST11.5WT11H2C4	37	-57.4	-95.8	-11.6	-272	-1646	-2748	-332.1	-7486
154	B1W11H11ST9.5WT11H0C5	47	-47.4	0.0	-11.6	-325	-1322	0	-322.9	-8062
155	B1W11H11ST9.5WT11H1C5	43	-47.4	-47.9	-11.6	-296	-1349	-1363	-329.4	-7790
156	B1W11H11ST9.5WT11H2C5	37	-47.4	-95.8	-11.6	-272	-1349	-2727	-329.6	-7486
157	B1W11H11ST10.5WT11H0C5	47	-52.4	0.0	-11.6	-325	-1461	0	-322.9	-8062
158	B1W11H11ST10.5WT11H1C5	43	-52.4	-47.9	-11.6	-296	-1491	-1363	-329.4	-7790
159	B1W11H11ST10.5WT11H2C5	37	-52.4	-95.8	-11.6	-272	-1503	-2748	-332.1	-7486
160	B1W11H11ST11.5WT11H0C5	47	-57.4	0.0	-11.6	-325	-1600	0	-322.9	-8062
161	B1W11H11ST11.5WT11H1C5	43	-57.4	-47.9	-11.6	-296	-1610	-1344	-324.9	-7790
162	B1W11H11ST11.5WT11H2C5	37	-57.4	-95.8	-11.6	-272	-1646	-2748	-332.1	-7486

Units: lb./in. for shear; lb.-in./in. for bending moment

#	Case	NLS	V_L^{DC}	V_L^{EF}	V_L^{DW}	V_L^{LL}	M_{pE}^{DC}	M_{pE}^{EF}	M_{pE}^{DW}	M_{pE}^{LL}
163	B1W12H12ST10WT12H0C3	55	-54.7	0.0	-12.7	-336	-1679	0	-389.6	-9163
164	B1W12H12ST10WT12H1C3	51	-54.7	-52.5	-12.7	-308	-1688	-1621	-391.6	-8909
165	B1W12H12ST10WT12H2C3	45	-54.7	-105.0	-12.7	-285	-1719	-3301	-398.8	-8622
166	B1W12H12ST11WT12H0C3	55	-60.2	0.0	-12.7	-336	-1847	0	-389.6	-9163
167	B1W12H12ST11WT12H1C3	51	-60.2	-52.5	-12.7	-308	-1857	-1621	-391.6	-8909
168	B1W12H12ST11WT12H2C3	45	-60.2	-105.0	-12.7	-285	-1879	-3280	-396.3	-8622
169	B1W12H12ST12WT12H0C3	55	-65.6	0.0	-12.7	-336	-2015	0	-389.6	-9163
170	B1W12H12ST12WT12H1C3	51	-65.6	-52.5	-12.7	-308	-2049	-1639	-396.1	-8909
171	B1W12H12ST12WT12H2C3	45	-65.6	-105.0	-12.7	-285	-2063	-3301	-398.8	-8622
172	B1W12H12ST10WT12H0C4	55	-54.7	0.0	-12.7	-336	-1679	0	-389.6	-9163
173	B1W12H12ST10WT12H1C4	51	-54.7	-52.5	-12.7	-308	-1688	-1621	-391.6	-8909
174	B1W12H12ST10WT12H2C4	45	-54.7	-105.0	-12.7	-285	-1719	-3301	-398.8	-8622
175	B1W12H12ST11WT12H0C4	55	-60.2	0.0	-12.7	-336	-1847	0	-389.6	-9163
176	B1W12H12ST11WT12H1C4	51	-60.2	-52.5	-12.7	-308	-1857	-1621	-391.6	-8909
177	B1W12H12ST11WT12H2C4	45	-60.2	-105.0	-12.7	-285	-1879	-3280	-396.3	-8622
178	B1W12H12ST12WT12H0C4	55	-65.6	0.0	-12.7	-336	-2015	0	-389.6	-9163
179	B1W12H12ST12WT12H1C4	51	-65.6	-52.5	-12.7	-308	-2049	-1639	-396.1	-8909
180	B1W12H12ST12WT12H2C4	45	-65.6	-105.0	-12.7	-285	-2063	-3301	-398.8	-8622
181	B1W12H12ST10WT12H0C5	55	-54.7	0.0	-12.7	-336	-1679	0	-389.6	-9163
182	B1W12H12ST10WT12H1C5	51	-54.7	-52.5	-12.7	-308	-1688	-1621	-391.6	-8909
183	B1W12H12ST10WT12H2C5	45	-54.7	-105.0	-12.7	-285	-1719	-3301	-398.8	-8622
184	B1W12H12ST11WT12H0C5	55	-60.2	0.0	-12.7	-336	-1847	0	-389.6	-9163
185	B1W12H12ST11WT12H1C5	51	-60.2	-52.5	-12.7	-308	-1857	-1621	-391.6	-8909
186	B1W12H12ST11WT12H2C5	45	-60.2	-105.0	-12.7	-285	-1879	-3280	-396.3	-8622
187	B1W12H12ST12WT12H0C5	55	-65.6	0.0	-12.7	-336	-2015	0	-389.6	-9163
188	B1W12H12ST12WT12H1C5	51	-65.6	-52.5	-12.7	-308	-2049	-1639	-396.1	-8909
189	B1W12H12ST12WT12H2C5	45	-65.6	-105.0	-12.7	-285	-2063	-3301	-398.8	-8622

Units: lb./in. for shear; lb.-in./in. for bending moment

Table E8. Bending moment and shear force values (2D model; AASHTO-LRFD BDS with rigid joints; 2-barrel culverts)

#	Case	NLS	V_L^{DC}	V_L^{EF}	V_L^{DW}	V_L^{LL}	V_R^{DC}	V_R^{EF}	V_R^{DW}	V_R^{LL}
1	B2W6H6ST7WT6H0C4	43	-22.6	0.0	-7.5	-273.4	-22.6	0.0	-7.5	43
2	B2W6H6ST7WT6H1C4	34	-22.6	-31.2	-7.5	-248.1	-22.6	-31.2	-7.5	34
3	B2W6H6ST7WT6H2C4	19	-22.6	-62.4	-7.5	-213.4	-22.6	-62.4	-7.5	19
4	B2W6H6ST8WT6H0C4	43	-25.8	0.0	-7.5	-272.0	-25.8	0.0	-7.5	43
5	B2W6H6ST8WT6H1C4	34	-25.8	-31.2	-7.5	-246.7	-25.8	-31.2	-7.5	34
6	B2W6H6ST8WT6H2C4	19	-25.8	-62.4	-7.5	-212.2	-25.8	-62.4	-7.5	19
7	B2W6H6ST9WT6H0C4	43	-29.0	0.0	-7.5	-270.8	-29.0	0.0	-7.5	43
8	B2W6H6ST9WT6H1C4	34	-29.0	-31.2	-7.5	-245.5	-29.0	-31.2	-7.5	34
9	B2W6H6ST9WT6H2C4	19	-29.0	-62.3	-7.5	-211.2	-29.0	-62.3	-7.5	19
10	B2W7H7ST7.5WT7H0C4	58	-28.7	0.0	-8.9	-292.3	-28.7	0.0	-8.9	58
11	B2W7H7ST7.5WT7H1C4	46	-28.7	-36.9	-8.9	-257.1	-28.7	-36.9	-8.9	46
12	B2W7H7ST7.5WT7H2C4	31	-28.7	-73.8	-8.9	-229.5	-28.7	-73.8	-8.9	31
13	B2W7H7ST8.5WT7H0C4	58	-32.5	0.0	-8.9	-291.2	-32.5	0.0	-8.9	58
14	B2W7H7ST8.5WT7H1C4	46	-32.5	-36.9	-8.9	-255.7	-32.5	-36.9	-8.9	46
15	B2W7H7ST8.5WT7H2C4	31	-32.5	-73.8	-8.9	-228.2	-32.5	-73.8	-8.9	31
16	B2W7H7ST9.5WT7H0C4	58	-36.3	0.0	-8.9	-290.3	-36.3	0.0	-8.9	58
17	B2W7H7ST9.5WT7H1C4	46	-36.3	-36.9	-8.9	-254.5	-36.3	-36.9	-8.9	46
18	B2W7H7ST9.5WT7H2C4	31	-36.3	-73.7	-8.9	-227.1	-36.3	-73.7	-8.9	31
19	B2W8H8ST8WT8H0C4	65	-35.4	0.0	-10.3	-308.8	-35.4	0.0	-10.3	65
20	B2W8H8ST8WT8H1C4	60	-35.4	-42.6	-10.3	-279.8	-35.4	-42.6	-10.3	60
21	B2W8H8ST8WT8H2C4	43	-35.4	-85.3	-10.3	-239.8	-35.4	-85.3	-10.3	43
22	B2W8H8ST9WT8H0C4	65	-39.8	0.0	-10.3	-307.3	-39.8	0.0	-10.3	65
23	B2W8H8ST9WT8H1C4	60	-39.8	-42.6	-10.3	-278.5	-39.8	-42.6	-10.3	60
24	B2W8H8ST9WT8H2C4	43	-39.8	-85.2	-10.3	-238.4	-39.8	-85.2	-10.3	43
25	B2W8H8ST10WT8H0C4	65	-44.1	0.0	-10.3	-306.1	-44.1	0.0	-10.3	65
26	B2W8H8ST10WT8H1C4	60	-44.1	-42.6	-10.3	-277.4	-44.1	-42.6	-10.3	60
27	B2W8H8ST10WT8H2C4	43	-44.1	-85.2	-10.3	-237.3	-44.1	-85.2	-10.3	43

Units: lb./in. for shear

#	Case	M_{pE}^{DC}	M_{pE}^{EF}	M_{pE}^{DW}	M_{pE}^{LL}	M_{nL}^{DC}	M_{nL}^{EF}	M_{nL}^{DW}	M_{nL}^{LL}	M_{nR}^{DC}	M_{nR}^{EF}	M_{nR}^{DW}	M_{nR}^{LL}
1	B2W6H6ST7WT6H0C4	-153	0	-49	-3384	264	0	90	2530	-264	0	-90	-2530
2	B2W6H6ST7WT6H1C4	-152	-203	-49	-2906	264	373	90	2358	-264	-373	-90	-2286
3	B2W6H6ST7WT6H2C4	-152	-406	-49	-2449	264	746	90	1534	-264	-746	-90	-1534
4	B2W6H6ST8WT6H0C4	-175	0	-50	-3412	300	0	90	2488	-300	0	-90	-2488
5	B2W6H6ST8WT6H1C4	-174	-204	-49	-2931	300	372	90	2317	-300	-372	-90	-2246
6	B2W6H6ST8WT6H2C4	-174	-407	-49	-2473	300	743	90	1571	-300	-743	-90	-1571
7	B2W6H6ST9WT6H0C4	-198	0	-50	-3432	335	0	89	2437	-335	0	-89	-2437
8	B2W6H6ST9WT6H1C4	-197	-205	-49	-2947	335	370	89	2268	-335	-370	-89	-2198
9	B2W6H6ST9WT6H2C4	-197	-409	-49	-2490	335	740	89	1584	-335	-740	-89	-1584
10	B2W7H7ST7.5WT7H0C4	-226	0	-69	-3990	398	0	126	2673	-398	0	-126	-2673
11	B2W7H7ST7.5WT7H1C4	-225	-283	-68	-3518	398	521	126	2562	-398	-521	-126	-2481
12	B2W7H7ST7.5WT7H2C4	-225	-565	-68	-3054	398	1042	126	1934	-398	-1042	-126	-1934
13	B2W7H7ST8.5WT7H0C4	-258	0	-69	-4027	448	0	125	2621	-448	0	-125	-2621
14	B2W7H7ST8.5WT7H1C4	-257	-284	-69	-3553	448	519	126	2518	-448	-519	-126	-2442
15	B2W7H7ST8.5WT7H2C4	-256	-566	-68	-3088	448	1039	126	1859	-448	-1039	-126	-1859
16	B2W7H7ST9.5WT7H0C4	-290	0	-69	-4055	497	0	125	2569	-497	0	-125	-2569
17	B2W7H7ST9.5WT7H1C4	-288	-285	-69	-3579	497	517	125	2469	-497	-517	-125	-2396
18	B2W7H7ST9.5WT7H2C4	-288	-568	-69	-3114	497	1034	125	1892	-497	-1034	-125	-1892
19	B2W8H8ST8WT8H0C4	-331	0	-95	-4592	568	0	168	2892	-568	0	-168	-2892
20	B2W8H8ST8WT8H1C4	-329	-389	-94	-4117	568	695	168	2690	-568	-695	-168	-2596
21	B2W8H8ST8WT8H2C4	-328	-776	-94	-3654	568	1390	168	2336	-568	-1390	-168	-2336
22	B2W8H8ST9WT8H0C4	-373	0	-95	-4631	635	0	167	2842	-635	0	-167	-2842
23	B2W8H8ST9WT8H1C4	-371	-390	-94	-4155	635	693	167	2645	-635	-693	-167	-2560
24	B2W8H8ST9WT8H2C4	-371	-778	-94	-3692	635	1385	167	2238	-635	-1385	-167	-2238
25	B2W8H8ST10WT8H0C4	-417	0	-95	-4659	701	0	167	2790	-701	0	-167	-2790
26	B2W8H8ST10WT8H1C4	-401	-377	-91	-4183	701	690	167	2597	-701	-690	-167	-2518
27	B2W8H8ST10WT8H2C4	-414	-780	-94	-3720	701	1380	167	2166	-701	-1380	-167	-2166

Units: lb.-in./in. for bending moment

#	Case	NLS	V_L^{DC}	V_L^{EF}	V_L^{DW}	V_L^{LL}	V_R^{DC}	V_R^{EF}	V_R^{DW}	V_R^{LL}
28	B2W9H9ST8.5WT9H0C4	81	-42.7	0.0	-11.7	-333.8	-42.7	0.0	-11.7	-333.8
29	B2W9H9ST8.5WT9H1C4	76	-42.7	-48.4	-11.7	-306.7	-42.7	-48.4	-11.7	-306.7
30	B2W9H9ST8.5WT9H2C4	55	-42.7	-96.7	-11.7	-246.3	-42.7	-96.7	-11.7	-259.7
31	B2W9H9ST9.5WT9H0C4	81	-47.6	0.0	-11.7	-332.1	-47.6	0.0	-11.7	-332.1
32	B2W9H9ST9.5WT9H1C4	76	-47.7	-48.3	-11.7	-305.1	-47.7	-48.3	-11.7	-305.1
33	B2W9H9ST9.5WT9H2C4	55	-47.7	-96.7	-11.7	-245.0	-47.7	-96.7	-11.7	-258.3
34	B2W9H9ST10.5WT9H0C4	81	-52.6	0.0	-11.7	-330.7	-52.6	0.0	-11.7	-330.7
35	B2W9H9ST10.5WT9H1C4	76	-52.6	-48.3	-11.7	-303.8	-52.6	-48.3	-11.7	-303.8
36	B2W9H9ST10.5WT9H2C4	55	-52.6	-96.6	-11.7	-243.9	-52.6	-96.6	-11.7	-257.2
37	B2W10H10ST9WT10H0C4	98	-50.6	0.0	-13.1	-351.3	-50.6	0.0	-13.1	-351.3
38	B2W10H10ST9WT10H1C4	83	-50.6	-54.1	-13.1	-314.9	-50.6	-54.1	-13.1	-314.9
39	B2W10H10ST9WT10H2C4	71	-50.6	-108.2	-13.1	-288.5	-50.6	-108.2	-13.1	-288.5
40	B2W10H10ST10WT10H0C4	98	-56.1	0.0	-13.1	-349.5	-56.1	0.0	-13.1	-349.5
41	B2W10H10ST10WT10H1C4	83	-56.1	-54.1	-13.1	-313.1	-56.1	-54.1	-13.1	-313.1
42	B2W10H10ST10WT10H2C4	71	-56.1	-108.1	-13.1	-286.9	-56.1	-108.1	-13.1	-286.9
43	B2W10H10ST11WT10H0C4	98	-61.7	0.0	-13.1	-348.1	-61.7	0.0	-13.1	-348.1
44	B2W10H10ST11WT10H1C4	83	-61.7	-54.0	-13.1	-311.7	-61.7	-54.0	-13.1	-311.7
45	B2W10H10ST11WT10H2C4	71	-61.7	-108.0	-13.1	-285.6	-61.7	-108.0	-13.1	-285.6
46	B2W11H11ST9.5WT11H0C4	105	-59.0	0.0	-14.5	-354.0	-59.0	0.0	-14.5	-354.0
47	B2W11H11ST9.5WT11H1C4	99	-59.0	-59.8	-14.5	-330.5	-59.0	-59.8	-14.5	-330.5
48	B2W11H11ST9.5WT11H2C4	87	-59.0	-119.6	-14.5	-307.2	-59.0	-119.6	-14.5	-307.2
49	B2W11H11ST10.5WT11H0C4	105	-65.2	0.0	-14.4	-352.2	-65.2	0.0	-14.4	-352.2
50	B2W11H11ST10.5WT11H1C4	99	-65.2	-59.8	-14.4	-328.6	-65.2	-59.8	-14.4	-328.6
51	B2W11H11ST10.5WT11H2C4	87	-65.2	-119.6	-14.4	-305.4	-65.2	-119.6	-14.4	-305.4
52	B2W11H11ST11.5WT11H0C4	105	-71.3	0.0	-14.4	-350.7	-71.3	0.0	-14.4	-350.7
53	B2W11H11ST11.5WT11H1C4	99	-71.3	-59.8	-14.4	-327.1	-71.3	-59.8	-14.4	-327.1
54	B2W11H11ST11.5WT11H2C4	87	-71.3	-119.5	-14.4	-304.0	-71.3	-119.5	-14.4	-304.0

Units: lb./in. for shear

#	Case	M_{pE}^{DC}	M_{pE}^{EF}	M_{pE}^{DW}	M_{pE}^{LL}	M_{nL}^{DC}	M_{nL}^{EF}	M_{nL}^{DW}	M_{nL}^{LL}	M_{nR}^{DC}	M_{nR}^{EF}	M_{nR}^{DW}	M_{nR}^{LL}
28	B2W9H9ST8.5WT9H0C4	-448	0	-121	-5167	778	0	216	3339	-778	0	-216	-3339
29	B2W9H9ST8.5WT9H1C4	-445	-497	-120	-4698	778	894	216	3217	-778	-894	-216	-3217
30	B2W9H9ST8.5WT9H2C4	-445	-991	-120	-4232	778	1788	216	2744	-778	-1788	-216	-2889
31	B2W9H9ST9.5WT9H0C4	-503	0	-121	-5215	865	0	215	3207	-865	0	-215	-3207
32	B2W9H9ST9.5WT9H1C4	-500	-498	-120	-4745	865	891	215	3090	-865	-891	-215	-3090
33	B2W9H9ST9.5WT9H2C4	-499	-994	-120	-4280	865	1783	215	2623	-865	-1783	-215	-2757
34	B2W9H9ST10.5WT9H0C4	-558	0	-121	-5252	951	0	215	3107	-951	0	-215	-3107
35	B2W9H9ST10.5WT9H1C4	-555	-499	-121	-4781	951	888	215	2997	-951	-888	-215	-2997
36	B2W9H9ST10.5WT9H2C4	-554	-996	-120	-4316	951	1777	215	2579	-951	-1777	-215	-2656
37	B2W10H10ST9WT10H0C4	-589	0	-150	-5720	1033	0	270	4044	-1033	0	-270	-4044
38	B2W10H10ST9WT10H1C4	-585	-617	-149	-5256	1033	1118	270	3928	-1033	-1118	-270	-3928
39	B2W10H10ST9WT10H2C4	-597	-1259	-152	-4793	1033	2236	270	3723	-1033	-2236	-270	-3723
40	B2W10H10ST10WT10H0C4	-656	0	-150	-5776	1142	0	269	3916	-1142	0	-269	-3916
41	B2W10H10ST10WT10H1C4	-652	-618	-149	-5311	1142	1115	270	3823	-1142	-1115	-270	-3823
42	B2W10H10ST10WT10H2C4	-665	-1261	-152	-4862	1142	2230	270	3662	-1142	-2230	-270	-3662
43	B2W10H10ST11WT10H0C4	-725	0	-151	-5820	1250	0	269	3944	-1250	0	-269	-3944
44	B2W10H10ST11WT10H1C4	-721	-620	-150	-5355	1250	1112	269	3850	-1250	-1112	-269	-3850
45	B2W10H10ST11WT10H2C4	-734	-1264	-153	-4919	1250	2224	269	3692	-1250	-2224	-269	-3690
46	B2W11H11ST9.5WT11H0C4	-777	0	-188	-6279	1336	0	330	5001	-1336	0	-330	-5001
47	B2W11H11ST9.5WT11H1C4	-775	-776	-188	-5935	1336	1367	330	4995	-1336	-1367	-330	-4995
48	B2W11H11ST9.5WT11H2C4	-775	-1551	-187	-5598	1336	2735	330	4945	-1336	-2735	-330	-4945
49	B2W11H11ST10.5WT11H0C4	-861	0	-188	-6362	1470	0	330	5003	-1470	0	-330	-5003
50	B2W11H11ST10.5WT11H1C4	-859	-778	-188	-6018	1470	1364	330	4999	-1470	-1364	-330	-4999
51	B2W11H11ST10.5WT11H2C4	-859	-1554	-188	-5676	1470	2729	330	4952	-1470	-2729	-330	-4952
52	B2W11H11ST11.5WT11H0C4	-946	0	-189	-6429	1603	0	329	5018	-1603	0	-329	-5018
53	B2W11H11ST11.5WT11H1C4	-944	-779	-188	-6085	1603	1361	329	5012	-1603	-1361	-329	-5012
54	B2W11H11ST11.5WT11H2C4	-943	-1557	-188	-5739	1603	2722	329	4966	-1603	-2722	-329	-4966

Units: lb.-in./in. for bending moment

#	Case	NLS	V_L^{DC}	V_L^{EF}	V_L^{DW}	V_L^{LL}	V_R^{DC}	V_R^{EF}	V_R^{DW}	V_R^{LL}
55	B2W12H12ST10WT12H0C4	121	-68.1	0.0	-15.8	-364.0	-68.1	0.0	-15.8	-364.0
56	B2W12H12ST10WT12H1C4	115	-68.1	-65.5	-15.8	-341.8	-68.1	-65.5	-15.8	-341.8
57	B2W12H12ST10WT12H2C4	103	-68.1	-131.1	-15.8	-321.2	-68.1	-131.1	-15.8	-321.2
58	B2W12H12ST11WT12H0C4	121	-74.9	0.0	-15.8	-362.2	-74.9	0.0	-15.8	-362.2
59	B2W12H12ST11WT12H1C4	115	-74.9	-65.5	-15.8	-340.0	-74.9	-65.5	-15.8	-340.0
60	B2W12H12ST11WT12H2C4	103	-74.9	-131.0	-15.8	-319.4	-74.9	-131.0	-15.8	-319.4
61	B2W12H12ST12WT12H0C4	121	-81.6	0.0	-15.8	-360.7	-81.6	0.0	-15.8	-360.7
62	B2W12H12ST12WT12H1C4	115	-81.6	-65.5	-15.8	-338.5	-81.6	-65.5	-15.8	-338.5
63	B2W12H12ST12WT12H2C4	103	-81.6	-131.0	-15.8	-317.8	-81.6	-131.0	-15.8	-317.8

Units: lb./in. for shear

#	Case	M_{pE}^{DC}	M_{pE}^{EF}	M_{pE}^{DW}	M_{pE}^{LL}	M_{nL}^{DC}	M_{nL}^{EF}	M_{nL}^{DW}	M_{nL}^{LL}	M_{nR}^{DC}	M_{nR}^{EF}	M_{nR}^{DW}	M_{nR}^{LL}
55	B2W12H12ST10WT12H0C4	-980	0	-226	-7060	1690	0	397	6086	-1690	0	-397	-6086
56	B2W12H12ST10WT12H1C4	-981	-934	-226	-6730	1691	1642	397	6017	-1691	-1642	-397	-6017
57	B2W12H12ST10WT12H2C4	-974	-1855	-224	-6397	1691	3284	397	5944	-1691	-3284	-397	-5944
58	B2W12H12ST11WT12H0C4	-1081	0	-226	-7147	1852	0	396	6085	-1852	0	-396	-6085
59	B2W12H12ST11WT12H1C4	-1082	-936	-226	-6817	1853	1639	396	6018	-1853	-1639	-396	-6018
60	B2W12H12ST11WT12H2C4	-1075	-1858	-225	-6487	1853	3278	396	5944	-1853	-3278	-396	-5944
61	B2W12H12ST12WT12H0C4	-1182	0	-226	-7218	2012	0	395	6090	-2012	0	-395	-6090
62	B2W12H12ST12WT12H1C4	-1177	-932	-225	-6889	2013	1635	395	6021	-2013	-1635	-395	-6021
63	B2W12H12ST12WT12H2C4	-1176	-1861	-225	-6561	2013	3270	395	5949	-2013	-3270	-395	-5949

Units: lb.-in./in. for bending moment

Table E9. Bending moment and shear force values (2D model; AASHTO-LRFD BDS with rigid joints; 3-barrel culverts)

#	Case	NLS	V_L^{DC}	V_L^{EF}	V_L^{DW}	V_L^{LL}	V_R^{DC}	V_R^{EF}	V_R^{DW}	V_R^{LL}
1	B3W6H6ST8WT6H0C4	43	-25.1	0.0	-7.3	-274.4	-20.8	0.0	-6.0	-259.0
2	B3W6H6ST8WT6H1C4	34	-25.1	-30.1	-7.3	-249.3	-20.8	-25.0	-6.0	-227.9
3	B3W6H6ST8WT6H2C4	19	-25.1	-60.1	-7.3	-214.5	-20.8	-50.0	-6.0	-189.6
4	B3W7H7ST8.5WT7H0C4	58	-31.7	0.0	-8.6	-293.3	-26.2	0.0	-7.1	-266.6
5	B3W7H7ST8.5WT7H1C4	46	-31.7	-35.7	-8.6	-258.7	-26.2	-29.6	-7.1	-239.3
6	B3W7H7ST8.5WT7H2C4	31	-31.7	-71.3	-8.6	-231.2	-26.2	-59.2	-7.1	-207.0
7	B3W8H8ST9WT8H0C4	65	-38.8	0.0	-10.0	-310.7	-32.0	0.0	-8.3	-277.1
8	B3W8H8ST9WT8H1C4	60	-38.8	-41.3	-10.0	-281.5	-32.0	-34.2	-8.3	-249.6
9	B3W8H8ST9WT8H2C4	43	-38.8	-82.6	-10.0	-241.8	-32.0	-68.3	-8.3	-218.9
10	B3W9H9ST9.5WT9H0C4	81	-46.6	0.0	-11.3	-336.4	-38.3	0.0	-9.4	-301.1
11	B3W9H9ST9.5WT9H1C4	76	-46.6	-46.9	-11.3	-309.2	-38.3	-38.8	-9.4	-272.8
12	B3W9H9ST9.5WT9H2C4	55	-46.6	-93.9	-11.3	-248.5	-38.3	-77.5	-9.4	-228.0
13	B3W10H10ST10WT10H0C4	98	-55.0	0.0	-12.7	-354.3	-45.1	0.0	-10.5	-319.6
14	B3W10H10ST10WT10H1C4	83	-55.0	-52.6	-12.7	-318.0	-45.1	-43.3	-10.5	-279.3
15	B3W10H10ST10WT10H2C4	71	-55.0	-105.2	-12.7	-291.3	-45.1	-86.7	-10.5	-253.0
16	B3W11H11ST10.5WT11H0C4	105	-63.9	0.0	-14.1	-357.4	-52.4	0.0	-11.6	-322.1
17	B3W11H11ST10.5WT11H1C4	99	-63.9	-58.2	-14.1	-333.9	-52.4	-47.9	-11.6	-295.2
18	B3W11H11ST10.5WT11H2C4	87	-63.9	-116.5	-14.1	-310.5	-52.4	-95.8	-11.6	-270.5
19	B3W12H12ST11WT12H0C4	121	-73.5	0.0	-15.4	-367.5	-60.2	0.0	-12.7	-334.2
20	B3W12H12ST11WT12H1C4	115	-73.5	-63.9	-15.4	-345.5	-60.2	-52.5	-12.7	-307.8
21	B3W12H12ST11WT12H2C4	103	-73.5	-127.8	-15.4	-324.8	-60.2	-105.0	-12.7	-284.8

Units: lb./in. for shear

#	Case	M_{pE}^{DC}	M_{pE}^{EF}	M_{pE}^{DW}	M_{pE}^{LL}	M_{nL}^{DC}	M_{nL}^{EF}	M_{nL}^{DW}	M_{nL}^{LL}	M_{nR}^{DC}	M_{nR}^{EF}	M_{nR}^{DW}	M_{nR}^{LL}	M_{pI}^{DC}	M_{pI}^{EF}	M_{pI}^{DW}	M_{pI}^{LL}
1	B3W6H6ST8WT6H0C4	-194	0	-57	-3357	257	0	73	2395	-235	0	-71	-2359	-77	0	-20	-2787
2	B3W6H6ST8WT6H1C4	-193	-235	-57	-2883	257	303	73	2221	-235	-294	-71	-2150	-77	-81	-20	-2366
3	B3W6H6ST8WT6H2C4	-193	-469	-57	-2427	258	607	73	1582	-235	-588	-71	-1620	-77	-162	-20	-1963
4	B3W7H7ST8.5WT7H0C4	-290	0	-80	-3952	390	0	104	2587	-346	0	-98	-2509	-119	0	-29	-3237
5	B3W7H7ST8.5WT7H1C4	-290	-331	-80	-3476	390	431	104	2437	-347	-407	-98	-2353	-118	-119	-29	-2812
6	B3W7H7ST8.5WT7H2C4	-289	-661	-80	-3017	390	863	104	2027	-347	-813	-98	-1900	-118	-237	-29	-2395
7	B3W8H8ST9WT8H0C4	-405	0	-106	-4535	559	0	141	2832	-486	0	-130	-2721	-171	0	-40	-3668
8	B3W8H8ST9WT8H1C4	-404	-436	-105	-4064	559	584	141	2612	-486	-537	-130	-2478	-171	-164	-40	-3241
9	B3W8H8ST9WT8H2C4	-404	-872	-105	-3600	559	1168	141	2487	-486	-1073	-130	-2145	-171	-327	-40	-2817
10	B3W9H9ST9.5WT9H0C4	-544	0	-135	-5090	768	0	184	3546	-656	0	-165	-2910	-236	0	-52	-4082
11	B3W9H9ST9.5WT9H1C4	-542	-555	-134	-4623	768	760	184	3409	-656	-684	-165	-2810	-236	-217	-52	-3656
12	B3W9H9ST9.5WT9H2C4	-541	-1108	-134	-4157	768	1521	184	2942	-656	-1369	-165	-2367	-236	-433	-52	-3226
13	B3W10H10ST10WT10H0C4	-718	0	-168	-5632	1021	0	232	4330	-859	0	-205	-3494	-310	0	-66	-4424
14	B3W10H10ST10WT10H1C4	-716	-695	-168	-5170	1021	961	232	4200	-859	-849	-205	-3417	-311	-274	-66	-4040
15	B3W10H10ST10WT10H2C4	-715	-1390	-168	-4708	1021	1923	232	3973	-859	-1699	-205	-3284	-315	-554	-67	-3624
16	B3W11H11ST10.5WT11H0C4	-915	0	-204	-6161	1322	0	287	5104	-1098	0	-249	-4514	-404	0	-82	-4520
17	B3W11H11ST10.5WT11H1C4	-916	-846	-204	-5787	1323	1187	287	4983	-1098	-1032	-249	-4516	-405	-342	-83	-4150
18	B3W11H11ST10.5WT11H2C4	-918	-1696	-205	-5456	1323	2373	287	4767	-1098	-2064	-249	-4486	-405	-684	-83	-3905
19	B3W12H12ST11WT12H0C4	-1146	0	-244	-6889	1675	0	347	5860	-1376	0	-298	-5549	-514	0	-101	-4953
20	B3W12H12ST11WT12H1C4	-1149	-1013	-245	-6559	1675	1436	347	5744	-1376	-1232	-298	-5487	-515	-418	-101	-4668
21	B3W12H12ST11WT12H2C4	-1150	-2027	-245	-6228	1675	2873	347	5543	-1376	-2464	-298	-5426	-515	-837	-101	-4436

Units: lb.-in./in. for bending moment

Table E10. Bending moment and shear force values (2D model; Proposed formula with rigid joints; 1-barrel culverts)

#	Case	NLS	V_L^{DC}	V_L^{EF}	V_L^{DW}	V_L^{LL}	M_{pE}^{DC}	M_{pE}^{EF}	M_{pE}^{DW}	M_{pE}^{LL}
1	B1W6H6ST7WT6H0C3	17	-18.2	0.0	-6.0	-243	-273	0	-90.6	-3834
2	B1W6H6ST7WT6H1C3	14	-18.2	-25.0	-6.0	-188	-273	-375	-90.6	-3020
3	B1W6H6ST7WT6H2C3	9	-18.2	-50.0	-6.0	-141	-273	-750	-90.6	-2328
4	B1W6H6ST8WT6H0C3	17	-20.8	0.0	-6.0	-243	-313	0	-90.6	-3834
5	B1W6H6ST8WT6H1C3	14	-20.8	-25.0	-6.0	-188	-313	-375	-90.6	-3020
6	B1W6H6ST8WT6H2C3	9	-20.8	-50.0	-6.0	-141	-313	-750	-90.6	-2328
7	B1W6H6ST9WT6H0C3	17	-23.4	0.0	-6.0	-243	-352	0	-90.6	-3834
8	B1W6H6ST9WT6H1C3	14	-23.4	-25.0	-6.0	-188	-352	-375	-90.6	-3020
9	B1W6H6ST9WT6H2C3	9	-23.4	-50.0	-6.0	-141	-352	-750	-90.6	-2328
10	B1W6H6ST7WT6H0C4	17	-18.2	0.0	-6.0	-243	-273	0	-90.6	-3834
11	B1W6H6ST7WT6H1C4	14	-18.2	-25.0	-6.0	-188	-273	-375	-90.6	-3020
12	B1W6H6ST7WT6H2C4	9	-18.2	-50.0	-6.0	-141	-273	-750	-90.6	-2328
13	B1W6H6ST8WT6H0C4	17	-20.8	0.0	-6.0	-243	-313	0	-90.6	-3834
14	B1W6H6ST8WT6H1C4	14	-20.8	-25.0	-6.0	-188	-313	-375	-90.6	-3020
15	B1W6H6ST8WT6H2C4	9	-20.8	-50.0	-6.0	-141	-313	-750	-90.6	-2328
16	B1W6H6ST9WT6H0C4	17	-23.4	0.0	-6.0	-243	-352	0	-90.6	-3834
17	B1W6H6ST9WT6H1C4	14	-23.4	-25.0	-6.0	-188	-352	-375	-90.6	-3020
18	B1W6H6ST9WT6H2C4	9	-23.4	-50.0	-6.0	-141	-352	-750	-90.6	-2328
19	B1W6H6ST7WT6H0C5	17	-18.2	0.0	-6.0	-243	-273	0	-90.6	-3834
20	B1W6H6ST7WT6H1C5	14	-18.2	-25.0	-6.0	-188	-273	-375	-90.6	-3020
21	B1W6H6ST7WT6H2C5	9	-18.2	-50.0	-6.0	-141	-273	-750	-90.6	-2328
22	B1W6H6ST8WT6H0C5	17	-20.8	0.0	-6.0	-243	-313	0	-90.6	-3834
23	B1W6H6ST8WT6H1C5	14	-20.8	-25.0	-6.0	-188	-313	-375	-90.6	-3020
24	B1W6H6ST8WT6H2C5	9	-20.8	-50.0	-6.0	-141	-313	-750	-90.6	-2328
25	B1W6H6ST9WT6H0C5	17	-23.4	0.0	-6.0	-243	-352	0	-90.6	-3834
26	B1W6H6ST9WT6H1C5	14	-23.4	-25.0	-6.0	-188	-352	-375	-90.6	-3020
27	B1W6H6ST9WT6H2C5	9	-23.4	-50.0	-6.0	-141	-352	-750	-90.6	-2328

Units: lb./in. for shear; lb.-in./in. for bending moment

#	Case	NLS	V_L^{DC}	V_L^{EF}	V_L^{DW}	V_L^{LL}	M_{pE}^{DC}	M_{pE}^{EF}	M_{pE}^{DW}	M_{pE}^{LL}
28	B1W7H7ST7.5WT7H0C3	24	-23.1	0.0	-7.1	-245	-410	0	-126.9	-4467
29	B1W7H7ST7.5WT7H1C3	18	-23.1	-29.6	-7.1	-194	-410	-525	-126.9	-3609
30	B1W7H7ST7.5WT7H2C3	13	-23.1	-59.2	-7.1	-151	-410	-1050	-126.9	-2878
31	B1W7H7ST8.5WT7H0C3	24	-26.2	0.0	-7.1	-245	-465	0	-126.9	-4467
32	B1W7H7ST8.5WT7H1C3	18	-26.2	-29.6	-7.1	-194	-465	-525	-126.9	-3609
33	B1W7H7ST8.5WT7H2C3	13	-26.2	-59.2	-7.1	-151	-465	-1050	-126.9	-2878
34	B1W7H7ST9.5WT7H0C3	24	-29.3	0.0	-7.1	-245	-520	0	-126.9	-4467
35	B1W7H7ST9.5WT7H1C3	18	-29.3	-29.6	-7.1	-194	-520	-525	-126.9	-3609
36	B1W7H7ST9.5WT7H2C3	13	-29.3	-59.2	-7.1	-151	-520	-1050	-126.9	-2878
37	B1W7H7ST7.5WT7H0C4	24	-23.1	0.0	-7.1	-245	-410	0	-126.9	-4467
38	B1W7H7ST7.5WT7H1C4	18	-23.1	-29.6	-7.1	-194	-410	-525	-126.9	-3609
39	B1W7H7ST7.5WT7H2C4	13	-23.1	-59.2	-7.1	-151	-410	-1050	-126.9	-2878
40	B1W7H7ST8.5WT7H0C4	24	-26.2	0.0	-7.1	-245	-465	0	-126.9	-4467
41	B1W7H7ST8.5WT7H1C4	18	-26.2	-29.6	-7.1	-194	-465	-525	-126.9	-3609
42	B1W7H7ST8.5WT7H2C4	13	-26.2	-59.2	-7.1	-151	-465	-1050	-126.9	-2878
43	B1W7H7ST9.5WT7H0C4	24	-29.3	0.0	-7.1	-245	-520	0	-126.9	-4467
44	B1W7H7ST9.5WT7H1C4	18	-29.3	-29.6	-7.1	-194	-520	-525	-126.9	-3609
45	B1W7H7ST9.5WT7H2C4	13	-29.3	-59.2	-7.1	-151	-520	-1050	-126.9	-2878
46	B1W7H7ST7.5WT7H0C5	24	-23.1	0.0	-7.1	-245	-410	0	-126.9	-4467
47	B1W7H7ST7.5WT7H1C5	18	-23.1	-29.6	-7.1	-194	-410	-525	-126.9	-3609
48	B1W7H7ST7.5WT7H2C5	13	-23.1	-59.2	-7.1	-151	-410	-1050	-126.9	-2878
49	B1W7H7ST8.5WT7H0C5	24	-26.2	0.0	-7.1	-245	-465	0	-126.9	-4467
50	B1W7H7ST8.5WT7H1C5	18	-26.2	-29.6	-7.1	-194	-465	-525	-126.9	-3609
51	B1W7H7ST8.5WT7H2C5	13	-26.2	-59.2	-7.1	-151	-465	-1050	-126.9	-2878
52	B1W7H7ST9.5WT7H0C5	24	-29.3	0.0	-7.1	-245	-520	0	-126.9	-4467
53	B1W7H7ST9.5WT7H1C5	18	-29.3	-29.6	-7.1	-194	-520	-525	-126.9	-3609
54	B1W7H7ST9.5WT7H2C5	13	-29.3	-59.2	-7.1	-151	-520	-1050	-126.9	-2878

Units: lb./in. for shear; lb.-in./in. for bending moment

#	Case	NLS	V_L^{DC}	V_L^{EF}	V_L^{DW}	V_L^{LL}	M_{pE}^{DC}	M_{pE}^{EF}	M_{pE}^{DW}	M_{pE}^{LL}
55	B1W8H8ST8WT8H0C3	27	-28.5	0.0	-8.3	-249	-584	0	-169.3	-5063
56	B1W8H8ST8WT8H1C3	24	-28.5	-34.2	-8.3	-199	-584	-700	-169.3	-4166
57	B1W8H8ST8WT8H2C3	17	-28.5	-68.3	-8.3	-157	-584	-1401	-169.3	-3401
58	B1W8H8ST9WT8H0C3	27	-32.0	0.0	-8.3	-249	-657	0	-169.3	-5063
59	B1W8H8ST9WT8H1C3	24	-32.0	-34.2	-8.3	-199	-657	-700	-169.3	-4166
60	B1W8H8ST9WT8H2C3	17	-32.0	-68.3	-8.3	-157	-657	-1401	-169.3	-3401
61	B1W8H8ST10WT8H0C3	27	-35.6	0.0	-8.3	-249	-730	0	-169.3	-5063
62	B1W8H8ST10WT8H1C3	24	-35.6	-34.2	-8.3	-199	-730	-700	-169.3	-4166
63	B1W8H8ST10WT8H2C3	17	-35.6	-68.3	-8.3	-157	-730	-1401	-169.3	-3401
64	B1W8H8ST8WT8H0C4	27	-28.5	0.0	-8.3	-249	-584	0	-169.3	-5063
65	B1W8H8ST8WT8H1C4	24	-28.5	-34.2	-8.3	-199	-584	-700	-169.3	-4166
66	B1W8H8ST8WT8H2C4	17	-28.5	-68.3	-8.3	-157	-584	-1401	-169.3	-3401
67	B1W8H8ST9WT8H0C4	27	-32.0	0.0	-8.3	-249	-657	0	-169.3	-5063
68	B1W8H8ST9WT8H1C4	24	-32.0	-34.2	-8.3	-199	-657	-700	-169.3	-4166
69	B1W8H8ST9WT8H2C4	17	-32.0	-68.3	-8.3	-157	-657	-1401	-169.3	-3401
70	B1W8H8ST10WT8H0C4	27	-35.6	0.0	-8.3	-249	-730	0	-169.3	-5063
71	B1W8H8ST10WT8H1C4	24	-35.6	-34.2	-8.3	-199	-730	-700	-169.3	-4166
72	B1W8H8ST10WT8H2C4	17	-35.6	-68.3	-8.3	-157	-730	-1401	-169.3	-3401
73	B1W8H8ST8WT8H0C5	27	-28.5	0.0	-8.3	-249	-584	0	-169.3	-5063
74	B1W8H8ST8WT8H1C5	24	-28.5	-34.2	-8.3	-199	-584	-700	-169.3	-4166
75	B1W8H8ST8WT8H2C5	17	-28.5	-68.3	-8.3	-157	-584	-1401	-169.3	-3401
76	B1W8H8ST9WT8H0C5	27	-32.0	0.0	-8.3	-249	-657	0	-169.3	-5063
77	B1W8H8ST9WT8H1C5	24	-32.0	-34.2	-8.3	-199	-657	-700	-169.3	-4166
78	B1W8H8ST9WT8H2C5	17	-32.0	-68.3	-8.3	-157	-657	-1401	-169.3	-3401
79	B1W8H8ST10WT8H0C5	27	-35.6	0.0	-8.3	-249	-730	0	-169.3	-5063
80	B1W8H8ST10WT8H1C5	24	-35.6	-34.2	-8.3	-199	-730	-700	-169.3	-4166
81	B1W8H8ST10WT8H2C5	17	-35.6	-68.3	-8.3	-157	-730	-1401	-169.3	-3401

Units: lb./in. for shear; lb.-in./in. for bending moment

#	Case	NLS	V_L^{DC}	V_L^{EF}	V_L^{DW}	V_L^{LL}	M_{pE}^{DC}	M_{pE}^{EF}	M_{pE}^{DW}	M_{pE}^{LL}
82	B1W9H9ST8.5WT9H0C3	35	-34.3	0.0	-9.4	-266	-798	0	-217.7	-5623
83	B1W9H9ST8.5WT9H1C3	32	-34.3	-38.8	-9.4	-216	-798	-901	-217.7	-4695
84	B1W9H9ST8.5WT9H2C3	21	-34.3	-77.5	-9.4	-161	-798	-1802	-217.7	-3899
85	B1W9H9ST9.5WT9H0C3	35	-38.3	0.0	-9.4	-266	-892	0	-217.7	-5623
86	B1W9H9ST9.5WT9H1C3	32	-38.3	-38.8	-9.4	-216	-892	-901	-217.7	-4695
87	B1W9H9ST9.5WT9H2C3	21	-38.3	-77.5	-9.4	-161	-892	-1802	-217.7	-3899
88	B1W9H9ST10.5WT9H0C3	35	-42.4	0.0	-9.4	-266	-985	0	-217.7	-5623
89	B1W9H9ST10.5WT9H1C3	32	-42.4	-38.8	-9.4	-216	-985	-901	-217.7	-4695
90	B1W9H9ST10.5WT9H2C3	21	-42.4	-77.5	-9.4	-161	-985	-1802	-217.7	-3899
91	B1W9H9ST8.5WT9H0C4	35	-34.3	0.0	-9.4	-266	-798	0	-217.7	-5623
92	B1W9H9ST8.5WT9H1C4	32	-34.3	-38.8	-9.4	-216	-798	-901	-217.7	-4695
93	B1W9H9ST8.5WT9H2C4	21	-34.3	-77.5	-9.4	-161	-798	-1802	-217.7	-3899
94	B1W9H9ST9.5WT9H0C4	35	-38.3	0.0	-9.4	-266	-892	0	-217.7	-5623
95	B1W9H9ST9.5WT9H1C4	32	-38.3	-38.8	-9.4	-216	-892	-901	-217.7	-4695
96	B1W9H9ST9.5WT9H2C4	21	-38.3	-77.5	-9.4	-161	-892	-1802	-217.7	-3899
97	B1W9H9ST10.5WT9H0C4	35	-42.4	0.0	-9.4	-266	-985	0	-217.7	-5623
98	B1W9H9ST10.5WT9H1C4	32	-42.4	-38.8	-9.4	-216	-985	-901	-217.7	-4695
99	B1W9H9ST10.5WT9H2C4	21	-42.4	-77.5	-9.4	-161	-985	-1802	-217.7	-3899
100	B1W9H9ST8.5WT9H0C5	35	-34.3	0.0	-9.4	-266	-798	0	-217.7	-5623
101	B1W9H9ST8.5WT9H1C5	32	-34.3	-38.8	-9.4	-216	-798	-901	-217.7	-4695
102	B1W9H9ST8.5WT9H2C5	21	-34.3	-77.5	-9.4	-161	-798	-1802	-217.7	-3899
103	B1W9H9ST9.5WT9H0C5	35	-38.3	0.0	-9.4	-266	-892	0	-217.7	-5623
104	B1W9H9ST9.5WT9H1C5	32	-38.3	-38.8	-9.4	-216	-892	-901	-217.7	-4695
105	B1W9H9ST9.5WT9H2C5	21	-38.3	-77.5	-9.4	-161	-892	-1802	-217.7	-3899
106	B1W9H9ST10.5WT9H0C5	35	-42.4	0.0	-9.4	-266	-985	0	-217.7	-5623
107	B1W9H9ST10.5WT9H1C5	32	-42.4	-38.8	-9.4	-216	-985	-901	-217.7	-4695
108	B1W9H9ST10.5WT9H2C5	21	-42.4	-77.5	-9.4	-161	-985	-1802	-217.7	-3899

Units: lb./in. for shear; lb.-in./in. for bending moment

#	Case	NLS	V_L^{DC}	V_L^{EF}	V_L^{DW}	V_L^{LL}	M_{pE}^{DC}	M_{pE}^{EF}	M_{pE}^{DW}	M_{pE}^{LL}
109	B1W10H10ST9WT10H0C3	44	-40.6	0.0	-10.5	-277	-1056	0	-272.3	-6153
110	B1W10H10ST9WT10H1C3	35	-40.6	-43.3	-10.5	-217	-1056	-1127	-272.3	-5196
111	B1W10H10ST9WT10H2C3	29	-40.6	-86.7	-10.5	-179	-1043	-2225	-268.9	-4439
112	B1W10H10ST10WT10H0C3	44	-45.1	0.0	-10.5	-277	-1174	0	-272.3	-6153
113	B1W10H10ST10WT10H1C3	35	-45.1	-43.3	-10.5	-217	-1174	-1127	-272.3	-5196
114	B1W10H10ST10WT10H2C3	29	-45.1	-86.7	-10.5	-179	-1159	-2225	-268.9	-4439
115	B1W10H10ST11WT10H0C3	44	-49.7	0.0	-10.5	-277	-1291	0	-272.3	-6153
116	B1W10H10ST11WT10H1C3	35	-49.7	-43.3	-10.5	-217	-1291	-1127	-272.3	-5196
117	B1W10H10ST11WT10H2C3	29	-49.7	-86.7	-10.5	-179	-1287	-2246	-271.4	-4439
118	B1W10H10ST9WT10H0C4	44	-40.6	0.0	-10.5	-277	-1056	0	-272.3	-6153
119	B1W10H10ST9WT10H1C4	35	-40.6	-43.3	-10.5	-217	-1056	-1127	-272.3	-5196
120	B1W10H10ST9WT10H2C4	29	-40.6	-86.7	-10.5	-179	-1043	-2225	-268.9	-4439
121	B1W10H10ST10WT10H0C4	44	-45.1	0.0	-10.5	-277	-1174	0	-272.3	-6153
122	B1W10H10ST10WT10H1C4	35	-45.1	-43.3	-10.5	-217	-1174	-1127	-272.3	-5196
123	B1W10H10ST10WT10H2C4	29	-45.1	-86.7	-10.5	-179	-1159	-2225	-268.9	-4439
124	B1W10H10ST11WT10H0C4	44	-49.7	0.0	-10.5	-277	-1291	0	-272.3	-6153
125	B1W10H10ST11WT10H1C4	35	-49.7	-43.3	-10.5	-217	-1291	-1127	-272.3	-5196
126	B1W10H10ST11WT10H2C4	29	-49.7	-86.7	-10.5	-179	-1287	-2246	-271.4	-4439
127	B1W10H10ST9WT10H0C5	44	-40.6	0.0	-10.5	-277	-1056	0	-272.3	-6153
128	B1W10H10ST9WT10H1C5	35	-40.6	-43.3	-10.5	-217	-1056	-1127	-272.3	-5196
129	B1W10H10ST9WT10H2C5	29	-40.6	-86.7	-10.5	-179	-1043	-2225	-268.9	-4439
130	B1W10H10ST10WT10H0C5	44	-45.1	0.0	-10.5	-277	-1174	0	-272.3	-6153
131	B1W10H10ST10WT10H1C5	35	-45.1	-43.3	-10.5	-217	-1174	-1127	-272.3	-5196
132	B1W10H10ST10WT10H2C5	29	-45.1	-86.7	-10.5	-179	-1159	-2225	-268.9	-4439
133	B1W10H10ST11WT10H0C5	44	-49.7	0.0	-10.5	-277	-1291	0	-272.3	-6153
134	B1W10H10ST11WT10H1C5	35	-49.7	-43.3	-10.5	-217	-1291	-1127	-272.3	-5196
135	B1W10H10ST11WT10H2C5	29	-49.7	-86.7	-10.5	-179	-1287	-2246	-271.4	-4439

Units: lb./in. for shear; lb.-in./in. for bending moment

#	Case	NLS	V_L^{DC}	V_L^{EF}	V_L^{DW}	V_L^{LL}	M_{pE}^{DC}	M_{pE}^{EF}	M_{pE}^{DW}	M_{pE}^{LL}
136	B1W11H11ST9.5WT11H0C3	47	-47.4	0.0	-11.6	-273	-1322	0	-322.9	-6771
137	B1W11H11ST9.5WT11H1C3	43	-47.4	-47.9	-11.6	-225	-1349	-1363	-329.4	-5921
138	B1W11H11ST9.5WT11H2C3	37	-47.4	-95.8	-11.6	-189	-1360	-2748	-332.1	-5197
139	B1W11H11ST10.5WT11H0C3	47	-52.4	0.0	-11.6	-273	-1461	0	-322.9	-6771
140	B1W11H11ST10.5WT11H1C3	43	-52.4	-47.9	-11.6	-225	-1491	-1363	-329.4	-5921
141	B1W11H11ST10.5WT11H2C3	37	-52.4	-95.8	-11.6	-189	-1503	-2748	-332.1	-5197
142	B1W11H11ST11.5WT11H0C3	47	-57.4	0.0	-11.6	-273	-1600	0	-322.9	-6771
143	B1W11H11ST11.5WT11H1C3	43	-57.4	-47.9	-11.6	-225	-1610	-1344	-324.9	-5921
144	B1W11H11ST11.5WT11H2C3	37	-57.4	-95.8	-11.6	-189	-1634	-2727	-329.6	-5197
145	B1W11H11ST9.5WT11H0C4	47	-47.4	0.0	-11.6	-273	-1322	0	-322.9	-6771
146	B1W11H11ST9.5WT11H1C4	43	-47.4	-47.9	-11.6	-225	-1349	-1363	-329.4	-5921
147	B1W11H11ST9.5WT11H2C4	37	-47.4	-95.8	-11.6	-189	-1360	-2748	-332.1	-5197
148	B1W11H11ST10.5WT11H0C4	47	-52.4	0.0	-11.6	-273	-1461	0	-322.9	-6771
149	B1W11H11ST10.5WT11H1C4	43	-52.4	-47.9	-11.6	-225	-1491	-1363	-329.4	-5921
150	B1W11H11ST10.5WT11H2C4	37	-52.4	-95.8	-11.6	-189	-1503	-2748	-332.1	-5197
151	B1W11H11ST11.5WT11H0C4	47	-57.4	0.0	-11.6	-273	-1600	0	-322.9	-6771
152	B1W11H11ST11.5WT11H1C4	43	-57.4	-47.9	-11.6	-225	-1610	-1344	-324.9	-5921
153	B1W11H11ST11.5WT11H2C4	37	-57.4	-95.8	-11.6	-189	-1634	-2727	-329.6	-5197
154	B1W11H11ST9.5WT11H0C5	47	-47.4	0.0	-11.6	-273	-1322	0	-322.9	-6771
155	B1W11H11ST9.5WT11H1C5	43	-47.4	-47.9	-11.6	-225	-1349	-1363	-329.4	-5921
156	B1W11H11ST9.5WT11H2C5	37	-47.4	-95.8	-11.6	-189	-1360	-2748	-332.1	-5197
157	B1W11H11ST10.5WT11H0C5	47	-52.4	0.0	-11.6	-273	-1461	0	-322.9	-6771
158	B1W11H11ST10.5WT11H1C5	43	-52.4	-47.9	-11.6	-225	-1491	-1363	-329.4	-5921
159	B1W11H11ST10.5WT11H2C5	37	-52.4	-95.8	-11.6	-189	-1503	-2748	-332.1	-5197
160	B1W11H11ST11.5WT11H0C5	47	-57.4	0.0	-11.6	-273	-1600	0	-322.9	-6771
161	B1W11H11ST11.5WT11H1C5	43	-57.4	-47.9	-11.6	-225	-1610	-1344	-324.9	-5921
162	B1W11H11ST11.5WT11H2C5	37	-57.4	-95.8	-11.6	-189	-1634	-2727	-329.6	-5197

Units: lb./in. for shear; lb.-in./in. for bending moment

#	Case	NLS	V_L^{DC}	V_L^{EF}	V_L^{DW}	V_L^{LL}	M_{pE}^{DC}	M_{pE}^{EF}	M_{pE}^{DW}	M_{pE}^{LL}
163	B1W12H12ST10WT12H0C3	55	-54.7	0.0	-12.7	-278	-1679	0	-389.6	-7579
164	B1W12H12ST10WT12H1C3	51	-54.7	-52.5	-12.7	-231	-1707	-1639	-396.1	-6687
165	B1W12H12ST10WT12H2C3	45	-54.7	-105.0	-12.7	-196	-1719	-3301	-398.8	-5923
166	B1W12H12ST11WT12H0C3	55	-60.2	0.0	-12.7	-278	-1847	0	-389.6	-7579
167	B1W12H12ST11WT12H1C3	51	-60.2	-52.5	-12.7	-231	-1857	-1621	-391.6	-6687
168	B1W12H12ST11WT12H2C3	45	-60.2	-105.0	-12.7	-196	-1879	-3280	-396.3	-5923
169	B1W12H12ST12WT12H0C3	55	-65.6	0.0	-12.7	-278	-2015	0	-389.6	-7579
170	B1W12H12ST12WT12H1C3	51	-65.6	-52.5	-12.7	-231	-2049	-1639	-396.1	-6687
171	B1W12H12ST12WT12H2C3	45	-65.6	-105.0	-12.7	-196	-2063	-3301	-398.8	-5923
172	B1W12H12ST10WT12H0C4	55	-54.7	0.0	-12.7	-278	-1679	0	-389.6	-7579
173	B1W12H12ST10WT12H1C4	51	-54.7	-52.5	-12.7	-231	-1707	-1639	-396.1	-6687
174	B1W12H12ST10WT12H2C4	45	-54.7	-105.0	-12.7	-196	-1719	-3301	-398.8	-5923
175	B1W12H12ST11WT12H0C4	55	-60.2	0.0	-12.7	-278	-1847	0	-389.6	-7579
176	B1W12H12ST11WT12H1C4	51	-60.2	-52.5	-12.7	-231	-1857	-1621	-391.6	-6687
177	B1W12H12ST11WT12H2C4	45	-60.2	-105.0	-12.7	-196	-1879	-3280	-396.3	-5923
178	B1W12H12ST12WT12H0C4	55	-65.6	0.0	-12.7	-278	-2015	0	-389.6	-7579
179	B1W12H12ST12WT12H1C4	51	-65.6	-52.5	-12.7	-231	-2049	-1639	-396.1	-6687
180	B1W12H12ST12WT12H2C4	45	-65.6	-105.0	-12.7	-196	-2063	-3301	-398.8	-5923
181	B1W12H12ST10WT12H0C5	55	-54.7	0.0	-12.7	-278	-1679	0	-389.6	-7579
182	B1W12H12ST10WT12H1C5	51	-54.7	-52.5	-12.7	-231	-1707	-1639	-396.1	-6687
183	B1W12H12ST10WT12H2C5	45	-54.7	-105.0	-12.7	-196	-1719	-3301	-398.8	-5923
184	B1W12H12ST11WT12H0C5	55	-60.2	0.0	-12.7	-278	-1847	0	-389.6	-7579
185	B1W12H12ST11WT12H1C5	51	-60.2	-52.5	-12.7	-231	-1857	-1621	-391.6	-6687
186	B1W12H12ST11WT12H2C5	45	-60.2	-105.0	-12.7	-196	-1879	-3280	-396.3	-5923
187	B1W12H12ST12WT12H0C5	55	-65.6	0.0	-12.7	-278	-2015	0	-389.6	-7579
188	B1W12H12ST12WT12H1C5	51	-65.6	-52.5	-12.7	-231	-2049	-1639	-396.1	-6687
189	B1W12H12ST12WT12H2C5	45	-65.6	-105.0	-12.7	-196	-2063	-3301	-398.8	-5923

Units: lb./in. for shear; lb.-in./in. for bending moment

Table E11. Bending moment and shear force values (2D model; Proposed formula with rigid joints; 2-barrel culverts)

#	Case	NLS	V_L^{DC}	V_L^{EF}	V_L^{DW}	V_L^{LL}	V_R^{DC}	V_R^{EF}	V_R^{DW}	V_R^{LL}
1	B2W6H6ST7WT6H0C4	43	-22.6	0.0	-7.5	-250.1	-22.6	0.0	-7.5	-250.1
2	B2W6H6ST7WT6H1C4	34	-22.6	-31.2	-7.5	-202.4	-22.6	-31.2	-7.5	-202.4
3	B2W6H6ST7WT6H2C4	19	-22.6	-62.4	-7.5	-157.1	-22.6	-62.4	-7.5	-157.1
4	B2W6H6ST8WT6H0C4	43	-25.8	0.0	-7.5	-248.8	-25.8	0.0	-7.5	-248.8
5	B2W6H6ST8WT6H1C4	34	-25.8	-31.2	-7.5	-201.2	-25.8	-31.2	-7.5	-201.2
6	B2W6H6ST8WT6H2C4	19	-25.8	-62.4	-7.5	-156.2	-25.8	-62.4	-7.5	-156.2
7	B2W6H6ST9WT6H0C4	43	-29.0	0.0	-7.5	-247.7	-29.0	0.0	-7.5	-247.7
8	B2W6H6ST9WT6H1C4	34	-29.0	-31.2	-7.5	-200.2	-29.0	-31.2	-7.5	-200.2
9	B2W6H6ST9WT6H2C4	19	-29.0	-62.3	-7.5	-155.5	-29.0	-62.3	-7.5	-155.5
10	B2W7H7ST7.5WT7H0C4	58	-28.7	0.0	-8.9	-262.5	-28.7	0.0	-8.9	-262.5
11	B2W7H7ST7.5WT7H1C4	46	-28.7	-36.9	-8.9	-206.5	-28.7	-36.9	-8.9	-206.5
12	B2W7H7ST7.5WT7H2C4	31	-28.7	-73.8	-8.9	-166.8	-28.7	-73.8	-8.9	-166.8
13	B2W7H7ST8.5WT7H0C4	58	-32.5	0.0	-8.9	-261.5	-32.5	0.0	-8.9	-261.5
14	B2W7H7ST8.5WT7H1C4	46	-32.5	-36.9	-8.9	-205.4	-32.5	-36.9	-8.9	-205.4
15	B2W7H7ST8.5WT7H2C4	31	-32.5	-73.8	-8.9	-165.8	-32.5	-73.8	-8.9	-165.8
16	B2W7H7ST9.5WT7H0C4	58	-36.3	0.0	-8.9	-260.7	-36.3	0.0	-8.9	-260.7
17	B2W7H7ST9.5WT7H1C4	46	-36.3	-36.9	-8.9	-204.5	-36.3	-36.9	-8.9	-204.5
18	B2W7H7ST9.5WT7H2C4	31	-36.3	-73.7	-8.9	-165.0	-36.3	-73.7	-8.9	-165.0
19	B2W8H8ST8WT8H0C4	65	-35.4	0.0	-10.3	-272.4	-35.4	0.0	-10.3	-272.4
20	B2W8H8ST8WT8H1C4	60	-35.4	-42.6	-10.3	-221.5	-35.4	-42.6	-10.3	-221.5
21	B2W8H8ST8WT8H2C4	43	-35.4	-85.3	-10.3	-172.2	-35.4	-85.3	-10.3	-172.2
22	B2W8H8ST9WT8H0C4	65	-39.8	0.0	-10.3	-271.1	-39.8	0.0	-10.3	-271.1
23	B2W8H8ST9WT8H1C4	60	-39.8	-42.6	-10.3	-220.5	-39.8	-42.6	-10.3	-220.5
24	B2W8H8ST9WT8H2C4	43	-39.8	-85.2	-10.3	-171.2	-39.8	-85.2	-10.3	-171.2
25	B2W8H8ST10WT8H0C4	65	-44.1	0.0	-10.3	-270.1	-44.1	0.0	-10.3	-270.1
26	B2W8H8ST10WT8H1C4	60	-44.1	-42.6	-10.3	-219.6	-44.1	-42.6	-10.3	-219.6
27	B2W8H8ST10WT8H2C4	43	-44.1	-85.2	-10.3	-170.4	-44.1	-85.2	-10.3	-170.4

Units: lb./in. for shear

#	Case	M_{pE}^{DC}	M_{pE}^{EF}	M_{pE}^{DW}	M_{pE}^{LL}	M_{nL}^{DC}	M_{nL}^{EF}	M_{nL}^{DW}	M_{nL}^{LL}	M_{nR}^{DC}	M_{nR}^{EF}	M_{nR}^{DW}	M_{nR}^{LL}
1	B2W6H6ST7WT6H0C4	-153	0	-49	-3096	264	0	90	2315	-264	0	-90	-2315
2	B2W6H6ST7WT6H1C4	-152	-203	-49	-2371	264	373	90	1923	-264	-373	-90	-1865
3	B2W6H6ST7WT6H2C4	-152	-406	-49	-1802	264	746	90	1129	-264	-746	-90	-1129
4	B2W6H6ST8WT6H0C4	-175	0	-50	-3121	300	0	90	2276	-300	0	-90	-2276
5	B2W6H6ST8WT6H1C4	-174	-204	-49	-2390	300	372	90	1890	-300	-372	-90	-1832
6	B2W6H6ST8WT6H2C4	-174	-407	-49	-1820	300	743	90	1156	-300	-743	-90	-1156
7	B2W6H6ST9WT6H0C4	-198	0	-50	-3139	335	0	89	2230	-335	0	-89	-2230
8	B2W6H6ST9WT6H1C4	-197	-205	-49	-2404	335	370	89	1850	-335	-370	-89	-1793
9	B2W6H6ST9WT6H2C4	-197	-409	-49	-1832	335	740	89	1166	-335	-740	-89	-1166
10	B2W7H7ST7.5WT7H0C4	-226	0	-69	-3583	398	0	126	2400	-398	0	-126	-2400
11	B2W7H7ST7.5WT7H1C4	-225	-283	-68	-2826	398	521	126	2058	-398	-521	-126	-1993
12	B2W7H7ST7.5WT7H2C4	-225	-565	-68	-2219	398	1042	126	1405	-398	-1042	-126	-1405
13	B2W7H7ST8.5WT7H0C4	-258	0	-69	-3616	448	0	125	2354	-448	0	-125	-2354
14	B2W7H7ST8.5WT7H1C4	-257	-284	-69	-2854	448	519	126	2023	-448	-519	-126	-1962
15	B2W7H7ST8.5WT7H2C4	-256	-566	-68	-2245	448	1039	126	1351	-448	-1039	-126	-1351
16	B2W7H7ST9.5WT7H0C4	-290	0	-69	-3641	497	0	125	2307	-497	0	-125	-2307
17	B2W7H7ST9.5WT7H1C4	-288	-285	-69	-2875	497	517	125	1983	-497	-517	-125	-1925
18	B2W7H7ST9.5WT7H2C4	-288	-568	-69	-2263	497	1034	125	1375	-497	-1034	-125	-1375
19	B2W8H8ST8WT8H0C4	-331	0	-95	-4050	568	0	168	2551	-568	0	-168	-2551
20	B2W8H8ST8WT8H1C4	-329	-389	-94	-3260	568	695	168	2129	-568	-695	-168	-2055
21	B2W8H8ST8WT8H2C4	-328	-776	-94	-2624	568	1390	168	1677	-568	-1390	-168	-1677
22	B2W8H8ST9WT8H0C4	-373	0	-95	-4085	635	0	167	2507	-635	0	-167	-2507
23	B2W8H8ST9WT8H1C4	-371	-390	-94	-3289	635	693	167	2094	-635	-693	-167	-2027
24	B2W8H8ST9WT8H2C4	-371	-778	-94	-2651	635	1385	167	1607	-635	-1385	-167	-1607
25	B2W8H8ST10WT8H0C4	-417	0	-95	-4110	701	0	167	2461	-701	0	-167	-2461
26	B2W8H8ST10WT8H1C4	-401	-377	-91	-3312	701	690	167	2056	-701	-690	-167	-1993
27	B2W8H8ST10WT8H2C4	-414	-780	-94	-2672	701	1380	167	1556	-701	-1380	-167	-1556

Units: lb.-in./in. for bending moment

#	Case	NLS	V_L^{DC}	V_L^{EF}	V_L^{DW}	V_L^{LL}	V_R^{DC}	V_R^{EF}	V_R^{DW}	V_R^{LL}
28	B2W9H9ST8.5WT9H0C4	81	-42.7	0.0	-11.7	-289.5	-42.7	0.0	-11.7	-289.5
29	B2W9H9ST8.5WT9H1C4	76	-42.7	-48.4	-11.7	-239.4	-42.7	-48.4	-11.7	-239.4
30	B2W9H9ST8.5WT9H2C4	55	-42.7	-96.7	-11.7	-174.8	-42.7	-96.7	-11.7	-184.3
31	B2W9H9ST9.5WT9H0C4	81	-47.6	0.0	-11.7	-288.0	-47.6	0.0	-11.7	-288.0
32	B2W9H9ST9.5WT9H1C4	76	-47.7	-48.3	-11.7	-238.1	-47.7	-48.3	-11.7	-238.1
33	B2W9H9ST9.5WT9H2C4	55	-47.7	-96.7	-11.7	-173.9	-47.7	-96.7	-11.7	-183.3
34	B2W9H9ST10.5WT9H0C4	81	-52.6	0.0	-11.7	-286.8	-52.6	0.0	-11.7	-286.8
35	B2W9H9ST10.5WT9H1C4	76	-52.6	-48.3	-11.7	-237.1	-52.6	-48.3	-11.7	-237.1
36	B2W9H9ST10.5WT9H2C4	55	-52.6	-96.6	-11.7	-173.1	-52.6	-96.6	-11.7	-182.6
37	B2W10H10ST9WT10H0C4	98	-50.6	0.0	-13.1	-299.7	-50.6	0.0	-13.1	-299.7
38	B2W10H10ST9WT10H1C4	83	-50.6	-54.1	-13.1	-242.5	-50.6	-54.1	-13.1	-242.5
39	B2W10H10ST9WT10H2C4	71	-50.6	-108.2	-13.1	-202.5	-50.6	-108.2	-13.1	-202.5
40	B2W10H10ST10WT10H0C4	98	-56.1	0.0	-13.1	-298.2	-56.1	0.0	-13.1	-298.2
41	B2W10H10ST10WT10H1C4	83	-56.1	-54.1	-13.1	-241.2	-56.1	-54.1	-13.1	-241.2
42	B2W10H10ST10WT10H2C4	71	-56.1	-108.1	-13.1	-201.3	-56.1	-108.1	-13.1	-201.3
43	B2W10H10ST11WT10H0C4	98	-61.7	0.0	-13.1	-297.0	-61.7	0.0	-13.1	-297.0
44	B2W10H10ST11WT10H1C4	83	-61.7	-54.0	-13.1	-240.0	-61.7	-54.0	-13.1	-240.0
45	B2W10H10ST11WT10H2C4	71	-61.7	-108.0	-13.1	-200.4	-61.7	-108.0	-13.1	-200.4
46	B2W11H11ST9.5WT11H0C4	105	-59.0	0.0	-14.5	-297.3	-59.0	0.0	-14.5	-297.3
47	B2W11H11ST9.5WT11H1C4	99	-59.0	-59.8	-14.5	-251.2	-59.0	-59.8	-14.5	-251.2
48	B2W11H11ST9.5WT11H2C4	87	-59.0	-119.6	-14.5	-213.3	-59.0	-119.6	-14.5	-213.3
49	B2W11H11ST10.5WT11H0C4	105	-65.2	0.0	-14.4	-295.8	-65.2	0.0	-14.4	-295.8
50	B2W11H11ST10.5WT11H1C4	99	-65.2	-59.8	-14.4	-249.8	-65.2	-59.8	-14.4	-249.8
51	B2W11H11ST10.5WT11H2C4	87	-65.2	-119.6	-14.4	-212.0	-65.2	-119.6	-14.4	-212.0
52	B2W11H11ST11.5WT11H0C4	105	-71.3	0.0	-14.4	-294.5	-71.3	0.0	-14.4	-294.5
53	B2W11H11ST11.5WT11H1C4	99	-71.3	-59.8	-14.4	-248.6	-71.3	-59.8	-14.4	-248.6
54	B2W11H11ST11.5WT11H2C4	87	-71.3	-119.5	-14.4	-211.0	-71.3	-119.5	-14.4	-211.0

Units: lb./in. for shear

#	Case	M_{pE}^{DC}	M_{pE}^{EF}	M_{pE}^{DW}	M_{pE}^{LL}	M_{nL}^{DC}	M_{nL}^{EF}	M_{nL}^{DW}	M_{nL}^{LL}	M_{nR}^{DC}	M_{nR}^{EF}	M_{nR}^{DW}	M_{nR}^{LL}
28	B2W9H9ST8.5WT9H0C4	-448	0	-121	-4481	778	0	216	2896	-778	0	-216	-2896
29	B2W9H9ST8.5WT9H1C4	-445	-497	-120	-3667	778	894	216	2512	-778	-894	-216	-2512
30	B2W9H9ST8.5WT9H2C4	-445	-991	-120	-3004	778	1788	216	1947	-778	-1788	-216	-2051
31	B2W9H9ST9.5WT9H0C4	-503	0	-121	-4523	865	0	215	2781	-865	0	-215	-2781
32	B2W9H9ST9.5WT9H1C4	-500	-498	-120	-3704	865	891	215	2412	-865	-891	-215	-2412
33	B2W9H9ST9.5WT9H2C4	-499	-994	-120	-3037	865	1783	215	1862	-865	-1783	-215	-1957
34	B2W9H9ST10.5WT9H0C4	-558	0	-121	-4554	951	0	215	2695	-951	0	-215	-2695
35	B2W9H9ST10.5WT9H1C4	-555	-499	-121	-3732	951	888	215	2339	-951	-888	-215	-2339
36	B2W9H9ST10.5WT9H2C4	-554	-996	-120	-3063	951	1777	215	1830	-951	-1777	-215	-1885
37	B2W10H10ST9WT10H0C4	-589	0	-150	-4880	1033	0	270	3450	-1033	0	-270	-3450
38	B2W10H10ST9WT10H1C4	-585	-617	-149	-4048	1033	1118	270	3025	-1033	-1118	-270	-3025
39	B2W10H10ST9WT10H2C4	-597	-1259	-152	-3364	1033	2236	270	2613	-1033	-2236	-270	-2613
40	B2W10H10ST10WT10H0C4	-656	0	-150	-4928	1142	0	269	3341	-1142	0	-269	-3341
41	B2W10H10ST10WT10H1C4	-652	-618	-149	-4090	1142	1115	270	2944	-1142	-1115	-270	-2944
42	B2W10H10ST10WT10H2C4	-665	-1261	-152	-3412	1142	2230	270	2570	-1142	-2230	-270	-2570
43	B2W10H10ST11WT10H0C4	-725	0	-151	-4966	1250	0	269	3365	-1250	0	-269	-3365
44	B2W10H10ST11WT10H1C4	-721	-620	-150	-4124	1250	1112	269	2965	-1250	-1112	-269	-2965
45	B2W10H10ST11WT10H2C4	-734	-1264	-153	-3452	1250	2224	269	2591	-1250	-2224	-269	-2590
46	B2W11H11ST9.5WT11H0C4	-777	0	-188	-5273	1336	0	330	4200	-1336	0	-330	-4200
47	B2W11H11ST9.5WT11H1C4	-775	-776	-188	-4512	1336	1367	330	3796	-1336	-1367	-330	-3796
48	B2W11H11ST9.5WT11H2C4	-775	-1551	-187	-3886	1336	2735	330	3433	-1336	-2735	-330	-3433
49	B2W11H11ST10.5WT11H0C4	-861	0	-188	-5343	1470	0	330	4202	-1470	0	-330	-4202
50	B2W11H11ST10.5WT11H1C4	-859	-778	-188	-4575	1470	1364	330	3800	-1470	-1364	-330	-3800
51	B2W11H11ST10.5WT11H2C4	-859	-1554	-188	-3940	1470	2729	330	3438	-1470	-2729	-330	-3438
52	B2W11H11ST11.5WT11H0C4	-946	0	-189	-5400	1603	0	329	4214	-1603	0	-329	-4214
53	B2W11H11ST11.5WT11H1C4	-944	-779	-188	-4626	1603	1361	329	3810	-1603	-1361	-329	-3810
54	B2W11H11ST11.5WT11H2C4	-943	-1557	-188	-3984	1603	2722	329	3447	-1603	-2722	-329	-3447

Units: lb.-in./in. for bending moment

#	Case	NLS	V_L^{DC}	V_L^{EF}	V_L^{DW}	V_L^{LL}	V_R^{DC}	V_R^{EF}	V_R^{DW}	V_R^{LL}
55	B2W12H12ST10WT12H0C4	121	-68.1	0.0	-15.8	-301.1	-68.1	0.0	-15.8	-301.1
56	B2W12H12ST10WT12H1C4	115	-68.1	-65.5	-15.8	-256.6	-68.1	-65.5	-15.8	-256.6
57	B2W12H12ST10WT12H2C4	103	-68.1	-131.1	-15.8	-220.6	-68.1	-131.1	-15.8	-220.6
58	B2W12H12ST11WT12H0C4	121	-74.9	0.0	-15.8	-299.6	-74.9	0.0	-15.8	-299.6
59	B2W12H12ST11WT12H1C4	115	-74.9	-65.5	-15.8	-255.2	-74.9	-65.5	-15.8	-255.2
60	B2W12H12ST11WT12H2C4	103	-74.9	-131.0	-15.8	-219.4	-74.9	-131.0	-15.8	-219.4
61	B2W12H12ST12WT12H0C4	121	-81.6	0.0	-15.8	-298.4	-81.6	0.0	-15.8	-298.4
62	B2W12H12ST12WT12H1C4	115	-81.6	-65.5	-15.8	-254.0	-81.6	-65.5	-15.8	-254.0
63	B2W12H12ST12WT12H2C4	103	-81.6	-131.0	-15.8	-218.4	-81.6	-131.0	-15.8	-218.4

Units: lb./in. for shear

#	Case	M_{pE}^{DC}	M_{pE}^{EF}	M_{pE}^{DW}	M_{pE}^{LL}	M_{nL}^{DC}	M_{nL}^{EF}	M_{nL}^{DW}	M_{nL}^{LL}	M_{nR}^{DC}	M_{nR}^{EF}	M_{nR}^{DW}	M_{nR}^{LL}
55	B2W12H12ST10WT12H0C4	-980	0	-226	-5840	1690	0	397	5034	-1690	0	-397	-5034
56	B2W12H12ST10WT12H1C4	-981	-934	-226	-5052	1691	1642	397	4516	-1691	-1642	-397	-4516
57	B2W12H12ST10WT12H2C4	-974	-1855	-224	-4395	1691	3284	397	4083	-1691	-3284	-397	-4083
58	B2W12H12ST11WT12H0C4	-1081	0	-226	-5912	1852	0	396	5034	-1852	0	-396	-5034
59	B2W12H12ST11WT12H1C4	-1082	-936	-226	-5117	1853	1639	396	4517	-1853	-1639	-396	-4517
60	B2W12H12ST11WT12H2C4	-1075	-1858	-225	-4457	1853	3278	396	4083	-1853	-3278	-396	-4083
61	B2W12H12ST12WT12H0C4	-1182	0	-226	-5971	2012	0	395	5037	-2012	0	-395	-5037
62	B2W12H12ST12WT12H1C4	-1177	-932	-225	-5171	2013	1635	395	4519	-2013	-1635	-395	-4519
63	B2W12H12ST12WT12H2C4	-1176	-1861	-225	-4508	2013	3270	395	4087	-2013	-3270	-395	-4087

Units: lb.-in./in. for bending moment

Table E12. Bending moment and shear force values (2D model; Proposed formula with rigid joints; 3-barrel culverts)

#	Case	NLS	V_L^{DC}	V_L^{EF}	V_L^{DW}	V_L^{LL}	V_R^{DC}	V_R^{EF}	V_R^{DW}	V_R^{LL}
1	B3W6H6ST8WT6H0C4	43	-25.1	0.0	-7.3	-251.0	-20.8	0.0	-6.0	-236.9
2	B3W6H6ST8WT6H1C4	34	-25.1	-30.1	-7.3	-203.3	-20.8	-25.0	-6.0	-185.9
3	B3W6H6ST8WT6H2C4	19	-25.1	-60.1	-7.3	-157.8	-20.8	-50.0	-6.0	-139.6
4	B3W7H7ST8.5WT7H0C4	58	-31.7	0.0	-8.6	-263.4	-26.2	0.0	-7.1	-239.4
5	B3W7H7ST8.5WT7H1C4	46	-31.7	-35.7	-8.6	-207.8	-26.2	-29.6	-7.1	-192.3
6	B3W7H7ST8.5WT7H2C4	31	-31.7	-71.3	-8.6	-168.0	-26.2	-59.2	-7.1	-150.4
7	B3W8H8ST9WT8H0C4	65	-38.8	0.0	-10.0	-274.1	-32.0	0.0	-8.3	-244.4
8	B3W8H8ST9WT8H1C4	60	-38.8	-41.3	-10.0	-222.8	-32.0	-34.2	-8.3	-197.6
9	B3W8H8ST9WT8H2C4	43	-38.8	-82.6	-10.0	-173.6	-32.0	-68.3	-8.3	-157.2
10	B3W9H9ST9.5WT9H0C4	81	-46.6	0.0	-11.3	-291.7	-38.3	0.0	-9.4	-261.1
11	B3W9H9ST9.5WT9H1C4	76	-46.6	-46.9	-11.3	-241.3	-38.3	-38.8	-9.4	-213.0
12	B3W9H9ST9.5WT9H2C4	55	-46.6	-93.9	-11.3	-176.4	-38.3	-77.5	-9.4	-161.8
13	B3W10H10ST10WT10H0C4	98	-55.0	0.0	-12.7	-302.2	-45.1	0.0	-10.5	-272.6
14	B3W10H10ST10WT10H1C4	83	-55.0	-52.6	-12.7	-244.9	-45.1	-43.3	-10.5	-215.1
15	B3W10H10ST10WT10H2C4	71	-55.0	-105.2	-12.7	-204.4	-45.1	-86.7	-10.5	-177.6
16	B3W11H11ST10.5WT11H0C4	105	-63.9	0.0	-14.1	-300.1	-52.4	0.0	-11.6	-270.5
17	B3W11H11ST10.5WT11H1C4	99	-63.9	-58.2	-14.1	-253.8	-52.4	-47.9	-11.6	-224.4
18	B3W11H11ST10.5WT11H2C4	87	-63.9	-116.5	-14.1	-215.5	-52.4	-95.8	-11.6	-187.8
19	B3W12H12ST11WT12H0C4	121	-73.5	0.0	-15.4	-304.0	-60.2	0.0	-12.7	-276.5
20	B3W12H12ST11WT12H1C4	115	-73.5	-63.9	-15.4	-259.4	-60.2	-52.5	-12.7	-231.0
21	B3W12H12ST11WT12H2C4	103	-73.5	-127.8	-15.4	-223.1	-60.2	-105.0	-12.7	-195.6

Units: lb./in. for shear

#	Case	M_{pE}^{DC}	M_{pE}^{EF}	M_{pE}^{DW}	M_{pE}^{LL}	M_{nL}^{DC}	M_{nL}^{EF}	M_{nL}^{DW}	M_{nL}^{LL}	M_{nR}^{DC}	M_{nR}^{EF}	M_{nR}^{DW}	M_{nR}^{LL}	M_{pI}^{DC}	M_{pI}^{EF}	M_{pI}^{DW}	M_{pI}^{LL}
1	B3W6H6ST8WT6H0C4	-194	0	-57	-3071	257	0	73	2191	-235	0	-71	-2158	-77	0	-20	-2549
2	B3W6H6ST8WT6H1C4	-193	-235	-57	-2352	257	303	73	1812	-235	-294	-71	-1754	-77	-81	-20	-1930
3	B3W6H6ST8WT6H2C4	-193	-469	-57	-1786	258	607	73	1164	-235	-588	-71	-1192	-77	-162	-20	-1444
4	B3W7H7ST8.5WT7H0C4	-290	0	-80	-3549	390	0	104	2323	-346	0	-98	-2253	-119	0	-29	-2906
5	B3W7H7ST8.5WT7H1C4	-290	-331	-80	-2792	390	431	104	1958	-347	-407	-98	-1891	-118	-119	-29	-2259
6	B3W7H7ST8.5WT7H2C4	-289	-661	-80	-2193	390	863	104	1473	-347	-813	-98	-1381	-118	-237	-29	-1741
7	B3W8H8ST9WT8H0C4	-405	0	-106	-4000	559	0	141	2498	-486	0	-130	-2400	-171	0	-40	-3235
8	B3W8H8ST9WT8H1C4	-404	-436	-105	-3217	559	584	141	2068	-486	-537	-130	-1962	-171	-164	-40	-2566
9	B3W8H8ST9WT8H2C4	-404	-872	-105	-2585	559	1168	141	1786	-486	-1073	-130	-1540	-171	-327	-40	-2022
10	B3W9H9ST9.5WT9H0C4	-544	0	-135	-4414	768	0	184	3075	-656	0	-165	-2524	-236	0	-52	-3540
11	B3W9H9ST9.5WT9H1C4	-542	-555	-134	-3609	768	760	184	2661	-656	-684	-165	-2194	-236	-217	-52	-2854
12	B3W9H9ST9.5WT9H2C4	-541	-1108	-134	-2950	768	1521	184	2088	-656	-1369	-165	-1680	-236	-433	-52	-2290
13	B3W10H10ST10WT10H0C4	-718	0	-168	-4805	1021	0	232	3694	-859	0	-205	-2981	-310	0	-66	-3774
14	B3W10H10ST10WT10H1C4	-716	-695	-168	-3981	1021	961	232	3234	-859	-849	-205	-2632	-311	-274	-66	-3111
15	B3W10H10ST10WT10H2C4	-715	-1390	-168	-3304	1021	1923	232	2788	-859	-1699	-205	-2305	-315	-554	-67	-2544
16	B3W11H11ST10.5WT11H0C4	-915	0	-204	-5174	1322	0	287	4286	-1098	0	-249	-3791	-404	0	-82	-3796
17	B3W11H11ST10.5WT11H1C4	-916	-846	-204	-4399	1323	1187	287	3788	-1098	-1032	-249	-3433	-405	-342	-83	-3154
18	B3W11H11ST10.5WT11H2C4	-918	-1696	-205	-3788	1323	2373	287	3310	-1098	-2064	-249	-3115	-405	-684	-83	-2711
19	B3W12H12ST11WT12H0C4	-1146	0	-244	-5698	1675	0	347	4848	-1376	0	-298	-4590	-514	0	-101	-4098
20	B3W12H12ST11WT12H1C4	-1149	-1013	-245	-4924	1675	1436	347	4311	-1376	-1232	-298	-4118	-515	-418	-101	-3504
21	B3W12H12ST11WT12H2C4	-1150	-2027	-245	-4278	1675	2873	347	3808	-1376	-2464	-298	-3728	-515	-837	-101	-3047

Units: lb.-in./in. for bending moment

Appendix F

Comparison of 2D and 3D Results

The following tables list the ratio of the extracted straining actions due to live loads from the 2D and 3D models for each case. The ratios listed in the following tables are for the following straining actions:

- 1-Barrel Cases
  - V_L = shear force left of 1st wall due to live load
  - M_{pE} = positive moment at 1st exterior midspan due to live load
- 2-Barrel Cases
  - V_L = shear force left of 1st wall due to live load
  - V_R = shear force right of 1st wall due to live load
  - M_{pE} = positive moment at 1st exterior midspan due to live load
  - M_{nL} = negative moment at left of 1st wall due to live load
  - M_{nR} = negative moment at right of 1st wall due to live load
- 3-Barrel Cases
  - V_L = shear force left of 1st wall due to live load
  - V_R = shear force right of 1st wall due to live load
  - M_{pE} = positive moment at 1st exterior midspan due to live load
  - M_{nL} = negative moment at left of 1st interior wall due to live load
  - M_{nR} = negative moment at right of 1st interior wall due to live load
  - M_{pI} = positive moment at 1st interior midspan due to live load

Note: each of the above listed variables is presented with superscripts indicating whether they results are from 2D- or 3D models. For example, M_{nL}^{2D} and M_{nL}^{3D} for the negative moment at left of 1st interior wall.

Table F1. Straining action ratios for 1-barrel cases

#	Case	$\frac{V_{L,LL}^{2D}}{V_{L,LL}^{3D}}$	$\frac{M_{pE,LL}^{2D}}{M_{pE,LL}^{3D}}$	#	Case	$\frac{V_{L,LL}^{2D}}{V_{L,LL}^{3D}}$	$\frac{M_{pE,LL}^{2D}}{M_{pE,LL}^{3D}}$
1	B1W6H6ST7WT6H0C3	0.596	1.199	82	B1W9H9ST8.5WT9H0C3	0.681	1.379
2	B1W6H6ST7WT6H1C3	0.768	1.399	83	B1W9H9ST8.5WT9H1C3	0.928	1.551
3	B1W6H6ST7WT6H2C3	0.975	1.511	84	B1W9H9ST8.5WT9H2C3	1.122	1.642
4	B1W6H6ST8WT6H0C3	0.598	1.197	85	B1W9H9ST9.5WT9H0C3	0.683	1.378
5	B1W6H6ST8WT6H1C3	0.770	1.397	86	B1W9H9ST9.5WT9H1C3	0.930	1.550
6	B1W6H6ST8WT6H2C3	0.975	1.509	87	B1W9H9ST9.5WT9H2C3	1.123	1.640
7	B1W6H6ST9WT6H0C3	0.599	1.196	88	B1W9H9ST10.5WT9H0C3	0.685	1.377
8	B1W6H6ST9WT6H1C3	0.772	1.395	89	B1W9H9ST10.5WT9H1C3	0.933	1.548
9	B1W6H6ST9WT6H2C3	0.977	1.506	90	B1W9H9ST10.5WT9H2C3	1.124	1.638
10	B1W6H6ST7WT6H0C4	0.596	1.199	91	B1W9H9ST8.5WT9H0C4	0.681	1.379
11	B1W6H6ST7WT6H1C4	0.768	1.399	92	B1W9H9ST8.5WT9H1C4	0.928	1.551
12	B1W6H6ST7WT6H2C4	0.975	1.511	93	B1W9H9ST8.5WT9H2C4	1.122	1.642
13	B1W6H6ST8WT6H0C4	0.598	1.197	94	B1W9H9ST9.5WT9H0C4	0.683	1.378
14	B1W6H6ST8WT6H1C4	0.770	1.397	95	B1W9H9ST9.5WT9H1C4	0.930	1.550
15	B1W6H6ST8WT6H2C4	0.975	1.509	96	B1W9H9ST9.5WT9H2C4	1.123	1.640
16	B1W6H6ST9WT6H0C4	0.599	1.196	97	B1W9H9ST10.5WT9H0C4	0.685	1.377
17	B1W6H6ST9WT6H1C4	0.772	1.395	98	B1W9H9ST10.5WT9H1C4	0.933	1.548
18	B1W6H6ST9WT6H2C4	0.977	1.506	99	B1W9H9ST10.5WT9H2C4	1.124	1.638
19	B1W6H6ST7WT6H0C5	0.596	1.199	100	B1W9H9ST8.5WT9H0C5	0.681	1.379
20	B1W6H6ST7WT6H1C5	0.768	1.399	101	B1W9H9ST8.5WT9H1C5	0.928	1.551
21	B1W6H6ST7WT6H2C5	0.975	1.511	102	B1W9H9ST8.5WT9H2C5	1.122	1.642
22	B1W6H6ST8WT6H0C5	0.598	1.197	103	B1W9H9ST9.5WT9H0C5	0.683	1.378
23	B1W6H6ST8WT6H1C5	0.770	1.397	104	B1W9H9ST9.5WT9H1C5	0.930	1.550
24	B1W6H6ST8WT6H2C5	0.975	1.509	105	B1W9H9ST9.5WT9H2C5	1.123	1.640
25	B1W6H6ST9WT6H0C5	0.599	1.196	106	B1W9H9ST10.5WT9H0C5	0.685	1.377
26	B1W6H6ST9WT6H1C5	0.772	1.395	107	B1W9H9ST10.5WT9H1C5	0.933	1.548
27	B1W6H6ST9WT6H2C5	0.977	1.506	108	B1W9H9ST10.5WT9H2C5	1.124	1.638

#	Case	$\frac{V_{L,LL}^{2D}}{V_{L,LL}^{3D}}$	$\frac{M_{pE,LL}^{2D}}{M_{pE,LL}^{3D}}$
28	B1W7H7ST7.5WT7H0C3	0.579	1.266
29	B1W7H7ST7.5WT7H1C3	0.880	1.455
30	B1W7H7ST7.5WT7H2C3	1.097	1.556
31	B1W7H7ST8.5WT7H0C3	0.582	1.265
32	B1W7H7ST8.5WT7H1C3	0.881	1.453
33	B1W7H7ST8.5WT7H2C3	1.096	1.554
34	B1W7H7ST9.5WT7H0C3	0.584	1.263
35	B1W7H7ST9.5WT7H1C3	0.882	1.451
36	B1W7H7ST9.5WT7H2C3	1.096	1.552
37	B1W7H7ST7.5WT7H0C4	0.579	1.266
38	B1W7H7ST7.5WT7H1C4	0.880	1.455
39	B1W7H7ST7.5WT7H2C4	1.097	1.556
40	B1W7H7ST8.5WT7H0C4	0.582	1.265
41	B1W7H7ST8.5WT7H1C4	0.881	1.453
42	B1W7H7ST8.5WT7H2C4	1.096	1.554
43	B1W7H7ST9.5WT7H0C4	0.584	1.263
44	B1W7H7ST9.5WT7H1C4	0.882	1.451
45	B1W7H7ST9.5WT7H2C4	1.096	1.552
46	B1W7H7ST7.5WT7H0C5	0.579	1.266
47	B1W7H7ST7.5WT7H1C5	0.880	1.455
48	B1W7H7ST7.5WT7H2C5	1.097	1.556
49	B1W7H7ST8.5WT7H0C5	0.582	1.265
50	B1W7H7ST8.5WT7H1C5	0.881	1.453
51	B1W7H7ST8.5WT7H2C5	1.096	1.554
52	B1W7H7ST9.5WT7H0C5	0.584	1.263
53	B1W7H7ST9.5WT7H1C5	0.882	1.451
54	B1W7H7ST9.5WT7H2C5	1.096	1.552

#	Case	$\frac{V_{L,LL}^{2D}}{V_{L,LL}^{3D}}$	$\frac{M_{pE,LL}^{2D}}{M_{pE,LL}^{3D}}$
109	B1W10H10ST9WT10H0C3	0.629	1.431
110	B1W10H10ST9WT10H1C3	0.899	1.628
111	B1W10H10ST9WT10H2C3	1.158	1.771
112	B1W10H10ST10WT10H0C3	0.631	1.430
113	B1W10H10ST10WT10H1C3	0.902	1.627
114	B1W10H10ST10WT10H2C3	1.159	1.769
115	B1W10H10ST11WT10H0C3	0.633	1.429
116	B1W10H10ST11WT10H1C3	0.905	1.625
117	B1W10H10ST11WT10H2C3	1.160	1.767
118	B1W10H10ST9WT10H0C4	0.629	1.431
119	B1W10H10ST9WT10H1C4	0.899	1.628
120	B1W10H10ST9WT10H2C4	1.158	1.771
121	B1W10H10ST10WT10H0C4	0.631	1.430
122	B1W10H10ST10WT10H1C4	0.902	1.627
123	B1W10H10ST10WT10H2C4	1.159	1.769
124	B1W10H10ST11WT10H0C4	0.633	1.429
125	B1W10H10ST11WT10H1C4	0.905	1.625
126	B1W10H10ST11WT10H2C4	1.160	1.767
127	B1W10H10ST9WT10H0C5	0.629	1.431
128	B1W10H10ST9WT10H1C5	0.899	1.628
129	B1W10H10ST9WT10H2C5	1.158	1.771
130	B1W10H10ST10WT10H0C5	0.631	1.430
131	B1W10H10ST10WT10H1C5	0.902	1.627
132	B1W10H10ST10WT10H2C5	1.159	1.769
133	B1W10H10ST11WT10H0C5	0.633	1.429
134	B1W10H10ST11WT10H1C5	0.905	1.625
135	B1W10H10ST11WT10H2C5	1.160	1.767

#	Case	$\frac{V_{L,LL}^{2D}}{V_{L,LL}^{3D}}$	$\frac{M_{pE,LL}^{2D}}{M_{pE,LL}^{3D}}$
55	B1W8H8ST8WT8H0C3	0.692	1.325
56	B1W8H8ST8WT8H1C3	0.902	1.503
57	B1W8H8ST8WT8H2C3	1.076	1.600
58	B1W8H8ST9WT8H0C3	0.694	1.324
59	B1W8H8ST9WT8H1C3	0.903	1.502
60	B1W8H8ST9WT8H2C3	1.076	1.598
61	B1W8H8ST10WT8H0C3	0.695	1.323
62	B1W8H8ST10WT8H1C3	0.905	1.500
63	B1W8H8ST10WT8H2C3	1.077	1.596
64	B1W8H8ST8WT8H0C4	0.692	1.325
65	B1W8H8ST8WT8H1C4	0.902	1.503
66	B1W8H8ST8WT8H2C4	1.076	1.600
67	B1W8H8ST9WT8H0C4	0.694	1.324
68	B1W8H8ST9WT8H1C4	0.903	1.502
69	B1W8H8ST9WT8H2C4	1.076	1.598
70	B1W8H8ST10WT8H0C4	0.695	1.323
71	B1W8H8ST10WT8H1C4	0.905	1.500
72	B1W8H8ST10WT8H2C4	1.077	1.596
73	B1W8H8ST8WT8H0C5	0.692	1.325
74	B1W8H8ST8WT8H1C5	0.902	1.503
75	B1W8H8ST8WT8H2C5	1.076	1.600
76	B1W8H8ST9WT8H0C5	0.694	1.324
77	B1W8H8ST9WT8H1C5	0.903	1.502
78	B1W8H8ST9WT8H2C5	1.076	1.598
79	B1W8H8ST10WT8H0C5	0.695	1.323
80	B1W8H8ST10WT8H1C5	0.905	1.500
81	B1W8H8ST10WT8H2C5	1.077	1.596

#	Case	$\frac{V_{L,LL}^{2D}}{V_{L,LL}^{3D}}$	$\frac{M_{pE,LL}^{2D}}{M_{pE,LL}^{3D}}$
136	B1W11H11ST9.5WT11H0C3	0.759	1.544
137	B1W11H11ST9.5WT11H1C3	1.023	1.762
138	B1W11H11ST9.5WT11H2C3	1.145	1.888
139	B1W11H11ST10.5WT11H0C3	0.761	1.543
140	B1W11H11ST10.5WT11H1C3	1.024	1.760
141	B1W11H11ST10.5WT11H2C3	1.146	1.886
142	B1W11H11ST11.5WT11H0C3	0.763	1.542
143	B1W11H11ST11.5WT11H1C3	1.025	1.759
144	B1W11H11ST11.5WT11H2C3	1.148	1.883
145	B1W11H11ST9.5WT11H0C4	0.759	1.544
146	B1W11H11ST9.5WT11H1C4	1.023	1.762
147	B1W11H11ST9.5WT11H2C4	1.145	1.888
148	B1W11H11ST10.5WT11H0C4	0.761	1.543
149	B1W11H11ST10.5WT11H1C4	1.024	1.760
150	B1W11H11ST10.5WT11H2C4	1.146	1.886
151	B1W11H11ST11.5WT11H0C4	0.763	1.542
152	B1W11H11ST11.5WT11H1C4	1.025	1.759
153	B1W11H11ST11.5WT11H2C4	1.148	1.883
154	B1W11H11ST9.5WT11H0C5	0.759	1.544
155	B1W11H11ST9.5WT11H1C5	1.023	1.762
156	B1W11H11ST9.5WT11H2C5	1.145	1.888
157	B1W11H11ST10.5WT11H0C5	0.761	1.543
158	B1W11H11ST10.5WT11H1C5	1.024	1.760
159	B1W11H11ST10.5WT11H2C5	1.146	1.886
160	B1W11H11ST11.5WT11H0C5	0.763	1.542
161	B1W11H11ST11.5WT11H1C5	1.025	1.759
162	B1W11H11ST11.5WT11H2C5	1.148	1.883

#	Case	$\frac{V_{L,LL}^{2D}}{V_{L,LL}^{3D}}$	$\frac{M_{pE,LL}^{2D}}{M_{pE,LL}^{3D}}$
163	B1W12H12ST10WT12H0C3	0.681	1.379
164	B1W12H12ST10WT12H1C3	0.928	1.551
165	B1W12H12ST10WT12H2C3	1.122	1.642
166	B1W12H12ST11WT12H0C3	0.683	1.378
167	B1W12H12ST11WT12H1C3	0.930	1.550
168	B1W12H12ST11WT12H2C3	1.123	1.640
169	B1W12H12ST12WT12H0C3	0.685	1.377
170	B1W12H12ST12WT12H1C3	0.933	1.548
171	B1W12H12ST12WT12H2C3	1.124	1.638
172	B1W12H12ST10WT12H0C4	0.681	1.379
173	B1W12H12ST10WT12H1C4	0.928	1.551
174	B1W12H12ST10WT12H2C4	1.122	1.642
175	B1W12H12ST11WT12H0C4	0.683	1.378
176	B1W12H12ST11WT12H1C4	0.930	1.550
177	B1W12H12ST11WT12H2C4	1.123	1.640
178	B1W12H12ST12WT12H0C4	0.685	1.377
179	B1W12H12ST12WT12H1C4	0.933	1.548
180	B1W12H12ST12WT12H2C4	1.124	1.638
181	B1W12H12ST10WT12H0C5	0.681	1.379
182	B1W12H12ST10WT12H1C5	0.928	1.551
183	B1W12H12ST10WT12H2C5	1.122	1.642
184	B1W12H12ST11WT12H0C5	0.683	1.378
185	B1W12H12ST11WT12H1C5	0.930	1.550
186	B1W12H12ST11WT12H2C5	1.123	1.640
187	B1W12H12ST12WT12H0C5	0.685	1.377
188	B1W12H12ST12WT12H1C5	0.933	1.548
189	B1W12H12ST12WT12H2C5	1.124	1.638

Table F2. Straining action ratios for 2-barrel cases

#	Case	$\frac{V_{cr-LL}^{2D}}{V_{cr-LL}^{3D}}$	$\frac{M_{pE,LL}^{2D}}{M_{pE,LL}^{3D}}$	$\frac{M_{n,cr-LL}^{2D}}{M_{n,cr-LL}^{3D}}$
1	B2W6H6ST7WT6H0C4	0.506	1.154	0.915
2	B2W6H6ST7WT6H1C4	0.684	1.391	1.005
3	B2W6H6ST7WT6H2C4	0.874	1.578	0.828
4	B2W6H6ST8WT6H0C4	0.513	1.162	0.931
5	B2W6H6ST8WT6H1C4	0.690	1.402	1.017
6	B2W6H6ST8WT6H2C4	0.878	1.593	0.810
7	B2W6H6ST9WT6H0C4	0.519	1.169	0.943
8	B2W6H6ST9WT6H1C4	0.696	1.411	1.025
9	B2W6H6ST9WT6H2C4	0.883	1.605	0.797
10	B2W7H7ST7.5WT7H0C4	0.536	1.214	0.918
11	B2W7H7ST7.5WT7H1C4	0.743	1.440	1.002
12	B2W7H7ST7.5WT7H2C4	0.943	1.603	0.893
13	B2W7H7ST8.5WT7H0C4	0.542	1.223	0.921
14	B2W7H7ST8.5WT7H1C4	0.750	1.451	1.014
15	B2W7H7ST8.5WT7H2C4	0.948	1.615	0.873
16	B2W7H7ST9.5WT7H0C4	0.548	1.230	0.920
17	B2W7H7ST9.5WT7H1C4	0.757	1.459	1.022
18	B2W7H7ST9.5WT7H2C4	0.954	1.624	0.857
19	B2W8H8ST8WT8H0C4	0.616	1.262	0.835
20	B2W8H8ST8WT8H1C4	0.814	1.478	0.903
21	B2W8H8ST8WT8H2C4	0.938	1.615	0.947
22	B2W8H8ST9WT8H0C4	0.624	1.272	0.841
23	B2W8H8ST9WT8H1C4	0.821	1.490	0.906
24	B2W8H8ST9WT8H2C4	0.943	1.628	0.923
25	B2W8H8ST10WT8H0C4	0.631	1.279	0.843
26	B2W8H8ST10WT8H1C4	0.828	1.498	0.906
27	B2W8H8ST10WT8H2C4	0.949	1.639	0.906

#	Case	$\frac{V_{cr-LL}^{2D}}{V_{cr-LL}^{3D}}$	$\frac{M_{pE,LL}^{2D}}{M_{pE,LL}^{3D}}$	$\frac{M_{n,cr-LL}^{2D}}{M_{n,cr-LL}^{3D}}$
28	B2W9H9ST8.5WT9H0C4	0.626	1.303	0.881
29	B2W9H9ST8.5WT9H1C4	0.855	1.509	0.944
30	B2W9H9ST8.5WT9H2C4	1.035	1.633	1.016
31	B2W9H9ST9.5WT9H0C4	0.633	1.313	0.862
32	B2W9H9ST9.5WT9H1C4	0.860	1.520	0.918
33	B2W9H9ST9.5WT9H2C4	1.040	1.645	0.988
34	B2W9H9ST10.5WT9H0C4	0.639	1.321	0.848
35	B2W9H9ST10.5WT9H1C4	0.866	1.529	0.899
36	B2W9H9ST10.5WT9H2C4	1.045	1.656	0.965
37	B2W10H10ST9WT10H0C4	0.604	1.341	0.953
38	B2W10H10ST9WT10H1C4	0.828	1.535	0.998
39	B2W10H10ST9WT10H2C4	1.041	1.685	1.056
40	B2W10H10ST10WT10H0C4	0.609	1.350	0.932
41	B2W10H10ST10WT10H1C4	0.833	1.545	0.972
42	B2W10H10ST10WT10H2C4	1.044	1.703	1.025
43	B2W10H10ST11WT10H0C4	0.614	1.358	0.923
44	B2W10H10ST11WT10H1C4	0.838	1.557	0.963
45	B2W10H10ST11WT10H2C4	1.048	1.718	1.022
46	B2W11H11ST9.5WT11H0C4	0.691	1.398	1.032
47	B2W11H11ST9.5WT11H1C4	0.895	1.621	1.085
48	B2W11H11ST9.5WT11H2C4	1.042	1.782	1.167
49	B2W11H11ST10.5WT11H0C4	0.697	1.412	1.048
50	B2W11H11ST10.5WT11H1C4	0.900	1.637	1.101
51	B2W11H11ST10.5WT11H2C4	1.045	1.800	1.182
52	B2W11H11ST11.5WT11H0C4	0.702	1.424	1.064
53	B2W11H11ST11.5WT11H1C4	0.905	1.650	1.117
54	B2W11H11ST11.5WT11H2C4	1.048	1.816	1.195
55	B2W12H12ST10WT12H0C4	0.671	1.482	1.156
56	B2W12H12ST10WT12H1C4	0.889	1.708	1.192
57	B2W12H12ST10WT12H2C4	1.098	1.870	1.250
58	B2W12H12ST11WT12H0C4	0.676	1.496	1.175
59	B2W12H12ST11WT12H1C4	0.894	1.725	1.210
60	B2W12H12ST11WT12H2C4	1.101	1.888	1.267
61	B2W12H12ST12WT12H0C4	0.682	1.508	1.194
62	B2W12H12ST12WT12H1C4	0.899	1.740	1.228
63	B2W12H12ST12WT12H2C4	1.105	1.900	1.283

Table F3. Straining action ratios for 3-barrel cases

#	Case	$\frac{V_{cr-LL}^{2D}}{V_{cr-LL}^{3D}}$	$\frac{M_{pE,LL}^{2D}}{M_{pE,LL}^{3D}}$	$\frac{M_{nL,LL}^{2D}}{M_{nL,LL}^{3D}}$	$\frac{M_{nR,LL}^{2D}}{M_{nR,LL}^{3D}}$	$\frac{M_{pI,LL}^{2D}}{M_{pI,LL}^{3D}}$
1	B3W6H6ST8WT6H0C4	0.515	1.149	0.877	0.977	1.100
2	B3W6H6ST8WT6H1C4	0.695	1.384	0.953	1.117	1.373
3	B3W6H6ST8WT6H2C4	0.885	1.575	0.864	0.945	1.591
4	B3W7H7ST8.5WT7H0C4	0.547	1.206	0.878	0.983	1.148
5	B3W7H7ST8.5WT7H1C4	0.758	1.431	0.963	1.099	1.409
6	B3W7H7ST8.5WT7H2C4	0.957	1.594	0.939	0.934	1.610
7	B3W8H8ST9WT8H0C4	0.630	1.252	0.848	0.977	1.188
8	B3W8H8ST9WT8H1C4	0.829	1.467	0.929	1.074	1.437
9	B3W8H8ST9WT8H2C4	0.952	1.602	0.999	0.954	1.619
10	B3W9H9ST9.5WT9H0C4	0.640	1.293	0.932	0.883	1.220
11	B3W9H9ST9.5WT9H1C4	0.868	1.497	0.991	0.972	1.459
12	B3W9H9ST9.5WT9H2C4	1.051	1.622	1.059	1.104	1.620
13	B3W10H10ST10WT10H0C4	0.617	1.329	1.011	0.948	1.246
14	B3W10H10ST10WT10H1C4	0.842	1.521	1.051	1.026	1.476
15	B3W10H10ST10WT10H2C4	1.055	1.662	1.106	1.126	1.621
16	B3W11H11ST10.5WT11H0C4	0.704	1.378	1.075	1.096	1.211
17	B3W11H11ST10.5WT11H1C4	0.910	1.598	1.106	1.187	1.466
18	B3W11H11ST10.5WT11H2C4	1.056	1.755	1.149	1.313	1.667
19	B3W12H12ST11WT12H0C4	0.683	1.458	1.136	1.236	1.283
20	B3W12H12ST11WT12H1C4	0.904	1.680	1.160	1.296	1.543
21	B3W12H12ST11WT12H2C4	1.113	1.842	1.188	1.400	1.756